TECHNISCHE UNIVERSITÄT
CHEMNITZ

(Metallo-)Dendrimers in Catalysis, Nanoparticle Stabilization and Biological Application

von der Fakultät für Naturwissenschaften der

Technischen Universität Chemnitz genehmigte

Dissertation

zur Erlangung des akademischen Grades

doctor rerum naturalium

(Dr. rer. nat.)

vorgelegt von Dipl.-Chem. Sascha Dietrich

geboren am 15.10.1982 in Stollberg/Erzgebirge

eingereicht am: 07. Oktober 2011

Erstgutachter: Prof. Dr. Heinrich Lang

Zweitgutachter: Prof. Dr. Michael Mehring

Tag der Verteidigung: 06. Januar 2012

http://nbn-resolving.de/urn:nbn:de:bsz:ch1-qucosa-82016

Bibliografische Beschreibung und Referat

Dietrich, S.

(Metallo-)Dendrimers in Catalysis, Nanoparticle Stabilization and Biological Application

Technische Universität Chemnitz, Fakultät für Naturwissenschaften
Dissertation 2011, 165 Seiten

Die vorliegende Dissertationsschrift befasst sich mit der Darstellung, Charakterisierung und Anwendung neuartiger (Metallo-)Dendrimere. Den Schwerpunkt der Arbeit bildet dabei die terminale Funktionalisierung (Poly)amidoamin-basierender Dendrimere kleiner Generationen.

Durch Standardpeptid-Knüpfungsreaktionen von 1,1´-(Diphenylphosphino)ferrocencarbonsäure an dendritische (Poly)amidoamine ist eine Serie entsprechend funktionalisierter Metallodendrimere zugänglich. Die metallorganischen, Dendrimer-immobilisierten Engruppen können durch Zugabe von $[Pd(\eta^3\text{-}C_3H_5)Cl]_2$ in heterobimetallische Übergangsmetallkomplexe umgewandelt werden und finden Einsatz als katalytisch aktive Systeme in *C*,*C*-Kreuzkupplungsreaktionen nach Heck.

Ein weiterer Gegenstand der Arbeit ist die terminale Modifikation von (dendritischen) Aminen mit (S_p)-2-(Diphenylphosphino)ferrocen-1-carbonsäure. Nach erfolgter Umsetzung mit $[Pd(\eta^3\text{-}C_3H_5)Cl]_2$ werden die erhaltenen planar-chiralen Verbindungen als Katalysatoren in asymmetrischen allylischen Substitutionsreaktionen eingesetzt.

Ferner ist die Darstellung (Oligo)ethylenglykolether-terminierter (Poly)amidoamin-Dendrimere beschrieben. Diese werden als Stabilisatoren zur *in-situ* Generierung von Gold- sowie Magnetit-Nanopartikeln eingesetzt. Der Einfluss der dendritischen Template auf die Kolloidgrößen und Morphologien sowie die Eigenschaften der gebildeten Hybridmaterialien werden aufgezeigt.

Darüber hinaus befasst sich die Arbeit mit der Verwendung biokompatibler (Oligo)ethylenglykolether-Dendrimere als Wirkstoffträger für Zytostatika bei der Krebstherapie. Die im Rahmen von *in vitro* Untersuchungen erhaltenen Ergebnisse werden präsentiert.

Stichworte: (Poly)amidoamine, (Metallo-)Dendrimer, Ferrocen, Palladium, Kreuzkupplung, (Oligo)ethylenglykole, Stabilisator, Nanopartikel, Gold, Magnetit, Zytostatika.

Selbstständigkeitserklärung

Hiermit erkläre ich an Eides statt, die vorliegende Promotionsarbeit mit dem Titel "(Metallo-)Dendrimers in Catalysis, Nanoparticle Stabilization and Biological Application" selbstständig und ohne unzulässige, fremde Hilfe angefertigt zu haben. Die Arbeit hat in dieser oder ähnlicher Form noch keiner anderen Prüfungsbehörde vorgelegen.

Chemnitz, den 09. Januar 2012

Zeitraum und Ort der Durchführung

Die vorliegende Promotionsarbeit wurde im Zeitraum von November 2007 bis Oktober 2011 unter Anleitung von Herrn Universitätsprofessor Dr. Heinrich Lang am Lehrstuhl für Anorganische Chemie der Technischen Universität Chemnitz durchgeführt.

Herrn Prof. Dr. Heinrich Lang
danke ich für die gewährten Freiheiten bei der Bearbeitung dieses Themas, die großzügige Unterstützung dieser Arbeit sowie das mir entgegengebrachte Vertrauen.

„Ein Gelehrter in seinem Laboratorium ist nicht nur ein Techniker; er steht auch vor den Naturgesetzen wie ein Kind vor der Märchenwelt.“

(Marie Curie, Nobelpreisträgerin)

Meinen Eltern, meinem Bruder und

meiner lieben Sophia

Table of Contents

Bibliografische Beschreibung und Referat ii
Selbstständigkeitserklärung iii
Table of Contents vii
List of Abbreviations xi
Präambel xvi
A Introduction 1
1. Dendrimers 1
2. Nanomaterials 4
3. References 7
B State of Knowledge 12
1. Dendrimers 12
1.1. Synthesis and Characterization 12
1.2. Functional Dendrimers 15
2. Characterization Techniques for Dendrimer-Nanomaterial Assemblies 24
3. Motivation 26
4. References 27
C Amidoamine-based Dendrimers with End-grafted Pd-Fe Units: Synthesis, Characterization and Their Use in the Heck Reaction 34
1. Introduction 34
2. Results and Discussion 35
2.1. Synthesis of Amidoamine Dendrimers 35
2.2. Synthesis of Metallo- and Selenium-Phosphine Amidoamine Dendrimers 36
2.3. Catalysis with Heterobimetallic Iron-Palladium Amidoamine Dendrimers 39
3. Conclusions 41
4. Experimental 42
4.1. Materials and Methods 42
4.2. Preparation of **2** 43
4.3. Preparation of **9-Fe** 43
4.4. Preparation of **5-Fe-Pd** 44
4.5. Preparation of **6-Fe-Pd** 44
4.6. Preparation of **7-Fe-Pd** 45
4.7. Preparation of **8-Fe-Pd** 46

4.8. Preparation of **9-Fe-Pd** 46
4.9. Preparation of **5-Fe-Se** 47
4.10. Preparation of **9-Fe-Se** 48
4.11. General Procedure for the Heck-Reaction 48
5. Acknowledgement 49
6. References 49

D A Preparation of Planar-Chiral Multidonor Phosphanyl-Ferrocene Carboxamides and Their Application as Ligands for Palladium-Catalyzed Asymmetric Allylic Alkylation. 52
1. Introduction 52
2. Results and Discussion 53
2.1. Syntheses and Characterization 53
2.2. Solid-State Structure of (S_p)–**2** 55
2.3. Catalytic Tests 57
3. Conclusions 58
4. Experimental 59
4.1. Materials and Methods 59
4.2. Preparation of Simple Amides. A General Procedure 59
4.3. Preparation of **6** 61
4.4. Preparation of (S_p,S_p)–**4** 61
4.5. Preparation of **7** 62
4.6. Preparation of (S_p,S_p,S_p)–**5** 62
4.7. Asymmetric Allylic Alkylation. A General Procedure 63
4.8. X-ray Crystallography 63
5. Acknowledgements 64
6. References 64

E Au Nanoparticles Stabilized by PEGylated Low-Generation PAMAM Dendrimers: Design, Characterization and Properties 68
1. Introduction 68
2. Materials and Methods 69
2.1. Synthesis of Stabilizers 69
2.2. Preparation Procedure for Gold Nanoparticles 70
3. Results and Discussion 70
3.1. Dendritic Stabilizers 70

3.2. Dendritic Stabilized Gold Nanoparticles 72
3.3. Physical and Chemical Characterization 73
4. Conclusion 79
5. Acknowledgement 80
6. Supplementary Material 80
7. References 80

F Design, Characterization and Magnetic Properties of Fe_3O_4-Nanoparticle Arrays Coated with PEGylated-Dendrimers 86
1. Introduction 86
2. Materials and Methods 88
2.1. Materials and Instruments 88
2.2. Synthesis Procedure for Fe_3O_4 Nanoparticles 89
3. Results and Discussion 91
3.1. Preparation and Characterization of Dendrimer-Surfaced Fe_3O_4 Nanoparticles 91
3.2. Magnetic Characterization of Dendrimer-Coated Fe_3O_4 Nanoparticles 96
4. Conclusion 99
5. Acknowledgement 100
6. References 100

G Dendrimer - Doxorubicin Conjugate for Enhanced Therapeutic Effects for Cancer 103
1. Introduction 103
2. Experimental Section 105
2.1. Materials and Methods 105
2.2. Synthesis of OEGylated Poly(amidoamine) Dendrimer **2** 106
2.3. Cell Viability Studies 107
2.4. Doxorubicin Loading and Release 107
2.5. *In Vitro* Cellular Uptake of Dendrimer-DOX Conjugate 109
3. Results and Discussion 109
3.1. Drug Loading and Release 109
3.2. Surface Potential of the Dendrimer-Drug Assembly 110
3.3. Structural Analysis of Dendrimer-DOX Conjugate 111
3.4. *In Vitro* DOX Release Profile from Dendrimer-Drug Conjugate 114
3.5. Cell Viability Studies of the Dendrimer-DOX Conjugate 117
3.6. Cellular Uptake by the Dendrimer-DOX Conjugate 118

3.7. Protein Adsorption Studies 119
4. Conclusions 119
5. Acknowledgements 120
6. Supplementary Material 120
7. References 121
H Summary 123
1. Summary 123
2. Zusammenfassung 129
Danksagung 136
I Appendix 137
1. Appendix Chapter C 137
2. Appendix Chapter D 139
3. Appendix Chapter E 140
4. Appendix Chapter F 142
5. Appendix Chapter G 144
Lebenslauf 145
Liste der Publikationen, Vorträge und Posterpräsentationen 147
Publikationen 147
Poster 148
Vorträge 149

List of Abbreviations

Å	Angstrom
$[a]_D$	Specific rotation
AC	Alternating current
Allyl	η^3-C_3H_5
AFM	Atomic force microscopy
a.u.	Arbitrary unit
Boc	*tert*-Butoxycarbonyl, $C(O)OC(CH_3)_3$
BSA	Bovine serum albumin
^{t}Bu	*tert*-Butyl, $^tC_4H_9$
CNTs	Carbon nanotubes
Cp	Cyclopentadienyl, η^5-C_5H_5
d	Days
DAAD	German Academic Exchange Service
ø	Average particle diameter
DLS	Dynamic light scattering
DMEM	Dulbecco´s modified eagle medium
DOX	Doxorubicin
DPX	Dibutyl phthalate in xylene, mounting medium
DSC	Differential scanning calorimetry
EDC	1-Ethyl-3-(3-dimethylaminopropyl)-carbodiimide
EDTA	Ethylenediaminetetraacetic acid

ee	Enantiomeric excess
Et	Ethyl, C_2H_5
Fc	Ferrocenyl, Fe(η^5-C_5H_5)(η^5-C_5H_4)
FC	Field cooled
FWHM	Full-width-at-half-maximum
Gen.	Dendrimer generation
G4OH	Dendrimer of 4th generation, hydroxyl-terminated
Hdpf	1´-(Diphenylphosphanyl)ferrocene-carboxylic acid
HeLa	Cervical cancer cell line
HOBT	1-Hydroxybenzotriazole
HPLC	High-performance liquid chromatography
hrs	Hours
IC_{50}	Half maximal inhibitory concentration
ICP-MS	Inductive-coupled plasma mass spectrometry
k_B	Boltzmann-constant
M	Molar
MALDI	Matrix-assisted laser desorption/ionization
MCF-7	Breast cancer cell line
Me	Methyl, CH_3
MEM	Minimum essential medium
MNPs	Magnetic nanoparticles
Mp	Melting point
MRI	Magnetic resonance imaging

MTS	3-(4,5-dimethylthiazol-2-yl)-5-(3-carboxymethoxyphenyl)-2-(4-sulfophenyl)-2H-tetrazolium
NPs	Nanoparticles
OEG	(Oligo)ethylene glycol
PAMAM	(Poly)amidoamine
PBS	Phosphate buffer saline
PCS	Photon correlation spectroscopy
PEG	(Poly)ethylene glycol
Ph	Phenyl, C_6H_5
PPI	(Poly)propyleneimine
^{i}Pr	*iso*-Propyl, $^{i}C_3H_7$
R	Single bonded organic group (alkyl, aryl)
RT	Room temperature
SBF	Simulated body fluid
SEM	Scanning electron microscopy
SERS	Surface-enhanced Raman scattering
SPIONs	Superparamagnetic iron oxide nanoparticles
SQUID	Superconducting quantum interference device
T_B	Blocking temperature
TEM	Transmission electron microscopy
ϑ	Temperature
TGA	Thermogravimetric analyses
TGA-MS	Coupled TGA-mass spectrometry

THF	Tetrahydrofuran, C_4H_8O
TOF	Turn-over-frequency
TON	Turn-over-number
VSM	Vibrating sample magnetometer
XPS	X-ray photoelectron spectroscopy
XRPD	X-ray powder diffraction
ζ-potential	Zeta-potential
ZFC	Zero-field cooled

MS	**Mass spectrometry**
ESI	Electrospray ionization
HR	high-resolution
M^+	Molecular-ion peak
TOF	Time-of-Flight
m/z	Mass-to-charge ratio

FT-IR	**Fourier transformed infrared spectroscopy**
ν	Stretching vibration
s	Strong
m	Medium
w	Weak

NMR	**Nuclear magnetic resonance**
δ	Chemical shift
br	Broad signal
d	Doublet
$^{n}J_{XY}$	Coupling constant over n bonds between core X and core Y
m	Multiplet
ppm	Parts per million
s	Singlet
t	Triplet
EA	**Elemental analysis**
Anal. Calc.	Calculated values
Found	Found values
UV/Vis	**Ultraviolet/visible light spectroscopy**
λ	Wavelength
ε	Coefficient of extinction

Präambel

Im Rahmen der im Zeitraum zwischen November 2007 und Oktober 2011 durchgeführten Promotionsarbeit an der Professur für Anorganische Chemie der Technischen Universität Chemnitz konnten bislang fünf das Thema der vorliegenden Promotionsschrift betreffende Publikationen erstellt werden. Diese veröffentlichten bzw. bei entsprechenden naturwissenschaftlichen Journalen zur Veröffentlichung eingereichten Arbeiten wurden vom Promovenden selbstständig unter Anleitung von Herrn Universitätsprofessor Dr. Heinrich Lang angefertigt. Die vom Promovenden geleisteten Eigenanteile in Publikationen, die als Ergebnis einer arbeitsgruppenübergreifenden Kooperation entstanden sind, werden an entsprechender Stelle gesondert ausgewiesen.

Alle diese Promotionsschrift betreffenden Manuskripte sind in englischer Sprache verfasst und in inhaltlich unveränderter Form als Kapitel C bis G eingefügt worden. Weiterhin wurden die Kapitel A Einleitung (Introduction), Kapitel B Kenntnisstand (State of Knowledge) und Kapitel H Zusammenfassung (Summary) sowie die Abschnitte Inhaltsverzeichnis (Table of Contents), verwendete Abkürzungen (List of Abbreviations) und Anhang (Appendix) in englischer Sprache erstellt.

Die Nummerierung der in der Dissertationsschrift aufgeführten chemischen Verbindungen erfolgt gemäß der Bezeichnung des Manuskriptes, in welchem die wissenschaftlichen Ergebnisse veröffentlicht wurden.

A Introduction

1. Dendrimers

In December 1953, the German chemist Hermann Staudinger was awarded with the Nobel Prize in Chemistry. Preceding to this award, he accomplished a pioneering research on the field of macromolecular chemistry and established the revolutionary concept of linking a large number of small monomer molecules by means of covalent bond formation to yield macromolecules. This certainly marked the beginning of a new era of molecular design of polymers. [A1]

Polymeric materials are exceptional with respect to their unique flexible and controllable preparation techniques as well as their extraordinary versatility of properties. Therefore, in the last decades, there was a tremendous development of various types of structural and functional macromolecular compounds like hyperbranched, star-shaped and radial symmetric polymers (dendrimers) (Scheme A1). [A1] [A2]

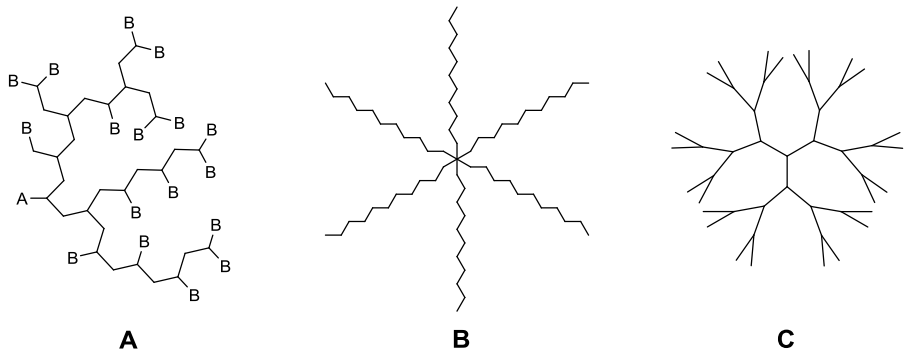

Scheme A1. Schematic illustration of a hyperbranched polymer (**A**), a star-shaped polymer (**B**) and a dendrimer (**C**). [A2]

In 1978, Vögtle [A3] published a seminal "cascade-like" synthetic strategy making accessible a new class of fascinating macromolecules which are now-a-days known as dendrimers (**C**). The word "dendrimer" originates from Greek (combining *dendron* meaning tree and *meros* meaning part) and refers to regular highly branched macromolecules [A4] that are in particular reminiscent of natural branching tree tops, blood vessels, nerve cells, corals and snowflakes. [A5] Apart from the distinctive chemical elegance, dendritic networks pertain to flexible, versatile and promising representatives of macromolecular chemistry.

In general, dendrimers are monodisperse, fractal-like polymers of well-defined three-dimensional globular shape, exhibiting a radial symmetry. [A6] Type **C** molecules are com-

posed of a central multifunctional core, repetitive branching units (generations) and terminal functional groups (periphery) (Scheme A2). [A7]

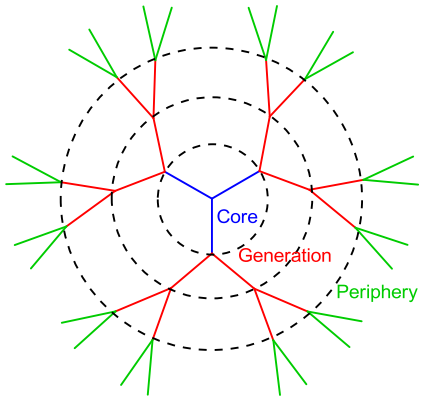

Scheme A2. Structure of a typical regular branched dendrimer.

The number n_i of repetitive units and terminal moieties, respectively, in the dendritic scaffold increases exponentially as a function of the dendrimer´s generation (i) (Equation A1). When the dendrimer grows in size, the terminal groups reside closer and closer to each other, resulting in a surface congestion, a phenomena that prevents further uniform growth for a monodisperse dendrimer. [A8]

$$n_i = f_c \cdot (f - 1)^i \qquad \text{(Eq. A1)}$$

n_i = number of repetitive units/terminal moieties; f_c = multiplicity of central core;
f = multiplicity of branching units; i = generation number.

In contrast to hyperbranched polymers (**A**), the precise dendritic architectures are constructed typically *via* iterative, consecutive synthesis processes, whereas the synthetic protocols rely on two different approaches: the divergent and the convergent methodology, employing protection and deprotection steps (Scheme A3). The divergent approach is based on the sequential addition of monomers to a branched building block (core), thus forming layer by layer (generations) within the structure. The convergent method constructs dendritic architectures starting from the periphery, elaborating inwards and finally attaching to a core for dendrimer assembly. [A6] As a consequence of both hierarchical synthesis strategies, size, molecular mass, monodisperseity, shape, chirality, density, viscosity, polarity, solubility, flexibility and surface chemistry of the resulting dendritic macromolecules can be controlled in an unique manner. [A9]

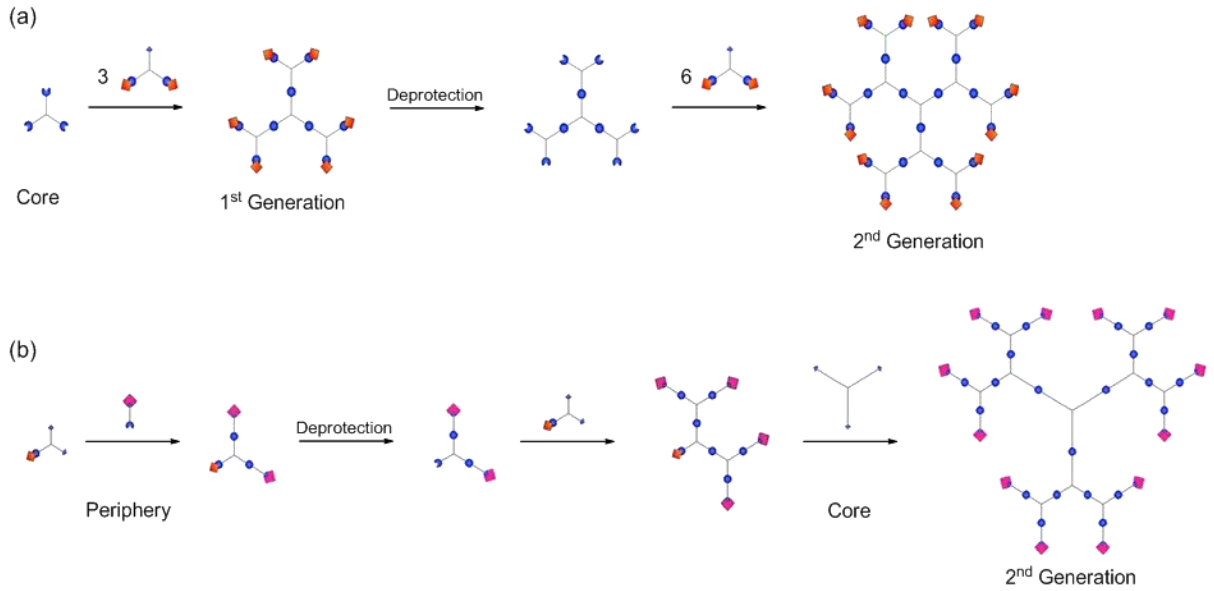

Scheme A3. Schematic representation of (a) divergent and (b) convergent synthesis of dendrimers. [A6]

Since Vögtle´s initial report about (poly)propyleneimine (PPI) dendrimers [A3], numerous dendritic systems have been prepared. [A10] Accordingly, Tomalia´s (poly)amidoamine (PAMAM) [A11], Fréchet´s (poly)aromatic ether [A12], Moore´s (poly)acetylene [A13] and Chapman´s (poly)silane dendrimers [A14] as well as Seebach´s (poly)ester [A15], Müllen´s (poly)phenylene [A16], Diederich´s (poly)etheramide [A17], Caminade´s (poly)phosphane [A18], Ford´s (poly)esteramide [A19] and Newkome´s "arborol" systems [A20] have received widespread attention, clearly reflecting the structural and chemical diversity of dendritic macromolecules. In addition, whereas the dendrimer´s exterior provide an excellent platform for terminal attachment of multiple close-packed functionalities, the present interior focal core, branching units as well as cavities around the focal core permit various opportunities for modification, *e.g.* to encapsulate both metal(ion)s as well as small organic molecule fragments (Scheme A4). [A21]

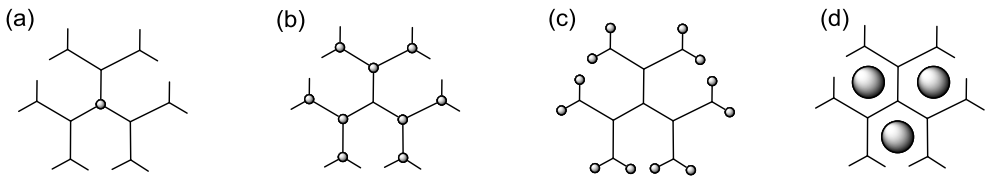

Scheme A4. Different types of dendrimer functionalization: (a) central, (b) branched, (c) terminal and (d) in intrinsic cavities.

During the last decade, the focus of the scientific interest in dendrimers shifted from initial synthetic directions towards various applications of these materials. [A8] Thus, different sized

dendrimers with tailored surface functionalities are becoming of interest from materials science perspective as these precise macromolecules facilitate unique novel chemical and physical properties, leading to promising potential applications including but not limited to catalysis [A22], optics [A23], sensors [A24], electronics [A25], cosmetics [A26], magnetic resonance imaging [A27], drug delivery systems [A28] and environmental remediation [A29].

2. Nanomaterials

In the 21st century, new demands arise in terms of efficiency, selectivity and environmental compatibility for both established as well as prospective chemical processes. Whereas in the past century chemical industry mainly focused on a high productivity, nowadays it faces rising energy and disposal costs. Moreover, there is an increasing social interest for environmentally compatible and sustainable chemistry. [A30, A31] One opportunity to overcome these current challenges is to further improve chemical processes with respect to energy and resource usage and hence reaching the goal of a "Green Chemistry". [A32] Among others, this can be achieved by magnitude minimization and simultaneous reactivity activation of the applied reactants.

In the last decades, a new direction of modern research has emerged, generally defined as "nanotechnology", wherein the term "nano" originates from Greek (*nanos*, meaning dwarf). It embraces research areas of chemistry, physics, biology, material science and mechanical engineering and involves the ability to fabricate, manipulate and characterize artificial structures of atoms or molecules at the nanometer level. These nanomaterials are sized between 1 to 100 nm in at least one dimension and exhibit new properties of matter at a level intermediate between macroscopic bulk solid and atomic/molecular systems. [A33] The unique physicochemical properties are strongly affected by the composition, size and shape of the appropriate nanometer-sized material. A significant feature of those nanoparticulate structures is the large surface-to-volume ratio. With decreasing particle diameter the unsaturated bonding and coordination sites of the surface atoms result in an enhanced chemical reactivity. [A33, A34]

In fact, the deliberate manufacturing and utilization of nanoparticles date back far in history. For example, the dying of glass by freshly precipitated colloidal gold solutions was already known in Roman times (*e.g.* the "Lycurgus Cup"). Dichroic hues have found wide application in glass and porcelain manufactories for several centuries. [A35] In the Middle Ages, Paracelsus postulated the health benefitting effect of "Aurum Potabile", a potable colloidal gold elixir.

Although nanoparticulate materials have been used throughout history, it was only in the 19th century when Faraday carried out initial systematic investigations on metal colloids. [A36] First scientific studies and descriptions on nanomaterials were established at the beginning of the 20th century by Zsigmondy, Ostwald, Mie and Feynman, resulting in many applied concepts in nanotechnology development. [A37 – A39]

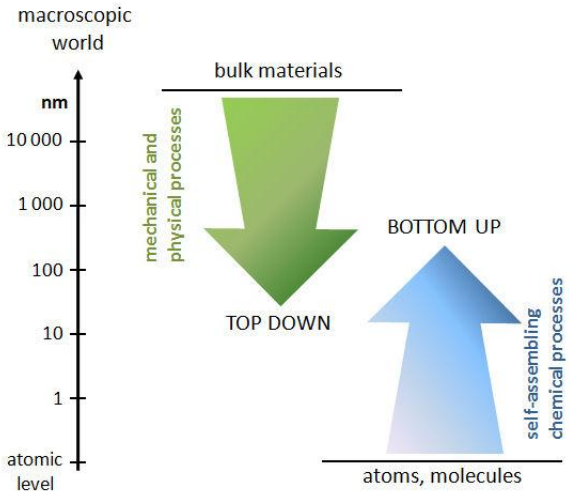

Scheme A5. Principle approaches for nanomaterials preparation. [A47]

The field of nanomaterial preparation has experienced an enormous progress to give a variety of anthropogenic nanoparticulate structures like fullerenes [A40], carbon nanotubes (CNTs) [A41], polymers [A42], dendrimers [A43], metals (homo- and bimetallic) [A44], (non-)metal oxides [A45] as well as metal sulfides and selenides [A46]. In principle, there are two different approaches for the synthesis of the entire nanomaterials: the Top-Down and the Bottom-Up method (Scheme A5). [A47] Whereas the Top-Down approach utilizes mechanical and physical processes (*e.g.* grinding, laser ablation) to crush bulk material into nanometer-sized particles, the Bottom-Up method forms specific nanomaterials by linking atoms/molecules *via* applied self-assembling chemical techniques (*e.g.* liquid/gas phase method, sol-gel process, hydrothermal synthesis, thermolysis, photochemical process). [A34, A35, A48]

Since small particles are thermodynamically unstable with respect to agglomeration to the bulk, a crucial aspect in colloid chemistry is the surface passivation of nanomaterials. Owing to the drastic increase in the chemical reactivity and attempts to minimize the surface, the nanoparticle exterior has to be saturated instantly after nucleation. The stabilization occurs by electrostatic repulsion and/or steric hindrance, [A37, A49] wherein prevention of the colloids to aggregate can be achieved by either surrounding with an electrical double layer formed by adsorbed ions (*e.g.* citrate, chloride) [A50] or by the adsorption of weakly bounded organic sur-

factant molecules (*e.g.* long-chain alkyl compounds, tensides, polymers, dendrimers), [A51] thus providing a protective layer (Scheme A6). [A33]

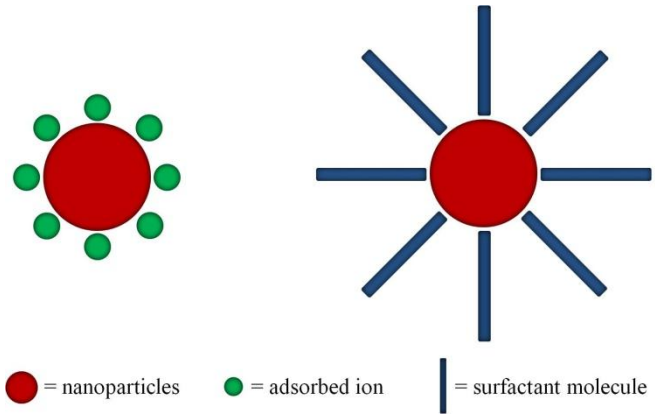

Scheme A6. Schematic illustration of electrostatic (left) and steric (right) stabilization of nanoparticles. [A33]

Moreover, the association of colloids and appropriate (stabilizing) molecular units introduces novel collective properties to the assembled composites that differ from the corresponding bulk materials. [A33] In correlation with the particle size, colloidal group-11 elements for example exhibit a particular optical absorption phenomenon in the visible range of the spectrum. [A35] This surface plasmon resonance is the result of collective oscillation modes of the confined electron-gas within the particles, initiated by the interaction of the electric field of the visible light (Scheme A7). [A52, A53] In consequence, the binding of substrates to the colloid´s surface facilitates an amplification of the appropriate molecular vibration signals up to 10^5-fold due to an enhancement in sensitivity (*e.g.* surface-enhanced Raman scattering (SERS)). [A54]

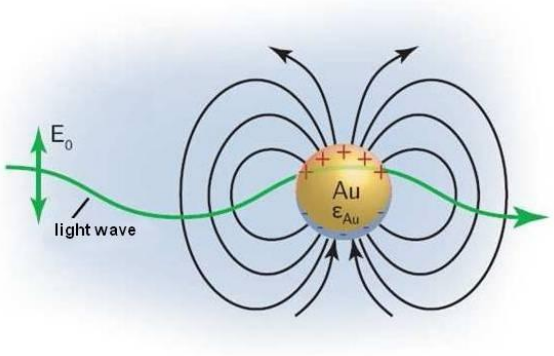

Scheme A7. Schematic surface plasmon resonance illustration. [A52, A53]

Nano-scaled assemblies are promising building blocks and hence provide a great variety of industrial applications due to their exceptional optical, electronic and catalytic properties, associated with manifold preparation methods available. Particularly, in modifying and upgrad-

ing a wide range of materials, the usage of nanostructures ranges from hardening and self-cleaning to antimicrobial surfaces, application in heterogeneous catalysis, ranging from classical synthesis chemistry to photocatalysis, includes the areas of luminescent, plasmonic and magnetic nanoparticles used in molecular biology as well as in medical diagnosis and therapy. In this respect, nanoparticulate pigments and luminophores, transparent conductive oxides and magnetic fluids also have to be mentioned. In terms of progressive miniaturization and material economization, nanodevices are of essential importance for flexible (printed) electronic circuit elements, light-emitting diods and visual display units as well as dye-sensitized solar cells and magnetic data-storage media. [A35]

3. References

[A1] R. Mülhaupt, *Angew. Chem. Int. Ed.* **2004**, *43*, 1054.

[A2] H. Frey, K. Lorenz, C. Lach, *Chem. Unserer Zeit* **1996**, *30*, 75.

[A3] (a) E. Buhleier, W. Wehner, F. Vögtle, *Synthesis* **1978**, 155;
(b) N. Feuerbacher, F. Vögtle, *Top. Curr. Chem.* **1998**, *197*, 2.

[A4] G.M. Dykes, *J. Chem. Technol. Biotechnol.* **2001**, *76*, 903.

[A5] F. Vögtle, G. Reichardt, N. Werner, *Dendritische Moleküle* **2007**, Teubner Verlag, Wiesbaden.

[A6] G.R. Newkome, E. He, C.N. Moorefield, *Chem. Rev.* **1999**, *99*, 1689.

[A7] B. Romagnoli, W. Hayes, *J. Mater. Chem.* **2002**, *12*, 767.

[A8] F.J. Stoddart, T. Welton, *Polyhedron* **1999**, *18*, 3575.

[A9] X. Camps, H. Schönberger, A. Hirsch, *Chem. Eur. J.* **1997**, *3*, 561.

[A10] (a) D. Astruc, *New. J. Chem.* **2011**, *35*, 764;
(b) D. Astruc, E. Boisselier, C. Ornelas, *Chem. Rev.* **2010**, *110*, 1857;
(c) D. Astruc, C. Ornelas, J. Ruiz, *Chem. Eur. J.* **2009**, *15*, 8936.

[A11] (a) D.A. Tomalia, H. Baker, J.R. Dewold, M. Hall, G. Kallos, S. Martin, J. Roeck, J. Ryder, P. Smith, *Polym. J.* **1985**, *17*, 117;
(b) D.A. Tomalia, H. Baker, J.R. Dewold, M. Hall, G. Kallos, S. Martin, J. Roeck, J. Ryder, P. Smith, *Macromolecules* **1986**, *19*, 2466.

[A12] C.J. Hawker, J.M.J. Fréchet, *J. Am. Chem. Soc.* **1990**, *112*, 7638.

[A13] (a) J.S. Moore, Z. Xu, *Macromolecules* **1991**, *24*, 5893;
(b) Z. Xu, J.S. Moore, *Angew. Chem. Int. Ed.* **1993**, *32*, 246;

(c) T. Kawaguchi, K.L. Wilkins, J.S. Moore, *J. Am. Chem. Soc.* **1995**, *117*, 2159.

[A14] T.M. Chapman, G.L. Hillyer, E.J. Mahan, K.A. Shaffer, *J. Am. Chem. Soc.* **1994**, *116*, 195.

[A15] D. Seebach, G.F. Herrmann, U.D. Lengweiler, B.M. Bachmann, W. Amrein, *Angew. Chem. Int. Ed.* **1996**, *35*, 2795.

[A16] (a) F. Morgenroth, E. Reuther, K. Müllen, *Angew. Chem. Int. Ed.* **1997**, *36*, 647;
(b) F. Morgenroth, C. Kübel, K. Müllen, *J. Mater. Chem.* **1997**, *7*, 1207.

[A17] B. Kenda, F. Diederich, *Angew. Chem. Int. Ed.* **1998**, *37*, 3152.

[A18] J.-P. Majoral, A.-M. Caminade, *Chem. Rev.* **1999**, *99*, 845.

[A19] Y. Pan, W.T. Ford, *J. Polym. Sci., Part A: Polym. Chem.* **2000**, *38*, 1533.

[A20] G.R. Newkome, Z.-Q. Yao, G.R. Baker, K. Gupta, *J. Org. Chem.* **1985**, *50*, 2003.

[A21] V. Biricova, A. Laznickova, *Bioorganic Chem.* **2009**, *37*, 185.

[A22] (a) D. Astruc, C. Ornelas, A.K. Diallo, J. Ruiz, *Molecules* **2010**, *15*, 4947;
(b) D. Méry, D. Astruc, *Coord. Chem. Rev.* **2006**, *250*, 1965;
(c) B. Helms, J.M.J. Fréchet, *Adv. Synth. Catal.* **2006**, *348*, 1125.

[A23] (a) S. R. Puniredd, C.M. Yin, Y.S. Hooi, *J. Colloid Interface Sci.* **2009**, *332*, 505;
(b) A. Tsuda, *Bullet. Chem. Soc. Jpn.* **2009**, *82*, 11.

[A24] D. Astruc, C. Ornelas, J. Ruiz, *Acc. Chem. Res.* **2008**, *41*, 841.

[A25] C.K. Song, B. Koo, C.K. Kim, *Jpn. J. Appl. Phys. 4B* **2002**, *41*, 2735.

[A26] G.T. Tolia, H.H. Choi, *Pharm. Tech.* **2008**, *32*, 88.

[A27] S. Langereis, A. Dirksen, T.M. Hackeng, M.H.P. van Genderen, E.W. Meijer, *New J. Chem.* **2007**, *31*, 1152.

[A28] Y. Cheng, L. Zhao, Y. Li, T. Xu, *Chem. Soc. Rev.* **2011**, *40*, 2673.

[A29] C.A. Cason, S.A. Oehrle, T.A. Fabré, C.D. Girten, K.A. Walters, D.A. Tomalia, K.L. Haik, H.A. Bullen, *J. Nanomater.* **2008**, 1.

[A30] J. Grunes, J. Zhu, G.A. Somorjai, *Chem. Commun.* **2003**, 2257.

[A31] E. de Jesús, J.C. Flores, *Ind. Eng. Chem. Res.* **2008**, *47*, 7968.

[A32] J.A. Gladysz, *Pure Appl. Chem.* **2001**, *73*, 1319.

[A33] G. Schmid (ed.), *Nanoparticles* **2004**, Wiley-VCH, Weinheim.

[A34] A. Gutsch, H. Mühlenberg, M. Krämer, *Small* **2005**, *1*, 30.

[A35] H. Goesmann, C. Feldmann, *Angew. Chem. Int. Ed.* **2010**, *49*, 1362.

[A36] M. Faraday, *Philos. Trans. R. Soc. London* **1857**, *147*, 145.

[A37] (a) W. Ostwald, *Z. Kolloidchem.* **1910**, *6*, 183;

(b) R. Zsigmondy, *Z. Kolloidchem.* **1912**, *198*, 217;

(c) H.D. Dörfler, *Grenzflächen und kolloid-disperse Systeme* **2002**, Springer, Berlin.

[A38] G. Mie, *Ann. Phys.* **1912**, *342*, 511.

[A39] R. Feynman, *Eng. Sci.* **1960**, *23*, 22.

[A40] A. Hirsch, M. Brettreich, *Fullerenes – Chemistry and Reactions* **2005**, Wiley-VCH, Weinheim.

[A41] (a) M.P. Anantram, S. Datta, Y.Q. Xue, *Phys. Rev. B* **2000**, *61*, 14219;

(b) W.A. de Heer, E. Al, *Science* **1995**, *270*, 1179.

[A42] (a) D. Wilms, S.-E. Stiriba, H. Frey, *Acc. Chem. Res.* **2010**, *43*, 129;

(b) P.H. Hess, P.H. Parker, *J. Appl. Polymer Sci.* **1966**, *10*, 1915;

(c) H. Hirai, *Macromol. Chem. Suppl.* **1985**, *14*, 55.

[A43] (a) T. Borkowski, P. Subik, A.M. Trzeciak, S. Wolowiec, *Molecules* **2011**, *16*, 427;

(b) A.K. Diallo, C. Ornelas, L. Salmon, J.R. Aranzaes, D. Astruc, *Angew. Chem. Int. Ed.* **2007**, *46*, 8644;

(c) M. Zhao, L. Sun, R.M. Crooks, *J. Am. Chem. Soc.* **1998**, *120*, 4877;

(d) L. Balogh, D.A. Tomalia, *J. Am. Chem. Soc.* **1998**, *120*, 7355;

(e) R.W.J. Scott, O.M. Wilson, R.M. Crooks, *J. Phys. Chem. B* **2005**, *109*, 692.

[A44] (a) J. Turkevitch, P.C. Stevenson, J. Hillier, *Disc. Faraday Soc.* **1951**, *11*, 55;

(b) N. Toshima, T. Yonezawa, *New J. Chem.* **1998**, 1179;

(c) K. Esumi, T. Itakura, K. Torigoe, *Colloids Surfaces A* **1994**, *82*, 111;

(d) P.R. van Rheenen, M.J. McKelvey, W.S. Glaunsinger, *J. Solid State Chem.* **1987**, *67*, 151;

(e) H. Ishizuka, T. Tano, K. Torigoe, K. Esumi, K. Meguro, *Colloids Surf.* **1992**, *63*, 337;

(f) A.C. Curtis, D.G. Duff, P.P. Edwards, D.A. Jefferson, B.F.G. Johnson, A.I. Kirkland, A.S. Wallace, *J. Phys. Chem.* **1988**, *92*, 2270;

(g) Q. Zhang, J. Ge, T. Pham, J. Goebl, Y. Hu, Z. Lu, Y. Yin, *Angew. Chem. Int. Ed.* **2009**, *48*, 3516.

[A45] (a) S. Laurent, D. Forge, M. Port, A. Roch, C. Robic, L. Vander Elst, R.N. Muller, *Chem. Rev.* **2008**, *108*, 2064;

(b) S. Chandra, K.C. Barick, D. Bahadur, *Adv. Drug Deliv. Rev.* **2011**, doi:10.1016/j.addr.2011.06.003.;

(c) N.K. Prasad, K. Rathinasamy, D. Panda, D. Bahadur, *J. Mater. Chem.* **2007**, *17*, 5042;

(d) L.D. Bonifacio, B.V. Lotsch, D.P. Puzzo, F. Scotognella, G.A. Ozin, *Adv. Mater.* **2009**, *21*, 1641;

(e) S. Colodrero, A. Mihi, L. Häggman, M. Ocana, G. Boschloo, A. Hagfeldt, H. Miguez, *Adv. Mater.* **2009**, *21*, 764.

[A46] (a) A. Henglein, *Ber. Bunsenges. Phys. Chem.* **1982**, *86*, 301;

(b) C.B. Murray, D.J. Norris, M.G. Bawendi, *J. Am. Chem. Soc.* **1993**, *115*, 8706;

(c) J.J. Ramsden, M. Grätzel, *J. Chem. Soc., Farad. Trans. 1* **1984**, *80*, 919;

(d) L.E. Brus, *J. Phys. Chem.* **1986**, *90*, 2555;

(e) L. Spanhel, M. Haase, H. Weller, A. Henglein, *J. Am. Chem. Soc.* **1987**, *109*, 5649;

(f) N. Herron, J.C. Calabrese, W.E. Farneth, Y. Wang, *Science* **1993**, *259*, 1426.

[A47] R. Shenhar, V.M. Rotello, *Acc. Chem. Res.* **2003**, *36*, 549.

[A48] (a) A.P. Newbery, B.Q. Han, E.J. Lavernia, C. Suryanarayana, J.A. Christodoulou, *Mater. Process. Handb.* **2007**, *13*, 1;

(b) Q. Zhang, J. Kano, F. Saito, *Handb. Powder Technol.* **2007**, *12*, 509;

(c) D. Vollath, *Nanomaterials* **2008**, Wiley-VCH, Weinheim;

(d) C.N.R. Rao, A. Müller, A.K. Cheetham, *The Chemistry of Nanomaterials* **2004**, Wiley-VCH, Weinheim;

(e) C. Burda, X. Chen, R. Narayanan, M.A. El-Sayed, *Chem. Rev.* **2005**, *105*, 1025;

(f) B.L. Cushing, V.L. Kolesnichenko, C.J. O´Connor, *Chem. Rev.* **2004**, *104*, 3893.

[A49] (a) J.T.G. Overbeek, J.W. Goodwin (ed.), *Colloidal Dispersions* **1981**, Royal Society of Chemistry, London;

(b) D. Myers, *Surfaces, Interfaces and Colloids* **1999**, Wiley-VCH, Weinheim.

[A50] J. Turkevitch, *Gold Bulletin* **1985**, *18*, 86.

[A51] (a) T.F. Tadros, *Applied Surfactants* **2005**, Wiley-VCH, Weinheim;

(b) C.S.S.R. Kumar (ed.), *Biofunctionalization of Nanomaterials* **2005**, Wiley-VCH, Weinheim;

(c) E. Boisselier, A.K. Diallo, L. Salmon, J. Ruiza, D. Astruc, *Chem. Commun.* **2008**, 4819.

[A52] (a) P.K. Khanna, R. Gokhale, V.V.V.S. Subbarao, A.K. Vishwanath, B.K. Das, C.V.V. Satyanarayana, *Mat. Chem. Phys.* **2005**, *92*, 229;

(b) A. Moores, F. Goettmann, *New J. Chem.* **2006**, *30*, 1121.

[A53] G. Schmid, B. Corain, *Eur. J. Inorg. Chem.* **2003**, *41*, 3081.

[A54] C.M. Niemeyer, *Angew. Chem. Int. Ed.* **2001**, *40*, 4128.

B State of Knowledge

As the present work covers multiple aspects within the field of applied dendrimer, metalorganic, organometallic and materials chemistry, the current Chapter B is subdivided into three sections giving an overview on significant fundamentals of related topics. In the first part, substantial synthesis methodologies and specific peculiarities of dendrimers are presented, followed by a selection of remarkable various functionalized dendritic architectures. Chapter B is complemented by a compilation focused on different characterization techniques which are essential for a complete material specification. However, as the entire paragraph provides a more general overview, the author would like to refer to the introduction sections of the respective Chapters C to G.

1. Dendrimers

1.1. Synthesis and Characterization

In 1941, Flory published a series of extensive monographs describing the theoretical evidence for the formation of highly branched three-dimensional macromolecular (nano)architectures. [B1] However, it was not until the late 1970s when Vögtle first reported about a seminal "cascade-like" synthetic methodology for the construction of a new class of architecturally fascinating macromolecules possessing regular highly branched and well-defined structures. Employing an exhaustive Michael addition reaction of diverse primary amines to acrylonitrile and a subsequent co-mediated reduction afforded the appropriate first "generation cascade-molecule" (Scheme B1). [B2] Further generational assembly of (poly)propyleneimine was accomplished *via* thus simple repetitive transformation sequences, the archetype of the divergent synthesis methodology.

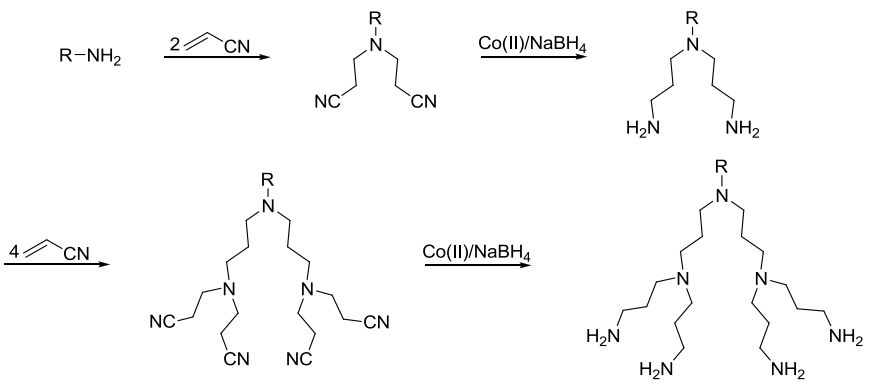

Scheme B1. "Cascade-like" synthesis of (poly)propyleneimine. [B2]

In the mid of the 1980s, Newkome and Tomalia independently complemented the basic concept of the divergent construction approach resulting in series of polyfunctional macromolecular architectures (synonymous "arborols" and "dendrimers"). [B3, B4] Whereas Newkome relied on the triester amidation for the assembly of polyols, [B5] Tomalia reported the first preparation of an entire series of "Starburst" (poly)amidoamine (PAMAM) dendrimers (Scheme B2). By applying addition and amidation cycles of primary amines to methacrylates, the formation of up to the 10th dendrimer´s generation was realized, exhibiting a multiplicity of intrinsic and terminal amine functionalities. [B6]

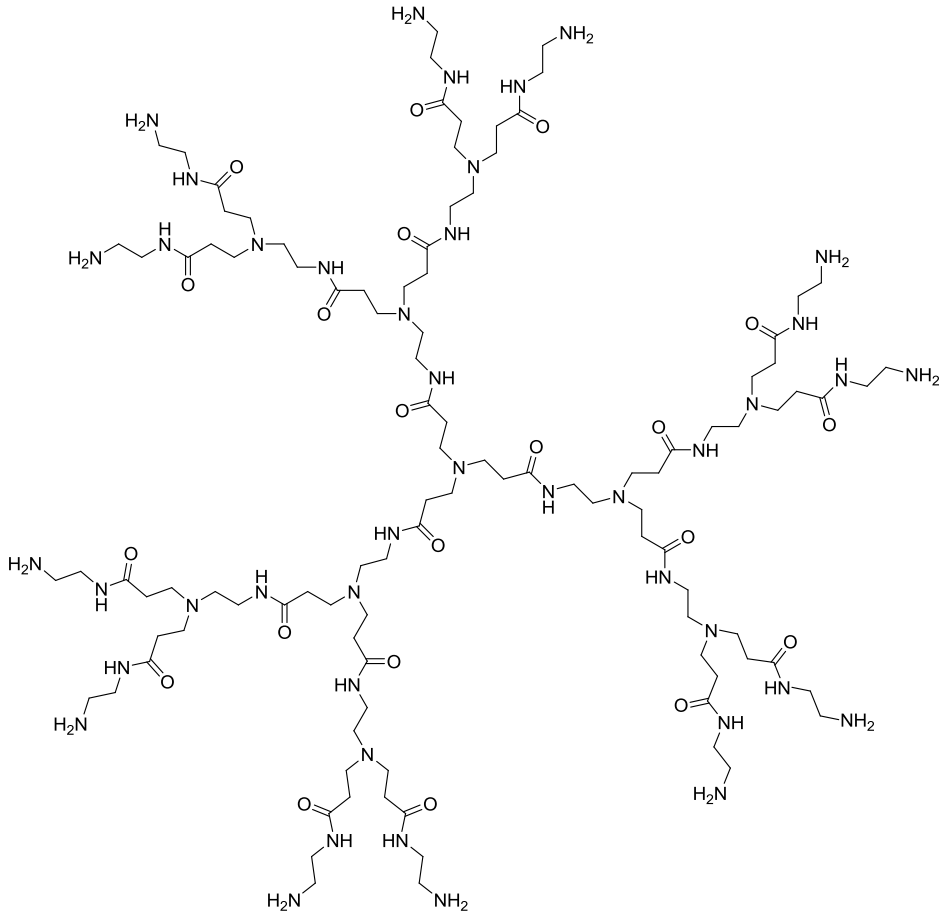

Scheme B2. Architecture of a 2nd generation (poly)amidoamine dendrimer. [B6]

Although the divergent approach is conceptually straightforward in terms of extended dendrimer constructions and multifunctional periphery modifications, synthetic problems occasionally encounter due to incomplete transformations, inadequate removal of contaminations as well as statistical defects within the dendritic structure. [B7]

More recently, the preparation of (poly)aryl ether dendrimers were reported by Fréchet and Hawker (Scheme B3). [B8] The eloquent utilization of selective alkylation of phenolic hydroxyl groups and the conversion of a benzylic alcohol to a benzylic bromide to generate a reac-

tive focal moiety established an alternate synthetic strategy, which was meant to overcome some of the problems associated with the divergent concept. [B9] In general, the convergent approach involves the synthesis of small "dendrons" (the later periphery), reacted to a multifunctional core in the last reaction step to give the assembled dendrimer. Notable attributes of the convergent protocol include a small number of required transformations, a variety of suitable reaction types, improved purifications and statistically minimized defects in the dendritic structure. [B10] However, due to steric hindrance in the final reaction step, the approach is restricted suitable for extended dendritic architectures formation.

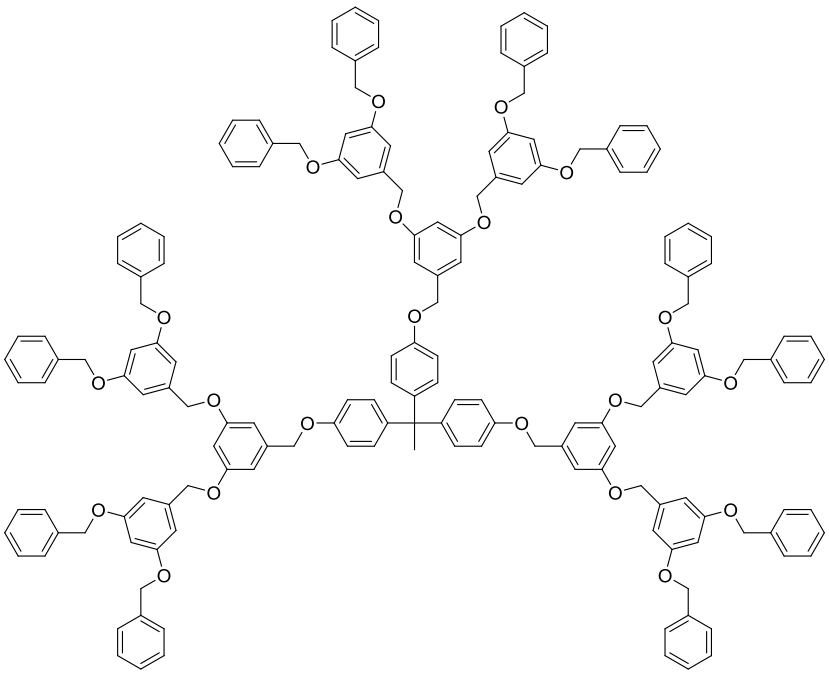

Scheme B3. Architecture of a Fréchet-type dendrimer. [B8]

The procedure initially pioneered by Fréchet was followed shortly thereafter by Miller and Neenan, who published the first series of aromatic-based, all-hydrocarbon dendrimers. [B11] A high rigidity was inherent to these systems. Over the next decades, many further types of significant and ecstatically pleasing dendrimer systems were developed and hence a great variety of dendritic scaffolds including amides, amines, silanes, carbosilanes (Scheme B4), siloxanes, carbosiloxanes, esters, ethers, carbohydrates and organometallic systems with defined nanoscopic dimensions were accessible. [B12 – B16]

Concomitant to synthetic progresses in dendrimer chemistry, reliable full characterization techniques for dendritic architectures had to be developed. Due to the size and symmetry of the entire macromolecules, definite purity analyses are rather complex. Various NMR experiments (^{1}H, ^{13}C, ^{29}Si, ^{31}P), elemental analysis, chromatography techniques (HPLC) and mass

spectrometries (MALDI, ESI) as well as microscopic examinations are implemented to identify potential imperfections in the dendrimer´s structure.

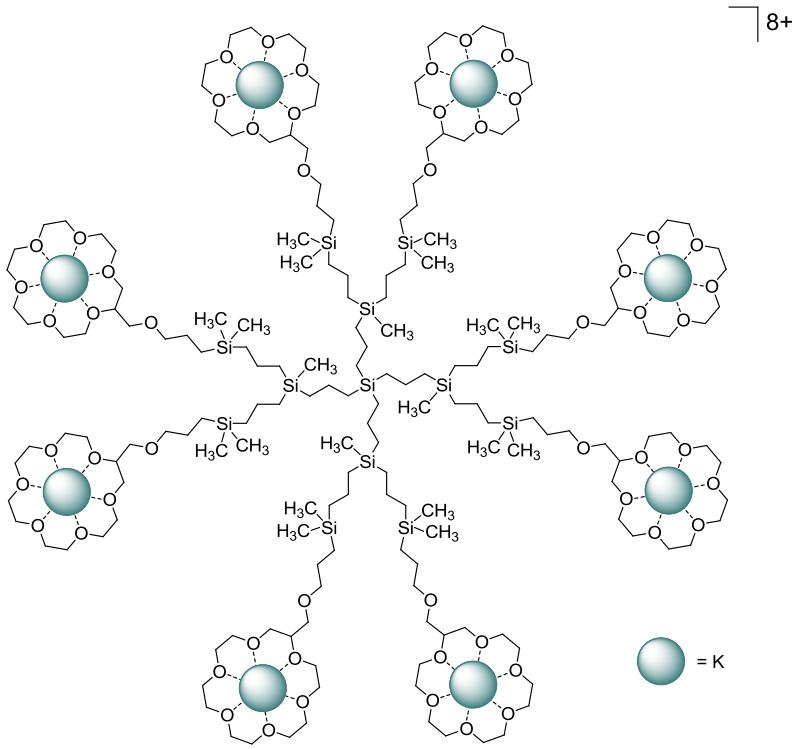

Scheme B4. Example for a crown-ether functionalized carbosilane dendrimer as a chelating ligand for K^+-ions, reported by Lang *et al.* in 2005. [B16]

1.2. Functional Dendrimers

Since Vögtle, Tomalia and Fréchet initially reported on dendrimers, research mainly focused on the preparation and characterization of a wide variety of dendritic macromolecules. [B13] Owing to the rising demand for materials with improved and novel properties, the emphasis in dendrimer research gradually shifted to investigate new classes of materials with highly controllable architectures and specific functionalities.

In principle, all of the functionalized dendrimer systems reported in literature can be categorized into one of the following classes (Chapter A, Scheme A4): (a) dendrimers incorporating a functional core; (b) dendrimers featuring functional branching units; (c) dendrimers possessing a functional periphery; and (d) dendrimers having loaded internal cavities. [B17]

Core-functionalized dendrimers are accessible by applying a convergent self-organization synthesis strategy, representing a versatile approach to form precise and regular materials. As the inner functionalization occurs in the final assembling reaction step, even sensitive core units can be incorporated. Apart from its crucial impact on multiplicity, size and shape, the

applied core unit also determines the dendrimer´s functionality. In this respect, chromophores [B18], electrochemical/redox- [B19] and catalytic [B20, B21] active as well as chiral moieties [B17] were placed in the center of dendrimer architectures.

Inside the dendritic structure, a unique and distinct (nano)environment is formed, suitable for the construction of dendrimer scaffolds by functional groups. Through specific incorporation of various active moieties (*e.g.* metal(ion)s, ammonium salts, amines, carbonyls, pyridines, fullerenes, fluorescence labels, crown ethers, liquid crystalline and chiral groups) [B22 – B25] an internal manipulation of dendrimers can be achieved. The resulting multifarious capabilities of appropriate intrinsic functionalized dendrimers were employed for example by Balzani and Vögtle in dendritic light-harvesting effects [B26], by Hirsch in photo-induced electron transfer processes [B27], by Moore in observation of dendritic antenna effects [B28], by Takahashi in a reversible morphological control of dendrimer structure by external chemical stimuli [B29], by Majoral in "burying" chiroptical properties [B30] and in biological systems as dendrimer protein mimetics [B31].

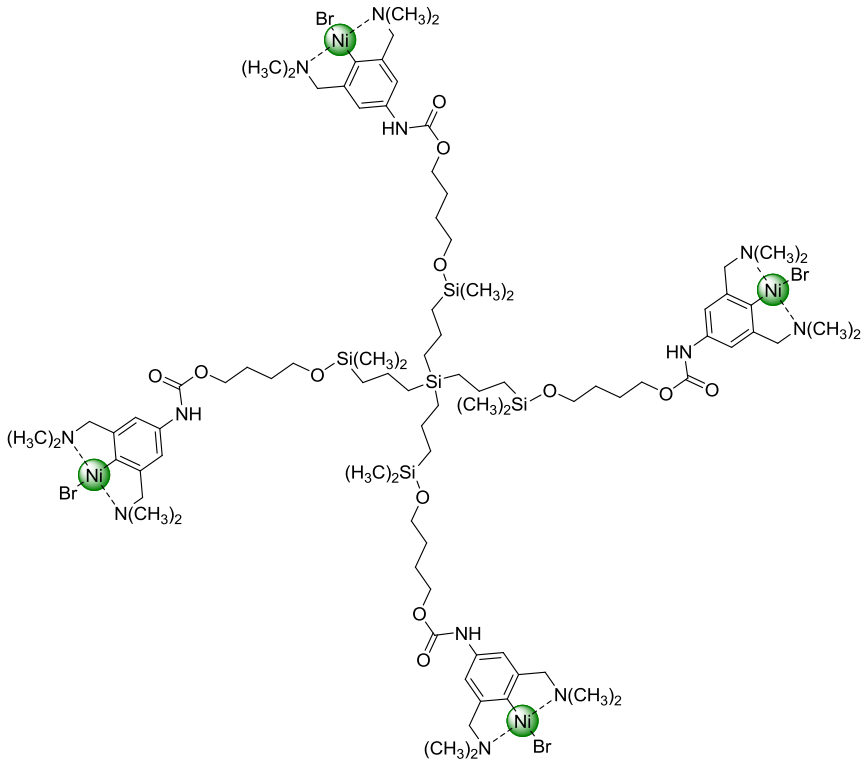

Scheme B5. Structure of van Koten´s carbosilane "NCN" pincer nickel dendrimer. [B41]

A range of studies certainly confirmed that the chemical and physical properties of dendritic (macro)molecules are highly affected by the peripheral moieties. Accordingly, terminal functionalities influence the stability, solubility, viscosity, flexibility, aggregation and chemical reactivity as well as spatial and surface shape of the dendrimer. [B22] As the number of termin-

al groups rises exponentially with the extension of generations, the periphery´s impact on the total molecule properties increases. Furthermore, multiplication of identical functional moieties in terms of peripheral dendritic immobilization might reveal a tremendous amplification of the termini´s effect ("dendritic effect"). Therefore, a molecule periphery functionalization is the most promising and straightforward option in terms of creating novel dendrimer properties.

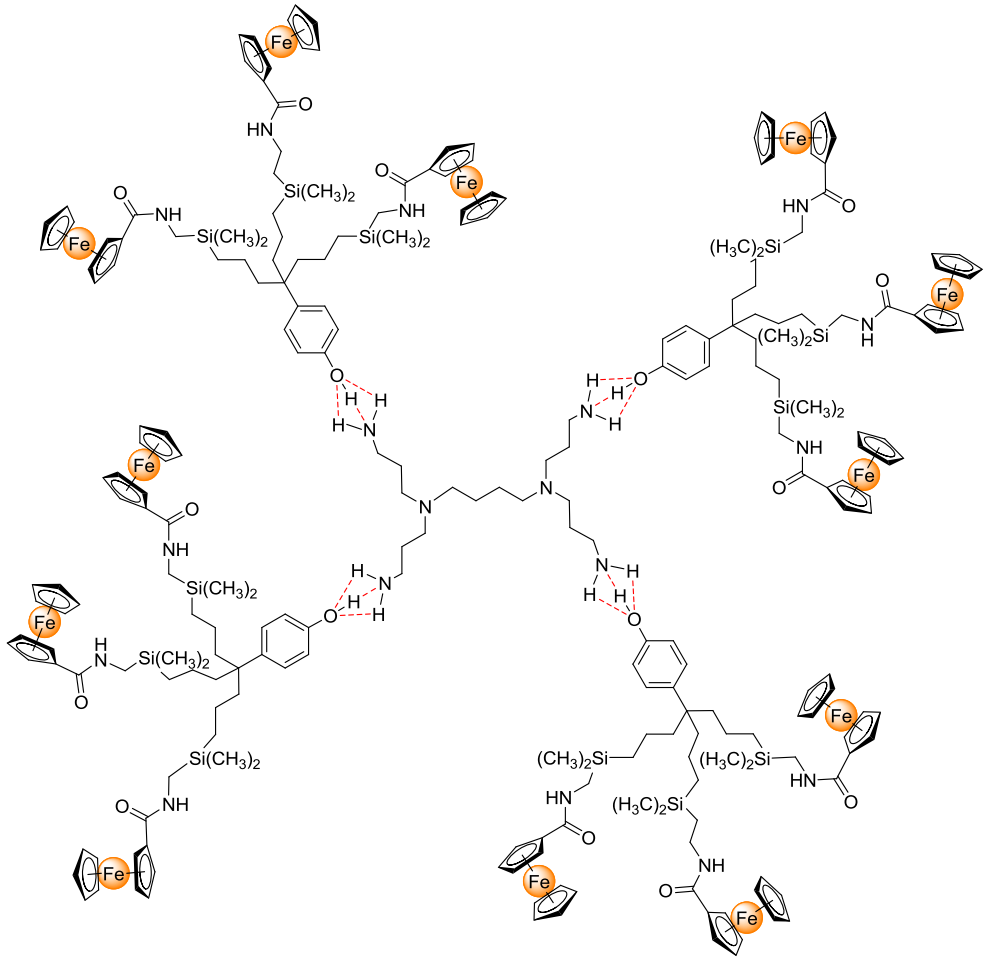

Scheme B6. Structure of Astruc´s non-covalent bonded dendrimer. [B44]

The commercially available (poly)propyleneimine and (poly)amidoamine of Vögtle and Tomalia, respectively, are frequently utilized primary amine (-NH_2) terminated dendrimers. Furthermore, divergent constructed dendritic scaffolds possessing CO_2H, CHO, OH, $P(X)R_2$ (R = H, alkyl, aryl, Cl; X = S, O) and Si-H groups are extensively described in literature. [B22, B32] Due to the outstanding accessibility of the peripheral moieties, further functionalization of, for example, primary amines (-NH_2) *via* applying appropriate coupling reactions with various carboxylic acid derivatives [B33], *N*-hydroxy succinimide esters [B34], sulfonic acid derivatives [B35], iso(thio)cyanates [B36] and urea derivates [B37] are widely approved. Of particular

interest is the subsequent terminal incorporation of metalorganic as well as organometallic fragments, [B38] forming a new class of supramolecular "metallodendrimers" that possess a series of novel physical, optical, electrochemical, photochemical, biological and catalytic properties. [B21, B38, B39]

In 1994, Puddephatt reported about the first dendrimer, decorated by organometallic $Pt^{(IV)}$ functionalities used as integral structural features of each generation. [B40] One of the first organometallic dendrimers applied in a homogeneous catalysis (Kharasch addition) was reported by van Koten and van Leeuwen in the same year. [B41] The periphery of a carbosilane dendrimer was adorned with "NCN" pincer supported $Ni^{(II)}$ groups (Scheme B5).

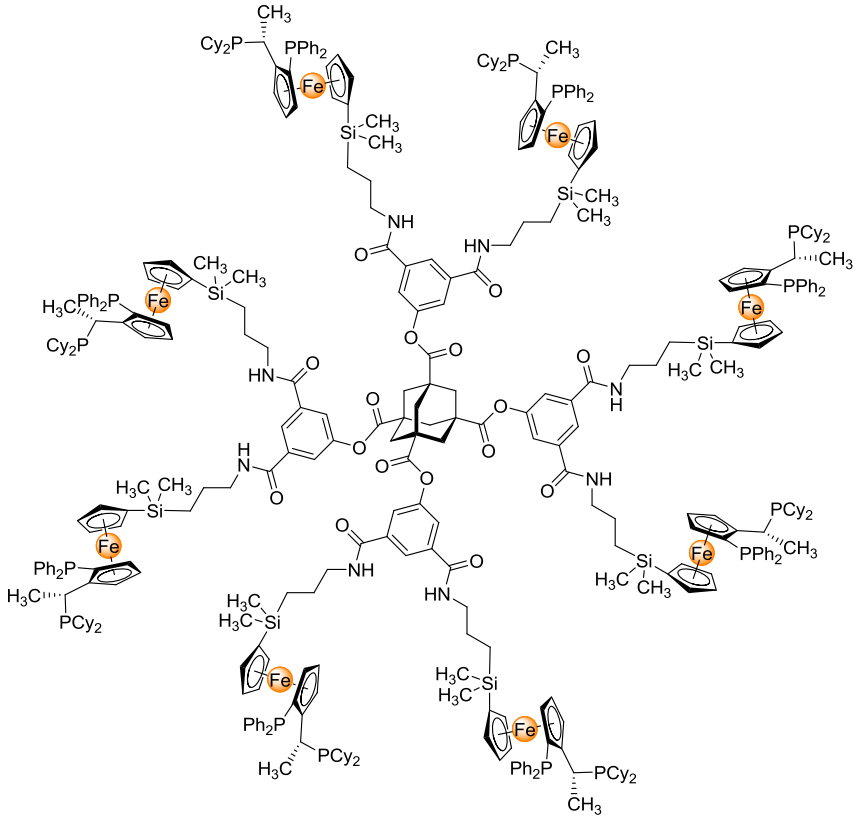

Scheme B7. Togni´s adamantane-1,3,5,7-tetracarboxylic acid cored dendrimer equipped with chiral ferrocenyl diphosphine ligands. [B46]

However, due to the high chemical and thermal stability as well as well-understood electrochemical properties, many reports deal with ferrocenyl moieties at dendrimer peripheries. In 1999, Moss [B42] and Cuadrado [B43] reviewed on the major aspects. A few years later, Astruc employed a non-covalent hydrogen bonding synthetic pathway to construct dendrimers with terminal organometallic ferrocene units (Scheme B6). [B44] At the same time, Majoral studied the chiroptical and electrochemical properties of chiral ferrocene fragments within phosphorus containing dendrimers. [B30, B45] Togni reported about the attachment of chiral "Josiphos"

ferrocenyl diphosphine groups to an adamantane-1,3,5,7-tetracarboxylic acid cored dendritic skeleton, proved as an effective support for Rh-catalyzed asymmetric hydrogenation of alkenes (Scheme B7). [B46] Cuadrado used a terminal ferrocenyl modified carbosilane dendrimer to demonstrate the first example of unambiguous electronic coupling within a dendritic framework. [B47] The pioneering work in the field of electronic communication was forwarded by Kaifer [B48], Salmon and Jutzi [B49] using alkylamine dendrimers as support. Furthermore, Cuadrado utilized various alkylamine dendrimer backbones with ferrocene and cobaltocenium moieties in a mixed manner (Scheme B8). [B50] Another versatile functionalization method of dendrimer´s periphery was reported by Astruc. By applying the principle of "click-chemistry", a ferrocenyl temini was introduced by reacting an azide-terminated dendrimer with ferrocenyl acetylene in a [3+2]-cycloaddition. [B51] The selection of applied organometallic terminated dendrimers listed here clearly indicates the wide variety and great potential in this field of chemistry.

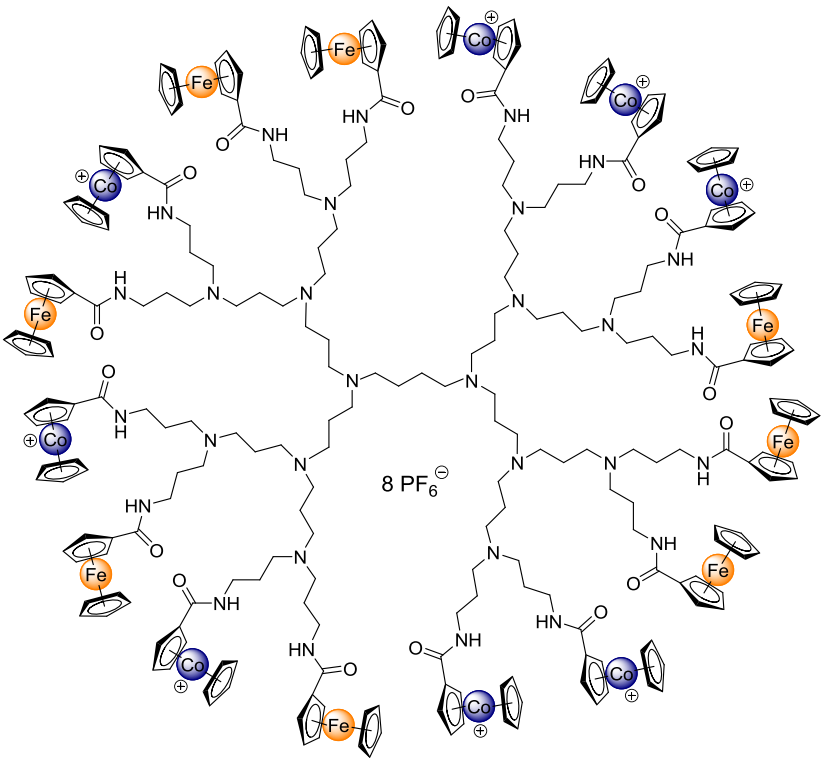

Scheme B8. Structure of Cuadrado´s mixed ferrocene-cobaltocenium dendrimer. [B50]

In the past decade, dendrimer-based therapeutics revolutionized the conventional health care and medical technology. [B52] Facilitating a great variety of biomedical applications, dendrimers can be employed as the drug itself or as the drug-carrier, in which the therapeutic agents are either encapsulated within the dendritic scaffold (host-guest) or conjugated to the dendrimer´s periphery in a (non-)covalent manner. In this respect, the construction of novel dendri-

mers with well-established biocompatible surface modifications such as (poly)ethylene glycols (PEG), amino acids, peptides and (poly)saccharides are propably the most effective strategies in antimicrobial, antiviral and anticancer therapies as well as tissue engineering. [B53, B54]

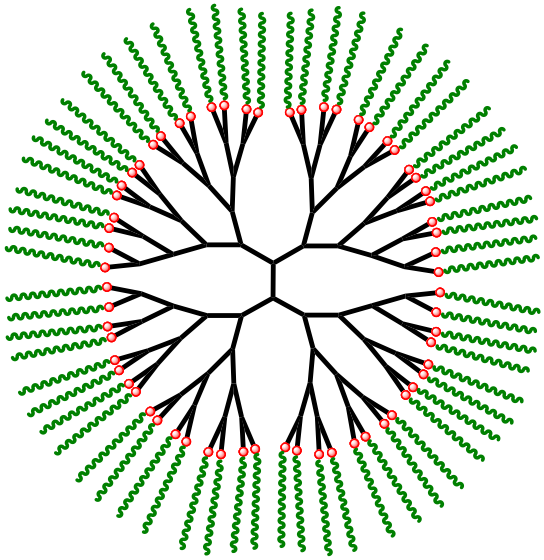

Scheme B9. Schematic illustration of Kono´s PEG-grafted PAMAM dendrimer; green line represents PEG chain. [B55]

In 2000, Kono synthesized a new biocompatible dendrimer using a PAMAM dendrimer as scaffold and PEG as surface terminals (Scheme B9). [B55] *In vivo* studies showed the benefit of that functionalization, a prolonged circulation and retention in the bloodstream as well as lower accumulation in organs. By optimization of the dendrimer size (generation) and length of terminated PEG chains, biodegradation and bioresortion behaviors can be manipulated. However, PEGlation reduces the ability for further covalent attachment of bioactive agents. In a separate study, the PEG chain (50 %) and doxorubicin (50 %) were conjugated to a polyester dendrimer using amino acids as spacers. The obtained bi-functionalized dendrimer was successfully applied in cancer chemotherapy investigations. [B56]

The concept of controlled release of bioactive compounds by covalent fragmentation of cleavable dendrimers is another promising emphasis in biochemistry. Shabat prepared a self-immolative phenol/*para*-aminophenol dendrimer conjugated with cytotoxic drugs for cancer therapy. Activated by adaptors in the stimuli-responsive cleavable delivery system, a remarkable drug release enhancement occurs accompanied with dendrimer degradation to excretable non-toxic compounds (Scheme B10). [B57]

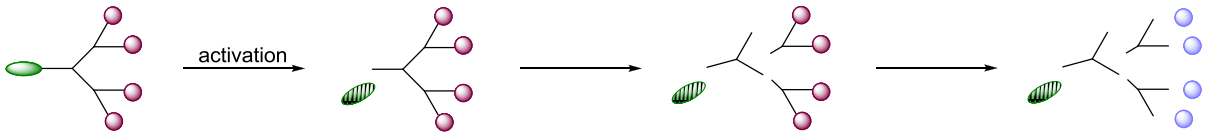

Scheme B10. Cleavage mechanism of self-immolative dendrimers for stimuli-responsive drug delivery. [B57]

While magnetic resonance imaging (MRI) has become a widely used non-invasive technique in disease diagnostics, however, a major limitation of MRI remains its inherent low sensitivity. To increase the MRI sensitivity, non-toxic contrast agents are applied. Currently gadolinium-complexes of precise structures are widely employed, as they are appreciated for a predominant signal enhancement. Unfortunately, a high dosage of the material is required due to non-specificity and fast renal excretion. One method to overcome these difficulties is to attach multiple MRI labels to a single dendritic scaffold. [B54] In a seminal work, Wiener conjugated several gadolinium chelating agents to different generations of Tomalia-type PAMAM dendrimers. The corresponding $Gd^{(III)}$ complexed dendritic structures have been successfully employed as multivalent MRI agents (Scheme B11). [B58 – B60]

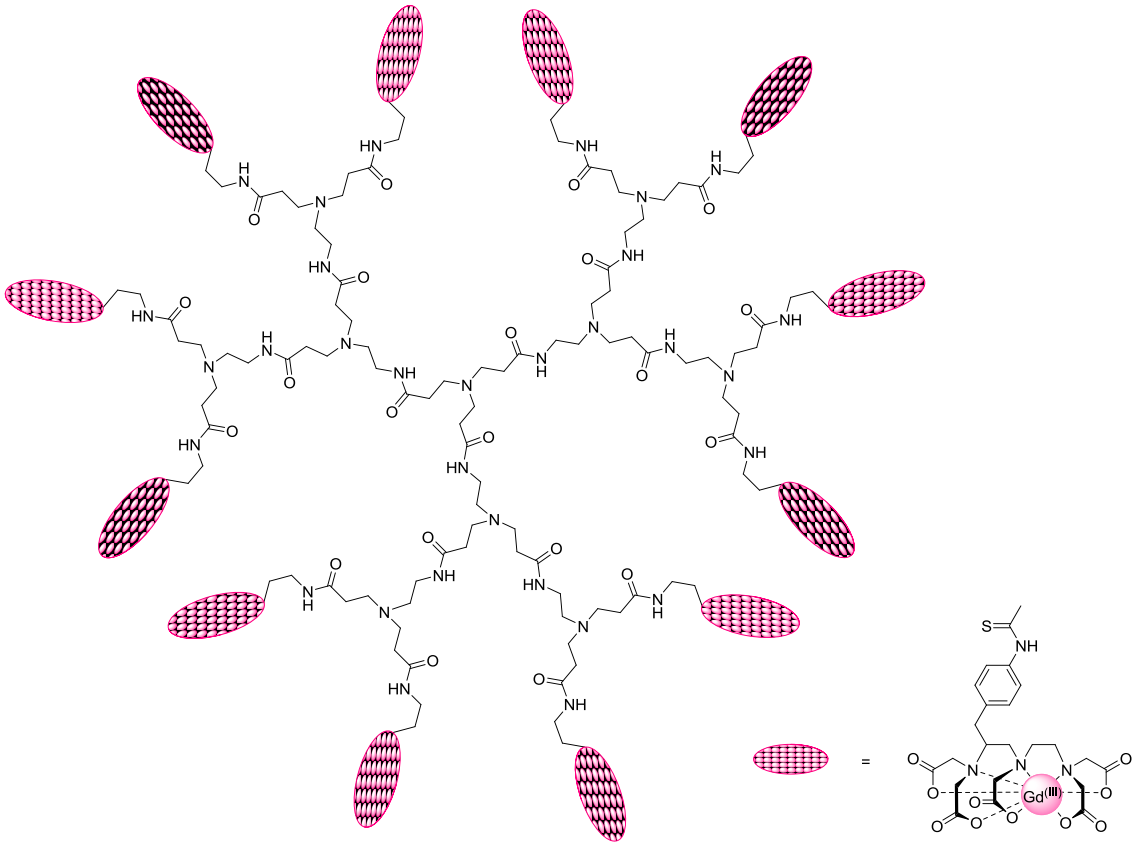

Scheme B11. Dendritic MRI contrast agent with $Gd^{(III)}$ complexes along the periphery. [B58]

Since the development of dendrimer chemistry, the peculiar interior cavities are regarded as suitable candidates for manifold applications in host-guest chemistry. Providing small localized and controlled microenvironments as well as conformational flexibility, dendrimers can serve as hosts for a non-covalent reversible intercalation of guest-molecules (*e.g.* drugs, pigments) forming a "dendritic box" assembly. [B61] In this respect, it was demonstrated that water-soluble dendrimers can "dissolve" small hydrophobic molecules within the interior scaffold similar to micelles. [B62] Newkome applied aliphatic dendrimers with carboxylate termini to bind lipophilic probes. [B61] Fréchet constructed an amphiphilic (poly)aromatic ether dendrimer with carboxylate end-groups to enhance solubility of pyrenes in water. [B63] In a similar manner, Martin utilized the hydrophobic interior of a dendritic micelle to catalyze reactions of guest molecules. [B64]

Beside the dendritic incorporation of small organic molecules, dendrimer cavities can be used to encapsulate metal, metal oxide as well as metal chalcogenide colloids. [B65] Based on the seminal work of Turkevich [B66] and Brust [B67] on colloidal gold stabilization techniques, in 1998, Tomalia, Crooks and Esumi independently implemented methodologies for metal nanoparticles (NPs) formation within hydroxy-terminated PAMAM dendrimer templates. Applying $Na[BH_4]$ as reducing agent to intrinsic coordinated metal ions, a wide range of appropriate dendritic stabilized metal nanoparticles (*e.g.* Cu, Au, Pt, Pd, Fe, Co, Ru and Rh) were formed (Scheme B12), [B68] whereby the employed surfactants serve both the kinetic control of the NPs size and the prevention of unintended aggregation.

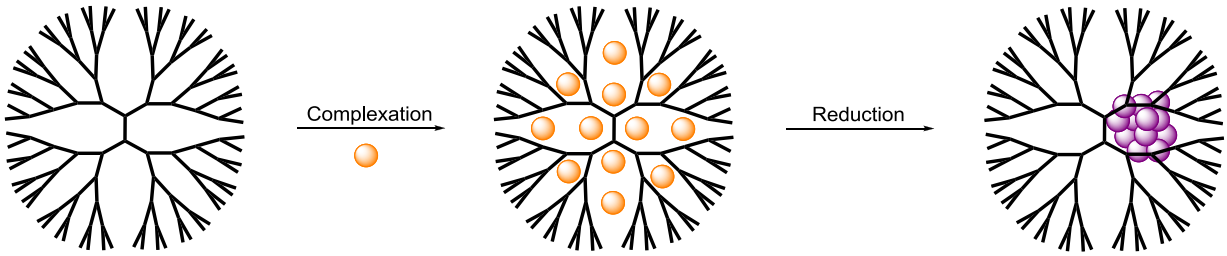

Scheme B12. Schematic representation of the formation of metal nanoparticles. [B68]

Once Reetz initial had showed the application of nanoparticulate Pd in homogeneous catalysis, [B69] El-Sayed employed PAMAM dendrimer-stabilized NPs in Suzuki cross-coupling reactions in 2001, investigating the effect of the dendrimer´s generation on the catalytic activity. [B70] The precise and predictable number of dendrimer-stabilized NPs offered the opportunity to study the influence of the NPs size and quantity on the catalytic efficiency. Regarding the size of the applied dendritic templates, Astruc reported about different types of the NPs stabilization. Dendrimers possessing a small size entirely surround the NPs surface to

give interdendrimer-stabilized colloids, whereas larger dendritic architectures form intradendrimer-encapsulated NPs. [B71] Furthermore, the encapsulation strategy of NPs was extended to bimetallic catalysts. A 4th generation PAMAM dendrimer with mixed Pd-Au and Pd-Pt NPs, respectively, proved to be more efficient in hydrogenation reactions than the analogous monometallic Pt or Pd catalyst. [B72 – B74] Due to dendrimer´s rigid open structure, substrates easily access to the NPs catalytic active sites. Moreover, dendritic templates are able to provide reactant and product selectivity as well as control of catalyst´s chemical composition, solubility and recovery, indicating the high potential of dendrimer nanocatalysts. [B74]

In addition, dendrimer architectures have attracted significant attention in surface coatings of metal oxide (*e.g.* NiO, ZnO, SiO_2, TiO_2, γ-Fe_2O_3, Fe_3O_4, Co_3O_4) as well as ferrite (*e.g.* $M_xFe_{2-x}O_3$, $M_xFe_{3-x}O_4$; M = Al, Zn, Mn, Co) colloids. According to relevant synthesis techniques available, a substantial progress was made over the past decade, covering a wide range of compositions and tunable sizes. [B75 – B78] Numerous chemical methods can be applied for preparation, wherein the wet chemical co-precipitation technique is probably the simplest and most efficient pathway to obtain for example dendrimer coated iron oxide NPs (Scheme B13). [B79] Among various types of metal oxides, magnetite (Fe_3O_4) colloids are of particular interest, due to remarkable size depending magnetic peculiarities of appropriate Fe_3O_4 nanostructures. According to Néel, the thermal fluctuations of magnetic moments cause a transition to superparamagnetism, when the diameter of magnetite particles is below a "critical size" (≈ 20 – 30 nm). [B80]

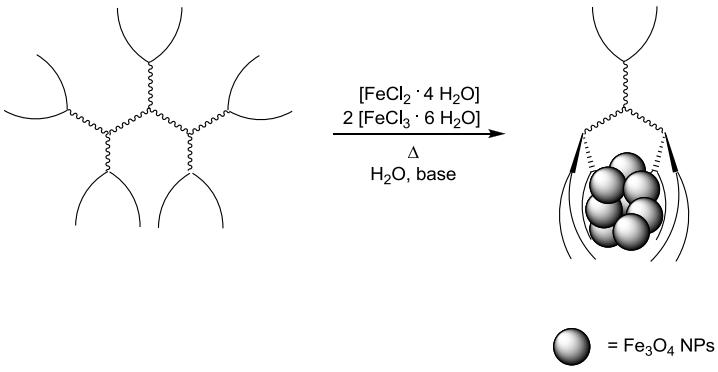

Scheme B13. Schematic illustration of magnetite (Fe_3O_4) NPs formation. [B79]

Owing to a non-toxic biocompatible support of the applied dendritic stabilizer as well as a magnetic Fe_3O_4 colloid size comparable to biological entities, the appropriate superparamagnetic magnetodendrimers emerged special interest in biomedical applications such as magnetic hyperthermia treatment of cancer, controlled drug delivery, cell separation, magnetic resonance imaging and biosensors. [B81] In this respect, Chandra demonstrated a facile approach for

the preparation of dendrimer coated magnetite NPs for drug delivery applications. [B82] Carboxylated PAMAM dendrimers were applied as composites in order to form nanometer-sized water-soluble magnetodendrimers by Bulte. [B83] Recently, Taratula reported about a multifunctional superparamagnetic iron oxide-(poly)propyleneimine dendrimer conjugate for enhanced cancer therapy. [B84]

As the above selection of multifunctional nano-sized dendritic assemblies clearly demonstrates, the area of biological nanocomposites is a highly promising and fast developing field that will lead to a plurality of novel capabilities in years to come. It is time to transform sophisticated scientific findings into future applications.

2. Characterization Techniques for Dendrimer-Nanomaterial Assemblies

The extensive characterization of dendritic templates as well as dendrimer-nanomaterial composites is essential for a precise structure and function correlation. Therefore, a combination of qualitative and quantitative characterization techniques is necessary, since a single method employed cannot result in a defined specification of such complex systems. In general, the material characteristics like identity, (phase) purity, morphology, size, size distribution, shape, crystallinity and structural composition are examined by applying a great variety of spectroscopy, spectrometry, microscopy, scattering as well as separation techniques. In the selection given below, the most relevant methods are summarized. [B85]

Nuclear magnetic resonance (NMR) spectroscopy measures the organic samples´ intrinsic magnetic moment of certain nuclei, typically for hydrogen (^{1}H) and carbon (^{13}C) as well as hetero-atoms like phosphorus (^{31}P) and silicon (^{29}Si). As one- and two-dimensional NMR spectroscopic methods provide physical, chemical, structural and environmental information about the species, NMR spectroscopy is definitely a versatile tool for the identity and purity characterization of dendrons and low-generation dendrimers. [B86]

In particular, for high-generation dendrimers purification and simultaneous characterization, on-line high-performance liquid chromatography (HPLC) techniques represent an exquisite ability. Based on physical and/or chemical interactions between the stationary phase in the column and a crude product mixture, elution is achieved to obtain separate product fractions. Distinct peaks within each HPLC trace provide the distribution and actual sample composition. [B86]

X-ray (powder) diffraction (XRD) is commonly used to determine the identity of functionalized nanoparticulated inorganic materials. By comparing the positions and intensities of experimental and reference peaks, one can establish the crystal structure of NPs, however, compared to bulk materials in the nano-scale more complicated structures can be formed. The crystallite size can be estimated from the line broadening of the XRD profile by Scherrer equation, wherein the crystal size is not equal to the NPs size, if the NPs are not single crystals. [B85] Although XRD is often the method of choice, due to line broadening certain quite similar NPs structures (*e.g.* Fe_3O_4 and γ-Fe_2O_3) cannot be resolved. Therefore, X-ray photoelectron spectroscopy (XPS) can be employed, to estimate the elemental composition and electronic states of the elements contributing to the material composite. [B85]

Transmission electron microscopy (TEM) imaging is a suitable common technique for the assessment of inorganic phases concerning crystallinity, atomic arrangements, lattice vacancies and structural defects. However, as samples are typically imaged in vacuum or low-pressure gas flow, *in-situ* liquid phase studies are excluded. Furthermore, due to extensive equipment, maintenance and sample preparation requirements, TEM is a relatively expensive examination method on an individual particle basis. Beside TEM further advanced microscopic techniques such as scanning electron microscopy (SEM) and atomic force microscopy (AFM) are capable tools in ascertaining the size and morphology of nano-sized structures. [B87]

Dynamic light scattering (DLS), also known as photon correlation spectroscopy (PCS), is probably the most common technique for in-solution-determination of the NPs size, shape and size distribution. The method gives access to the hydrodynamic radius of the whole mono- or polydisperse colloidal sample in a simple, non-invasive, non-destructive and relatively economical process. Due to the Brownian motion of particles, fluctuations in the scattered light intensity occur, that are used to determine the particle diffusion coefficient which is directly related to the hydrodynamic radius *via* the Stokes-Einstein relationship. [B86, B88]

The colloidal stability is analyzed through zeta(ζ)-potential, in an indirect measurement of the surface charges that prevent the NPs aggregation by electrostatic repulsion. It corresponds to a potential difference between the outer Helmholtz plane and the particles surface, providing information on the nature of the nano-encapsulated material. [B87]

Among optical characterization techniques, UV/Vis spectroscopy is often used for *in-situ* observation of coordination processes between metal ions and dendrimers. Furthermore, the intrinsic UV/Vis absorbance features can be used to monitor pertinent nanomaterial properties

such as concentration, size, shape and aggregation state. Metal NPs, in particular Au, Ag and Cu exhibit a strong absorption in the visible region termed as surface plasmon resonance band, which is sensitive to colloids size, shape and composition. [B85]

As Fourier transformed infrared spectroscopy (FT-IR) measures the distinctive absorption of IR radiation by an (in)organic sample, the method is frequently used to demonstrate the conjugation of an applied surfactant to a nano-scaled material through the appearance and shifting of characteristic spectral bands. Moreover, the complexation type and strength of dendritic functional groups to an appropriate metal species can by ascertained. [B86]

Recently, thermal characterization techniques like thermogravimetric analyses (TGA) and differential scanning calorimetry (DSC) are used for the quantitative determination of dendritic components grafted on nanocomposite surfaces. By utilization of a high-precision balance, changes in the sample´s weight relative to changes in temperature are revealed. Applying coupled TGA-MS (MS = mass spectrometry) systems, an accurate specification of stabilization fragments can be achieved. [B85]

Mass spectrometric analyses comprise sample based mass-to-charge ratio technologies. In particular, inductively coupled plasma mass spectrometry (ICP-MS) techniques are suitable for determination of metal and metal oxide quantities in nano-structured composites. However, application of ICP-MS is fairly limited due to costly instrumentations required and sample destruction during the analytic process. [B86]

3. Motivation

Within the macromolecular chemistry, dendrimers represent undeniably one of the most versatile classes of molecules. The fascinating chemical elegance of dendritic architectures matched with the precise control of both the intrinsic scaffold´s structure as well as the straightforward terminal functionalization predestines dendrimers for a great variety of applications serving highest precision. However, sterically demanding high-generation dendrimers require multifarious and time consuming syntheses as well as extensive purification and characterization techniques, making these kinds of macromolecules less attractive for a wider area of applications due to economical reasons.

That status resulted in the motivation for the research work introduced in the present doctoral thesis. The task was to develop a synthesis methodology making accessible series of comparable novel well-defined (poly)amidoamine-based dendrimers of low-generations, facilitat-

ing a straightforward and more time efficient access to readily functionalizable and fully characterizable dendritic architectures. Furthermore, esteemed features like the monodisperse easy accessible open molecular structure and the plurality of capable donating moieties should likewise be integrated. Applying appropriate ligand, metal organic and organometallic modifications to the dendrimers´ periphery, the thus obtained promising oligomers were applied as templates in various fields of applications like (asymmetric) homogeneous catalyses (Chapter C + D), metal and metal oxide nanoparticles formations (Chapter E + F) as well as in biomedical processes as drug-carriers (Chapter G).

4. References

[B1] (a) P.J. Flory, *J. Am. Chem. Soc.* **1941**, *63*, 3096;
(b) P.J. Flory, *J. Am. Chem. Soc.* **1952**, *74*, 2718.

[B2] E. Buhleier, W. Wehner, F. Vögtle, *Synthesis* **1978**, 155.

[B3] G.R. Newkome, Z. Yao, G.R. Baker, V.K Gupta, P.S. Russo, M.J. Saunders, *J. Am. Chem. Soc.* **1986**, *108*, 849.

[B4] D.A. Tomalia, H. Baker, J.R. Dewald, M. Hall, G. Kallos, S. Martin, J. Roeck, J. Ryder, P. Smith, *Polym. J.* **1985**, *17*, 117.

[B5] G.R. Newkome, Z. Yao, G.R. Baker, V.K Gupta, *J. Org. Chem.* **1985**, *50*, 2003.

[B6] D.A. Tomalia, H. Baker, J.R. Dewald, M. Hall, G. Kallos, S. Martin, J. Roeck, J. Ryder, P. Smith, *Macromolecules* **1986**, *19*, 2466.

[B7] G.M. Dykes, *J. Chem. Technol. Biotechnol.* **2001**, *76*, 903.

[B8] C. Hawker, J.M.J. Fréchet, *J. Chem. Soc., Chem. Commun.* **1990**, 1010.

[B9] C. Hawker, J.M.J. Fréchet, *J. Am. Chem. Soc.* **1990**, *112*, 7638.

[B10] G.R. Newkome, E. He, C.N. Moorefield, *Chem. Rev.* **1999**, *99*, 1689.

[B11] T.M. Miller, T.X. Neenan, *Chem. Mater.* **1990**, *2*, 346.

[B12] G.R. Newkome, C.N. Moorefield, F. Vögtle, *Dendrimer and Dendrons* **2001**, Wiley-VCH, Weinheim.

[B13] A.W. Bosman, H.M. Janssen, E.W. Meijer, *Chem. Rev.* **1999**, *99*, 1665.

[B14] (a) D.Y. Son, Z. Rappoport, Y. Apeloig, *The Chemistry of Organic Silicon Compounds* **2001**, Wiley-VCH, New York;
(b) J.M. Majoral, A.M. Caminade, *Chem. Rev.* **1999**, *99*, 845.

[B15] (a) R. Buschbeck, H. Lang, *J. Organomet. Chem.* **2005**, *690*, 1198;

(b) R. Buschbeck, H. Sachse, H. Lang, *J. Organomet. Chem.* **2005**, *690*, 751.

[B16] R. Buschbeck, H. Lang, *J. Organomet. Chem.* **2005**, *690*, 696.

[B17] B. Romagnoli, W. Hayes, *J. Mater. Chem.* **2002**, *12*, 767.

[B18] V. Balzani, P. Ceroni, A. Juris, M. Venturi, S. Campagna, F. Puntoriero, S. Serroni, *Coord. Chem. Rev.* **2001**, *219-221*, 545.

[B19] (a) C.B. Gorman, J.C. Smith, M.W. Hager, B.L. Parkhurst, H. Sierzputowska-Gracz, C.A. Haney, *J. Am. Chem. Soc.* **1999**, *121*, 9958;

(b) C.M. Cardona, T.D. McCarley, A.E. Kaifer, *J. Org. Chem.* **2000**, *65*, 1857;

(c) D.L. Stone, D.K. Smith, P.T. McGrail, *J. Am. Chem. Soc.* **2002**, *124*, 856.

[B20] A.V. Davis, M. Driffild, D.K. Smith, *Org. Lett.* **2001**, *3*, 3075.

[B21] L.J. Twyman, A.S.H. King, I.K. Martin, *Chem. Soc. Rev.* **2002**, *31*, 69.

[B22] F. Vögtle, G. Reichardt, N. Werner, *Dendritische Moleküle* **2007**, Teubner Verlag, Wiesbaden.

[B23] (a) T. Nagasaki, S. Tamagaki, K. Ogini, *Chem. Lett.* **1997**, 717;

(b) J.F. Li, K.A. Krandall, P. Chu, V. Percec, R.G. Petschek, C. Rosenblatt, *Macromolecules* **1996**, *29*, 7813;

(c) P. Murer, D. Seebach, *Helv. Chim. Acta* **1998**, *81*, 603.

[B24] (a) C. Larré, D. Brosselles, C. Turrin, B. Donnadieu, A.M. Caminade, J.P. Majoral, *J. Am. Chem. Soc.* **1998**, *120*, 13070;

(b) L. Brauge, A.M. Caminade, J.P. Majoral, S. Slomkowski, M. Wolszczak, *Macromolecules* **2001**, *34*, 5599.

[B25] H.F. Chow, T.K.K. Mong, M.F. Nongrum, C.W. Wan, *Tetrahedron* **1998**, *54*, 8543.

[B26] (a) S. Campagna, S. Serroni, V. Balzani, G. Denti, A. Juris, M. Venturi, *Acc. Chem. Res.* **1998**, *31*, 29;

(b) S. Campagna, S. Serroni, V. Balzani, A. Juris, M. Venturi, *Chem. Rev.* **1996**, *96*, 756;

(c) J. Issberner, F. Vögtle, L. De Cola, V. Balzani, *Chem. Eur. J.* **1997**, *3*, 706;

(d) V. Balzani, P. Ceroni, M. Maestri, C. Saudan, V. Vicinelli, *Top. Curr. Chem.* **2003**, *228*, 159.

[B27] M. Braun, S. Atalick, D.M. Guldi, H. Lang, M. Brettreich, S. Burghardt, M. Hatzimarinaki, E. Ravanelli, M. Prato, R. van Eldik, A. Hirsch, *Chem. Eur. J.* **2003**, *9*, 3867.

[B28] (a) C. Devadoss, P. Bharathi, J.S. Moore, *Angew. Chem. Int. Ed.* **1997**, *36*, 1709;

(b) C. Devadoss, P. Bharathi, J.S. Moore, *J. Am. Chem. Soc.* **1996**, *118*, 9635.

[B29] K. Onitsuka, A. Iuchi, M. Fugimoto, S. Takahashi, *Chem. Commun.* **2001**, 741.

[B30] C.O. Turrin, J. Chiffre, D. de Montauzon, G. Balavoine, E. Manoury, A.M. Caminade, J.P. Majoral, *Organometallics* **2002**, *21*, 1891.

[B31] (a) T.D. Pallin, J.P. Tam, *Chem. Commun.* **1996**, 1345;
(b) C. Douat-Casassus, T. Dabre, J.L. Reymond, *J. Am. Chem. Soc.* **2004**, *126*, 7817.

[B32] P. Marchand, L. Griffe, A.M. Caminade, J.P. Majoral, M. Destarac, F. Leising, *Org. Lett.* **2004**, *6*, 1309.

[B33] (a) S. Stevelmans, J.C.M. van Hest, J.F.G.A. Jansen, D.A.F.J. van Boxtel, E.M.M. de Brabander-van den Berg, E.W. Meijer, *J. Am. Chem. Soc.* **1996**, *118*, 7398;
(b) C. Valério, J.L. Fillaut, J. Ruiz, J. Guittard, J.C. Blais, D. Astruc, *J. Am. Chem. Soc.* **1997**, *119*, 2588;
(c) A.I. Cooper, J.D. Londono, G. Wignall, J.B. McClain, E.T. Samulski, J.S. Lin, A. Dobrynin, M. Rubinstein, A.L.C. Burke, J.M.J. Fréchet, J.M. DeSimone, *Nature* **1997**, *389*, 368;
(d) R. Roy, D. Zanini, S.J. Meunier, A. Romanowska, *J. Chem. Soc., Chem. Commun.* **1993**, 1869.

[B34] (a) J.F.G.A. Jansen, E.M.M. de Brabander-van den Berg, E.W. Meijer, *Science* **1994**, *266*, 1226;
(b) A.P.H.J. Schenning, C. Elissen-Román, J.W. Wener, M.W.P.L. Baars, S.J. van der Gaast, E.W. Meijer, *J. Am. Chem. Soc.* **1998**, *120*, 8199.

[B35] (a) J.F.G.A. Jansen, H.W.I. Peerlings, E.M.M. de Brabander-van den Berg, E.W. Meijer, *Angew. Chem. Int. Ed.* **1995**, *34*, 1206;
(b) A. Archut, F. Vögtle, L. De Cola, G.C. Azzellini, V. Balzani, P.S. Ramanujam, R.H. Berg, *Chem. Eur. J.* **1998**, *4*, 699.

[B36] (a) T.K. Lindhorst, C. Kieburg, *Angew. Chem. Int. Ed.* **1996**, *35*, 1953;
(b) D. Zanini, R. Roy, *J. Org. Chem.* **1998**, *63*, 3486;
(c) U. Boas, A.J. Karlsson, B.F.W. de Waal, E.W. Meijer, *J. Org. Chem.* **2001**, *66*, 2136.

[B37] (a) G.R. Newkome, C.D. Weis, C.N. Moorefield, G.R. Baker, B.J. Childs, J. Epperson, *Angew. Chem. Int. Ed.* **1998**, *37*, 307;
(b) S. Rosenfeldt, N. Dingenouts, M. Ballauf, N. Werner, F. Vögtle, P. Linder, *Macromolecules* **2002**, *35*, 8098.

[B38] P.A. Chase, R.J.M. Klein Gebbink, G. van Koten, *J. Organomet. Chem.* **2004**, *689*, 4016.

[B39] (a) D. Astruc, F. Chardac, *Chem. Rev.* **2001**, *101*, 2991;

(b) G.E. Oosterom, J.N.H. Reek, P.C.J. Kamer, P.W.N.M. van Leeuwen, *Angew. Chem. Int. Ed.* **2001**, *40*, 1828;

(c) R. Kreiter, A.W. Kleij, R.J.M. Klein Gebbink, G. van Koten, *Top. Curr. Chem.* **2001**, *217*, 593;

(d) S. Hecht, J.M.J. Fréchet, *Angew. Chem. Int. Ed.* **2001**, *40*, 74.

[B40] (a) S. Achar, R.J. Puddephatt, *Angew. Chem. Int. Ed.* **1994**, *33*, 847;

(b) S. Achar, R.J. Puddephatt, *J. Chem. Soc., Chem. Commun.* **1994**, 1895.

[B41] J.W.J. Knapen, A.W. van der Made, J.C. De Wilde, P.W.N.M. van Leeuwen, P. Wijkens, D.M. Grove, G. van Koten, *Nature* **1994**, *372*, 659.

[B42] M.A. Hearshaw, J.R. Moss, *Chem. Commun. 1999*, 1.

[B43] I. Cuadrado, M. Morán, C.M. Casado, B. Alonzo, J. Losada, *Coord. Chem. Rev.* **1999**, 395.

[B44] M.C. Daniel, J. Ruiz, D. Astruc, *J. Am. Chem. Soc.* **2003**, 125, 1150.

[B45] (a) A.M. Caminade, V. Maraval, R. Laurent, C.O. Turrin, P. Sutra, J. Leclaire, L. Griffe, P. Marchand, C. Baudoin-Dehoux, C. Rebout, J.P. Majoral, *C. R. Chim.* **2003**, 6, 791.

[B46] (a) A. Togni, C. Breutel, A. Schnyder, F. Spindler, H. Landert, A. Tijani, *J. Am. Chem. Soc.* **1994**, *116*, 4062;

(b) A. Togni, N. Bieler, U. Burckhardt, C. Köllner, G. Pioda, R. Schneider, A. Schyder, *Pure Appl. Chem.* **1999**, 71, 1531.

[B47] I. Cuadrado, C.M. Casado, B. Alonso, M. Morán, J. Losada, V. Belsky, *J. Am. Chem. Soc.* **1997**, *119*, 7613.

[B48] J. Alvarez, T. Ren, A.E. Kaifer, *Organometallics* **2001**, *20*, 3543.

[B49] A. Salmon, P. Jutzi, *J. Organomet. Chem.* **2001**, *637-639*, 595.

[B50] C.M. Casado, B. González, I. Cuadrado, B. Alonso, M. Morán, J. Losada, *Angew. Chem. Int. Ed.* **2000**, *39*, 2135.

[B51] D. Astruc, C. Ornelas, J. Ruiz, *Acc. Chem. Res.* **2008**, *41*, 841.

[B52] Y. Cheng, L. Zhao, Y. Lic, T. Xu, *Chem. Soc. Rev.* **2011**, *40*, 2673.

[B53] (a) S. Svenson, *Eur. J. Pharm. Biopharm.* **2009**, *71*, 445;

(b) V. Mishra, U. Gupta and N. K. Jain, *J. Biomater. Sci., Polym. Ed.* **2009**, *20*, 141.

[B54] M.A. Mintzer, M.W. Grinstaff, *Chem. Soc. Rev.* **2011**, *40*, 173.

[B55] (a) C. Kojima, K. Kono, K. Maruyama, T. Takagishi, *Bioconjugate Chem.* **2000**, *11*, 910;

(b) Y. Haba, A. Harada, T. Takagishi, K. Kono, *Polymer* **2005**, *46*, 1813.

[B56] S.J. Guillaudeu, M.E. Fox, Y.M. Haidar, E.E. Dy, F.C. Szoka Jr., J.M.J. Fréchet, *Bioconjugate Chem.* **2008**, *19*, 461.

[B57] (a) M. Shamis, H.N. Lode, D. Shabat, *J. Am. Chem. Soc.* **2004**, *126*, 1726;

(b) R.J. Amir, N. Pessah, M. Shamis, D. Shabat, *Angew. Chem. Int. Ed.* **2003**, *42*, 4494.

[B58] (a) E. Wiener, M.W. Brechbiel, H. Brothers, R.L. Magin, O.A. Gansow, D.A. Tomalia, P.C. Lauterbur, *Magn. Reson. Med.* **1994**, *31*, 1;

(b) E. Wiener, F.P. Auteri, J.W. Chen, M.W. Brechbiel, O.A. Gansow, D.S. Schneider, R.L. Belford, R.B. Clarkson, P.C. Lauterbur, *J. Am. Chem. Soc.* **1996**, *118*, 7774.

[B59] S. Langereis, A. Dirksen, T.M. Hackeng, M.H.P. van Genderen, E.W. Meijer, *New J. Chem.* **2007**, *31*, 1152.

[B60] L.M. de Leon-Rodriguez, A.J.M. Lubag, C.R. Malloy, G.V. Martinez, R.J. Gillies, A.D. Sherry, *Acc. Chem. Res.* **2009**, *42*, 948.

[B61] G.R. Newkome, C.N. Moorefield, G.R. Baker, M.J. Saunders, S.H. Grossman, *Angew. Chem. Int. Ed.* **1991**, *30*, 1178.

[B62] (a) L.J. Twyman, A.E. Beezer, R. Esfand, M.J. Hardy, J.C. Mitchell, *Tetrahedron Lett.* **1999**, *40*, 1743;

(b) Y. Sayed-Sweet, D.M. Hedstrand, R. Spinder, D.A. Tomalia, *J. Mater. Chem.* **1997**, *7*, 1199;

(c) Y. Pan, W.T. Ford, *Macromolecules* **2000**, *33*, 3731.

[B63] C. Hawker, K.L. Wooley, J.M.J. Fréchet, *J. Chem. Soc., Perkin Trans. 1* **1993**, 1287.

[B64] L.J. Twyman, I.K. Martin, *Tetrahedron Lett.* **2001**, *42*, 1123.

[B65] H. Goesmann, C. Feldmann, *Angew. Chem. Int. Ed.* **2010**, *49*, 1362.

[B66] (a) J. Turkevitch, P.C. Stevenson, J. Hillier, *Discuss. Faraday Soc.* **1951**, *11*, 55;

(b) J. Turkevitch, G. Kim, *Science* **1970**, *169*, 873;

(c) J. Turkevitch, *Gold Bull.* **1985**, *18*, 86.

[B67] (a) M. Brust, A. Walker, D. Bethell, D.J. Schiffrin, R. Whyman, *Chem. Commun.* **1994**, 801;

(b) M. Brust, D. Bethell, D.J. Schiffrin, C.J. Kiely, *Adv. Mater.* **1995**, *7*, 795;

(c) R. Levy, N.T.K. Thanh, R.C. Doty, I. Hussain, R.J. Nichols, D.J. Schiffrin, M. Brust, D.G. Fernig, *J. Am. Chem. Soc.* **2004**, *126*, 10076.

[B68] (a) L. Balogh, D.A. Tomalia, *J. Am. Chem. Soc.* **1998**, *120*, 7355;

(b) D.A. Tomalia, A.M. Naylor, W.A. Goddard, *Angew. Chem. Int. Ed.* **1990**, *29*, 138;

(c) M. Zhao, L. Sun, R.M. Crooks, *J. Am. Chem. Soc.* **1998**, *120*, 4877;

(d) R.W. J. Scott, O.M. Wilson, R.M. Crooks, *J. Phys. Chem. B* **2005**, *109*, 692;

(e) K. Esumi, A. Suzuki, N. Aihara, K. Usui, K. Torigoe, *Langmuir* **1998**, *14*, 3157;

(f) K. Esumi, A. Kameo, A. Suzuki, K. Torigoe, *Colloids Surf. A* **2001**, *189*, 155.

[B69] M.T. Reetz, R. Breinbauer, K. Wanninger, *Tetrahedron Lett.* **1996**, *37*, 4499.

[B70] Y. Li, M.A. El-Sayed, *J. Phys. Chem. B* **2001**, *105*, 8938.

[B71] C. Ornelas, L. Salmon, J.R. Aranzaes, D. Astruc, *Chem. Commun.* **2007**, 4946.

[B72] D. Astruc, F. Lu, J.R. Aranzaes, *Angew. Chem. Int. Ed.* **2005**, *44*, 7852.

[B73] Y.M. Chung, H.K. Rhee, *J. Mol. Catal. A* **2003**, *206*, 291.

[B74] (a) L.K. Yeung, C.T. Lee, K.P. Jonston, R.M. Crooks, *Chem. Commun.* **2001**, 2290;

(b) R.W. Scott, A.F. Datye, R.M. Crooks, *J. Am. Chem. Soc.* **2003**, *125*, 3708.

[B75] S. Chandra, K.C. Barick, D. Bahadur, *Adv. Drug Deliv. Rev.* **2011**, doi:10.1016/j.addr.2011.06.003.

[B76] J. Giri, T. Sriharsha, D. Bahadur, *J. Mater. Chem.* **2004**, *14*, 875.

[B77] A.S. de Dios, M.E. Díaz-García, *Anal. Chim. Acta* **2010**, *666*, 1.

[B78] L. Chen, J. Xu, D.A. Tanner, R. Phelan, M. van der Meulen, J.D. Holmes, M.A. Morris, *Chem. Eur. J.* **2009**, *15*, 440.

[B79] S. Laurent, D. Forge, M. Port, A. Roch, C. Robic, L. van der Elst, R.N. Muller, *Chem. Rev.* **2008**, *108*, 2064.

[B80] R. Qiao, C. Yang, M. Gao, *J. Mater. Chem.* **2009**, *19*, 6274.

[B81] N.K. Prasad, K. Rathinasamy, D. Panda, D. Bahadur, *J. Mater. Chem.* **2007**, *17*, 5042.

[B82] S. Chandra, S. Mehta, S. Nigam, D. Bahadur, *New J. Chem.* **2010**, *34*, 648.

[B83] (a) E. Strable, J.W.M. Bulte, B. Moskowitz, K. Vivekanandan, M. Allen, T. Douglas, *Chem. Mater.* **2001**, *13*, 2201;

(b) J.W.M. Bulte, T. Douglas, B. Witwer, S.C. Zhang, E. Strable, B. Lewis, H. Zywicke, B. Miller, P. van Gelderen, B.M. Moskowitz, I.D. Duncan, J.A. Frank, *Nat. Biotechnol.* **2001**, *19*, 1141.

[B84] O. Taratula, O. Garbuzenk, R. Savla, Y.A. Wang, H. He, T. Minko, *Curr. Drug Deliv.* **2011**, *8*, 5.

[B85] L.M. Bronstein, Z.B. Shifrina, *Chem. Rev.* **2011**, *111*, 5301.

[B86] K.E. Sapsford, K.M. Tyner, B.J. Dair, J.R. Deschamps, I.L. Medintz, *Anal. Chem.* **2011**, *83*, 4453.

[B87] S. Sundar, J. Kundu, S.C. Kundu, *Sci. Technol. Adv. Mater.* **2010**, *11*, 014104.

[B88] G. Lespes, J. Gigault, *Anal. Chim. Acta* **2011**, *692*, 26.

C Amidoamine-based Dendrimers with End-grafted Pd-Fe Units: Synthesis, Characterization and Their Use in the Heck Reaction

Sascha Dietrich, Anja Nicolai and Heinrich Lang

Published in *J. Organomet. Chem.* **2011**, *696*, 739 – 747.

1. Introduction

Since the early work of G. van Koten [C1] on homogeneous catalysts immobilized on soluble inert silicon-based dendrimer supports there is a rapid development in this field of chemistry recognized which merges heterogeneous and homogeneous catalysis, respectively [C2]. Metallodendrimers depending on their size properties take advantage of a simple catalyst separation and recovery [C3]. Furthermore, immobilization on a dendrimer support may influence the activity (positive or negative dendritic effect) and/or selectivity of a catalytic reaction, when compared with their monomeric analogs. In addition to silicon-containing dendritic frameworks, amidoamine dendrimers with their nitrogen and amide functionalities give advantage as high capacity chelating molecules for the stabilization of catalytic active species during the catalytic process [C4]. So far, dendrimers with peripherally attached mononuclear organometallic or metal-organic chiral and non-chiral units including nickel [C5], palladium [C6, C7], platinum [C8], cobalt [C9], rhodium [C10, C11] and ruthenium [C12] fragments have been applied in a variety of homogeneous catalyses. In this context, the utilization of ferrocenyl phosphine functionalized supports in combination with diverse palladium sources to *in-situ* generate catalytic active species in carbon-carbon cross coupling reactions has widely been described [C13]. About the use of individual heterobimetallic end-grafted organometallics featuring at least one catalytic active transition metal atom has to the best of our knowledge not been reported in dendrimer chemistry so far, however, very recently a method was reported to prepare the PAMAM-based dendrimer G4OH-$(Pt^{2+})_x(Ru^{3+})_y$ by subsequent addition of $K_2[PtCl_4]$ and $[RuCl_3]$, respectively, to dendrimer G4OH in an aqueous solution [C14]. Nevertheless, the proposed heterobimetallic Pt-Ru complexes were not isolated.

With this in mind and as a continuation of our research in the field of dendrimers [C15] and carbon-carbon cross-coupling reactions [C16], we here describe the immobilization of catalytic active palladium ferrocenyl phosphines using amidoamine dendrimers. The use of the appro-

priate supported heterobimetallic Fe-Pd systems as catalysts in the Heck-Mizoroki [C17 – C19] (reaction of iodobenzene with *tert*-butyl acrylate) reaction is reported.

2. Results and Discussion

2.1. Synthesis of Amidoamine Dendrimers

Amidoamine dendrimers were prepared by a divergent consecutive synthesis procedure firstly described by Tomalia and coworkers [C20]. This synthesis methodology was applied to the preparation of **2** as depicted in Scheme C1. After appropriate work-up, this dendrimer with its five terminal amino functionalities could be isolated as a colorless oil in almost quantitative yield (Experimental Part).

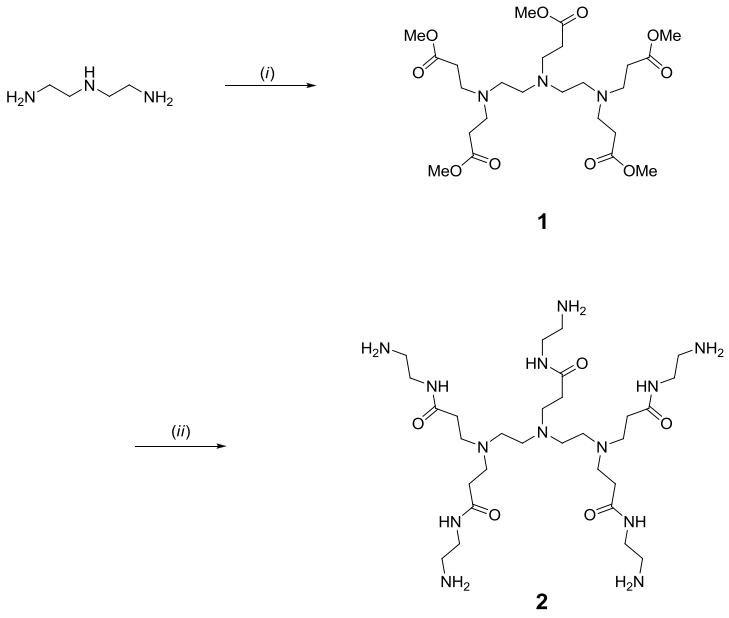

((*i*) CH_2CHCO_2Me, methanol, 25 °C, 72 hrs; (*ii*) $H_2NCH_2CH_2NH_2$, methanol, 25 °C, 72 hrs).

Scheme C1. Synthesis of amidoamine dendrimer **2**.

Dendrimer **2** was characterized by elemental analysis, FT-IR and NMR (^1H, $^{13}C\{^1H\}$) spectroscopy. As for related amidoamine compounds [C21a] the NMR spectroscopic characterization of **2** revealed single resonance patterns for the $C(O)CH_2CH_2$, $C(O)CH_2$, $HNCH_2$, CH_2NH_2 and NH_2 fragments of which, as expected, the latter group appears as a broad signal (Experimental Part). Most characteristic in the FT-IR spectrum of **2** is the observation of three very distinctive absorptions at 3365 (ν_{NH}), 1640 ($\nu_{C(O)}$, amide I) and 1560 cm^{-1} ($\nu_{C(O)}$, amide II) (Experimental Part).

2.2. Synthesis of Metallo- and Selenium-Phosphine Amidoamine Dendrimers

The Iron-palladium organometallic moieties were attached to the dendrimer periphery *via* peptide coupling by treatment of (diphenylphosphino)ferrocenyl carboxylic acid (**3**) [C21b] with the NH_2-functionalized amidoamine support (**2**) under standard peptide coupling conditions in presence of HOBT (= *h*ydrox*y*b*e*nzo*t*riazole) and EDC (= 1-*e*thyl-3-(3-*d*imethylaminopropyl)*c*arbodiimide), respectively, which was further reacted with $[Pd(\eta^3\text{-}C_3H_5)Cl]_2$ (**4**) [C21c] to give heterobimetallic **9-Fe-Pd** (Scheme C2). Organometallic **9-Fe-Pd** was obtained in an overall yield of 26 % (Experimental Part).

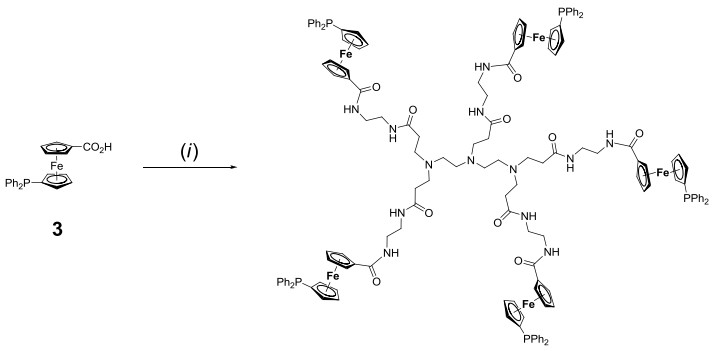

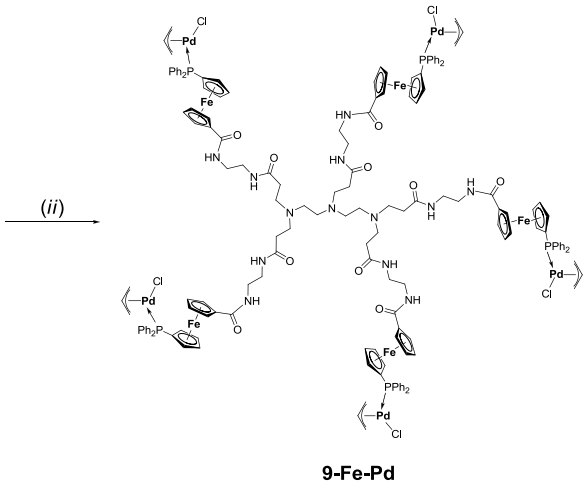

((*i*) **2**, HOBT (= *h*ydrox*y*b*e*nzo*t*riazole), EDC (= 1-*e*thyl-3-(3-*d*imethylaminopropyl)-*c*arbodiimide, dichloromethane, 0 → 25 °C, 12 hrs; (*ii*) $[Pd(\eta^3\text{-}C_3H_5)Cl]_2$ (**4**), dichloromethane, 25 °C, 1 h).

Scheme C2. Synthesis of heterobimetallic **9-Fe-Pd**.

For comparison, the organometallic molecules **5-Fe-Pd** − **8-Fe-Pd** were synthesized in a consecutive reaction sequence using the same reaction conditions as described for the synthesis of **9-Fe-Pd** (Figure C1).

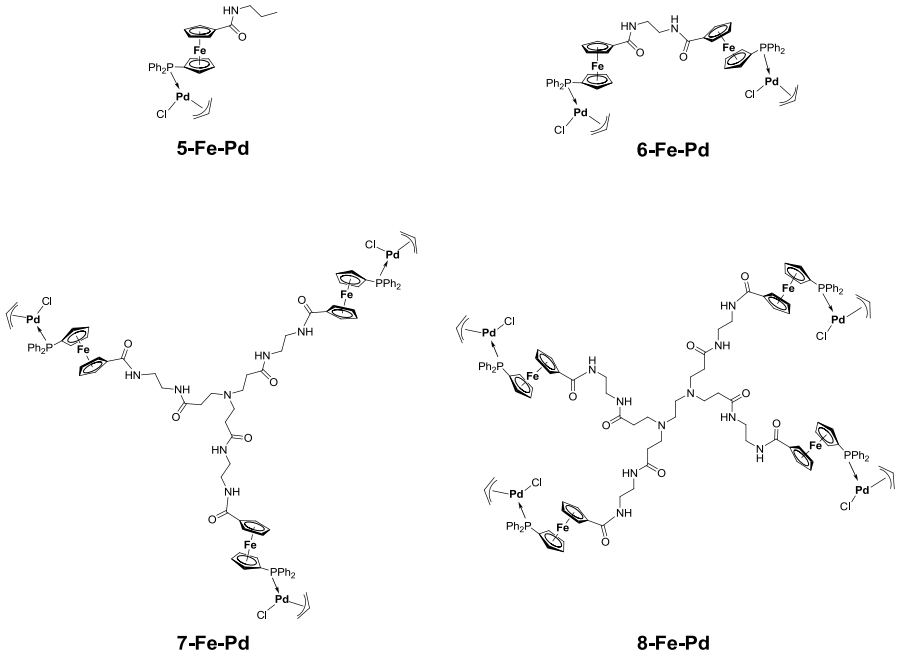

Figure C1. Heterobimetallic amidoamines **5-Fe-Pd** – **8-Fe-Pd**.

Compounds **9-Fe** and **5-Fe-Pd** – **9-Fe-Pd** are odorless, stable to air and moisture, dissolve in polar organic solvents, *e.g.* in dichloromethane and tetrahydrofuran, while being poorly soluble in benzene and toluene. Dendrimer **9-Fe** featuring as terminal group the ferrocenyl diphenylphosphine is an orange colored solid, whereas the defined coordination compounds Fe-Pd (**5-Fe-Pd** – **9-Fe-Pd**) are bright yellow.

All ferrocenyl and heterobimetallic Fe-Pd metallodendrimers **9-Fe** and **5-Fe-Pd** – **9-Fe-Pd** gave correct elemental analyses. As the unimolecular amidoamine molecule **2**, the appropriate metallodendrimer **9-Fe-Pd** shows separated and well-resolved signals with the expected coupling pattern in the NMR spectra (Experimental Part).

The successful attaching of **3** to the amidoamine scaffold **2** can nicely be proofed by FT-IR and NMR spectroscopy. In FT-IR spectroscopy the absorption at ca. 1670 ($\nu_{C(O)}$) disappears, proofing complete consumption of the carboxylic acid (**3**). The formation of the amide connectivity can best be figured with ^{1}H NMR spectroscopy. For example, the signal of the terminal NH_2 moiety is shifted to lower field at 7.82 ppm in course of the reaction [C21a]. In the $^{13}C\{^{1}H\}$ NMR spectra the resonance of the carbonyl carbon atom of the carboxylic acid (**3**) is shifted from 177 to ca. 170 ppm [C21b] (Experimental Part).

The presence of a diphenylphosphine ferrocenyl sandwich unit in **9-Fe** is discernable by the appearance of a singlet at -17.9 ppm in the $^{31}P\{^{1}H\}$ NMR (Experimental Part). Through coordination of the phosphorus atom to palladium as given in heterobimetallic compound **9-Fe-Pd** a representative shift to lower field occurs (13.3 ppm). The chemical shift of the datively-bonded Ph_2P group is, as expected, almost independent of the appropriate amidoamine scaffold [C22]. The newly introduced [Pd(η^3-C_3H_5)Cl] organometallic fragment in **5-Fe-Pd** – **9-Fe-Pd** can also be recognized in the ^{1}H and $^{13}C\{^{1}H\}$ NMR spectra. In the ^{1}H NMR spectra the allyl moieties give rise to three distinctive resonances at ca. 2.8 (CH-*anti*), 3.8 (CH-*syn*) and 5.5 ppm (CH-*centered*) as a result of the different chemical environment within the allyl unit, while in $^{13}C\{^{1}H\}$ spectroscopy two signals can be assigned at ca. 62 (CH_2) and 118 ppm (CH) (Experimental Part) [C23].

The σ - donor properties of phosphines can be quantified by the phosphorus-selenium coupling constant $^{1}J_{(31P\text{-}77Se)}$ of the appropriate seleno derivatives [C24]. Therefore, we reacted the phosphino ferrocenyl amidoamines **9-Fe** and **5-Fe** with selenium in dichloromethane at ambient temperature to obtain the appropriate seleno-phosphine derivatives **9-Fe-Se** and **5-Fe-Se** (Figure C2) to classify the electronic properties of the immobilized phosphino ferrocenes and range them with conventionally phosphines. After appropriate work-up, **5-Fe-Se** and **9-Fe-Se** were isolated as orange solids in almost quantitative yield (Experimental Part).

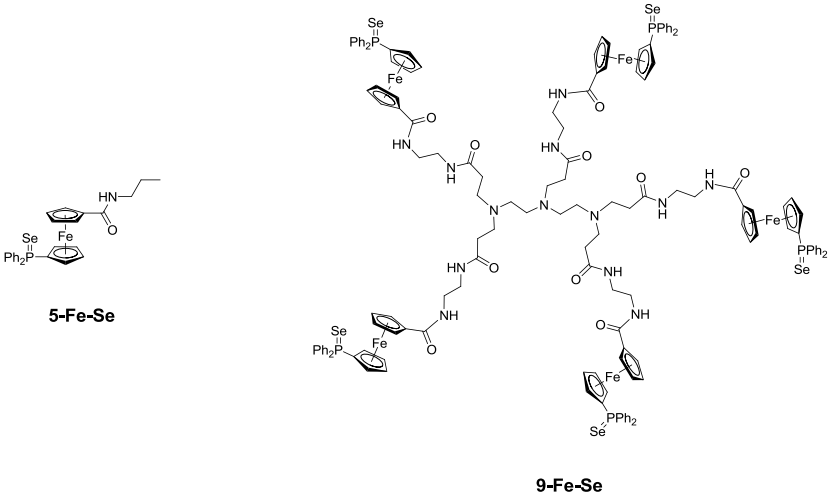

Figure C2. Seleno-phosphines **5-Fe-Se** and **9-Fe-Se**.

The phosphorus-selenium coupling constants of **5-Fe-Se** and **9-Fe-Se** were determined to $^{1}J_{(31P\text{-}77Se)}$ = 720 Hz (**5-Fe-Se**) and 723 Hz (**9-Fe-Se**), being slightly decreased, when compared with $FcPh_2P{=}Se$ ($^{1}J_{(31P\text{-}77Se)}$ = 731 Hz) and $Ph_3P{=}Se$ ($^{1}J_{(31P\text{-}77Se)}$ = 729 Hz) [C25]. Obviously, the immobilization on the scaffold has no negative impact on the σ – donor proper-

ties of the phosphines. Furthermore, the phosphorus-selenium coupling constants indicate no influence according to the number of the immobilized diphenylphosphino ferrocenyl fragments.

2.3. Catalysis with Heterobimetallic Iron-Palladium Amidoamine Dendrimers

To enrich the family of existing Heck catalysts, we applied the above described heterobimetallic Fe-Pd phosphines **5-Fe-Pd** – **9-Fe-Pd** in vinylation reactions, as metal-containing phosphines and particularly those based on a ferrocene scaffold have played a very important role in many organic transformations catalyzed by palladium complexes [C26]. In comparative studies these newly synthesized compounds showed to be efficient catalysts in the carbon-carbon cross coupling of iodobenzene with *tert*-butyl acrylate. The results obtained for dendrimers **6-Fe-Pd** – **9-Fe-Pd** are compared with the parent model **5-Fe-Pd** and are comparatively discussed in terms of the potential ability of the amidoamine scaffold stabilizing catalytic active palladium species. The homogeneous palladium-catalyzed vinylation was performed as described by Boys and Butler [C27]. Thus, the appropriate organic coupling reagents (3.0 mmol iodobenzene (**10**), 3.1 mmol *tert*-butyl acrylate (**11**)) were reacted in a toluene-acetonitrile mixture of ratio 1:1 (*v/v*), in the presence of NEt^iPr_2 (3.1 mmol) as a base, [CuI] (two equivalents) as reducing reagent [C27] and a (pre)catalyst loading of 0.5 mol% of palladium at a comparative mild reaction temperature (80 °C) (Reaction C1, Figure C3, Table C1, Experimental Part). The initial reaction rate, conversion, TON (= *t*urn-*o*ver-*n*umber) and TOF (= *t*urn-*o*ver-*f*requency) data are reported.

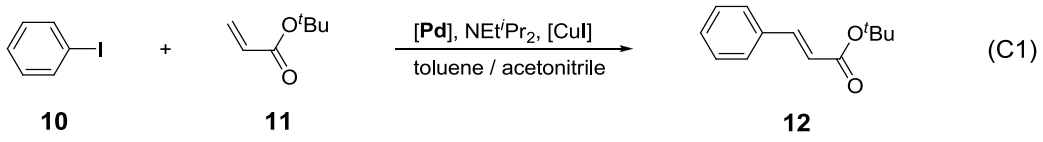

10 **11** **12** (C1)

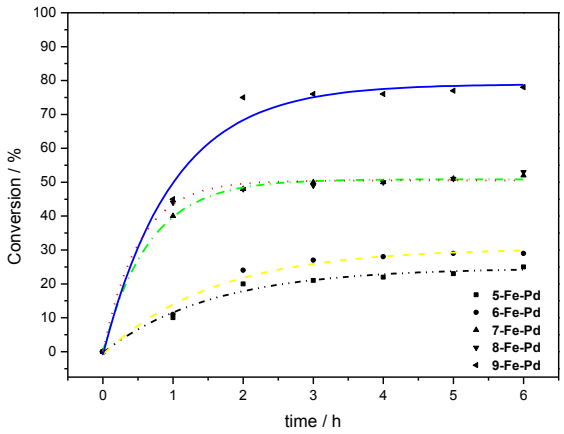

Figure C3. Kinetic investigation of **5-Fe-Pd** – **9-Fe-Pd** in the Heck-Mizoroki carbon-carbon cross-coupling reaction of iodobenzene (**10**) with *tert*-butyl acrylate (**11**) to give *E*-*tert*-butyl cinnamate (**12**) (0.5 mol% (pre)catalyst; conversion time 0 – 6 hrs).

Table C1. Results of the Heck-Mizoroki *C,C*-cross-coupling of iodobenzene with *tert*-butyl acrylate by **5-Fe-Pd** – **9-Fe-Pd**.

Compd.	**5-Fe-Pd**	**6-Fe-Pd**	**7-Fe-Pd**	**8-Fe-Pd**	**9-Fe-Pd**
Yield of **12** [%] [a]	44	48	61	63	88
TON [b]	88	96	122	126	176
TOF [1/h] [c]	20	24	80	88	90

[a] Yields are determined by ^{1}H NMR spectroscopy with acetylferrocene as standard relative to *E*-*tert*-butyl cinnamate (**12**), reaction time 24 hrs; [b] Mol product/mol [Pd]; [c] Mol product/mol [Pd])/2, determined after 1 h.

From Figure C3 and Table C1 it can be seen that the best productivity is reached with catalyst **9-Fe-Pd** possessing the highest number of terminal heterobimetallic Fe-Pd-units. It can also be recognized that there is a positive synergistic effect most pronounced between **5-Fe-Pd** / **6-Fe-Pd**, **7-Fe-Pd** / **8-Fe-Pd** and **9-Fe-Pd** (Figure C3). As the electronic properties of all the compounds are similar ($^{1}J_{(^{31}P\text{-}^{77}Se)}$, *vide supra*), the different catalytic activity is most likely caused by cooperative effects between the catalytic active palladium-species formed and the amino groups of the amidoamine scaffold. The higher the number of terminal metal frag-

ments and of intrinsic amino units, the higher is the catalytic activity for the embedded palladium catalyst. Similar results of a positive "dendritic effect" on chemical yields, which means that the activity is improved by increasing the number of terminal metal-containing groups, have been reported recently [C3c, C16e, C28, C29]. For all heterobimetallic Fe-Pd systems concomitant precipitation of metallic palladium occurs during the catalytic reaction, which decreases in the series **5-Fe-Pd** / **6-Fe-Pd** > **7-Fe-Pd** / **8-Fe-Pd** > **9-Fe-Pd**.

By means of the Hg(0) drop test, reaction mixtures of iodobenzene (**10**), *tert*-butyl acrylate (**11**) and 0.5 mol% of **8-Fe-Pd** as (pre)catalyst are quenched with metallic mercury (Figure C4) at certain times [C30]. Quenching after the catalytically active system is formed (t = 45 min) extinguishes the catalytic activity instantly, while adding mercury at the beginning of the catalysis (t = 0 min) even prevents the formation of a catalytic active palladium species. This observations of poisoning implies heterogeneous Heck-Mizoroki reactions promoted by Pd(0) particles [C31].

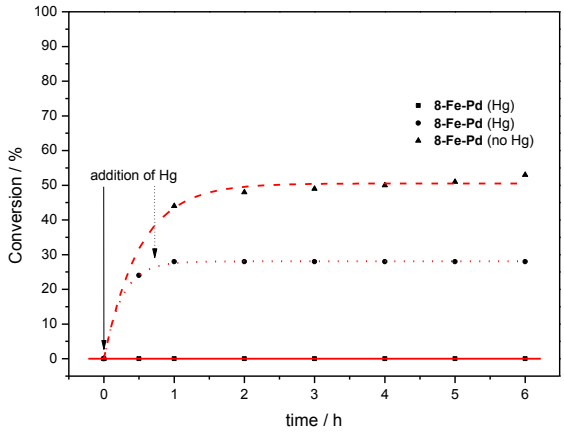

Figure C4. Hg(0) drop tests of **8-Fe-Pd** in the Heck-Mizoroki reactions by addition of metallic mercury at certain times (t = 0 min; t = 45 min) and without the addition of mercury for comparison.

3. Conclusions

The preparation and characterization of well-defined Fe-Pd phosphine functionalized amidoamines $N(CH_2CH_2C(O)NHCH_2CH_2NHC(O)(Fe(\eta^5\text{-}C_5H_4)(\eta^5\text{-}C_5H_4PPh_2(Pd(\eta^3\text{-}C_3H_5)Cl))))_3$, $[CH_2N(CH_2CH_2C(O)NHCH_2CH_2NHC(O)(Fe(\eta^5\text{-}C_5H_4)(\eta^5\text{-}C_5H_4PPh_2(Pd(\eta^3\text{-}C_3H_5)Cl))))_2]_2$, $(Fe((\eta^5\text{-}C_5H_4PPh_2(Pd(\eta^3\text{-}C_3H_5)Cl))(\eta^5\text{-}C_5H_4))C(O)HNCH_2CH_2NHC(O)CH_2CH_2)N[CH_2CH_2\text{-}N(CH_2CH_2C(O)NHCH_2CH_2NHC(O)(Fe(\eta^5\text{-}C_5H_4)(\eta^5\text{-}C_5H_4PPh_2(Pd(\eta^3\text{-}C_3H_5)Cl))))_2]_2$, (Fe-

(η^5-C_5H_4(PPh_2(Pd(η^3-C_3H_5)Cl))(η^5-$C_5H_4C(O)NH^nC_3H_7$))) and [Fe(η^5-C_5H_4(PPh_2(Pd(η^3-C_3H_5)Cl))(η^5-$C_5H_4C(O)NHCH_2$))]$_2$, for comparison, using consecutive divergent growth methodologies including addition, amidation and complexation reactions is described. These molecules are unique because they feature as end-grafted moieties heterobimetallic ferrocenyl-based palladium allyl chlorides. These individual metallodendrimers were successfully employed as homogeneous Heck catalysts in the vinylation of iodobenzene with *tert*-butyl acrylate to give *E*-*tert*-butyl cinnamate. The newly prepared Fe-Pd-catalysts are less active than the catalyst systems reported earlier with any combination of *N*-heterocyclic carbenes [C32], bulky electron-rich chelating bis(phosphines) [C33], palladacycles [C34], secondary phosphates or phosphonium salts [C29a, C35], however, the systems prepared show synergistic and cooperative effects resulting in higher yields and productivities with increasing numbers of end-grafted Fe-Pd phosphine moieties. Due to the larger organic matrix with its specific, intrinsic amine functionalities the amidoamine scaffold with the most immobilized heterobimetallic iron-palladium features is best suited for the stabilization of the catalytic active species.

4. Experimental

4.1. Materials and Methods

Syntheses were performed under a dry and deoxygenated dinitrogen atmosphere using standard Schlenk techniques unless otherwise stated. All solvents were carefully dried by standard procedures over the appropriate drying agents and distilled immediately prior to use. The reagents that where purchased commercially were used without further purification. (Diphenylphosphino)ferrocenyl carboxylic acid (**3**) [C21b], [Pd(η^3-C_3H_5)Cl]$_2$ (**4**) [C21c] and **5-Fe** – **8-Fe** [C16e] were prepared according to published procedures.

^{1}H, ^{13}C{^{1}H} and ^{31}P{^{1}H} NMR spectra were recorded with a Bruker Avance III 500 MHz spectrometer. Chemical shifts δ are given in ppm (parts per million) using the particular solvent or H_3PO_4 as external standard as reference signal. Coupling constants *J* are given in Hertz (Hz). FT-IR spectra were recorded with a FT Nicolet IR 200 instrument in the range of 500 to 4000 cm^{-1}. The melting points were obtained using capillaries with an electro thermal melting point apparatus. Microanalyses were performed with a C,H,N-analyzer FLASHEA 1112 Series (Thermo Inc.).

4.2. Preparation of $H_2NCH_2CH_2NHC(O)CH_2CH_2)N(CH_2CH_2N(CH_2CH_2C(O)NH-CH_2CH_2NH_2)_2)_2$ (2)

Poly(amidoamine)dendrimer **2** was synthesized by a preparation procedure firstly described by Tomalia *et al.* [C21a], in a two step synthesis methodology using 1.0 g (9.7 mmol) of diethylenetriamine in 20 mL of methanol. After subsequent addition of methyl acrylate (10 g, 116 mmol) at 25 °C an excess of ethylenediamine (33.5 mL, 0.5 mol) was added in a single portion. After 3 days of stirring all volatiles were evaporated in oil-pump vacuum, whereby **2** was obtained as colorless oil (6.5 g, 99 %, based on diethylenetriamine). Anal. Calc. for $C_{29}H_{63}N_{13}O_5$ (673.9): C, 51.69; H, 9.42; N, 27.02. Found: C, 52.03; H, 9.67; N, 27.19. ^{1}H NMR (δ, $CDCl_3$): 1.45 (bs, 10 H, NH_2), 2.37 (m, 10 H, CH_2C(O)), 2.56 (br, 8 H, NCH_2CH_2N), 2.74 (t, 10 H, $^3J_{HH}$ = 6.9 Hz, NCH_2CH$_2$C(O)), 2.78 (t, 10 H, $^3J_{HH}$ = 6.3 Hz, CH_2NH$_2$), 3.25 (t, 10 H, $^3J_{HH}$ = 6.3 Hz, NHCH_2), 7.66 (m, 5 H, C(O)NH). ^{13}C{^{1}H} NMR (δ, $CDCl_3$): 32.1 (*C*H$_2$C(O)), 41.3 (NH*C*H$_2$), 42.3 (*C*H$_2$NH$_2$), 51.4 (N*C*H$_2$CH$_2$N), 52.0 (NCH$_2$*C*H$_2$N), 54.2 (N*C*H$_2$CH$_2$C(O)), 168.4 (*C*(O)). FT-IR (NaCl, cm^{-1}): 3365 (vs, ν_{NH2}), 1640 (vs, $\nu_{C(O)}$, amide I), 1560 (s, $\nu_{C(O)}$, amide II).

4.3. Preparation of $((Fe(\eta^5\text{-}C_5H_4PPh_2)(\eta^5\text{-}C_5H_4))C(O)HNCH_2CH_2NHC(O)CH_2CH_2)$-$N[CH_2CH_2N(CH_2CH_2C(O)NHCH_2CH_2NHC(O)(Fe(\eta^5\text{-}C_5H_4)(\eta^5\text{-}C_5H_4PPh_2)))_2]_2$ (9-Fe)

300 mg (0.45 mmol) of **2** in 20 mL of dichloromethane was mixed with 950 mg (2.3 mmol) of (diphenylphosphino)ferrocenyl carboxylic acid (**3**) and 310 mg (2.3 mmol) of HOBT. After stirring for 1 h at 0 °C, 355 mg (2.3 mmol) of EDC in 30 mL of dichloromethane was slowly added. The resulting reaction mixture was stirred overnight at 25 °C and afterwards was subsequently washed with 20 mL of an aqueous solution of ammonium chloride (0.5 M). After drying the organic layer over $MgSO_4$ the solvents were removed under reduced pressure. The crude product was purified by column chromatography (column size: 10 x 3 cm, alumina) using dichloromethane as eluent. After evaporation of all volatiles in oil-pump vacuum molecule **9-Fe** was obtained as an air stable, orange colored solid (350 mg, 30 %, based on **2**). Mp: 125 °C. Anal. Calc. for $C_{144}H_{148}Fe_5N_{13}O_{10}P_5$ (2654.9): C, 65.15; H, 5.62; N, 6.86. Found: C, 64.63; H, 5.23; N, 6.39. ^{1}H NMR (δ, $CDCl_3$): 2.09 (bs, 20 H, NCH_2CH_2C(O)), 2.51 (m, 8 H, NCH_2CH_2N), 3.31 (m, 20 H, HNCH_2CH_2NH), 4.00 (m, 10 H, H_α/$C_5H_4PPh_2$), 4.07 (m, 10 H, H_β/C_5H_4C(O)), 4.29 (m, 10 H, H_β/$C_5H_4PPh_2$), 4.64 (m, 10 H, H_α/C_5H_4C(O)), 7.18 – 7.31 (m, 50 H, C_6H_5), 7.82 (m, 10 H, NH). ^{13}C{^{1}H} NMR (δ, $CDCl_3$): 29.7 (*C*H$_2$C(O)), 39.3

(HN*C*H$_2$CH$_2$NH), 40.4 (HNCH$_2$*C*H$_2$NH), 50.9 (N*C*H$_2$CH$_2$C(O)), 51.6 (N*C*H$_2$CH$_2$N), 51.9 (NCH$_2$*C*H$_2$N), 69.5 (*C*$_\alpha$/C$_5$H$_4$C(O)), 71.9 (*C*$_\beta$/C$_5$H$_4$C(O)), 73.1 (d, $^3J_{CP}$ = 3 Hz, *C*$_\beta$/C$_5$H$_4$C(PPh$_2$)), 74.4 (d, $^2J_{CP}$ = 13 Hz, *C*$_\alpha$/C$_5$H$_4$C(PPh$_2$)), 76.6 (*C*$_i$/C$_5$H$_4$C(O)), 77.5 (d, $^1J_{CP}$ = 8 Hz, *C*$_i$/C$_5$H$_4$C(PPh$_2$)), 128.4 (d, $^3J_{CP}$ = 6 Hz, *C*$_m$/C$_6$H$_5$), 128.8 (*C*$_p$/C$_6$H$_5$), 133.5 (d, $^2J_{CP}$ = 19 Hz, *C*$_o$/C$_6$H$_5$), 138.5 (d, $^1J_{CP}$ = 10 Hz, *C*$_i$/C$_6$H$_5$), 170.9 (*C*(O)), 173.6 (C(O)). ^{31}P{^{1}H} NMR (δ, CDCl$_3$): -17.9 (*P*Ph$_2$). FT-IR (KBr, cm^{-1}): 3300 (m, ν_{NH}), 1640 (s, $\nu_{C(O)}$, amide I), 1540 (s, $\nu_{C(O)}$, amide II).

4.4. Preparation of (Fe(η^5-C$_5$H$_4$(PPh$_2$(Pd(η^3-C$_3$H$_5$)Cl))(η^5-C$_5$H$_4$C(O)NH^{n}C$_3$H$_7$))) (5-Fe-Pd)

180 mg (0.4 mmol) of (Fe(η^5-C$_5$H$_4$(PPh$_2$)(η^5-C$_5$H$_4$C(O)NH^{n}C$_3$H$_7$))) (**5-Fe**) were dissolved in dichloromethane (20 mL) and 75 mg (0.21 mmol) of [Pd(η^3-C$_3$H$_5$)Cl]$_2$ (**4**) were added in a single portion. After 1 h of stirring at 25 °C, **5-Fe-Pd** was purified by precipitation from dichloromethane (5 mL) by addition of 20 mL of *n*-hexane. The precipitate was washed twice with 10 mL portions of *n*-hexane. After appropriate work-up, the title compound was isolated as a bright yellow solid (230 mg, 90 %, based on **5-Fe**). Mp: 150 °C. Anal. Calc. for C$_{29}$H$_{31}$ClFeNOPPd (638.3): C, 54.57; H, 4.90; N, 2.91. Found: C, 54.44; H, 5.12; N, 2.99. ^{1}H NMR (δ, CDCl$_3$): 0.96 (t, 3 H, $^3J_{HH}$ = 7.4 Hz, C*H*$_3$), 1.65 (m, 2 H, CH$_2$C*H*$_2$CH$_3$), 2.85 (m, 1H, C*H-anti*), 3.30 (m, 2 H, C*H*$_2$CH$_2$CH$_3$), 3.78 (m, 1 H, C*H-syn*), 4.26 (m, 2 H, *H*$_\alpha$/C$_5$H$_4$PPh$_2$), 4.57 (m, 2 H, *H*$_\beta$/C$_5$H$_4$C(O)), 5.02 (m, 2 H, *H*$_\beta$/C$_5$H$_4$PPh$_2$), 5.15 (m, 2 H, *H*$_\alpha$/C$_5$H$_4$C(O)), 5.55 (m, 1 H, C*H-centered*), 7.18 (m, 1 H, N*H*), 7.31 – 7.78 (m, 10 H, C$_6$H$_5$). ^{13}C{^{1}H} NMR (δ, CDCl$_3$): 11.7 (*C*H$_3$), 23.2 (CH$_2$*C*H$_2$CH$_3$), 41.5 (*C*H$_2$CH$_2$CH$_3$), 61.9 (*C*H$_2$-*syn*/*anti*), 70.3 (*C*$_\alpha$/C$_5$H$_4$C(O)), 71.9 (*C*$_\beta$/C$_5$H$_4$C(O)), 73.5 (d, $^3J_{CP}$ = 5 Hz, *C*$_\beta$/C$_5$H$_4$C(PPh$_2$)), 74.3 (d, $^1J_{CP}$ = 47 Hz, *C*$_i$/C$_5$H$_4$C(PPh$_2$)), 76.4 (d, $^2J_{CP}$ = 16 Hz, *C*$_\alpha$/C$_5$H$_4$C(PPh$_2$)), 78.5 (*C*$_i$/C$_5$H$_4$C(O)), 118.2 (*C*H-*centered*), 128.5 (d, $^3J_{CP}$ = 6 Hz, *C*$_m$/C$_6$H$_5$), 130.2 (*C*$_p$/C$_6$H$_5$), 133.1 (d, $^2J_{CP}$ = 12 Hz, *C*$_o$/C$_6$H$_5$), 135.9 (d, $^1J_{CP}$ = 44 Hz, *C*$_i$/C$_6$H$_5$), 169.2 (*C*(O)). ^{31}P{^{1}H} NMR (δ, CDCl$_3$): 11.6 (*P*Ph$_2$). FT-IR (KBr, cm^{-1}): 3315 (m, ν_{NH}), 1645 (s, $\nu_{C(O)}$, amide I), 1540 (s, $\nu_{C(O)}$, amide II), 1480 (w, $\nu_{\eta 3\text{-}C3H5}$).

4.5. Preparation of [Fe(η^5-C$_5$H$_4$(PPh$_2$(Pd(η^3-C$_3$H$_5$)Cl))(η^5-C$_5$H$_4$C(O)NHCH$_2$]$_2$ (6-Fe-Pd)

Compound **6-Fe-Pd** was synthesized in the same manner as **5-Fe-Pd**, whereby 150 mg (0.18 mmol) of [Fe(η^5-C$_5$H$_4$(PPh$_2$))(η^5-C$_5$H$_4$C(O)NHCH$_2$)]$_2$ (**6-Fe**) were reacted with 70 mg (0.2

mmol) of [Pd(η^3-C_3H_5)Cl]$_2$ (**4**). After appropriate work-up, **6-Fe-Pd** was obtained as a bright yellow solid (200 mg, 92 %, based on **6-Fe**). Mp: 160 °C. Anal. Calc. for $C_{54}H_{52}Cl_2Fe_2N_2O_2P_2Pd_2$ (1218.4): C, 53.23; H, 4.30; N, 2.30. Found: C, 53.46; H, 4.31; N, 2.20. ^{1}H NMR (δ, $CDCl_3$): 2.67 (m, 2H, C*H-anti*), 3.59 (m, 4 H, CH_2), 3.86 (m, 2 H, C*H-syn*), 4.03 (m, 4 H, H_α/$C_5H_4PPh_2$), 4.27 (m, 4 H, H_β/$C_5H_4C(O)$), 4.44 (m, 4 H, H_β/$C_5H_4PPh_2$), 4.80 (m, 4 H, H_α/$C_5H_4C(O)$), 5.68 (m, 2 H, C*H-centered*), 7.12 (m, 2 H, N*H*), 7.38 – 7.71 (m, 20 H, C_6H_5). ^{13}C{^{1}H} NMR (δ, $CDCl_3$): 40.6 (*C*H_2), 61.7 (*C*H_2-*syn*/*anti*), 70.2 (C_α/$C_5H_4C(O)$), 72.6 (C_β/$C_5H_4C(O)$), 73.7 (d, $^3J_{CP}$ = 9 Hz, C_β/$C_5H_4C(PPh_2)$), 74.5 (d, $^1J_{CP}$ = 44 Hz, C_i/$C_5H_4C(PPh_2)$), 76.4 (d, $^2J_{CP}$ = 14 Hz, C_α/$C_5H_4C(PPh_2)$), 77.5 (C_i/$C_5H_4C(O)$), 118.3 (*C*H-*centered*), 128.6 (d, $^3J_{CP}$ = 9 Hz, C_m/C_6H_5), 130.3 (C_p/C_6H_5), 133.2 (d, $^2J_{CP}$ = 12 Hz, C_o/C_6H_5), 135.4 (d, $^1J_{CP}$ = 44 Hz, C_i/C_6H_5), 170.7 (*C*(O)). ^{31}P{^{1}H} NMR (δ, $CDCl_3$): 11.4 (*P*Ph_2). FT-IR (KBr, cm^{-1}): 3315 (m, ν_{NH}), 1640 (s, $\nu_{C(O)}$, amide I), 1535 (s, $\nu_{C(O)}$, amide II), 1485 (w, $\nu_{\eta 3\text{-}C3H5}$).

4.6. Preparation of N($CH_2CH_2C(O)NHCH_2CH_2NHC(O)$(Fe($\eta^5$-$C_5H_4$)($\eta^5$-$C_5H_4PPh_2$-(Pd($\eta^3$-$C_3H_5$)Cl))))$_3$ (7-Fe-Pd)

Compound **7-Fe-Pd** was synthesized in the same way as **5-Fe-Pd**, whereby 140 mg (0.09 mmol) of N($CH_2CH_2C(O)NHCH_2CH_2NHC(O)$(Fe($\eta^5$-$C_5H_4$)($\eta^5$-$C_5H_4PPh_2$)))$_3$ (**7-Fe**) were reacted with 50 mg (0.135 mmol) of [Pd(η^3-C_3H_5)Cl]$_2$ (**4**). After appropriate work-up, **7-Fe-Pd** was obtained as a bright yellow solid (165 mg, 88 %, based on **7-Fe**). Mp: 165 °C. Anal. Calc. for $C_{93}H_{99}Cl_3Fe_3N_7O_6P_3Pd_3$ (2096.9): C, 53.27; H, 4.76; N, 4.68. Found: C, 53.13; H, 4.91; N, 4.52. ^{1}H NMR (δ, $CDCl_3$): 2.37 (m, 6 H, CH_2C(O)), 2.72 (m, 6 H, NC$H_2$$CH_2$C(O)), 2.97 (m, 3 H, C*H-anti)*, 3.43 (bs, 12 H, HNCH_2CH_2NH), 3.84 (m, 3 H, C*H-syn*), 4.01 (m, 6 H, H_α/$C_5H_4PPh_2$), 4.29 (m, 6 H, H_β/$C_5H_4C(O)$), 4.53 (m, 6 H, H_β/$C_5H_4PPh_2$), 4.99 (m, 6 H, H_α/$C_5H_4C(O)$), 5.64 (m, 3 H, C*H-centered*), 7.29 – 7.81 (m, 30 H, C_6H_5), 7.87 (m, 6 H, N*H*). ^{13}C{^{1}H} NMR (δ, $CDCl_3$): 29.9 (NCH_2*C*H_2C(O)), 39.6 (HN*C*$H_2$$CH_2$NH), 39.9 (HNC$H_2$*C*$H_2$NH), 50.0 (N*C*$H_2$$CH_2$C(O)), 59.9 (*C*$H_2$-*syn*/*anti*), 69.9 ($C_\alpha$/$C_5H_4C(O)$), 72.4 ($C_\beta$/$C_5H_4C(O)$), 73.6 (d, $^3J_{CP}$ = 7 Hz, C_β/$C_5H_4C(PPh_2)$), 73.9 (d, $^1J_{CP}$ = 43 Hz, C_i/$C_5H_4C(PPh_2)$), 74.5 (d, $^2J_{CP}$ = 15 Hz, C_α/$C_5H_4C(PPh_2)$), 77.5 (C_i/$C_5H_4C(O)$), 118.4 (*C*H-*centered*), 128.3 (d, $^3J_{CP}$ = 10 Hz, C_m/C_6H_5), 130.3 (C_p/C_6H_5), 132.7 (d, $^2J_{CP}$ = 12 Hz, C_o/C_6H_5), 135.6 (d, $^1J_{CP}$ = 42 Hz, C_i/C_6H_5), 170.6 (*C*(O)), 171.9 (*C*(O)). ^{31}P{^{1}H} NMR (δ,

$CDCl_3$): 12.5 (*P*Ph_2). FT-IR (KBr, cm^{-1}): 3300 (m, ν_{NH}), 1640 (s, $\nu_{C(O)}$, amide I), 1540 (s, $\nu_{C(O)}$, amide II), 1480 (w, $\nu_{\eta 3\text{-}C3H5}$).

4.7. Preparation of [$CH_2N(CH_2CH_2C(O)NHCH_2CH_2NHC(O)(Fe(\eta^5\text{-}C_5H_4)(\eta^5\text{-}C_5H_4PPh_2$ ($Pd(\eta^3\text{-}C_3H_5)Cl)))_2]_2$ (8-Fe-Pd)

The title compound **8-Fe-Pd** was synthesized by using the same synthesis methodology as **5-Fe-Pd**, whereby 275 mg (0.13 mmol) of [$CH_2N(CH_2CH_2C(O)NHCH_2CH_2NHC(O)(Fe(\eta^5$-$C_5H_4)(\eta^5$-$C_5H_4PPh_2)))_2]_2$ (**8-Fe**) were reacted with 100 mg (0.27 mmol) of [$Pd(\eta^3$-$C_3H_5)Cl]_2$ (**4**). After appropriate work-up, **8-Fe-Pd** was obtained as a bright yellow solid (240 mg, 65 %, based on **8-Fe**). Mp: 170 °C. Anal. Calc. for $C_{126}H_{136}Cl_4Fe_4N_{10}O_8P_4Pd_4$ (2833.3): C, 53.41; H, 4.84; N, 4.94. Found: C, 53.74; H, 4.96; N, 5.28. ^{1}H NMR (δ, $CDCl_3$): 2.34 (m, 8 H, CH_2C(O)), 2.42 (m, 4 H, CH_2N), 2.74 (m, 8 H, NC$H_2$$CH_2$C(O)), 2.84 (m, 4 H, C*H-anti)*, 3.38 (m, 16 H, HNCH_2CH_2NH), 3.81 (m, 4 H, C*H-syn*), 4.07 (m, 8 H, H_α/$C_5H_4PPh_2$), 4.28 (m, 8 H, H_β/C_5H_4C(O)), 4.55 (m, 8 H, H_β/$C_5H_4PPh_2$), 5.01 (m, 8 H, H_α/C_5H_4C(O)), 5.61 (m, 4 H, C*H-centered*), 7.28 – 7.78 (m, 40 H, C_6H_5), 8.18 (m, 8 H, N*H*). ^{13}C{^{1}H} NMR (δ, $CDCl_3$): 34.8 (*C*H_2C(O)), 39.3 (HN*C*$H_2$$CH_2$NH), 40.4 (HNC$H_2$*C*$H_2$NH), 53.5 (N*C*$H_2$$CH_2$C(O)), 56.7 (*C*$H_2$N), 61.2 (*C*$H_2$-*syn*/*anti*), 70.4 ($C_\alpha$/$C_5H_4$C(O)), 72.4 ($C_\beta$/$C_5H_4$C(O)), 73.8 (d, $^3J_{CP}$ = 7 Hz, C_β/C_5H_4C(PPh_2)), 74.5 (d, $^1J_{CP}$ = 48 Hz, C_i/C_5H_4C(PPh_2)), 76.2 (C_α/C_5H_4C(PPh_2)), 77.9 (C_i/C_5H_4C(O)), 118.3 (*C*H-*centered*), 128.5 (d, $^3J_{CP}$ = 10 Hz, C_m/C_6H_5), 130.4 (C_p/C_6H_5), 133.1 (d, $^2J_{CP}$ = 12 Hz, C_o/C_6H_5), 133.6 (d, $^1J_{CP}$ = 48 Hz, C_i/C_6H_5), 169.9 (*C*(O)), 170.4 (*C*(O)). ^{31}P{^{1}H} NMR (δ, $CDCl_3$): 13.4 (*P*Ph_2). FT-IR (KBr, cm^{-1}): 3300 (m, ν_{NH}), 1645 (s, $\nu_{C(O)}$, amide I), 1535 (s, $\nu_{C(O)}$, amide II), 1480 (w, $\nu_{\eta 3\text{-}C3H5}$).

4.8. Preparation of ($(Fe(\eta^5\text{-}C_5H_4PPh_2(Pd(\eta^3\text{-}C_3H_5)Cl))(\eta^5\text{-}C_5H_4))C(O)HNCH_2CH_2$-$NHC(O)CH_2CH_2)N[CH_2CH_2N(CH_2CH_2C(O)NHCH_2CH_2NHC(O)(Fe(\eta^5$-$C_5H_4)(\eta^5\text{-}C_5H_4$-$PPh_2(Pd(\eta^3\text{-}C_3H_5)Cl))))_2]_2$ (9-Fe-Pd)

Dendrimer **9-Fe-Pd** was synthesized in the same manner as **5-Fe-Pd**, whereby 150 mg (0.06 mmol) of ($Fe((\eta^5$-$C_5H_4PPh_2)(\eta^5$-$C_5H_4))C(O)HNCH_2CH_2NHC(O)CH_2CH_2)N[CH_2CH_2N$-$(CH_2CH_2C(O)NHCH_2CH_2NHC(O)(Fe(\eta^5$-$C_5H_4)(\eta^5$-$C_5H_4PPh_2)))_2]_2$ (**9-Fe**) were reacted with 55 mg (0.15 mmol) of [$Pd(\eta^3$-$C_3H_5)Cl]_2$ (**4**). After appropriate work-up, **9-Fe-Pd** was obtained as a bright yellow solid (180 mg, 85 %, based on **9-Fe**). Mp: 170 °C. Anal. Calc. for $C_{159}H_{173}Cl_5Fe_5N_{13}O_{10}P_5Pd_5$ (3569.6): C, 53.50; H, 4.88; N, 5.10. Found: C, 54.02; H, 4.75; N, 5.43. ^{1}H NMR (δ, $CDCl_3$): 2.31 (m, 20 H, NCH_2CH_2C(O)), 2.58 (m, 8 H, NCH_2CH_2N), 2.76

(m, 5 H, C*H-anti)*, 3.31 (m, 20 H, HNCH_2CH_2NH), 3.79 (m, 5 H, C*H-syn*), 4.04 (m, 10 H, H_α/$C_5H_4PPh_2$), 4.28 (m, 10 H, H_β/$C_5H_4C(O)$), 4.53 (m, 10 H, H_β/$C_5H_4PPh_2$), 5.01 (m, 10 H, H_α/$C_5H_4C(O)$), 5.62 (m, 5 H, C*H-centered*), 7.27 – 7.76 (m, 50 H, C_6H_5), 7.89 (m, 10 H, N*H*). $^{13}C\{^1H\}$ NMR (δ, $CDCl_3$): 34.6 (*C*H_2C(O)), 39.5 (HN*C*H_2CH$_2$NH), 40.1 (HNCH$_2$*C*H_2NH), 50.9 (N*C*H_2CH$_2$C(O)), 53.5 (*C*H_2N), 61.3 (*C*H_2-*syn*/*anti*), 70.3 (C_α/$C_5H_4C(O)$), 72.5 (C_β/$C_5H_4C(O)$), 73.9 (d, $^3J_{CP}$ = 7 Hz, C_β/$C_5H_4C(PPh_2)$), 74.5 (d, $^1J_{CP}$ = 46 Hz, C_i/$C_5H_4C(PPh_2)$), 77.2 (C_α/$C_5H_4C(PPh_2)$), 77.8 (C_i/$C_5H_4C(O)$), 118.4 (*C*H-*centered*), 128.5 (d, $^3J_{CP}$ = 11 Hz, C_m/C_6H_5), 130.4 (C_p/C_6H_5), 133.2 (d, $^2J_{CP}$ = 11 Hz, C_o/C_6H_5), 133.4 (d, $^1J_{CP}$ = 44 Hz, C_i/C_6H_5), 170.0 (*C*(O)), 170.8 (*C*(O)). $^{31}P\{^1H\}$ NMR (δ, $CDCl_3$): 13.3 (*P*Ph_2). FT-IR (KBr, cm^{-1}): 3295 (m, ν_{NH}), 1640 (s, $\nu_{C(O)}$, amide I), 1540 (s, $\nu_{C(O)}$, amide II), 1480 (w, $\nu_{\eta^3\text{-}C_3H_5}$).

4.9. Preparation of (Fe(η^5-C_5H_4(PPh$_2$(Se))(η^5-$C_5H_4C(O)NH^nC_3H_7$))) (5-Fe-Se)

50 mg (0.11 mmol) of (Fe(η^5-C_5H_4(PPh_2)(η^5-$C_5H_4C(O)NH^nC_3H_7$))) (**5-Fe**) were dissolved in 10 mL of dichloromethane and 8 mg (0.11 mmol) of selenium were added in a single portion. After 1 h of stirring at 25 °C, the suspension was filtered through a pad of Celite. After evaporation the title compound could be isolated as an orange solid (55 mg, 98 %, based on **5-Fe**). Anal. Calc. for $C_{26}H_{26}FeNOPSe$ (534.3): C, 58.45; H, 4.91; N, 2.62. Found: C, 58.16; H, 5.22; N, 2.54. ^1H NMR (δ, $CDCl_3$): 0.97 (t, 3 H, $^3J_{HH}$ = 7.3 Hz, C*H*$_3$), 1.67 (m, 2 H, CH$_2$C*H*$_2$CH$_3$), 3.33 (m, 2 H, C*H*$_2$CH$_2$CH$_3$), 3.92 (m, 2 H, H_α/$C_5H_4PPh_2$), 4.24 (m, 2 H, H_β/$C_5H_4C(O)$), 4.62 (m, 2 H, H_β/$C_5H_4PPh_2$), 4.89 (m, 2 H, H_α/$C_5H_4C(O)$), 7.39 (m, 1 H, N*H*), 7.45 – 7.68 (m, 10 H, C_6H_5). $^{13}C\{^1H\}$ NMR (δ, $CDCl_3$): 11.8 (*C*H_3), 23.2 (CH$_2$*C*H_2CH$_3$), 41.4 (*C*H_2CH$_2$CH$_3$), 71.2 (C_α/$C_5H_4C(O)$), 71.5 (C_β/$C_5H_4C(O)$), 73.4 (d, $^3J_{CP}$ = 10 Hz, C_β/$C_5H_4C(PPh_2)$), 75.1 (d, $^2J_{CP}$ = 12 Hz, C_α/$C_5H_4C(PPh_2)$), 75.5 (d, $^1J_{CP}$ = 88 Hz, C_i/$C_5H_4C(PPh_2)$), 79.1 (C_i/$C_5H_4C(O)$), 128.4 (d, $^3J_{CP}$ = 12 Hz, C_m/C_6H_5), 131.7 (C_p/C_6H_5), 132.1 (d, $^1J_{CP}$ = 11 Hz, C_i/C_6H_5), 133.2 (d, C_o/C_6H_5), 169.1 (*C*(O)). $^{31}P\{^1H\}$ NMR (δ, $CDCl_3$): 30.9 ($^1J_{(^{31}P\text{-}^{77}Se)}$ = 720 Hz). FT-IR (KBr, cm^{-1}): 3300 (m, ν_{NH}), 1645 (s, $\nu_{C(O)}$, amide I), 1540 (s, $\nu_{C(O)}$, amide II), 560 (s, $\nu_{P(Se)}$).

4.10. Preparation of ((Fe(η^5-C_5H_4(PPh_2(Se)))(η^5-C_5H_4))C(O)HNCH_2CH_2NHC(O)-CH_2CH_2)N[CH_2CH_2N(CH_2CH_2C(O)NHCH_2CH_2NHC(O)(Fe(η^5-C_5H_4)(η^5-C_5H_4-(PPh_2(Se)))))$_2$]$_2$ (9-Fe-Se)

Compound **9-Fe-Se** was synthesized as described for **5-Fe-Se** using 55 mg (0.02 mmol) of (Fe((η^5-$C_5H_4PPh_2$)(η^5-C_5H_4))C(O)HNCH_2CH_2NHC(O)CH_2CH_2)N[CH_2CH_2N(CH_2CH_2C(O)-NHCH_2CH_2NHC(O)(Fe(η^5-C_5H_4)(η^5-$C_5H_4PPh_2$)))$_2$]$_2$ (**9-Fe**) and 8 mg (0.11 mmol) of selenium. After appropriate work-up, compound **9-Fe-Se** was obtained as an air stable, orange colored solid (50 mg, 85 %, based on **9-Fe**). Anal. Calc. for $C_{144}H_{148}Fe_5N_{13}O_{10}P_5Se_5$ (3049.7): C, 56.71; H, 4.89; N, 5.97. Found: C, 56.31; H, 4.94; N, 6.02. ^{1}H NMR (δ, $CDCl_3$): 2.03 (m, 20 H, NCH_2CH_2C(O)), 2.67 (m, 8 H, NCH_2CH_2N), 3.47 (m, 20 H, HNCH_2CH_2NH), 4.15 (m, 10 H, H_α/$C_5H_4PPh_2$), 4.32 (m, 10 H, H_β/C_5H_4C(O)), 4.59 (m, 10 H, H_β/$C_5H_4PPh_2$), 4.88 (m, 10 H, H_α/C_5H_4C(O)), 7.45 – 7.67 (m, 50 H, C_6H_5), 7.72 (m, 10 H, N*H*). ^{13}C{^{1}H} NMR (δ, $CDCl_3$): 29.8 (*C*H_2C(O)), 39.7 (HN*C*H_2CH_2NH), 40.5 (HNCH_2*C*H_2NH), 50.3 (N*C*H_2CH_2C(O)), 51.6 (N*C*H_2CH_2N), 51.9 (NCH_2*C*H_2N), 70.1 (C_α/C_5H_4C(O)), 72.1 (C_β/C_5H_4C(O)), 73.7 (d, $^3J_{CP}$ = 8 Hz, C_β/C_5H_4C(PPh_2)), 75.4 (d, $^2J_{CP}$ = 11 Hz, C_α/C_5H_4C(PPh_2)), 75.6 (d, $^1J_{CP}$ = 88 Hz, C_i/C_5H_4C(PPh_2)), 78.2 (C_i/C_5H_4C(O)), 128.3 (d, $^3J_{CP}$ = 12 Hz, C_m/C_6H_5), 131.5 (C_p/C_6H_5), 132.2 (d, $^1J_{CP}$ = 11 Hz, C_i/C_6H_5), 133.2 (C_o/C_6H_5), 170.1 (*C*(O)), 173.2 (C(O)). ^{31}P{^{1}H} NMR (δ, $CDCl_3$): 30.7 ($^1J_{(^{31}P\text{-}^{77}Se)}$ = 723 Hz). FT-IR (KBr, cm^{-1}): 3300 (m, ν_{NH}), 1645 (s, $\nu_{C(O)}$, amide I), 1540 (s, $\nu_{C(O)}$, amide II), 560 (s, $\nu_{P(Se)}$).

4.11. General Procedure for the Heck-Reaction

Iodobenzene (615 mg, 3.0 mmol), *tert*-butyl acrylate (395 mg, 3.1 mmol), EtN^iPr_2 (410 mg, 3.1 mmol) and acetylferrocene (114 mg, 0.5 mmol) were dissolved in 20 mL of a toluene/acetonitrile mixture (ratio 1:1, v/v) and loaded with the respective catalyst (**6-Fe-Pd** – **9-Fe-Pd** or **5-Fe-Pd**, 0.5 mol% palladium). Two equivalents of [CuI] (6 mg, 0.0315 mmol) were added in a single portion. The reaction suspension was stirred at 80 °C and samples (1 mL) were taken in periods of 1 h. The samples were filtered through a pad of Silica gel with diethyl ether as eluent. All volatiles were evaporated from the respective samples under reduced pressure. The conversions were determined by ^{1}H NMR spectroscopy.

5. Acknowledgement

This study was generously supported by the State of Saxony (Landesgraduierten Stipendium S.D.), the Edgar-Heinemann-Fellowship of the TU Chemnitz (A.N.), the Deutsche Forschungsgemeinschaft and the Fonds der Chemischen Industrie.

6. References

[C1] J.W.J. Kapen, A.W. van der Made, J.C. de Wilde, P.W.N.M. van Leeuwen, P. Wijkens, D.M. Grove, G. van Koten, *Nature* **1994**, 372, 659.

[C2] (a) D.E. Bergbreiter, J. Tian, C. Hongfa, *Chem. Rev.* **2009**, *109*, 530;
(b) A.W. Kleij, R.A. Gossage, R.J.M. Klein Gebbink, N. Brinkmann, EdJ. Reijserse, U. Kragl, M. Lutz, A.L. Spek, G. van Koten, *J. Am. Chem. Soc.* **2000**, *122*, 1211;
(b) D. Astruc, F. Chardac, *Chem. Rev.* **2001**, *101*, 2991;
(d) S.-H. Hwang, C.D. Shreiner, C.N. Moorefield, G.R. Newkome, *New J. Chem.* **2007**, *31*, 1192.

[C3] (a) D. Astruc, E. Boisselier, C. Ornelas, *Chem. Rev.* **2010**, *110*, 1857;
(b) G.E. Oosterom, J.N.H. Reek, P.C.J. Kamer, P.W.N.M. van Leuwen, *Angew. Chem.* **2001**, *113*, 1878;
(c) M. Ooe, M. Murata, T. Mizugaki, K. Ebitani, K. Kaneda, *J. Am. Chem. Soc.* **2004**, *126*, 1604.

[C4] K.A. Krot, A.F. Danil de Namor, A. Aguilar-Cornejo, K.B. Nolan, *Inorg. Chim. Acta* **2005**, *358*, 3497.

[C5] R. Malgas, S.F. Mapolie, S.O. Ojwach, G.S. Smith, J. Darkwa, *Catal. Commun.* **2008**, *9*, 1612.

[C6] P. Servin, R. Laurent, A. Romerosa, M. Peruzzini, J.-P. Majoral, A.-M. Caminade, *Organometallics* **2008**, *27*, 2066.

[C7] M.T. Reetz, G. Lohmer, R. Schwickardi, *Angew. Chem. Int. Ed.* **1997**, *36*, 1526.

[C8] L.K. Yeung, R.M. Crooks, *Nano Lett.* **2001**, *1*, 14.

[C9] (a) K. Takada, G.D. Storrier, J.I. Goldsmith, H.D. Abruna, *J. Phys. Chem. B* **2001**, *105*, 2404;
(b) K. Vassilev, S. Turmanova, M. Dimitrova, S. Boneva, *Eur. Polym. J.* **2009**, 45, 2269.

[C10] L.I. Rodriguez, O. Rossell, M. Seco, G. Muller, *J. Organomet. Chem.* **2009**, *694*, 938.

[C11] (a) A. Togni, *Angew. Chem.* **1996**, *108*, 1581;
(b) C. Köllner, B. Pugin, A. Togni, *J. Am. Chem. Soc.* **1998**, *120*, 10274;
(c) R. Schneider, C. Köllmer, I. Weber, A. Togni, *Chem. Commun.* **1999**, 2415.

[C12] C. Jahier, S. Nlate, *J. Organomet. Chem.* **2009**, *694*, 637.

[C13] (a) T.E. Pickett, F.X. Roca, C.J. Richards, *J. Org. Chem.* **2003**, *68*, 2592;
(b) J.F. Jensen, M. Johannsen, *Org. Lett.* **2003**, *5*, 3025;
(c) J.C. Hierso, A. Fihri, R. Amardeil, P. Meunier, H. Doucet, M. Santelli, *Organometallics* **2003**, *22*, 4490;
(d) D. Vinci, N. Martins, O. Saidi, J. Bacsa, A. Brigas, J. Xiao, *Can. J. Chem.* **2009**, *87*, 171;
(e) M.D. Sliger, G.A. Broker, S.T. Griffin, R.D. Rogers, K.H. Shaughnessy, *J. Organomet. Chem.* **2005**, *690*, 1478;
(f) C. Baillie, L. Zhang, J. Xiao, *J. Org. Chem.* **2004**, *69*, 7779;
(g) N. Kataoka, Q. Shelby, J.P. Stambuli, J.F. Hartwig, *J. Org. Chem.* **2002**, *67*, 5553.

[C14] Y. Gu, G. Wu, X.F. Hu, D.A. Chen, T. Hansen, H.C. zur Loye, H.J. Ploehn, *J. Power Sources* **2010**, *195*, 425.

[C15] R. Buschbeck, H. Lang, *Inorg. Chem. Commun.* **2004**, *7*, 1213.

[C16] (a) A. Jakob, B. Milde, P. Ecorchard, C. Schreiner, H. Lang, *J. Organomet. Chem.* **2008**, *693*, 3821;
(b) M. Lamac, J. Tauchman, S. Dietrich, I. Cisarova, H. Lang, P. Stepnicka, *Appl. Organomet. Chem.* **2010**, *24*, 326;
(c) D. Schaarschmidt, H. Lang, *Catal. Commun.* **2010**, *11*, 581;
(d) D. Schaarschmidt, H. Lang, *Eur. J. Inorg. Chem.* **2010**, 4811;
(e) J. Kühnert, M. Lamac, K. Demel, A. Nicolai, H. Lang, P. Stepnicka, *J. Mol. Catal. A* **2008**, *285*, 41.

[C17] H.A. Dieck, V. Heck, *J. Am. Chem. Soc.* **1974**, *96*, 1133.

[C18] B. Cornils, W.A. Herrmann, *Applied Homogenous Catalysis with Organometallic Compounds* **1996**, Wiley-VCH, Weinheim.

[C19] I.P. Beletskaya, A.V. Cheprakov, *Chem. Rev.* **2000**, *100*, 3009.

[C20] D.A. Tomalia, *United States Patent* **1985**, *4507466*.

[C21] (a) D.A. Tomalia, H. Baker, J.R. Dewald, M. Hall, G. Kallos, S. Martin, J. Roeck, J. Smith, P. Smith, *Polym. J.* **1985**, *17*, 117;
(b) J. Podlaha, P. Stepnicka, J. Ludvik, I. Cisarova, *Organometallics* **1996**, *15*, 543;

(c) N. Marion, O. Navarro, J. Mei, E.D. Stevens, N.M. Scott, S.P. Nolan, *J. Am. Chem. Soc.* **2006**, *128*, 4101.

[C22] C. Schreiner, *Ph.D. Thesis* **2010**, TU Chemnitz/Germany.

[C23] B. Domhöver, W.J. Kläui, *J. Organomet. Chem.* **1996**, *522*, 207.

[C24] (a) S. Jeulin, S. Duprat de Paule, V. Ratovelomanana-Vidal, J.-P. Genet, N. Champion, P. Dellis, *Angew. Chem. Int. Ed.* **2004**, *43*, 320;

(b) R.P. Pinnel, C.A. Megerle, S.L. Manatt, P.A. Kroon, *J. Am. Chem. Soc.* **1973**, *95*, 977;

(c) D.W. Allen, I.W. Nowell, *J. Chem. Soc. Dalton Trans.* **1985**, 2505.

[C25] A. Muller, S. Otto, A. Broodt, *Dalton Trans.* **2008**, 650.

[C26] O.V. Gusev, T.A. Peganova, A.M. Kalsin, N.V. Vologdin, P.V. Petrovskii, K.A. Lyssenko, A.V. Tsvetkov, I.P. Beletskaya, *Organometallics* **2006**, *25*, 2750.

[C27] A.L. Boyes, I.R. Butler, S.C. Quayle, *Tetrahedron Lett.* **1998**, *39*, 7763.

[C28] (a) T.R. Krishna, N. Jayaraman, *Tetrahedron* **2004**, *60*, 10325;

(b) G.S. Smith, S.F. Mapolie, *J. Mol. Catal. A: Chem.* **2004**, *213*, 187.

[C29] (a) M.T. Reetz, G. Lohmar, R. Schwickardi, *Angew. Chem. Int. Ed.* **1998**, *37*, 481;

(b) M.T. Reetz, G. Lohmar, R. Schwickardi, *Angew. Chem. Int. Ed.* **1997**, *36*, 1526.

[C30] M.R. Eberhard, *Org. Lett.* **2004**, *6*, 2125.

[C31] N.T.S. Phan, M. Van der Sluys, C.W. Jones, *Adv. Synth. Catal.* **2006**, *348*, 609.

[C32] G.D. Frey, J. Schütz, E. Herdtweck, W.A. Herrmann, *Organometallics* **2005**, *24*, 4416.

[C33] N.G. Andersen, M. Parvez, R. McDonald, B.A. Keay, *Can. J. Chem.* **2004**, *82*, 141.

[C34] T. Rosner, J. Le Bars, A. Pfaltz, D.G. Blackmond, *J. Am. Chem. Soc.* **2001**, *123*, 1848.

[C35] (a) G.C. Fu, *Acc. Chem. Res.* **2008**, *41*, 1555;

(b) A.F. Littke, G.C. Fu, *J. Am. Chem. Soc.* **2001**, *123*, 6989.

D A Preparation of Planar-Chiral Multidonor Phosphanyl-Ferrocene Carboxamides and Their Application as Ligands for Palladium-Catalyzed Asymmetric Allylic Alkylation

Martin Lamač, Jiří Tauchman, Sascha Dietrich, Ivana Císařová, Heinrich Lang and Petr Štěpnička

Published in *Appl. Organometal. Chem.* **2010**, *24*, 326 – 331.

The issues presented in the subsequent section are the result of an inter-institutional cooperation with the research group of ac. Prof. Dr. Petr Štěpnička at Charles University in Prague (Czech Republic).

In this respect, the author of the present doctoral thesis synthesized and fully characterized the dendritic amidoamines **7** and (S_p,S_p,S_p)−**5** under supervision of Prof. Dr. Heinrich Lang in Chemnitz. The syntheses of the remaining compounds as well as the catalytic tests were performed by Martin Lamač, Jiří Tauchman and ac. Prof. Dr. Petr Štěpnička in Prague. The X-ray crystallographic investigations were accomplished by Dr. Ivana Císařová.

1. Introduction

The use of dendrimeric molecules as supporting scaffolds to catalytic systems has recently gained considerable attention largely because it can lead to multifunctional catalysts, which can be recycled while often retaining high activity and selectivity of their corresponding homogeneous, low-molecular weight counterparts. Dendrimers for catalytic applications, mostly with phosphane donor sites, are typically prepared with a single functional moiety in (or close to) the core of the hyperbranched structure, or with several functional units attached at the periphery. The latter approach is particularly attractive as it may result in unique materials showing unusual reactivity due to the formation of specific microcompartments within the highly functionalized structures. [D1]

In view of our previous work aimed at the preparation, coordination behaviour and catalytic chemistry of ferrocene-based phosphanylcarboxylic acids [D2] and the corresponding carboxamide derivatives, [D3] we recently synthesized dendrimer like assemblies containing several covalently bonded terminal 1´-(diphenylphosphanyl)ferrocen-1-yl groups at the exterior. [D4]

For the synthesis of the latter molecules, we made use of the amidation reaction between 1´-(diphenylphosphanyl)ferrocene-1-carboxylic acid (Hdpf) [D5, D2a] and the terminal NH_2 groups of first-generation poly(amidoamine) dendrimers (PAMAM). [D6, D7] Even these relatively simple compounds containing one to four phosphanylferrocenyl moieties exerted a distinct positive dendritic effect on the reaction rate in palladium-catalyzed Suzuki–Miyaura and Heck–Mizoroki reactions. This led us to design, prepare and study analogous compounds derived from the planar-chiral isomer of Hdpf, viz. (S_p)-2-(diphenylphosphanyl)ferrocene-1-carboxylic acid [(S_p)–**1**]. [D8]

With this contribution, we report on the preparation of several amides derived from (S_p)–**1** and small PAMAM-like amines or related model compounds (Scheme D1) and on their use as ligands in palladium-catalyzed asymmetric allylic alkylation. [D9] These newly prepared donors not only widen the scope of the chiral phosphanyl-carboxamide ligands synthesized so far from (S_p)–**1**, [D3e, D8a, D8b, D10] but also further demonstrate the alternative approach towards the preparation of chiral phosphanylferrocenyl dendrimers. [D11]

2. Results and Discussion

2.1. Syntheses and Characterization

The series of phosphanylferrocenyl amides was designed comprising both simple monoferrocenyl derivatives analogous to the compounds studied earlier [D3e] and their larger PAMAM-like congeners (Scheme D1). Compounds **2** – **5** were obtained by the reactions of (S_p)-2-(diphenylphosphanyl)ferrocene-1-carboxylic acid [(S_p)–**1**] [D8] with appropriate terminal amines in the presence of peptide coupling agents [D12] (Scheme D1).

The starting amines were synthesized as described in the literature (see Experimental) except for the precursor to compound **4**, which was obtained *via* the coupling of N-Boc protected 1,2-diaminoethane (**8**) and *β*-alanine (**9**) followed by removal of the protecting groups and was isolated as dihydrochloride **6** (Scheme D2).

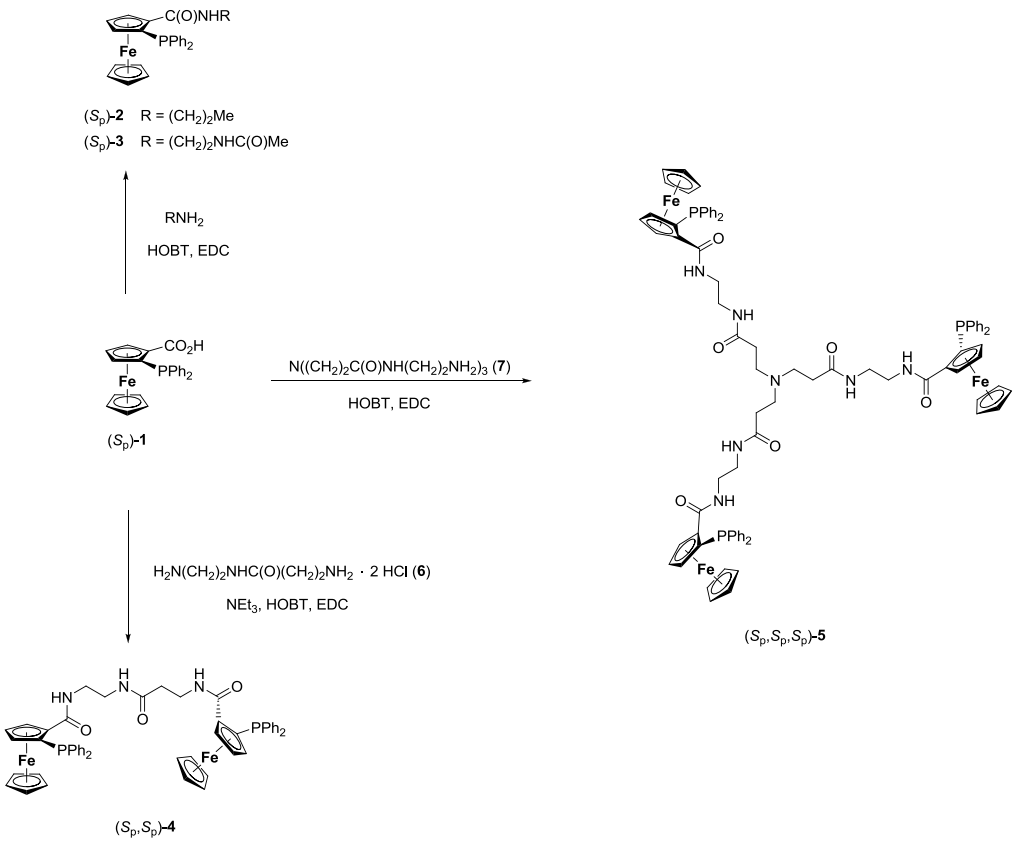

Scheme D1. Preparation of phosphane-amide ligands **2** – **5** (EDC = 1-ethyl-3-[3-(dimethylamino)propyl]carbodiimide, HOBT = 1-hydroxybenzotriazole).

The amidation reactions with small amines proceeded very well and afforded the products in good to excellent isolated yields. In the case of larger molecules, however, the isolation was complicated by chemical similarity and overall high polarity of the main and side products, which resulted in relatively lower yields (cf. the synthesis of compound **5**). Finally, an attempted preparation of a penta(amidoferrocenyl) derivative from $\{H_2N(CH_2)_2$-$NHC(O)(CH_2)_2\}_2NCH_2CH_2N\{(CH_2)_2C(O)NH(CH_2)_2NH_2\}CH_2CH_2N\{(CH_2)_2C(O)NH(CH_2)_2$ $NH_2\}_2$ analogously to the synthesis of **5** was unsuccessful due to complications during the isolation step.

Amido-phosphanes **2** – **5** were characterized by multinuclear NMR spectroscopy, electrospray (ESI) mass spectrometry and by optical rotation. In the ^{1}H and ^{13}C NMR spectra, they showed signals typical for 1,2-disubstituted ferrocene moieties and signals due to the amide substituents. The ^{13}C NMR spectra further comprised resonances of the amide C═O groups due to the ferrocenyl-bound amide units (a doublet with $^{3}J_{PC}$ = 3 – 4 Hz) and the organic linkers (singlets), all in the narrow range δ_C ca 170.3 – 173.2. $^{31}P\{^{1}H\}$ NMR spectra of **2**, **3** and **5** displayed single resonances at δ_P around -20, whereas the unsymmetric diphosphane **4** expec-

tedly showed two signals. On the other hand, the unsymmetric diphosphane **4** showed two signals at very similar positions (δ_P -19.7 and -19.8). In ESI mass spectra, compounds **2** – **5** gave rise to characteristic pseudomolecular ions ($[M + Z]^+$, Z = H, Na or K; $[M - H]^-$).

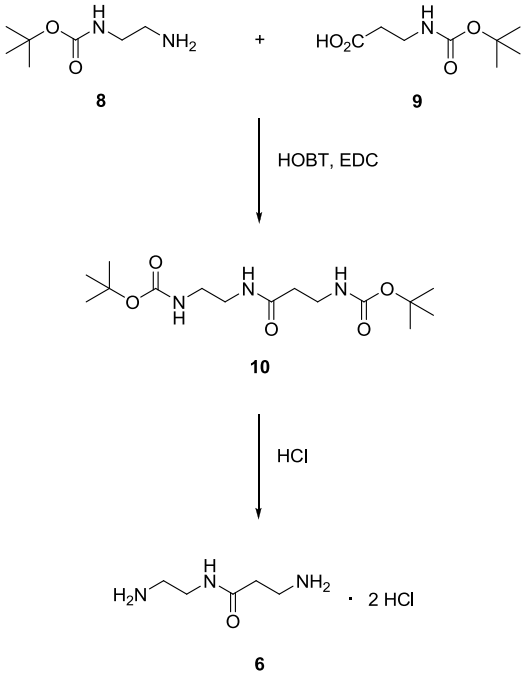

Scheme D2. Preparation of the starting amido-diamine dihydrochloride **6** (see legend to Scheme D1).

2.2. Solid-State Structure of (S_p)–2

The solid-state structure of (S_p)–**2** was established by single-crystal X-ray diffraction analysis. A view of the molecular structure is presented in Figure D1 together with selected geometric data. The structure of (S_p)–**2** is not unexpected and corroborates both the connectivity and chirality at the ferrocene moiety. Besides, the molecular geometry compares well with the structural data reported for (S_p)-1-(*N*-benzylcarbamoyl)-2-(diphenylphosphanyl)ferrocene [D3e] and (S_p)-2-(diphenylphosphanoyl)-1-ferrocene-1-carboxylic acid. [D8c]

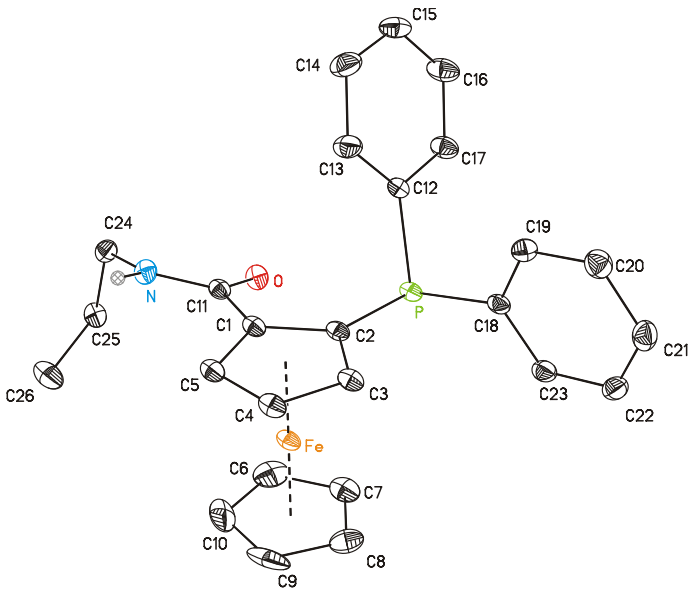

Figure D1. View of the molecular structure of (S_p)–**2** showing the atom labeling scheme. Displacement ellipsoids are drawn at the 30 % probability level. Selected distances and angles: Fe–Cg1 1.6443(7), Fe–Cg2 1.653(1), P–C2 1.826(1), P–C12 1.837(2), P–C18 1.850(2), C1–C11 1.487(2), C11–O 1.240(2), C11–N 1.343(2), N–C24 1.465(2) Å;<Cp1,Cp2 1.8(1), C2–C1–C11 124.7(1), C5–C1–C11 126.9(1), C1–C11–O 121.4(1), C1–C11–N 115.4(1), O–C11–N 123.2(1), C11–N–C24 121.2(1), C1–C2–P 126.9(1), C3–C2–P 126.7(1), C2–P–C12 103.23(6), C2–P–C18 97.60(7), C12–P–C18 99.29(7). The ring planes are defined as follows: Cp1 = C(1–5), Cp2 = C(6–10); Cg1 and Cg2 denote the respective ring centroids.

The ferrocene moiety in (S_p)–**2** exerts balanced Fe–Cg distances and negligible tilting [dihedral angle of the mean cyclopentadienyl ring planes being 1.8(1)°]. As indicated by the relatively minor differences in the pairs of adjacent C2/C5–C1–C11 and C1/C3–C2–P angles being 2.2 and 0.2°, respectively and further by the torsion angle C11–C1–C2–P being 0.6(2)°, the substituents bind symmetrically to the ferrocene scaffold without any notable torsional deformation. On the other hand, the carbamoyl group (C11,O,N) is rotated from the plane of its bonding cyclopentadienyl ring by as much as 20.5(2)° with its bulkier $N(CH_2)_2CH_3$ moiety pointing above the ferrocene unit and away from the PPh_2 group. In the crystal, individual molecules of (S_p)–**2** aggregate into infinite chains by means of N–H· · ·O hydrogen bonds between proximal molecules related by crystallographic 2_1 screw axis (Figure D2). A similar packing arrangement has been noted in the structure of the aforementioned *N*-benzyl amide.

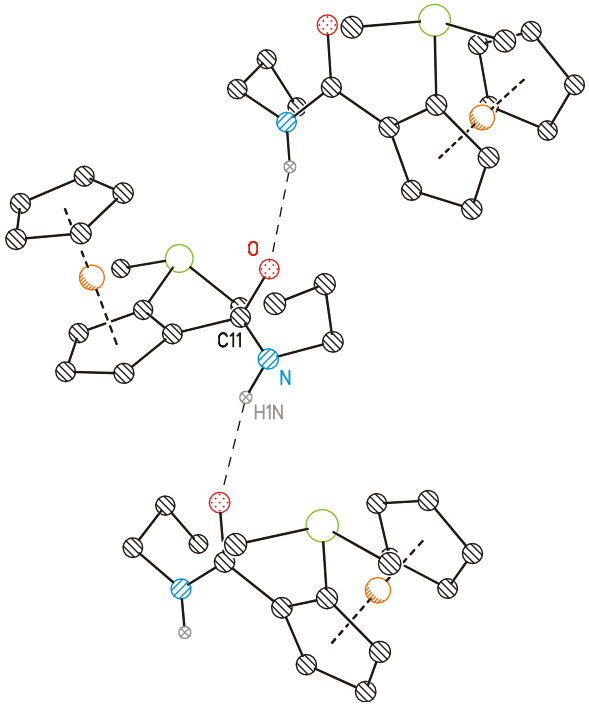

Figure D2. A section of the infinite hydrogen bonded chain in the structure of (S_p)–**2**. Only pivotal phenyl ring carbons and H-bonded hydrogen atoms are shown for clarity. Hydrogen bond parameters, N–H1N· · ·O´:N· · ·O´ = 3.006(2) Å, N–H1N· · ·O´ = 161° (prime-labeled atoms are generated by the (2 - *x*, *y* - 1/2, 1 - *z*) symmetry operation).

2.3. Catalytic Tests

Although asymmetric palladium-catalyzed allylic alkylation is both a valuable synthetic tool and a widely used benchmark test, [D9] there have been published only a few reports concerning the use of chiral, dendrimer-supported phosphanes as ligands for this reaction. [D11d, D13] In the present case, we have employed asymmetric allylic alkylation because it allows for a comparison of the newly prepared multidonor phosphanylferrocene carboxamides with the related ligands. For testing, we used the alkylation of the symmetrical substrate 1,3-diphenylprop-2-en-1-yl acetate (**11**) with *in-situ* generated malonate anion (Scheme D3).

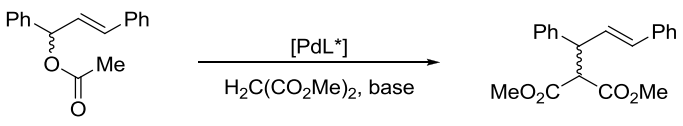

11 **12**

Scheme D3. The model asymmetric allyic alkylation reaction.

The results summarized in Table D1 clearly show that there was only relatively minor variation in the *ee* upon increasing the number of the chiral 2-phosphanylferrocenyl units per li-

gand molecule, the (*R*)–**12** always being the major product. In terms of enantioselectivity, the reaction outcome was similar to or slightly better than that achieved with simple benzylic amides derived from acid (S_p)–**1** [D3e] and considerably better than that reported for analogous, donor-unsymmetric chiral-pocket bisamides. [D10a]

Table D1. Application of the chiral phosphano-amides **2** – **5** to palladium-catalyzed enantioselective allylic alkylation[a].

Entry	Ligand	Additive	Conversion	ee[b]
1	(S_p)−**2**	None	65	82
2	(S_p)−**3**	None	70	91
3	(S_p,S_p)−**4**	None	7	87
4	(S_p,S_p,S_p)−**5**	None	22	88
5	(S_p)−**3**	LiOAc	13	84
6	(S_p)−**3**	NaOAc	45	92
7	(S_p)−**3**	KOAc	33	92
8	(S_p)−**3**	RbOAc	57	93
9	(S_p)−**3**	CsOAc	96	91

[a] The results are an average of two independent runs. For detailed conditions, see Experimental.
[b] (*R*)–**12** was the dominating component of the enantiomeric mixture in all cases.

On the other hand, the conversions achieved with ligands **2** – **5** were far from complete after 24 hrs and varied greatly with the ligand structure, being lower with the larger ligands (Table D1). Fortunately, however, the conversion could be varied significantly upon adding alkali-metal acetates a catalytic base additives to *N*,*O*-bis(trimethylsilyl)acetamide. With ligand (S_p)–**3**, which performed best in the series of ligands tested and caesium acetate as the base additive, the conversion was nearly complete within 24 hrs while the degree of asymmetric induction remained unaffected (Table D1).

3. Conclusions

Oligoamides bearing one to three (S_p)-2-(diphenylphosphanyl)ferrocen-1-yl pendant groups at the periphery are readily available *via* amide coupling of (S_p)-2-(diphenylphosphanyl)ferrocene-1-carboxylic acid with appropriate terminal amines. When combined with bis[chlorido(η^3-allyl)palladium(II)] as a metal source, these donors give rise to efficient

catalysts for asymmetric allylic alkylation of 1,3-diphenylallyl acetate. Whereas the enantioselectivity varies only slightly with the ligand structure (maximum *ee* being 93 %), the reaction rate changes considerably more, being lower with the larger donor molecules. However, the reaction can be improved by adding an appropriate alkalimetal acetate as a catalytic base additive.

4. Experimental

4.1. Materials and Methods

All syntheses were performed under an argon atmosphere. Dichloromethane was dried over anhydrous potassium carbonate and distilled under argon. Acetone and methanol were distilled under argon. Acid (S_p)–**1**, [D8c] *N*-(2-aminoethyl)acetamide, [D14] *tert*-butyl *N*-(2-aminoethyl)carbamate (**8**) [D15] and 3-[(*tert*-butoxycarbonyl)amino]propanoic acid (**9**) [D16] were prepared according to the literature procedures.

NMR spectra were recorded on a Varian Unity Inova 400 spectrometer at 25 °C (^{1}H, 399.95; ^{13}C, 100.58 and ^{31}P, 161.90 MHz). Chemical shifts (δ/ppm) are given relative to internal tetramethylsilane (^{13}C and ^{1}H) or to external 85 % aqueous H_3PO_4 (^{31}P). Low-resolution electrospray (ESI) mass spectra were measured with a Bruker Esquire 3000 spectrometer on methanol solutions whereas the high-resolution data were obtained with a Thermo Fisher Scientific LCQ Fleet spectrometer. Optical rotations were determined with an Autopol III automatic polarimeter (Rudolph Research) at room temperature.

4.2. Preparation of Simple Amides. A General Procedure

N-(3-Dimethylaminopropyl)-*N*-ethylcarbodiimide (EDC) was slowly added to a mixture of acid (S_p)–**1**, 1-hydroxybenzotriazole (HOBT) and dry dichloromethane (10 – 15 mL) while cooling in an ice bath. The resultant mixture was stirred at 0 °C for 5 min, whereupon the solids dissolved to give a clear orange-red solution. The appropriate amine was introduced (dissolved in a small amount of dichloromethane) and stirring was continued at room temperature for 20 h. Then, the mixture was washed successively with 1 M HCl, saturated aqueous $NaHCO_3$ solution and with brine. The organic phase was separated, dried over $MgSO_4$ and evaporated under vacuum, leaving and orange residue, which was subsequently purified by column chromatography (silica gel, dichloromethane-methanol 20:1, v/v) to give the desired amide after evaporation under vacuum.

4.2.1. (S_p)-2-(Diphenylphosphanyl)-1-(*N*-*n*-propylcarbamoyl)ferrocene [(S_p)–**2**]

Starting with (S_p)–**1** (208 mg, 0.50 mmol), HOBT (76 mg, 0.51 mmol), EDC (0.15 mL, 0.75 mmol) and *n*-propylamine (35 mg, 0.60 mmol), the general procedure afforded amide (S_p)–**2** as an orange oil, which slowly crystallized at 4 °C. Yield: 205 mg (91 %). $[\alpha]_D$ = -201° (*c* = 1.0, $CHCl_3$); ^{1}H NMR ($CDCl_3$): δ = 0.87 (t, $^3J_{HH}$ = 7.5 Hz, 3 H, C*H*$_3$), 1.50 (m, 2 H, C*H*$_2$), 3.30 (m, 2 H, C*H*$_2$), 3.79 (m, 1 H, C_5H_3), 4.11 (s, 5 H, C_5H_5), 4.45 (m, 1 H, C_5H_3), 5.18 (m, 1 H, C_5H_3), 7.12 – 7.59 (m, 11 H, P*Ph*$_2$ and N*H*); ^{13}C{^{1}H} NMR ($CDCl_3$): δ = 11.45 (*C*H$_3$), 22.91, 41.37 (2 · *C*H$_2$), 70.79 (*C*$_5$H$_5$), 71.35 (C_5H_3 *C*H), 73.79 (d, J_{PC} = 2 Hz, C_5H_3 *C*H), 74.25 (d, J_{PC} = 4 Hz, C_5H_3 *C*H), 74.72 (d, J_{PC} = 9 Hz, C_5H_3 *C*$_{ipso}$), 81.35 (d, J_{PC} = 20 Hz, C_5H_3 *C*$_{ipso}$), 128.36 (d, $^3J_{PC}$ = 7 Hz, PPh_2 *C*H$_m$), 128.40 (PPh_2 *C*H$_p$) 128.43 (d, $^3J_{PC}$ = 6 Hz, PPh_2 *C*H$_m$), 129.75 (PPh_2 *C*H$_p$), 132.10 (d, $^2J_{PC}$ = 17 Hz, PPh_2 *C*H$_o$), 135.13 (d, $^2J_{PC}$ = 21 Hz, PPh_2 *C*H$_o$), 135.92, 137.84 (2 · d, $^1J_{PC}$ = 6 Hz, PPh_2 *C*$_{ipso}$), 170.04 (d, $^3J_{PC}$ = 4 Hz, *C*ONH); ^{31}P{^{1}H} NMR ($CDCl_3$) = δ -20.1 (s); MS ESI$^+$: *m/z* = 456 ([M + H]$^+$), 478 ([M + Na]$^+$), 494 ([M + K]$^+$); MS ESI$^-$: *m/z* = 454 ([M - H]$^-$); HR MS (ESI$^+$) calcd. for $C_{26}H_{27}{}^{56}FeNOP$ ([M + H]$^+$) 456.1174, found 456.1172.

4.2.2. (S_p)-2-(Diphenylphosphanyl)-1-{*N*-[2-(acetylamino)ethyl]carbamoyl}ferrocene [(S_p)–**3**]

Following the general procedure, acid (S_p)–**1** (83 mg, 0.20 mmol), HOBT (30 mg, 0.22 mmol), EDC (0.05 mL, 0.30 mmol) and *N*-(2-aminoethyl)acetamide (26 mg, 0.25 mmol) gave amide (S_p)–**3** as an orange solid foam. Yield: 62 mg (62 %). $[\alpha]_D$ = -147° (*c* = 1.0, $CHCl_3$); ^{1}H NMR ($CDCl_3$): δ = 1.84 (s, 3 H, C*H*$_3$), 3.25 – 3.59 (m, 4 H, C*H*$_2$), 3.81 (m, 1 H, C_5H_3), 4.12 (s, 5 H, C_5H_5), 4.47 (m, 1 H, C_5H_3), 5.11 (m, 1 H, C_5H_3), 6.02 (br s, 1 H, N*H*COMe), 7.13 – 7.58 (m, 11 H, P*Ph*$_2$ and C_5H_3CONH); ^{13}C{^{1}H} NMR ($CDCl_3$): δ = 23.21 (*C*H$_3$), 39.45, 40.87 (2 · *C*H$_2$), 70.91 (*C*$_5$H$_5$), 71.65 (C_5H_3 *C*H), 73.18 (d, J_{PC} = 2 Hz, C_5H_3 *C*H), 74.46 (d, J_{PC} = 4 Hz, C_5H_3 *C*H), 75.42 (d, J_{PC} = 10 Hz, C_5H_3 *C*$_{ipso}$), 80.41 (d, J_{PC} = 18 Hz, C_5H_3 *C*$_{ipso}$), 128.40 – 128.55 (m, PPh_2 *C*H$_m$ and *C*H$_p$), 129.83 (PPh_2 *C*H$_p$), 131.87 (d, $^2J_{PC}$ = 17 Hz, PPh_2 *C*H$_o$), 135.13 (d, $^2J_{PC}$ = 21 Hz, PPh_2 *C*H$_o$), 135.82, 138.18 (2 · d, $^1J_{PC} \approx$ 6 Hz, PPh_2 *C*$_{ipso}$), 170.66 (CH_3*C*ONH), 171.70 (d, $^3J_{PC} \approx$ 3 Hz, C_5H_3*C*ONH); ^{31}P{^{1}H} NMR ($CDCl_3$): δ = -19.8 (s); MS ESI$^+$: *m/z* = 499 ([M + H]$^+$), 521 ([M + Na]$^+$), 537 ([M + K]$^+$); MS ESI$^-$: *m/z* = 497 ([M - H]$^-$); HR MS (ESI$^+$) calcd. for $C_{27}H_{27}{}^{56}FeN_2O_2P$ (M$^+$) 498.1160, found 498.1156.

4.3. Preparation of 2-[*N*-(2-aminoethyl)carbamoyl]ethylamine dihydrochloride (6)

A suspension of 3-[(*tert*-butoxycarbonyl)amino]propanoic acid (**9**; 1.89 g, 10.0 mmol) and HOBT (1.5 g, 11.0 mmol) in dichloromethane (100 mL) was cooled in an ice bath. EDC (2.2 ml, 12.0 mmol) was slowly introduced and the mixture was stirred at 0 °C for 5 min. To the resulting clear solution, a solution of *tert*-butyl (2-aminoethyl)carbamate (**8**; 1.92 g, 12.0 mmol) in dichloromethane (20 mL) was added and the reaction mixture was stirred at room temperature for 20 h. Then, it was washed with saturated aqueous citric acid and brine (50 mL each). The organic phase was dried over $MgSO_4$ and evaporated under vacuum, leaving a pale yellow viscous oil. Subsequent purification by column chromatography (silica gel, dichloromethane-methanol, 10:1 v/v) gave **10** as a colourless solid. Yield: 2.96 g (89 %). ^{1}H NMR ($CDCl_3$): δ = 1.43, 1.44 (2 · s, 9 H, C*Me*$_3$), 2.39 (t, ^3J = 5.8 Hz, 2 H, COC*H*$_2$), 3.20 – 3.45 (m, 6 H, C*H*$_2$), 4.99, 5.21, 6.40 (3 · br s, 1 H, N*H*); HR MS (ESI$^+$) calcd. for $C_{15}H_{29}N_3NaO_5$ ([M + Na]$^+$) 354.1999, found 354.2001.

In the next step, the Boc-protected derivative **10** (500 mg, 1.51 mmol) was dissolved in acetone (30 mL, in air) and dry HCl gas was bubbled through the stirred solution for 15 min, causing separation of a fine white precipitate. The mixture was stirred for another 2 hrs and then evaporated to dryness under vacuum. The resulting colourless solid was identified as pure dihydrochloride **6** and was used directly in the following synthesis without any further purification. ^{1}H NMR (D_2O): δ = 2.73 (t, ^3J = 6.7 Hz, 2 H, C*H*$_2$), 3.17 (t, ^3J = 5.8 Hz, 2 H, C*H*$_2$), 3.29 (t, ^3J = 6.6 Hz, 2 H, C*H*$_2$), 3.54 (t, ^3J = 5.9 Hz, 2 H, C*H*$_2$), 4.77 (br s, 6 H, N*H*$_3^+$); HR MS (ESI$^+$) calcd. for $C_5H_{14}N_3O$([**6**-H-2Cl]$^+$, *i.e.* monodeprotonated cation) 132.1131, found 132.1130.

4.4. Preparation of Compound (S_p,S_p)–4

EDC (0.05 mL, 0.30 mmol) was added to a mixture of (S_p)–**1** (83 mg, 0.20 mmol), HOBT (30 mg, 0.22 mmol) and dichloromethane (10 mL) with cooling in an ice bath. After stirring for 5 min, the resulting clear orange-red solution of the pre-formed active ester was added to a suspension of compound **6** (35 mg, 0.15 mmol) in triethylamine (0.1 mL, 0.72 mmol) and dichloromethane (10 mL). The heterogeneous mixture was stirred at room temperature for 22 hrs and worked up in the same manner as described in the general procedure. Yield: 68 mg (74 %) of (*S*p,*S*p)–**4**; an orange solid foam.

4.5. Preparation of Amino-Amide 7

Compound **7** was obtained by a two-step procedure as reported previously by Tomalia *et al*. [D17] Methyl acrylate (14.5 g, 0.168 mol) and excess 1,2-diaminoethane (49.0 g, 0.815 mol) were successively added to a solution of ammonia in methanol (4 mL, 0.028 mol) and the reaction mixture was stirred at room temperature for 72 h. Subsequent removal of the volatiles under vacuum yielded **7** as a colourless oil (10.0 g, 99 % based on the ammonia).

4.6. Preparation of Compound (S_p,S_p,S_p)–5

Acid (S_p)–**1** (230 mg, 0.55 mmol) and HOBT (75 mg, 0.55 mmol) were added to a solution of **7** (64 mg, 0.18 mmol) in dichloromethane (20 mL) while cooling in an ice bath. After stirring at 0 °C for 1 h, a solution of EDC (100 mg, 0.65 mmol) in dichloromethane (5 mL) was introduced slowly. The resulting mixture was stirred at room temperature overnight, washed with aqueous ammonium chloride solution (0.5 M), dried over $MgSO_4$ and evaporated under reduced pressure. The product was isolated by column chromatography on alumina using dichloromethane-ethanol (100:1 v/v) as the eluent. Subsequent evaporation afforded amide (*S*p,*S*p,*S*p)–**5** as an orange amorphous solid. Yield: 150 mg (54 %). ^{1}H NMR ($CDCl_3$): δ = 2.19 (unresolved t, 2 H), 2.44 – 2.69 (br m, 2 H), 3.18 – 3.37 (m, 4 H) (4 · C*H*$_2$); 3.78 (m, 1 H, C_5H_3), 4.13 (s, 5 H, C_5H_5), 4.42 (t, J = 2.6 Hz, 1 H, C_5H_3), 5.08 m, 1 H, C_5H_3), 7.07 (br unresolved t, 1 H, N*H*), 7.12 – 7.57 (m, 11 H, P*Ph*$_2$ + N*H*); ^{13}C{^{1}H} NMR ($CDCl_3$): δ = 33.86 (br), 39.61, 40.01 and 49.90 (4 · *C*H$_2$), 70.96 (*C*$_5$H$_5$), 71.51 (C$_5$H$_3$ *C*H), 72.51 (d, J_{PC} = 2 Hz, C$_5$H$_3$ *C*H), 74.42 (d, J_{PC} = 4 Hz, C$_5$H$_3$ *C*H), 80.37 (d, J_{PC} = 17 Hz, C$_5$H$_3$ *C*$_{ipso}$), 128.1 – 128.5 (m, PPh$_2$, four *C*H$_m$ + one *C*H$_p$), 129.45 (PPh$_2$ *C*H$_p$), 132.04 (d, $^2J_{PC}$ = 18 Hz, PPh$_2$ *C*H$_o$), 135.13 (d, $^2J_{PC}$ = 21 Hz, PPh$_2$ *C*H$_o$), 136.97, 138.98 (2 · d, $^1J_{PC}$ = 8 Hz, PPh$_2$ *C*$_{ipso}$), 171.17 (d, $^3J_{PC}$ = 3 Hz, C$_5$H$_3$*C*ONH), 173.2 (br, CH$_2$*C*ONH) (note: the signal due to C$_5$H$_3$ *C*$_{ipso}$ is probably obscured by another resonance); ^{31}P{^{1}H} NMR ($CDCl_3$): δ = -19.6; MS ESI$^+$: *m/z* = 1548 ([M + H]$^+$), 1570 ([M + Na]$^+$), 1586 ([M + K]$^+$); HR MS (ESI$^+$) calcd. for $C_{84}H_{85}{}^{56}Fe_3N_7O_6P_3$ ([M + H]$^+$) 1548.3817, found 1548.3818.

4.7. Asymmetric Allylic Alkylation. A General Procedure

Ligand (12.5 μmol), [{Pd(η^3-C_3H_5)Cl}$_2$] (2.3 mg, 6.3 μmol) and alkali metal acetate (25 μmol; if appropriate) were mixed with dry dichloromethane (3 mL) and the mixture was stirred at room temperature for 15 min. Racemic 1,3-diphenylprop-2-en-1-yl acetate (**11**; 63 mg, 0.25 mmol) was introduced next, followed after stirring for another 5 min by *N*,*O*-bis(trimethylsilyl)acetamide (BSA; 0.19 mL, 0.75 mmol) and dimethyl malonate (0.09 mL, 0.75 mmol). The reaction mixture was stirred at room temperature for 24 hrs and then washed with saturated aqueous NH_4Cl solution (2 · 5ml). The organic layer was separated, dried over $MgSO_4$ and concentrated under vacuum. Subsequent purification by flash chromatography (silica gel; hexane-ethyl acetate, 3:1 v/v) afforded the mixture of the alkylation product and the starting acetate **11**. The conversions were determined by ^{1}H NMR spectroscopy. Enantiomeric excesses were established from ^{1}H NMR spectra recorded in C_6D_6 in the presence of the chiral lanthanide shift reagent tris(3-trifluoroacetyl-*d*-camphorato)-europium(III). The configuration of the major component was assigned on the basis of optical rotation of the mixture. [D18]

4.8. X-ray Crystallography

Single-crystals of (S_p)–**2** suitable for X-ray diffraction analysis were selected directly from the reaction batch (orange-brown block, 0.38 × 0.50 × 0.55 mm^3). Full-set diffraction data ($\pm h$ $\pm k$ $\pm l$; $2\theta \leq 55°$) were collected with a Nonius KappaCCD image plate diffractometer equipped with a Cryostream Cooler (Oxford Cryosystems) at 150(2) K using graphite monochromatized MoK_α radiation (λ = 0.71073 Å) and were analysed with the HKL program package. [D19]

The phase problem was solved by direct methods (SIR97 [D20]) and the structure was refined by full-matrix least squares procedure based on F^2 (SHELXL97 [D21]). All non-hydrogen atoms were refined with anisotropic displacement parameters. The amide hydrogen atom (H1N) was identified on a difference density map and refined as a riding atom with U_{iso}(H1N) = 1.2 U_{eq}(N). The remaining hydrogen atoms were included in calculated positions and refined as riding atoms with U_{iso}(H) assigned to a multiple of U_{eq}(C) of their bonding carbon atom. Geometric parameters and structural drawings were obtained with a recent version of PLATON program. [D22]

Crystallographic data: $C_{26}H_{26}FeNOP$, M = 455.3g mol^{-1}, monoclinic, space group $P2_1$ (no. 4), a = 9.6809(1), b = 9.6817(2), c = 11.8994(2) Å; β = 100.897(1)°, V = 1095.19(3) Å^3, Z = 2, D = 1.381 g mL^{-1}, μ(Mo K$_\alpha$) = 0.779 mm^{-1}; 28 930 diffractions of which 5026 were unique and 4895 observed according to $I_o > 2\sigma(I_o)$ criterion (R_{int} = 1.65 %); 272 parameters, R (observed diffractions) = 2.15 %, R (all data) = 2.26 %, wR (all data) = 5.31 %, Flack´s enantiomorph parameter: 0.002(9).

The crystallographic data for (S_p)-**2** have been deposited at the Cambridge Crystallographic Centre as supplementary publication CCDC-749434. This data can be obtained free of charge from the Cambridge Crystallographic Centre, *via* http://www.ccdc.cam.ac.uk/data request/cif.

5. Acknowledgements

This work was financially supported by the Czech Science Foundation (project no. 104/09/0561), the Deutsche Forschungsgemeinschaft and the Fond der Chemischen Industrie. It is also a part of the long-term research projects supported by the Ministry of Education of the Czech Republic (project nos LC06070 and MSM0021620857).

6. References

[D1] For recent reviews, see: (a) A.-M. Caminade, P. Servin, R. Laurent, J.-P. Majoral, *Chem. Soc. Rev.* **2008**, *37*, 56;

(b) R. van Heerbeek, P.C.J. Kamer, P.W.N.M. van Leeuwen, J.N.H. Reek, *Chem. Rev.* **2002**, *102*, 3717;

(c) A. Berger, R.J.M.K. Gebbink, G. van Koten, *Top. Organomet. Chem.* **2006**, *20*, 1;

(d) J.K. Kassube, L.H. Gade, *Top. Organomet. Chem.* **2006**, *20*, 61;

(e) B. Helms, J.M.J. Fréchet, *Adv. Synth. Catal.* **2006**, *348*, 1125;

(f) D. Méry, D. Astruc, *Coord. Chem. Rev.* **2006**, *250*, 1965;

(g) J.N.H. Reek, S. Arévalo, R. van Heerbeek, P.C.J. Kamer, P.W.N.M. van Leeuwen, *Adv. Catal.* **2006**, *49*, 71.

[D2] (a) P. Stepnicka, *Eur. J. Inorg. Chem.* **2005**, 3787; (review).

For recent examples, see: (b) P. Stepnicka, I. Cisarova, *Collect. Czech. Chem. Commun.* **2006**, *71*, 279;

(c) M. Lamac, I. Cisarova, P. Stepnicka, *Eur. J. Inorg. Chem.* **2007**, 2274;

(d) M. Lamac, I. Cisarova, P. Stepnicka, *Collect. Czech. Chem. Commun.* **2007**, *72*, 985;

(e) J. Kühnert, M. Lamac, T. Rüffer, B. Walfort, P. Stepnicka, H. Lang, *J. Organomet. Chem.* **2007**, *692*, 4303;

(f) C. Bianchini, A. Meli, W. Oberhauser, A.M. Segarra, E. Passaglia, M. Lamac, P. Stepnicka, *Eur. J. Inorg. Chem.* **2008**, 441;

(g) M. Lamac, J. Cvacka, P. Stepnicka, *J. Organomet. Chem.* **2008**, *693*, 3430;

(h) M. Lamac, I. Cisarova, P. Stepnicka, *New J. Chem.* **2009**, *33*, 1549;

(i) J. Kühnert, P. Ecorchard, H. Lang, *Eur. J. Inorg. Chem.* **2008**, 5125.

[D3] (a) D. Drahonovsky, I. Cisarova, P. Stepnicka, H. Dvorakova, P. Malon, D. Dvorak, *Collect. Czech. Chem. Commun.* **2001**, *66*, 588;

(b) L. Meca, D. Dvorak, J. Ludvik, I. Cisarova, P. Stepnicka, *Organometallics* **2004**, *23*, 2541;

(c) P. Stepnicka, J. Schulz, I. Cisarova, K. Fejfarova, *Collect. Czech. Chem. Commun.* **2007**, *72*, 453;

(d) J. Kühnert, M. Dusek, J. Demel, H. Lang, P. Stepnicka, *Dalton Trans.* **2007**, 2802;

(e) M. Lamac, J. Tauchman, I. Cisarova, P. Stepnicka, *Organometallics* **2007**, *26*, 5042;

(f) J. Kühnert, I. Cisarova, M. Lamac, P. Stepnicka, *Dalton Trans.* **2008**, 2454;

(g) J. Tauchman, I. Cisarova, P. Stepnicka, *Organometallics* **2009**, *28*, 3288;

(h) J. Schulz, I. Cisarova, P. Stepnicka, *J. Organomet. Chem.* **2009**, *694*, 2519;

(i) P. Stepnicka, M. Krupa, M. Lamac, I. Cisarova, *J. Organomet. Chem.* **2009**, *694*, 2987.

[D4] J. Kühnert, M. Lamac, J. Demel, A. Nicolai, H. Lang, P. Stepnicka, *J. Mol. Catal. A: Chem.* **2008**, *285*, 41.

[D5] J. Podlaha, P. Stepnicka, J. Ludvik, I. Cisarova, *Organometallics* **1996**, *15*, 543.

[D6] D.A. Tomalia, H. Baker, J. Dewald, M. Hall, G. Kallos, S. Martin, J. Roeck, J. Ryder, P. Smith, *Polym. J.* **1985**, *17*, 117.

[D7] For the use of phosphane-terminated PAMAM dendrimers in catalysis, see: (a) S.C. Bourque, F. Maltais, W.-J. Xiao, O. Tardif, H. Alper, P. Arya, L.E. Manzer, *J. Am. Chem. Soc.* **1999**, *121*, 3035;

(b) H. Alper, P. Arya, S.C. Bourque, G.R. Jefferson, L.E. Manzer, *Can. J. Chem.* **2000**, *78*, 920;

(c) A. Gong, Q. Fan, Y. Chen, H. Liu, C. Chen, F. Xi, *J. Mol. Catal. A: Chem.* **2000**, *159*, 225;

(d) S. Antebi, P. Arya, L.E. Manzer, H. Alper, *J. Org. Chem.* **2002**, *67*, 6623;

(e) Y. Ribourdouille, G.D. Engel, M. Richard-Plouet, L.H. Gade, *Chem. Commun.* **2003**, 1228;

(f) J.P.K. Reynhardt, H. Alper, *J. Org. Chem.* **2003**, *68*, 8353;

(g) P.P. Zweni, H. Alper, *Adv. Synth. Catal.* **2004**, *346*, 849;

(h) J.P.K. Reynhardt, Y. Yang, A. Sayari, H. Alper, *Chem. Mater.* **2004**, *16*, 4095;

(i) R. Touzani, H. Alper, *J. Mol. Catal. A: Chem.* **2005**, *227*, 197;

(j) J.P.K. Reynhardt, Y. Yang, A. Sayari, H. Alper, *Adv. Synth. Catal.* **2005**, *347*, 1379;

(k) P. Li, S. Kawi, *J. Catal.* **2008**, *257*, 23;

(l) J.K. Kassube, L.H. Gade, *Adv. Synth. Catal.* **2009**, *351*, 739;

(m) M. Bernechea, E. de Jesus, C. Lopez-Mardomingo, P. Terreros, *Inorg. Chem.* **2009**, *48*, 4491.

[D8] (a) J.M. Longmire, B. Wang, X. Zhang, *Tetrahedron Lett.* **2000**, *41*, 5435;

(b) S.-L. You, X.-L. Hou, L.-X. Dai, B.-X. Cao, J. Sun, *Chem. Commun.* **2000**, 1933;

(c) P. Stepnicka, *New J. Chem.* **2002**, *26*, 567.

[D9] (a) B.M. Trost, D.L. van Vranken, *Chem. Rev.* **1996**, *96*, 395;

(b) B.M. Trost, M.L. Crawley, *Chem. Rev.* **2003**, *103*, 2921;

(c) B.M. Trost, *J. Org. Chem.* **2004**, *69*, 5813;

(d) T. Hayashi, Asymmetric allylic substitution and grignard cross-coupling, in *Catalytic Asymmetric Synthesis* (Ed.: I. Ojima), chapter 7.1, pp. 325, VCH: New York, **1993**;

(e) G. Helmchen, *J. Organomet. Chem.* **1999**, *576*, 203;

(f) T. Hayashi, Asymmetric catalysis with chiral ferrocenylphosphine ligands, in *Ferrocenes: Homogeneous Catalysis, Organic Synthesis, Materials Science* (Eds.: A. Togni, T. Hayashi), chapter 2, pp. 105, VCH: Weinheim, **1995**.

[D10] (a) S.-L. You, X.-L.Hou, L.-X. Dai, *J. Organomet. Chem.* **2001**, *637 − 639*, 762;

(b) S.-L. You, X.-L. Hou, L.-X. Dai, X.-Z. Zhu, *Org. Lett.* **2001**, *3*, 149;

(c) J.M. Longmire, B. Wang, X. Zhang, *J. Am. Chem. Soc.* **2002**, *124*, 13400.

[D11] The approaches used to date are the amidation reaction between carboxy-terminated dendrimers with chiral ferrocene diphosphanes equipped with amine anchoring groups: (a) C. Köllner, B. Pugin, A. Togni, *J. Am. Chem. Soc.* **1997**, *120*, 10274;
(b) R. Schneider, C. Köllner, I. Weber, A. Togni, *Chem. Commun.* **1999**, 2415;
(c) C. Köllner, A. Togni, *Can. J. Chem.* **2001**, *79*, 1762;
and condensation between a 4-hydroxyphenyl group attached to a chiral ferrocene molecule and terminal -P(S)Cl_2 group of a dendrimer: (d) L. Routaboul, S. Vincendeau, C.-O. Turrin, A.-M. Caminade, J.-P. Majoral, J.-C. Daran, E. Manoury, *J. Organomet. Chem.* **2007**, *692*, 1064.

[D12] H.-B. Kraatz, *J. Inorg. Polym. Mater.* **2005**, *15*, 83.

[D13] R. Laurent, A.-M. Caminade, J.-P. Majoral, *Tetrahedron Lett.* **2005**, *46*, 6503.

[D14] M. Jasinski, G. Mloston, P. Mucha, A. Linden, H. Heimgartner, *Helv. Chim. Acta* **2007**, *90*, 1765.

[D15] A.J. Lowe, G.A. Dyson, F.M. Pfeffer, *Eur. J. Org. Chem.* **2008**, 1559.

[D16] J.A. McCubbin, M.L. Maddess, M. Lautens, *Org. Lett.* **2006**, *8*, 2993.

[D17] D.A. Tomalia, J.R. Dewald, *US Patent* **1985**, *4507466*.

[D18] T. Hayashi, A. Yamamoto, T. Hagihara, Y. Ito, *Tetrahedron Lett.* **1986**, *27*, 191.

[D19] (a) Z. Otwinowski, W. Minor, *HKL Denzo* and *Scalepack* Program Package, Nonius BV, Delft;
For a reference, see: (b) Z. Otwinowski, W. Minor, *Meth. Enzymol.* **1997**, *276*, 307.

[D20] A. Altomare, M.C. Burla, M. Camalli, G.L. Cascarano, C. Giacovazzo, A. Guagliardi, A.G.G. Moliterni, G. Polidori, R. Spagna, *J. Appl. Crystallogr.* **1999**, *32*, 115.

[D21] G.M. Sheldrick, *SHELXL97. Program for Crystal Structure Refinement from Diffraction Data*, University of Göttingen: Germany, **1997**.

[D22] A.L. Spek, *Platon – a Multipurpose Crystallographic Tool*, Utrecht University: Utrecht, **2003**, and updates. Available from: http://www.cryst.chem.uu.nl/platon/.

E Au Nanoparticles Stabilized by PEGylated Low-Generation PAMAM Dendrimers: Design, Characterization and Properties

Sascha Dietrich, Steffen Schulze, Michael Hietschold and Heinrich Lang

Published in *J. Colloid Interface Sci.* **2011**, *359*, 454 – 460.

1. Introduction

Transition metal nanoparticles (NPs) are of significant interest in physics, biology, chemistry and material sciences [E1]. As these materials have at least one dimension between 1 and 100 nm, their unique physical and chemical properties are strongly affected by the particle size, size distribution, shape and particle-to-particle interaction [E2]. In particular, group-11 NPs play an important role in the field of optic [E3], catalytic [E4], electronic [E5], chemical sensing [E6] and bio-medical approaches [E7]. Nanostructured colloids can be obtained by Top-Down and Bottom-Up processes [E8], resulting in the design of new generations of nanodevices and smart materials to link the current technologies with future demands [E9]. Various synthetic strategies have been reported continuously to generate NPs of noble metals [E10], whereas the chemical reduction of metal ions to zero-valent metal NPs in aqueous or organic solvents in the presence of stabilizing agents is most common [E11]. The organic coatings provide stabilization to the nanoparticles surface and act as protectives to prevent aggregation. As stabilizing components mostly ethylene glycol [E12], polymers/co-polymers [E13] or dendrimers [E14] with donating functionalities including N, O, P and S donor atoms are used. (Poly)amidoamine (PAMAM)-based dendrimers are outstanding candidates as templates and stabilizers because of their regular structure and chemical versatility [E15], having intrinsic amino and amido functionalities as well as terminal amino [E16], hydroxyl [E17] and (poly)ethylene glycol (PEG) [E18] groups or substituted saccharides [E19]. Originally, Tomalia [E20] and Crooks [E21] reported on an efficient encapsulation of copper NPs in a (poly)amidoamine matrix providing dendrimer-metal nanocomposites, followed by a number of reports dealing with the application of dendrimers for the formation of stable colloidal metal NP solutions, such as Ag [E22], Au [E23], Ni [E24], Pd [E25] and Pt [E26]. Recently, the synthesis and structural analysis of heterobimetallic PdAu [E27], PtAu [E28] and NiAu [E29] dendrimer-

encapsulated core-shell NPs for catalytic and magnetic applications have been reported as well.

In all the above-mentioned investigations the dendritic (poly)amidoamine templates used for the stabilization of the appropriate NPs were dendrimers of 2nd to 10th generation [E30], having a large interior with tertiary amines binding to the corresponding metal centers. Although these dendritic networks are of particularly chemical elegance exhibiting a monodisperse and high radial symmetry their multifarious and time consuming synthesis as well as extensive purification make them less attractive for applications, due to economical reasons. Recently, in this respect Astruc showed the encapsulation and stabilization of Au NPs by an arene-cored (poly)ethylene glycol-terminated dendrimer formed by "click" chemistry providing 27, 81 and 243 tethers (Gen. 0 to 2) [E14a]. These dendritic precursors which are accessible after a plurality of complex synthetic steps allow the formation of 2 to 4 nm sized Au NPs.

Herein, we report a two-step synthesis methodology for a novel series of well-defined (poly)amidoamine-based dendrimers of low-generation (Gen. 0) and related amidoamine model compounds functionalized with terminal ethylene glycol ethers of various chain lengths providing multiple donating functionalities. Our approach facilitates a straightforward and more time efficient access to flexible dendritic surfactants, whose identity and purity are still well characterisable (*e.g.* by NMR techniques) compared to other applied dendrimers [E14, E20, E21]. Furthermore, our biocompatible organic coatings are also more effective than monodentate stabilizers such as triphenylphosphine [E31] or alkanethioles [E32], as they provide more donating functionalities per gram. Bearing up to ten tentacles, the molecules described here act as promising templates in the formation of Au NPs using $H[AuCl_4]$ as gold source and $Na[BH_4]$ as reducing agent. The sufficient surfactant sizes and determination of the minimum requirements for (poly)ethylene glycol-based nanotemplates as well as temporal stability studies on inorganic and/or organic hybrid colloids are presented.

2. Materials and Methods

2.1. Synthesis of Stabilizers

All synthesis procedures were performed under a dry and deoxygenated dinitrogen atmosphere using standard Schlenk techniques unless otherwise stated. All organic solvents were carefully dried by standard procedures over the appropriate drying agents and distilled immediately prior to use. Hydrogen tetrachloroaurate(III) hydrate (**12**), sodium borohydride, ethy-

lene glycol methyl ether acrylate (**9**) and poly(ethylene glycol) methyl ether acrylate (average M_n ca. 480 g · mol^{-1}) (**11**) were purchased from SIGMA ALDRICH and were used without further purification. Di(ethylene glycol) ethyl ether acrylate (**10**) was distilled prior to use. The poly(amidoamine)dendrimers $N(CH_2CH_2C(O)NHCH_2CH_2NH_2)_3$ (**6**), $[CH_2N-(CH_2CH_2C(O)NHCH_2CH_2NH_2)_2]_2$ (**7**) and $(H_2NCH_2CH_2NHC(O)CH_2CH_2)N[CH_2CH_2N-(CH_2CH_2C(O)NHCH_2CH_2NH_2)_2]_2$ (**8**) as well as the corresponding di(ethylene glycol) functionalized amidoamine $(R_2NCH_2CH_2NHC(O)CH_2CH_2)N[CH_2CH_2N(CH_2CH_2C(O)-NHCH_2CH_2NR_2)_2]_2$ (**5b**, R = $CH_2CH_2C(O)O(CH_2CH_2O)_2C_2H_5$) were synthesized according to previously published procedures [E33, E34, E37]. Detailed experimental instructions for **1**, **2**, **3a** – **3c**, **4** and **5a** – **5c** are given in the supplementary material available.

2.2. Preparation Procedure for Gold Nanoparticles

In-situ (dendrimer) stabilized Au NPs were prepared in solution [E11]. This methodology involves two steps: (a) The preparation of the corresponding (dendritic) amidoamine-based ethylene glycol Au(III) system, whereas the appropriate metallodendrimer was synthesized by combining the respective dendrimer (10 mL) with $H[AuCl_4]$ (10 mL) in tetrahydrofuran at 25 °C in different ratios (dendrimer:Au(III) = 1:1 (2 mmol · L^{-1}: 2 mmol · L^{-1}), 1:5 (0.4 mmol · L^{-1}: 2 mmol · L^{-1}), 1:10 (0.2 mmol · L^{-1}: 2 mmol · L^{-1}), 1:50 (0.04 mmol · L^{-1}: 2 mmol · L^{-1}) or 1:100 (0.02 mmol · L^{-1}: 2 mmol · L^{-1})). The resulting yellow colored mixture was stirred for additional 15 min followed by (b) the reduction of the respective Au(III) ions to zero-valent Au NPs. Therefore, freshly prepared saturated $Na[BH_4]$ in tetrahydrofuran was added dropwise under vigorous stirring. The mixture was further aged for 30 min, while the solution color changed from yellow to intensive purple.

3. Results and Discussion

3.1. Dendritic Stabilizers

The amidoamine-based dendrimers with end-grafted ethylene glycol ether tentacles (Chart E1) were prepared by a divergent consecutive synthesis procedure including Michael addition and amidation cycles, a method which was firstly described by Tomalia and coworkers [E33]. This methodology was applied for the straightforward and more time efficient synthesis of (poly)ethylene glycol-functionalized dendrimers $N(CH_2CH_2C(O)NHCH_2CH_2NR_2)_3$ (**3a**, R = $CH_2CH_2C(O)OCH_2CH_2OCH_3$; **3b**, R = $CH_2CH_2C(O)O(CH_2CH_2O)_2C_2H_5$; **3c**, R =

$CH_2CH_2C(O)O(CH_2CH_2O)_9CH_3$), $[CH_2N(CH_2CH_2C(O)NHCH_2CH_2NR_2)_2]_2$ (**4**, R = $CH_2CH_2C(O)O(CH_2CH_2O)_2C_2H_5$) and $(R_2NCH_2CH_2NHC(O)CH_2CH_2)N[CH_2CH_2N$-$(CH_2CH_2C(O)NHCH_2CH_2NR_2)_2]_2$ (**5a**, R = $CH_2CH_2C(O)OCH_2CH_2OCH_3$; **5b**, R = $CH_2CH_2C(O)O(CH_2CH_2O)_2C_2H_5$; **5c**, R = $CH_2CH_2C(O)O(CH_2CH_2O)_9CH_3$).

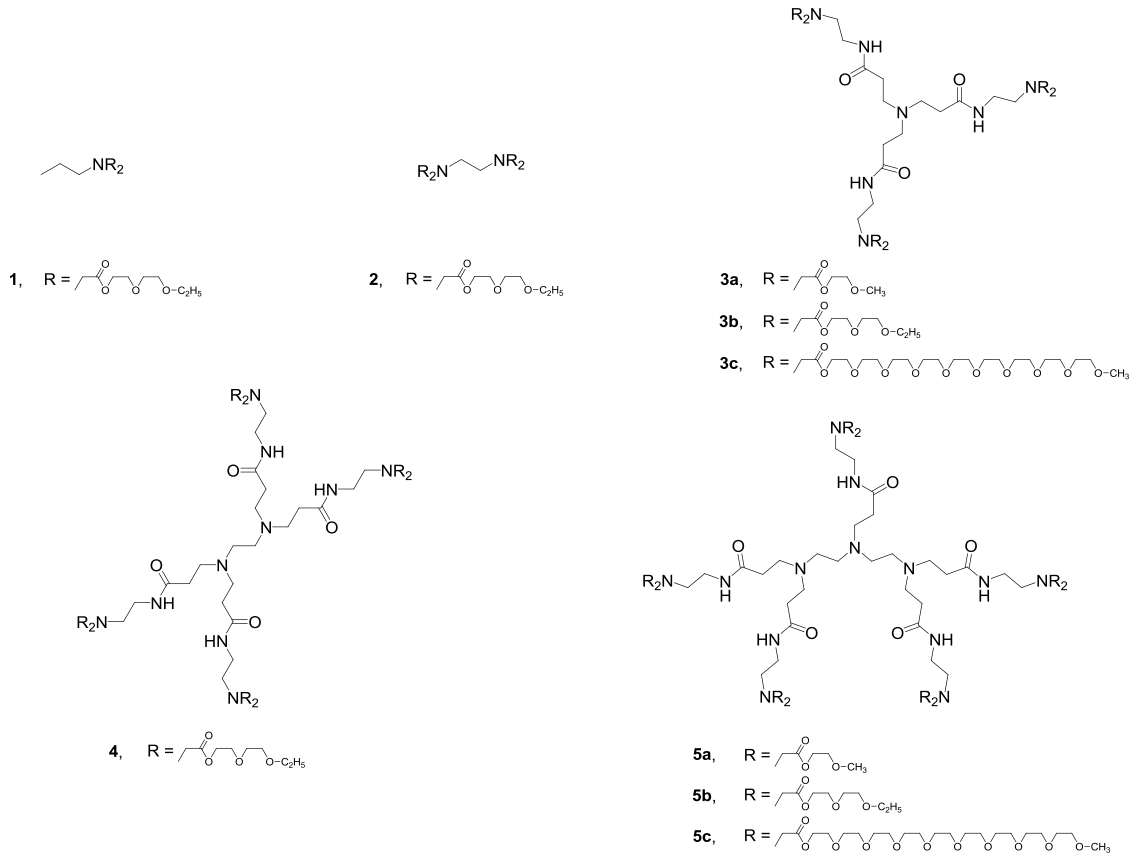

Chart E1. (Poly)ethylene glycol-functionalized PAMAM dendrimers **3a** – **3c**, **4**, **5a** – **5c** and for comparison, amines **1** and **2**.

Michael addition of the terminal amino functionalities of dendritic molecules $N(CH_2CH_2C(O)NHCH_2CH_2NH_2)_3$ (**6**), $[CH_2N(CH_2CH_2C(O)NHCH_2CH_2NH_2)_2]_2$ (**7**) and $(H_2NCH_2CH_2NHC(O)CH_2CH_2)N[CH_2CH_2N(CH_2CH_2C(O)NHCH_2CH_2NH_2)_2]_2$ (**8**) to ethylene glycol methyl ether acrylate (**9**), di(ethylene glycol) ethyl ether acrylate (**10**) and poly(ethylene glycol) methyl ether acrylate (**11**), respectively, gave the appropriate biocompatible dendrimers **3a** – **3c**, **4**, **5a** – **5c** featuring 6, 8, or even 10 ethylene glycol ether-termini of various sizes and hence, feature multiple σ-donor capabilities (Chart E1) [E37]. Exemplarily, the synthesis of **3b** is shown in Reaction E1.

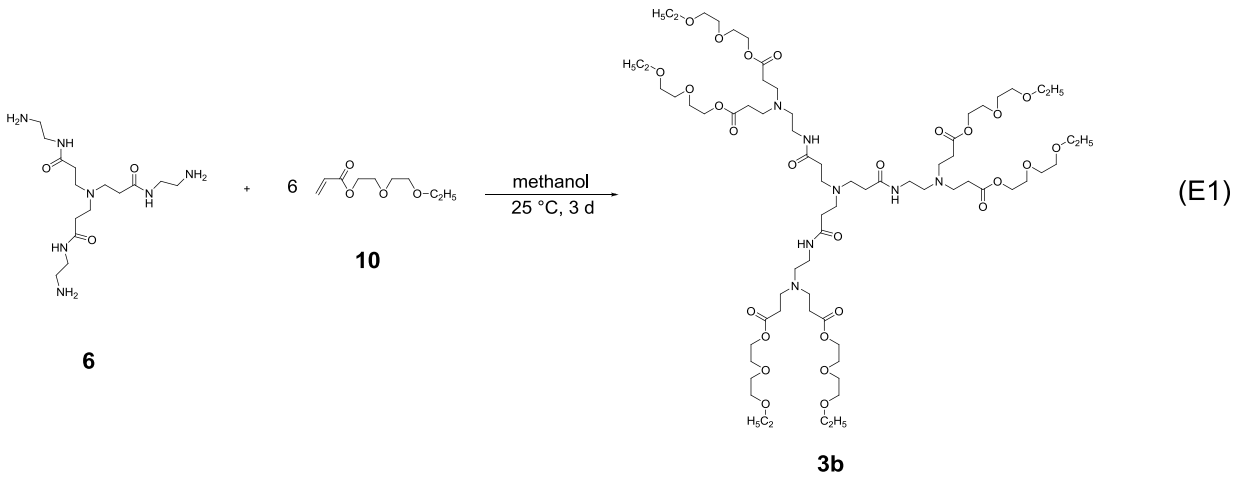

(E1)

After appropriate work-up, dendrimers **3a** – **3c**, **4** and **5a** – **5c** were isolated as odorless oils in almost quantitative yield (Experimental Section). For comparison, the di(ethylene glycol) ethyl ether-functionalized amines **1** and **2** were accessible using the same reaction conditions as described for the synthesis of **3** – **5** (Experimental Section).

Molecules **1** – **5** were characterized by NMR (^{1}H, ^{13}C{^{1}H}), FT-IR and UV/Vis spectroscopy as well as high resolution mass spectrometry. As the unimolecular amino compounds **1** and **2** the ^{1}H NMR spectra of **3a** – **3c**, **4** and **5a** – **5c** show single resonance signals for the C*H*$_2$C(O)O ($\delta \approx$ 2.45 ppm), C(O)OC*H*$_2$ ($\delta \approx$ 4.25 ppm), C*H*$_2$OC*H*$_2$ ($\delta \approx$ 3.60 ppm) and C*H*$_3$ ($\delta \approx$ 1.25 and 3.35 ppm, respectively) moieties. Furthermore, the amidoamine dendrimers exhibit a broad distinctive resonance signal at ca. 7.0 ppm for the C(O)N*H* unit. In the ^{13}C{^{1}H} NMR spectra of all compounds the carbonyl carbon atoms are observed between ca. 172 ppm, while the CH_2, CH_3 building blocks are found at 12 – 73 ppm.

The progress of the reaction of attaching the (poly)ethylene glycols to the (amido)amine scaffold can be monitored by FT-IR spectroscopy, since as an evidence for the complete consumption of the appropriate amino educts, the absorption band of the terminal NH_2 group at ca. 3365 cm^{-1} (ν_{NH}) disappears [E34].

3.2. Dendritic Stabilized Gold Nanoparticles

The nanotemplating properties of the synthesized (poly)ethylene glycol-functionalized amines **1** and **2** as well as the PAMAM-based dendrimers **3a** – **3c**, **4** and **5a** – **5c** featuring intrinsic tertiary amine and ether groups were examined for the stabilization of Au NPs in tetrahydrofuran solutions using consecutive steps. Based on the number of di(ethylene glycol)

termini, the addition of half equivalents of $H[AuCl_4]$ (**12**) to **1**, **2**, **3a** – **3c**, **4** and **5a** – **5c** resulted in the formation of the appropriate intensively yellow colored Au(III) containing metallodendrimers **3a-Au(III)** – **3c-Au(III)**, **4-Au(III)**, **5a-Au(III)** – **5c-Au(III)**, **1-Au(III)** and **2-Au(III)**, respectively. All the Au(III) loaded compounds **1-Au(III)** – **5-Au(III)** were then reduced chemically by addition of $Na[BH_4]$. For completion of the reaction vigorously stirring for 30 min was required during the color changed from yellow to purple indicating the formation of zero-valent Au colloids **1-Au(0)** – **5-Au(0)** stabilized by the appropriate templating agent.

3.3. Physical and Chemical Characterization

The formation of Au NPs within the stabilizing system was examined by FT-IR spectroscopic measurements. A bathochromic absorption shift of the C−O−C stretching vibration of ca. 30 cm^{-1} compared to the appropriate non-coordinated species was thereby observed. Furthermore, electron diffraction patterns were taken, whereas the resulting pattern for the **5b**-stabilized Au NPs is exemplarily shown in Figure E1a. The displayed ring pattern can be indexed as derived from (111), (002), (022), (222), (113), (024) and (133) lattice planes of gold (Figure E1b).

(a)

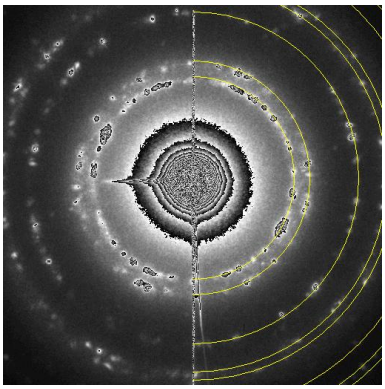

(b)

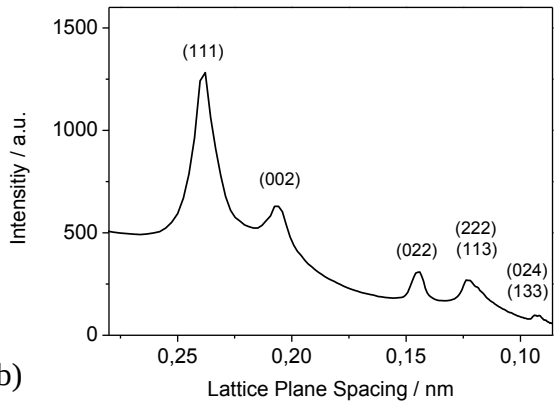

Figure E1. Selected area diffraction patterns (a) and resulting Miller indices (b) derived from lattice planes of gold NPs obtained from **5b-Au(0)**.

To investigate the optical properties of the hybrid materials UV/Vis spectroscopic studies of **1-Au(0)**, **2-Au(0)**, **3b-Au(0)**, **4-Au(0)** and **5b-Au(0)** were carried out (Figure E2). The obtained spectra show strong absorptions in the range of 450 – 700 nm due to plasmon oscillation modes of the electrons in the Au NPs [E35]. The higher the number of end-grafted di(ethylene glycol) ethyl ether-functionalities, the stronger the absorption, the narrower the

curve´s shape and the more the absorption maximum is hypsochromic shifted (**3b-Au(0)**: λ_{max} = 541 nm; **5b-Au(0)**: λ_{max} = 532 nm). As a result thereof, dendritic stabilizer **5b** produces smaller NPs (Figure E2) [E36].

For determination of the Full-Width-at-Half-Maximum (FWHM) of the plasmon band deconvolution of the UV/Vis data was performed using four Gaussian shaped overlapping absorptions until the sum of the Gaussian functions closely matches the measured spectra. The FWHM of **5b-Au(0)** is 2525 cm^{-1}, whereas **3b-Au(0)** possess a FWHM of 3450 cm^{-1} and hence, a broader NP size distribution than in **5b-Au(0)**. Furthermore, using **1** as stabilizing agent for Au NPs a very wide absorption was observed. Deposition of a gold layer occurs contemporary and proofs that molecule **1** cannot provide an adequate quantity of donor atoms to stabilize the surface of the Au colloids (**1-Au(0)**) [E14]. As a conclusion of the UV/Vis studies (Figure E2) within this series of **1-Au(0)** – **5b-Au(0)**, dendrimer **5b** is the most suitable for the formation of Au NPs having smallest particle diameters as well as narrow size distributions.

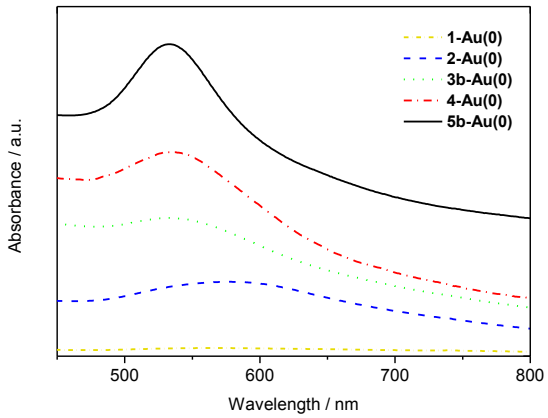

Figure E2. UV/Vis absorptions of di(ethylene glycol) ethyl ether-functionalized **1-Au(0)**, **2-Au(0)**, **3b-Au(0)**, **4-Au(0)** and **5b-Au(0)** in tetrahydrofuran (ϑ = 25 °C; c = 1.0 mmol · L^{-1}).

Estimation of the maximum loading of stabilized Au NPs within the dendritic template was achieved by embedding various amounts of Au colloids in the organic matrix of **5b**. The resulting UV/Vis absorption spectra for **5b**:Au ratios 1:1, 1:10, 1:50, or 1:100 are depicted in Figure E3. The spectra for the ratios **5b**:Au of 1:1 (FWHM = 2345 cm^{-1}) and 1:10 (FWHM = 2870 cm^{-1}), respectively, exhibit absorption peaks at about 525 and 530 nm. In addition, the absorbance of **5b**-stabilized Au NPs increases concomitantly with the loading of zero-valent gold colloids from **5b**:Au = 1:1 to 1:10. However, the curves for **5b**:Au of 1:50 (FWHM = 4695 cm^{-1}) and 1:100 are very broad, caused by an exceeding of **5b**´s stabilizing capacity re-

sulting in enlarged particle sizes due to aggregation of Au NPs, which is in accordance with the experimental observations that metallic Au precipitated. These results correspond well with literature, where lower loadings yield smaller particles [E14].

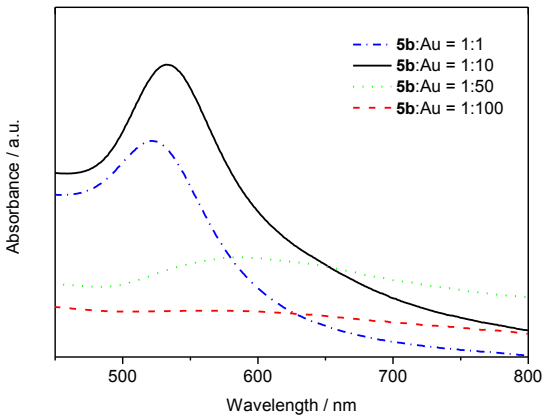

Figure E3. UV/Vis absorption spectra of various **5b**:Au ratios (1:1, 1:10, 1:50 and 1:100) in tetrahydrofuran (ϑ = 25 °C; c = 1.0 mmol · L^{-1}).

To investigate the influence of different ethylene glycol chain lengths on the stabilization capability for Au NPs, tri- and penta-amino terminated PAMAM-dendrimers **6** and **8** were modified with ethylene glycol methyl ether acrylate (**9**) and poly(ethylene glycol) methyl ether acrylate (**11**) to give **3a**, **5a**, **3c** and **5c** (Chart E1), using the same reactions conditions as described for the synthesis of **3b**. Figure E4 shows the changes occurring in the absorption spectra, when Au NPs were stabilized by dendrimers **5a**, **5b** and **5c**. The absorption patterns of the surface plasmon resonance derived from **5b-Au(0)** and **5c-Au(0)** are more sharp compared to **5a-Au(0)**, exhibiting a FWHM value of 2715 cm^{-1}. Furthermore, as the intensity of the absorption is increased, within this series dendritic templates **5b** and **5c** result in the formation of small Au NPs (*vide infra*; Figures E6 and E7).

In addition, we proceeded temporal stability studies of the ethylene glycol-terminated PAMAM-based dendrimers. From Figure E5 it can be seen that **5c** is capable to encapsulate Au NPs for more than eight weeks and thus, prevents macroscopic particle aggregation. The UV/Vis spectra display absorption curves centered at ca. 530 nm after reduction with $Na[BH_4]$. The curve´s shape becomes broader and the absorption´s intensity is slightly decreased after aging for 8 weeks, as the Au NPs agglomerate to macroscopic colloids. In comparison, Au NPs embedded in dendritic **5a** and **5b**, respectively, are stable for several hours to some days, only.

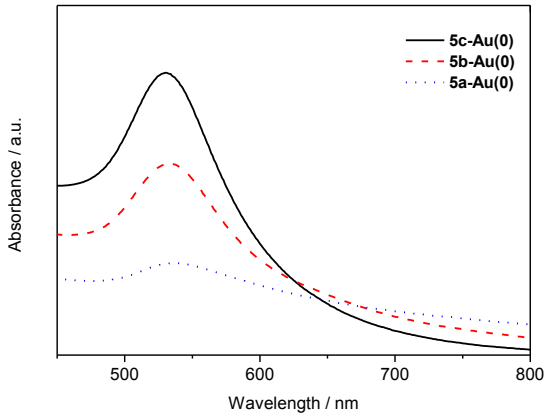

Figure E4. Comparison of the UV/Vis absorption spectra of Au NPs stabilized by **5a**, **5b** and **5c**, respectively, bearing ethylene glycol units of different lengths (tetrahydrofuran; ϑ = 25 °C; c = 1.0 mmol · L^{-1}).

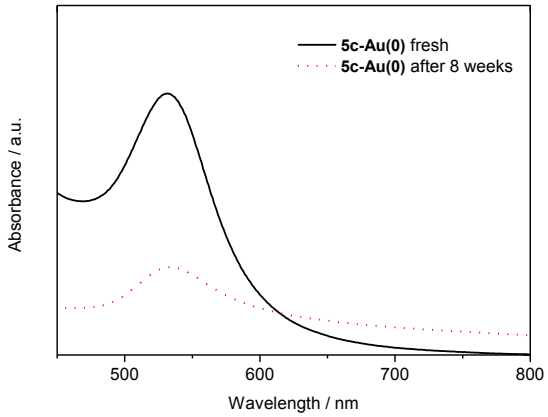

Figure E5. UV/Vis absorption spectra of **5c-Au(0)** for long-term stability investigations (tetrahydrofuran; ϑ = 25 °C; c = 1.0 mmol · L^{-1}).

These UV/Vis spectroscopic results indicate that the poly(ethylene glycol) methyl ether attached to the dendrimers periphery can result in the formation of well-grown Au NPs and in a high colloidal stability for several weeks.

The actual particle size, size distribution and particle shape were determined by transmission electron microscopy (TEM) and verified by dynamic light scattering (DLS) studies. The data show the appearance of the formed Au NPs coated by (amido)amine stabilizer **5b** and **1** for comparison (Figure E6). The colloidal gold solutions obtained at ambient temperature for stabilizer **5b** showed well-defined particles. Apparently, the Au NPs sizes depend on the number of terminal groups. The particle sizes decrease concomitantly with the number of attached di(ethylene glycol) ethyl ether functionalities. As already expected from UV/Vis and

FWHM analyses (*vide supra*), from Figure E6 it can be seen that Au NPs stabilized by **5b** (ø = 4.0 (± 0.9) nm) are smaller and exhibit a more narrow size distribution as compared to particles embedded in **3b** (ø = 6.8 (± 5.3) nm) and **1** (ø = 37.3 (± 13.4) nm), respectively. On the basis of observations made by TEM and FT-IR spectroscopy, the particles might grow within the dendritic template and hence, a higher number of terminal ethylene glycol results in a better encapsulation, preventing aggregation and precipitation of the Au NPs. Furthermore, the shape of the generated gold particles is affected by the number of terminal di(ethylene glycol) ethyl ether groups as well. While **5b** forms more or less regular spherical shaped Au NPs, ligand **1** results in formation and short stabilization of enlarged anisotropic particles exhibiting multiple morphologies, *e.g.* spheres, rods and prisms (Figure E6b).

(a)

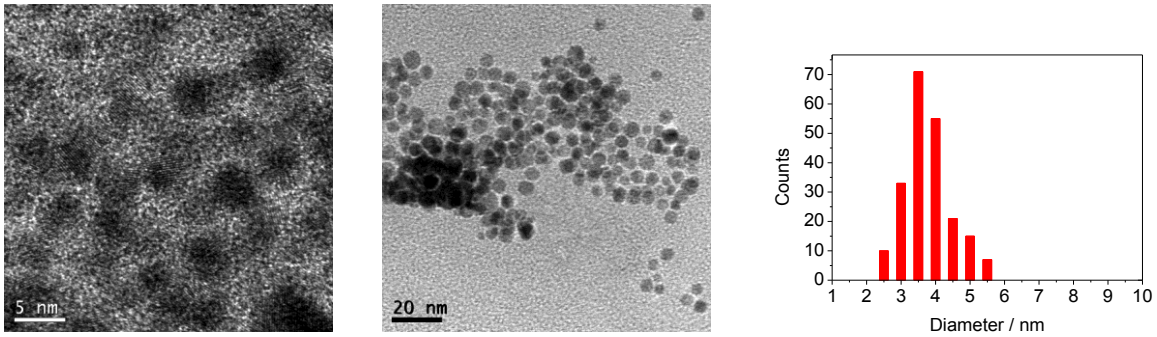

(b)

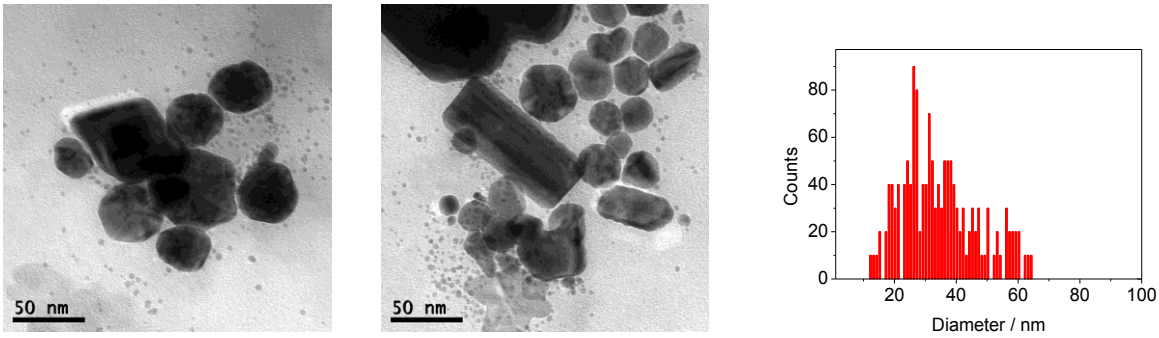

Figure E6. TEM micrographs and particle size distribution of spherical Au NPs stabilized by **5b (**ø = 4.0 (± 0.9) nm) (a) and multiple shaped Au NPs stabilized by **1** (ø = 37.3 (± 13.4) nm) (b).

In addition, the chain length´s effect of the ethylene glycol-moiety attached on dendrimer´s periphery on the colloid size is not simple, *i.e.* the colloids formed by **5a** (ø = 9.4 (± 3.4) nm) are larger than those generated by template **5b (**ø = 4.0 (± 0.9) nm). For Au NPs stabilized using **5c** slightly increased particle diameters of 7.6 (± 1.8) nm were found (Figure E7a). In agreement with literature dealing with low-generation dendrimers as colloid stabilizers, for

the interpretation of these results, for example, different (stable) conformers of the dendrimers in solution have to be considered. In dependence on the terminal ethylene glycol ether functionality the structure and the flexibility of the corresponding dendrimer as Au NPs template is crucial for the resulting colloid size and shape [E13, E22]. However, the applied dendritic surfactants with merely ten (poly)ethylene glycol tentacles are able to generate gold colloid sizes in the same range or only slightly increased to Astruc´s complex dendritic arene-cored (poly)ethylene glycol-terminated system providing 27, 81 or even 243 tethers [E14a].

(a)

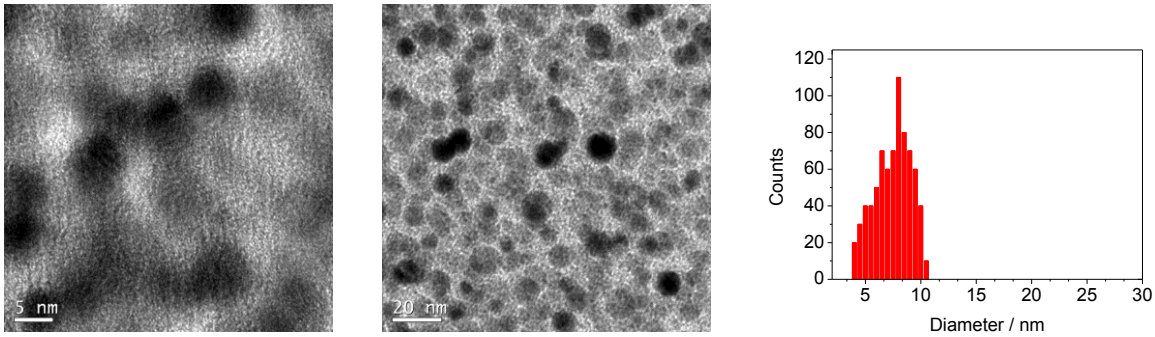

(b)

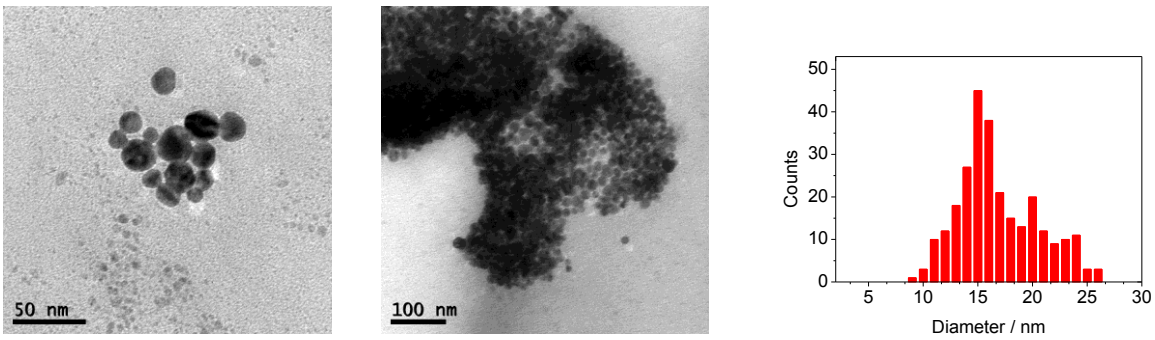

Figure E7. TEM images and particle size distributions of (a) freshly prepared **5c-Au(0)** (ø = 7.6 (± 1.9) nm) and (b) **5c-Au(0)** (ø = 16.9 (± 3.8) nm) aged for 8 weeks.

Moreover, to perform temporal stability studies long-term investigations of **5a-Au(0)** – **5c-Au(0)** were examined by TEM. The study demonstrates that **5c** encapsulated Au colloids aged for more than 8 weeks (Figure E7b) have an average diameter of 16.9 (± 3.8) nm and almost retaining spherical shape. **5c** obviously offers the best "host-guest conditions" for a long term, whereas Au NPs embedded in dendritic **5a** and **5b** (ø = 14.4 (± 3.2) nm; obtained after 3 days) aggregate in a period of 8 hours up to 5 days.

Table E1. Particle sizes generated by dendrimer **5b** and varied stabilizer:Au ratios.

Entry	Ratio (Stabilizer:Gold)	Particle Size
1	1:1	5.3 (± 1.1) nm
2	1:10	9.1 (± 1.7) nm
3	1:50	58.5 (± 14.5) nm
4	1:100	42.2 (± 8.7) nm

It is well known that the particle diameter of the Au NPs can be controlled by the molar ratio of Au and the appropriate stabilizer [E15]. This correlation was evaluated using stabilizing agent 5b loaded with various amounts of $H[AuCl_4]$ to achieve different molar ratios of 5b:Au (1:1, 1:10, 1:50, 1:100) (Table E1). In accordance with UV/Vis spectroscopic data reported (*vide supra*), transmission electron microscopy images implied, when the molar ratio of 5b and Au is sufficiently low (5b:Au = 1:1, 1:10) stable colloidal solutions of small uniform spherical shaped Au NPs are generated (5b:Au = 1:1; ø = 5.3 (± 1.1) nm). Higher concentrations of Au (5b:Au = 1:50, 1:100) resulted in irregular shaped Au NPs of increased average diameters (5b:Au = 1:100; ø = 42.2 (± 8.7) nm). Macroscopic metal precipitation occurs upon reduction of the dendritic Au(III) complex.

4. Conclusion

A novel series of well-defined (poly)amidoamine-based dendrimers $N(CH_2CH_2C(O)NHCH_2CH_2NR_2)_3$, $[CH_2N(CH_2CH_2C(O)NHCH_2CH_2NR_2)_2]_2$ and $(R_2NCH_2CH_2NHC(O)CH_2CH_2)N[CH_2CH_2N(CH_2CH_2C(O)NHCH_2CH_2NR_2)_2]_2$ functionalized with terminal ethylene glycol methyl ether- (R = $CH_2CH_2C(O)OCH_2CH_2OCH_3$), di(ethylene glycol) ethyl ether- (R = $CH_2CH_2C(O)O(CH_2CH_2O)_2C_2H_5$) and poly(ethylene glycol) methyl ether moieties (R = $CH_2CH_2C(O)O(CH_2CH_2O)_9CH_3$) were prepared by a straightforward synthesis methodology enabling a more time efficient access to low-generation (Gen. 0) dendritic surfactants providing multiple donating functionalities. However, among other complex syn-

thesized, sterically demanding, high generation dendrimers used in this field by Astruc [E2b], Amis [E14b], Tomalia [E20b] and Crooks [E21b] the more flexible, versatile, biocompatible and well characterisable organics presented here can serve as readily accessible efficient stabilizers and templating agents for gold colloids.

Using the *in-situ* reduction of the appropriate Au(III)-loaded metallodendrimers with $Na[BH_4]$ gave nascent, small sized Au NPs. In dependence on the dendritic structure, the adjusted stabilizer:gold ratio and the reaction time gold colloids of spherical shapes and average particle sizes in the range of 4.0 (± 0.9) to 58.5 (± 14.5) nm are created.

In summary, it can be stated that even small PAMAM-based dendritic stabilizers (low-generation dendrimers) can act efficiently as templates for nanoparticle formation.

5. Acknowledgement

This study was generously supported by the Deutsche Forschungsgemeinschaft, the Fonds der Chemischen Industrie and the State of Saxony (Landesgraduierten fellowship, Sascha Dietrich).

6. Supplementary Material

Supporting information with detailed experimental instructions for the synthesis of **1**, **2**, **3a** – **3c**, **4** and **5a** – **5c** are available with the corresponding ^{1}H NMR, $^{13}C\{^{1}H\}$ NMR, FT-IR and UV/Vis absorption spectra as well as data on microanalyses and high resolution mass spectrometry.

7. References

[E1] (a) S. Park, K. Hamad-Schifferli, *Curr. Opin. Chem. Biol.* **2010**, *14*, 616;
(b) M.Z. Ahmad, S. Akhter, G.K. Jain, M. Rahman, S.A. Pathan, F.J. Ahmad, R.K. Khar, *Expert Opin. Drug Delivery* **2010**, *7*, 927;
(c) M. Wang, M. Thanou, *Pharmacol. Res.* **2010**, *62*, 90;
(d) A. Ethirajan, K. Landfester, *Chem. Eur. J.* **2010**, *16*, 9398;
(e) R. Costi, A.E. Saunders, U. Banin, *Angew. Chem. Int. Ed.* **2010**, *49*, 4878;
(f) R. Klajn, J. Fraser Stoddart, B.A. Grzybowski, *Chem. Soc. Rev.* **2010**, *39*, 2203;

(g) C. Marambio-Jones, E.M.V. Hoek, *J. Nanopart. Res.* **2010**, *12*, 1531;

(h) V. Polshettiwar, R.S. Varma, *Green Chem.* **2010**, *12*, 743;

(i) D. Le Corre, J. Bras, A. Dufresne, *Biomacromolecules* **2010**, *11*, 1139.

[E2] (a) S.-A. Dong, S.-P. Zhou, *Mater. Sci. Eng. B.* **2007**, *140*, 153;

(b) M.-C. Daniel, D. Astruc, *Chem. Rev.* **2004**, *104*, 293;

(c) C.J. Murphy, T.K. Sau, A.M. Gole, C.-J. Orendorff, J. Gao, L. Gou, S.E. Hunyadi, T. Li, *J. Phys. Chem. B.* **2005**, *109*, 13857;

(d) J.L. Elechiguerra, J. Reyes-Gasga, M.J. Yacaman, *J. Mater. Chem.* **2006**, *16*, 3906;

(e) N. Garg, C. Scholl, A. Mohanty, R. Jin, *Langmuir* **2010**, *26*, 10271.

[E3] (a) S. Link, A. Beeby, S.F. Gerald, M.A. El-Sayed, T.G. Schaaff, R.L. Whetten, *J. Phys. Chem. B.* **2002**, *106*, 3410;

(b) G. Palui, S. Ray, A. Banerjee, *J. Mater. Chem.* **2009**, *19*, 3457;

(c) P.V. Kamat, *J. Phys. Chem. B.* **2002**, *106*, 7729;

(d) T. Goodson, O. Varnavski, Y. Wang, *Int. Rev. Phys. Chem.* **2004**, *23*, 109;

(e) H. Aleali, L. Sarkhosh, M. Eslamifar, R. Karimzadeh, N. Mansour, *Jpn. J. Appl. Phys.* **2010**, *49*, 085002;

(f) S. Link, M.A. El-Sayed, *Int. Rev. Phys. Chem.* **2000**, *19*, 409.

[E4] (a) M. Daté, M. Okumura, S. Tsubota, M. Haruta, *Angew. Chem. Int. Ed.* **2004**, *43*, 2129;

(b) V.R. Reddy, *Synlett* **2006**, *11*, 1791;

(c) S.-H. Hwang, C.D. Shreiner, C.N. Moorefield, G.R. Newkome, *New. J. Chem.* **2007**, *31*, 1192;

(d) M. Steffan, A. Jakob, P. Claus, H. Lang, *Catal. Commun.* **2009**, *10*, 437;

(e) R.M. Crooks, M. Zhao, L. Sun, V. Chechik, L.K. Yeung, *Acc. Chem. Res.* **2001**, *34*, 181;

(f) M.S. Chen, D.W. Goodman, *Science* **2004**, *306*, 252;

(g) R. Narayanan, *Molecules* **2010**, *15*, 2124;

(h) Lisa Starkey Ott, R.G. Finke, *Coord. Chem. Rev.* **2007**, *251*, 1075;

(i) A.Z. Moshfegh, *J. Phys. D: Appl. Phys.* **2009**, *42*, 233001;

(j) G. Kyriakou, S.K. Beaumont, S.M. Humphrey, C. Antonetti, R.M. Lambert, *ChemCatChem* **2010**, *22*, 1444;

(k) R. Narayanan, M.A. El-Sayed, *J. Phys. Chem. B* **2005**, *109*, 12663;

(l) C. Harding, V. Habibpour, S. Kunz, A. Nam-Su Farnbacher, U. Heiz, B. Yoon, U. Landman, *J. Am. Chem. Soc.* **2009**, *131*, 538.

[E5] (a) D.L. Feldheim, C.D. Kealing, *Chem. Soc. Rev.* **1998**, *27*, 1;

(b) M. Reches, E. Gazit, *Science* **2003**, *300*, 625;

(c) O. Carny, D.E. Shalev, E. Gazit, *Nano Lett.* **2006**, *6*, 1594;

(d) B.J. Privett, J. Ho Shin, M.H. Schoenfisch, *Anal. Chem.* **2010**, *82*, 4723.

[E6] (a) Y. Kim, R.C. Johnson, J.T. Hupp, *Nano Lett.* **2001**, *1*, 165;

(b) S.O. Obare, R.E. Hollowell, C.J. Murphy, *Langmuir* **2002**, *18*, 10407;

(c) K.-S. Lee, M.A. El-Sayed, *J. Phys. Chem. B.* **2006**, *110*, 19220;

(d) I. Koh, L. Josephson, *Sensors* **2009**, *9*, 8130;

(e) Y. Shen, M. Kuang, Z. Shen, J. Nieberle, H. Duan, H. Frey, *Angew. Chem. Int. Ed.* **2008**, *47*, 2227.

[E7] (a) N.L. Rosi, C.A. Mirkin, *Chem. Rev.* **2005**, *105*, 1547;

(b) S. Srivastava, B. Samanta, B.J. Jordan, R. Hong, Q. Xiao, M.T. Touminen, V.M. Rotello, *J. Am. Chem. Soc.* **2007**, *129*, 11776;

(c) M. De, P.S. Ghosh, V.M. Rotello, *Adv. Mater.* **2008**, *30*, 4225;

(d) X. Huang, S. Neretina, M.A. El-Sayed, *Adv. Mater.* **2009**, *21*, 4880;

(e) S.-E. Stiriba, H. Frey, R. Haag, *Angew. Chem. Int. Ed.* **2002**, *41*, 1329.

[E8] (a) O.D. Velev, S. Gupta, *Adv. Mater.* **2009**, *21*, 1897;

(b) S. Eustis, M.A. El-Sayed, *Chem. Soc. Rev.* **2006**, *35*, 209;

(c) G.M. Whitesides, J.C. Love, *Sci. Am.* **2001**, 39.

[E9] (a) H. Wohltjen, A.-W. Snow, *Anal. Chem.* **1998**, *70*, 2856;

(b) A.G. Kanaras, F.S. Kamounah, K. Schaumburg, C.J. Kiely, M. Brust, *Chem. Commun.* **2002**, 2249;

(c) M. Calderón, M.A. Quadir, M. Strumia, R. Haag, *Biochimie* **2010**, *92*, 1242.

[E10] (a) J. Zeng, J. Huang, W. Lu, X. Wang, B. Wang, S. Zhang, J. Hou, *Adv. Mater.* **2007**, *19*, 2172;

(b) Y. Xiang, J.M. McLellan, Y. Yin, Y. Xia, *Angew. Chem. Int. Ed.* **2007**, *46*, 790;

(c) M. Sakamoto, M. Fujistuka, T. Majima, *J. Photochem. Photobiol. C* **2009**, *10*, 33.

[E11] (a) P. Pengo, S. Polizzi, M. Battagliarin, L. Pasquato, P. Scrimin, *J. Mater. Chem.* **2003**, *13*, 2471;

(b) G. Schmid, B. Corain, *Eur. J. Inorg. Chem.* **2003**, 3081.

[E12] (a) V. Delmas, S. Grugeon, R. Herrera Urbina, P.-Y. Silvert, K. Tekaia-Elshsissen, *Nanostruct. Mater.* **1999**, *11*, 1277;

(b) C.-H. Wang, C.-J. Liu, C.-L. Wang, T.-E. Hua, J.M. Obliosca, K.H. Lee, Y. Hwu, C.-S. Yang, R.-S. Liu, H.-M. Lin, J.-H. Je, G. Margaritondo, *J. Phys. D: Appl. Phys.* **2008**, *41*, 1;

(c) M. Maccarini, G. Briganti, S. Rucareanu, X.-D. Lui, R. Sinibaldi, M. Sztucki, R.B. Lennox, *J. Phys. Chem. C* **2010**, *114*, 6937.

[E13] (a) J. Zhou, J. Ralston, R. Sedev, D.A. Beattie, *J. Colloid Interface Sci.* **2009**, *331*, 251;

(b) G. A. Nimola, K. Pandian, *Colloids and Surfaces A: Physiochem. Eng. Aspects* **2006**, *290*, 138;

(c) G.V. Ramesh, S. Porel, T.P. Radhakrishnan, *Chem. Soc. Rev.* **2009**, *38*, 2646.

[E14] (a) E. Boisselier, A.K. Diallo, L. Salmon, C. Ornelas, J. Riuz, D. Astruc, *J. Am. Chem. Soc.* **2010**, *132*, 2729;

(b) F. Gröhn, B.J. Bauer, Y.A. Akpalu, C.L. Jackson, E.J. Amis, *Macromolecules* **2000**, *33*, 6042;

(c) K. Esumi, *Colloid Chemistry II, Top. Curr. Chem.* **2003**, *227*, 31;

(d) R. Haag, F. Vögtle, *Angew. Chem. Int. Ed.* **2004**, *43*, 272.

[E15] (a) F. Divsar, A. Nomani, M. Chaloosi, I. Haririan, *Microchim. Acta* **2009**, *165*, 421;

(b) C. Zhai, C. Wei, J. Xu, P. Yang, Y. Du, *Colloid Journal* **2009**, *71*, 764;

(c) D.A. Tomalia, *Prog. Polym. Sci.* **2005**, *30*, 294.

[E16] (a) Y.G. Kim, S.-K. Oh, R.M. Crooks, *Chem. Mater.* **2004**, *16*, 167;

(b) Y. Chen, Y.-M. Zhang, Y. Liu, *Chem. Commun.* **2010**, 5622.

[E17] X. Shi, S. Wang, H. Sun, J.R. Baker Jr., *Soft Matter* **2007**, *3*, 71.

[E18] (a) Y. Umeda, C. Kojima, A. Harada, H. Horinaka, K. Kono, *Bioconjugate Chem.* **2010**, *21*, 1559;

(b) R.C. Hedden, B.J. Bauer, A.P. Smith, F. Gröhn, E. Amis, *Polymer* **2002**, *43*, 5473;

(c) M. Calderón, M.A. Quadir, S.K. Sharma, R. Haag, *Adv. Mater.* **2010**, *22*, 190.

[E19] (a) K. Torigoe, A. Tasaki, T. Yoshimura, K. Sakai, K. Esumi, Y. Takamatsu, S.C. Sharma, H. Sakai, M. Abe, *Colloids and Surfaces A: Physiochem. Eng. Aspects* **2008**, *326*, 184;

(b) K. Esumi, T. Hosoya, A. Suzuki, K. Torigoe, *Langmuir* **2000**, *16*, 2978.

[E20] (a) L. Balogh, D.A. Tomalia, *J. Am. Chem. Soc.* **1998**, *120*, 7355;

(b) L. Balogh, R. Valluzzi, G.L. Hagnauer, K.S. Laverdure, S.P. Gido, D.A. Tomalia, *J. Nanopart. Res.* **1999**, *3*, 353.

[E21] (a) M. Zhao, L. Sun, R.M. Crooks, *J. Am. Chem. Soc.* **1998**, *120*, 4877;

(b) R.M. Crooks, B.I. Lemon, L. Sun, L.K. Yeung, M. Zhao, *Top. Curr. Chem.* **2001**, *212*, 81.

[E22] (a) M.F. Ottiviani, R. Valluzzi, L. Balogh, *Macromolecules* **2002**, *35*, 5105;

(b) G. Li, Y. Luo, H. Tan, *J. Solid State Chem.* **2005**, *178*, 1038;

(c) G. Li, Y. Luo, W. Lu, J. Li, Y. Jin, S. Guo, *Chin. J. Chem.* **2010**, *28*, 633;

(d) M. Kavitha, M.R. Parida, E. Prasad, C. Vijayan, P.C. Deshmukh, *Macromol. Chem. Phys.* **2009**, *210*, 1310.

[E23] (a) M.E. Garcia, L.A. Baker, R.M. Crooks, *Anal. Chem.* **1999**, *71*, 256;

(b) L. Yu, A. Andriola, *Talanta* **2010**, *82*, 869;

(c) C. Peng, H. Wang, R. Guo, M. Shen, X. Cao, M. Zhu, G. Zhang, X. Shi, *J. Appl. Polym. Sci.* **2011**, *119*, 1673.

[E24] (a) S. Qiu, Z. Zhou, J. Dong, G. Chen, *J. Tribol.* **2001**, *123*, 441;

(b) M.R. Knecht, J.C. Garcia-Martinez, R.M. Crooks, *Chem. Mater.* **2006**, *18*, 5039.

[E25] (a) A.K. Diallo, C. Ornelas, L. Salmon, J.R. Aranzaes, D. Astruc, *Angew. Chem. Int. Ed.* **2007**, *46*, 8644;

(b) M. Bernechea, E. de Jesús, C. López-Mardomingo, P. Terreros, *Inorg. Chem.* **2009**, *48*, 4491;

(c) M.V. Gomez, J. Guerra, A.H. Velders, R.M. Crooks, *J. Am. Chem. Soc.* **2009**, *131*, 341.

[E26] (a) M.R. Knecht, M.G. Weir, V.S. Myers, W.D. Pyrz, H. Ye, V. Petkov, D.J. Buttrey, A.I. Frenkel, R.M. Crooks, *Chem. Mater.* **2008**, *20*, 5218;

(b) D. Yamamoto, S. Watanabe, M.T. Miyahara, *Langmuir* **2010**, *26*, 2339;

(c) F. Gröhn, G. Kim, B.J. Bauer, E. Amis, *Macromolecules* **2001**, *34*, 2179.

[E27] M.G. Weir, M.R. Knecht, A.I. Frenkel, R.M. Crooks, *Langmuir* **2010**, *26*, 1137.

[E28] (a) H. Lang, S. Maldonado, K.J. Stevenson, B.D. Chandler, *J. Am. Chem. Soc.* **2004**, *126*, 12949;

(b) B.J. Auten, H. Lang, B.D. Chandler, *Applied Catalysis B: Environmental* **2008**, *81*, 225.

[E29] B.J. Auten, B.P. Hahn, G. Vijayaraghavan, K.J. Stevenson, B.D. Chandler, *J. Phys. Chem. C* **2008**, *112*, 5365.

[E30] S. Chandra, H. Lang, *Mat. Chem. Phys.* **2009**, *114*, 926.

[E31] R. Sharma, G.P. Holland, V.C. Solomon, H. Zimmermann, S. Schiffenhaus, S.A. Amin, D.A. Buttry, J.L. Yarger, *J. Phys. Chem. C* **2009**, *113*, 16387.

[E32] (a) M. Brust, C.J. Kiely, *Colloid Surface A* **2002**, *202*, 175;

(b) M. Brust, M. Walker, D. Bethell, D.J. Schiffrin, R. Whyman, *J. Chem. Soc., Chem. Commun.* **1994**, 801;

(c) J.C. Garcia-Martinez, R.M. Crooks, *J. Am. Chem. Soc.* **2004**, *126*, 16170;

(d) V.V. Agrawal, N. Varghese, G.U. Kulkarni, C.N.R. Rao, *Langmuir* **2008**, *24*, 2494.

[E33] D.A. Tomalia, *United States Patent* **1985**, *4507466*.

[E34] S. Dietrich, A. Nicolai, H. Lang, *J. Organomet. Chem.* **2011**, *696*, 739.

[E35] P.K. Khanna, R. Gokhale, V.V.V.S. Subbarao, A.K. Vishwanath, B.K. Das, C.V.V. Satyanarayana, *Mat. Chem. Phys.* **2005**, *92*, 229.

[E36] W. Haiss, N.T.K. Thanh, J. Aveyard, D.G. Fernig, *Anal. Chem.* **2007**, *79*, 4215.

[E37] S. Chandra, S. Dietrich, H. Lang, D. Bahadur, *J. Mater. Chem.* **2011**, *21*, 5729.

F Design, Characterization and Magnetic Properties of Fe_3O_4-Nanoparticle Arrays Coated with PEGylated-Dendrimers

Sascha Dietrich, Sudeshna Chandra, Colin Georgi, Senoy Thomas, Denys Makarov, Steffen Schulze, Michael Hietschold, Manfred Albrecht, Dhirendra Bahadur and Heinrich Lang

Submitted to *Mat. Chem. Phys.* **2011**.

The following section´s results were generated in a multifarious collaboration between Chemnitz University of Technology and the Indian Institute of Technology Bombay (India).

The applied dendritic stabilizers **1** – **4** and **5a** – **c** were synthesized and completely characterized in the Department of Inorganic Chemistry headed by Prof. Dr. Heinrich Lang in Chemnitz. During a DAAD granted research stay in India the author of the present doctoral thesis further prepared the appropriate dendrimer coated Fe_3O_4 nanoparticles under supervision of Dr. Sudeshna Chandra and Prof. Dr. Dhirendra Bahadur in the Department of Metallurgical Engineering and Materials Science in Bombay. Subsequently, the chemical identity and particle properties of the obtained magnetite colloids were determined by the Solid Surfaces Analysis Group by Dr. Steffen Schulze and Prof. Dr. Michael Hietschold at the Institute of Physics in Chemnitz. The magnetic peculiarities were analyzed by Dr. Senoy Thomas, Dr. Denys Makarov and Prof. Dr. Manfred Albrecht of the Department of Surface and Interface Physics (TU Chemnitz).

1. Introduction

Magnetic nanoparticles (MNPs) have generated considerable interest in the scientific world especially in the area of biomedicine and technology, particularly, magnetic storage media [F1], magnetic inks for ink-jet printing [F2], biosensing [F3], targeted drug delivery [F4] and contrast agents in magnetic resonance imaging (MRI) [F5]. The importance of the NPs is attributed to the fact that they represent a critical link between the current technology and future application due to their small size, large surface to volume ratio and size dependent properties like superparamagnetism [F6]. The superparamagnetic behavior of MNPs is of immense inter-

est for *in vivo* applications, as they lose their magnetism after removal of the magnetic field. Thus, the potential benefit of MNPs is to use the localized magnetic field to attract the particle to the chosen site, to hold them until completion of the therapy and then remove them [F7]. Iron oxide NPs are generally synthesized in either aqueous or organic solutions and thus require sophisticated coatings for stability under physiological conditions [F8]. The coatings provide stabilization to the MNPs against aggregation in both a biological medium and in a magnetic field. In general, NPs can be stabilized with monomeric stabilizers [F9] (carboxylates, phosphates and sulphates), polymers [F10] (dextran, PEG and chitosan), inorganic materials [F11] (silica), liposomes [F12] and dendrimers [F13]. Out of many stabilizers, dendrimers have an added advantage of not only providing stability to the MNPs in solution but also help in binding various biological ligands to the surface of the colloids. The unique structural features of the dendrimers allow them to be used as stabilizers either as templates under fast reduction and nucleation chemistry or by entrapment under mild reduction condition. Moreover, the dendrimers have an added advantage of being capable for entrapping guest molecules or drugs within themselves and can also provide surface to guest molecules for attachment. Stable internal encapsulation of the drug is provided by the covalent scaffold of the dendrimers thus making them efficient drug carriers. Recent advances in dendrimer chemistry have shown that carboxyl-terminated (poly)amidoamine (PAMAM) dendrimers with folic acid modifications can be assembled onto the surface of iron oxide nanoparticles for intracellular uptake studies [F14]. Recently, Saboktakin *et al.* [F15] reported superparamagnetic iron oxide nanoparticles (SPIONs) coated with acetylated PAMAM dendrimers as controlled release systems for parental administration of mesalamine drug. Efforts have been continuously made to demonstrate the ability of dendritic molecules to deliver MNPs into cells, however, not much success has been achieved. Martin *et al.* [F16] aimed at modulating the uptake of SPIONs by cells for *in vitro* labeling using polyester dendron having multiple peripheral guanidine groups. This dendritic guanidine was found to have good penetrating capability upon conjugation with SPIONs and also enhanced the cellular uptake. Folate targeted PEG conjugate of PAMAM dendrimers [F17] was used as drug delivery system for controlled release of antiarthiritic drug, indomethacin with reduced side effects and higher targeting efficiency. The application of PEGylated diaminobutane poly(propylene imine) dendrimers [F18] as drug carrier was evaluated for solubilizing and release of betamethasone corticosteroids.

In spite of significant progress in the synthesis of magnetic nanoparticles, preventing agglomeration or precipitation of MNPs remains an important issue. Stability still is a crucial para-

meter for almost any application of the magnetic nanoparticles. The main difficulty arises due to the susceptibility of the nanoparticles towards oxidation which increases with decrease in particle size [F19]. Therefore, it is essential to develop efficient strategies for improving the chemical stability of the nanoparticles. This can be achieved by protecting the nanoparticles with an impenetrable layer which prevents the oxygen to reach the particle surface.

Towards this direction, we report here on a straightforward and time efficient approach facilitating *in-situ* synthesis of dendritic stabilized MNPs using the chemical co-precipitation method. The readily accessible flexident biocompatible organic coatings with ethylene glycol-based tentacles provide stability to the MNPs surface and hence, protect from particle coagulation. The resulted MNPs were characterized with TEM, XPRD, TGA, FT-IR and SQUID-VSM magnetometry.

2. Materials and Methods

2.1. Materials and Instruments

All synthesis procedures were performed under dinitrogen atmosphere. Water was deoxygenated prior to use. Iron (II) chloride tetrahydrate, iron (III) chloride hexahydrate, ammonium hydroxide solution and methanol were purchased from SIGMA ALDRICH and used without further purification. The (poly)amidoamine (PAMAM)-based dendrimers **3**, **4** and **5a** – **5c** as well as amines **1** and **2** were synthesized according to previously published procedures [F20].
Size and morphology of the magneto-dendrimer NPs were determined using TEM imaging, performed on a PHILIPS CM 20 operated at 200 kV, while the structure of the powder samples was identified by X-ray powder diffraction (XRPD) on a STOE-STAD IP diffractometer with Cu-K_α (1.5405 Å) radiation. The surface coating was examined by FT-IR spectroscopy recorded with a FT Nicolet IR 200 instrument. Thermogravimetric experiments were performed on a METTLER-TOLEDO TGA/DSC1 1100 system with an UMX1 balance. Mass spectrometry coupled thermogravimetric experiments were determined by using a METTLER-TOLEDO TGA/DSC1 1600 system with a MX1 balance coupled with a PFEIFFER VACUUM MS ThermoStar GSD 301 T2 mass spectrometer. Magnetic properties of the magnetite nanoparticles were studied by a QUANTUM DESIGN SQUID-VSM. Field cooled (FC) and zero field cooled (ZFC) magnetization measurements were performed in the temperature range 5 K to 300 K at two different magnetic fields of 100 Oe and 200 Oe. Field dependent magnetization measurements were also recorded for the samples at various temperatures be-

tween 5 K and 300 K in the field range -70 kOe to +70 kOe. For ZFC measurements, the samples were cooled in a zero magnetic field from 300 K to 5 K and at 5 K a small magnetic field of ≈ 100 Oe or 200 Oe was applied. The magnetic moment was measured on warming the samples to 300 K (ZFC magnetization). Next, the magnetic moment was measured by cooling the sample from 300 K down to 5 K keeping the applied field unchanged (FC magnetization).

2.2. Synthesis Procedure for Fe_3O_4 Nanoparticles

In a typical experiment, *in-situ* dendritic stabilized Fe_3O_4 NPs were prepared by the chemical co-precipitation method in a 250 mL round bottom flask equipped with a mechanical stirrer, gas inlet and condenser. [$FeCl_2 \cdot 4\ H_2O$] and two equivalents of [$FeCl_3 \cdot 6\ H_2O$] were dissolved in deoxygenated distilled water and kept at 70 °C for 15 min. N_2 gas was kept passing through the aqueous mixture during the whole experimental process. While vigorously stirring the reaction mixture, an appropriate amount (molar ratio stabilizer-to-Fe_3O_4 = 1:10, 1:100, 1:1000) of the respective (dendritic) stabilizer dissolved in 3 mL of methanol was added in a single portion. After alkaline hydrolysis (pH 8.5) by adding a slight excess of NH_4OH in solution (25 %), the appropriate Fe_3O_4 colloids were obtained as a black precipitate in virtually quantitative yield and isolated by magnetoseparation, decantation and washed twice with 25 mL of distilled water and methanol. The products were dried at 25 °C for 24 hrs.

Data for **1**-stabilized colloids (**1**:Fe_3O_4 = 1:100): 10 mg (0.023 mmol) **1**, 0.46 g (2.3 mmol) [$FeCl_2 \cdot 4\ H_2O$] and 1.24 g (4.6 mmol) [$FeCl_3 \cdot 6\ H_2O$] in 70 mL H_2O.

Data for **2**-stabilized colloids (**2**:Fe_3O_4 = 1:100): 10 mg (0.012 mmol) **2**, 0.24 g (1.2 mmol) [$FeCl_2 \cdot 4\ H_2O$] and 0.66 g (2.4 mmol) [$FeCl_3 \cdot 6\ H_2O$] in 40 mL H_2O.

Data for **3**-stabilized colloids (**3**:Fe_3O_4 = 1:100): 10 mg (0.007 mmol) **3**, 0.14 g (0.7 mmol) [$FeCl_2 \cdot 4\ H_2O$] and 0.38 g (1.4 mmol) [$FeCl_3 \cdot 6\ H_2O$] in 20 mL H_2O.

Data for **4**-stabilized colloids (**4**:Fe_3O_4 = 1:100): 10 mg (0.005 mmol) **4**, 0.1 g (0.5 mmol) [$FeCl_2 \cdot 4\ H_2O$] and 0.27 g (1.0 mmol) [$FeCl_3 \cdot 6\ H_2O$] in 15 mL H_2O.

Data for **5a**-stabilized colloids (**5a**:Fe_3O_4 = 1:1000): 10 mg (0.005 mmol) **5a**, 1.01 g (5 mmol) [$FeCl_2 \cdot 4\ H_2O$] and 2.72 g (10 mmol) [$FeCl_3 \cdot 6\ H_2O$] in 150 mL H_2O.

Data for **5b**-stabilized colloids (**5b**:Fe_3O_4 = 1:10): 150 mg (0.06 mmol) **5b**, 120 mg (0.6 mmol) [$FeCl_2 \cdot 4\ H_2O$] and 320 mg (1.2 mmol) [$FeCl_3 \cdot 6\ H_2O$] in 18 mL H_2O.

Data for **5b**-stabilized colloids (**5b**:Fe_3O_4 = 1:100): 75 mg (0.029 mmol) **5b**, 580 mg (2.9 mmol) [$FeCl_2 \cdot 4\ H_2O$] and 1.58 g (5.8 mmol) [$FeCl_3 \cdot 6\ H_2O$] in 90 mL H_2O.

Data for **5b**-stabilized colloids (**5b**:Fe_3O_4 = 1:1000): 10 mg (0.0039 mmol) **5b**, 770 mg (3.9 mmol) [$FeCl_2 \cdot 4\ H_2O$] and 2.11 g (7.8 mmol) [$FeCl_3 \cdot 6\ H_2O$] in 120 mL H_2O.

Data for **5c**-stabilized colloids (**5c**:Fe_3O_4 = 1:1000): 20 mg (0.0036 mmol) **5c**, 720 mg (3.6 mmol) [$FeCl_2 \cdot 4\ H_2O$] and 1.96 g (7.2 mmol) [$FeCl_3 \cdot 6\ H_2O$] in 110 mL H_2O.

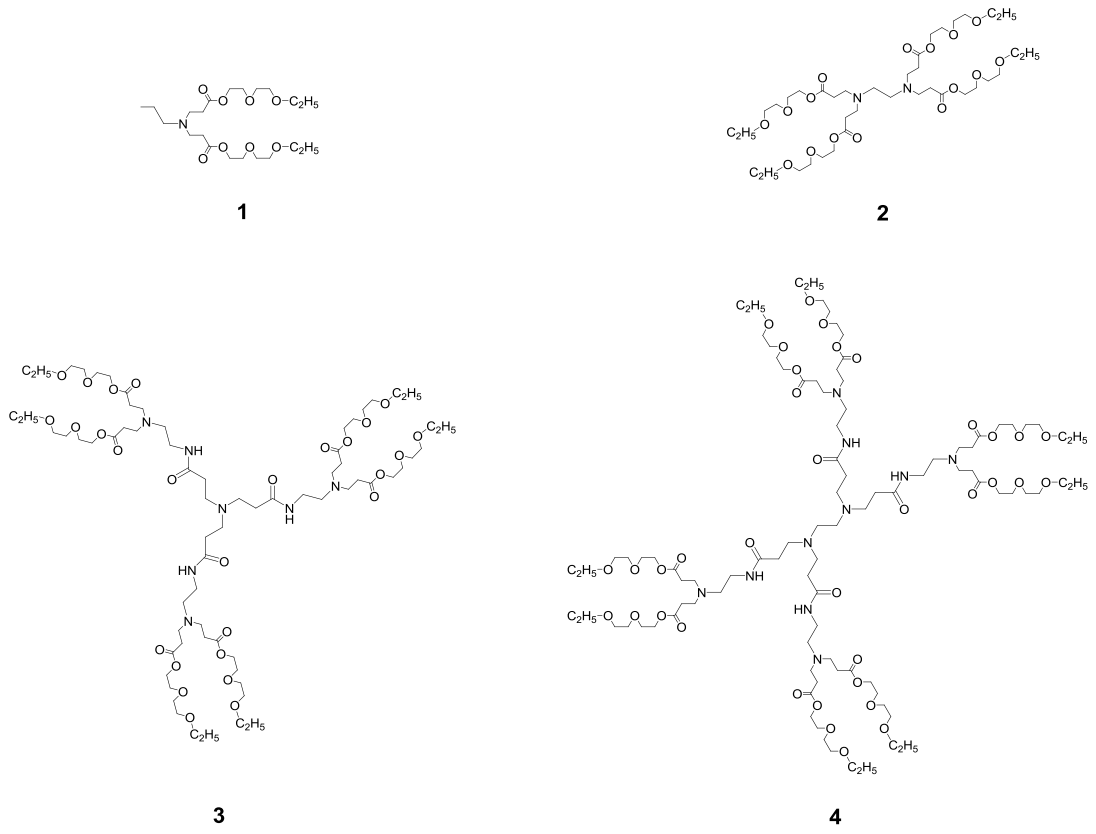

Chart F1. (Di)ethylene glycol-functionalized PAMAM-dendrimers **3** and **4** as well as amines **1** and **2**, for comparison [F20].

3. Results and Discussion

3.1. Preparation and Characterization of Dendrimer-Surfaced Fe_3O_4 Nanoparticles

End-grafted ethylene glycol ether-functionalized amidoamine-based low-generation dendrimers **3**, **4** (Chart F1) and **5a** – **5c** (Scheme F1) as well as amines **1** and **2** (Chart F1) were prepared according to published procedures [F20]. The obtained biocompatible PEGylated dendritic nanoreactors of type $N(CH_2CH_2C(O)NHCH_2CH_2NR_2)_3$ (**3**, R = $CH_2CH_2C(O)O(CH_2CH_2O)_2C_2H_5$), $[CH_2N(CH_2CH_2C(O)NHCH_2CH_2NR_2)_2]_2$ (**4**, R = $CH_2CH_2C(O)O(CH_2CH_2O)_2C_2H_5$) and $(R_2NCH_2CH_2NHC(O)CH_2CH_2)N[CH_2CH_2N(CH_2CH_2C(O)NHCH_2CH_2NR_2)_2]_2$ (**5a**, R = $CH_2CH_2C(O)OCH_2CH_2OCH_3$; **5b**, R = $CH_2CH_2C(O)O(CH_2CH_2O)_2C_2H_5$; **5c**, R = $CH_2CH_2C(O)O(CH_2CH_2O)_9CH_3$) as well as amines **1** and **2** were applied as surfactants during the formation of iron oxide NPs by the controlled co-precipitation method from Fe^{2+} and Fe^{3+} salts in an alkaline medium [F21].

The resulting black colored Fe_3O_4 colloids with dendrimer coating were stable in aqueous solution. No bulk precipitate was observed in the reactions performed using mild conditions with slightly elevated temperatures (70 °C). After separation from the supernatant solution, the functionalized Fe_3O_4 NPs were dried at ambient temperature for 24 hrs (Scheme F2).

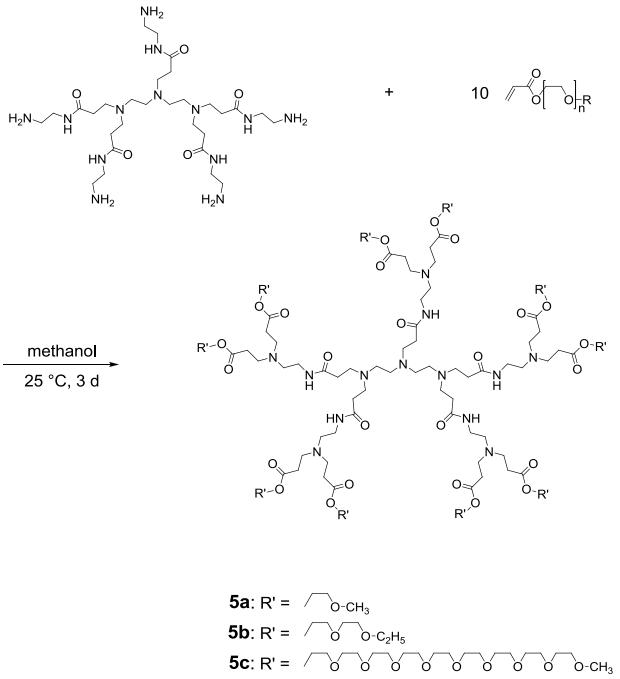

Scheme F1. Synthesis of (oligo)ethylene glycol ether-functionalized amidoamine-based low-generation dendrimers **5a** – **5c** [F20].

The nature of the chemical bonding in the newly formed hybrid materials was investigated using FT-IR spectroscopy. Figure F1 shows the FT-IR spectra of **5b** and **5b**-coated Fe_3O_4 nanoparticles. In the spectrum of **5b**-stabilized MNPs the vibration bands at around 585 and 440 cm^{-1} indicate the formation of Fe_3O_4 as these peaks result from symmetric Fe−O stretching and antisymmetric Fe−O vibrations, respectively [F22].

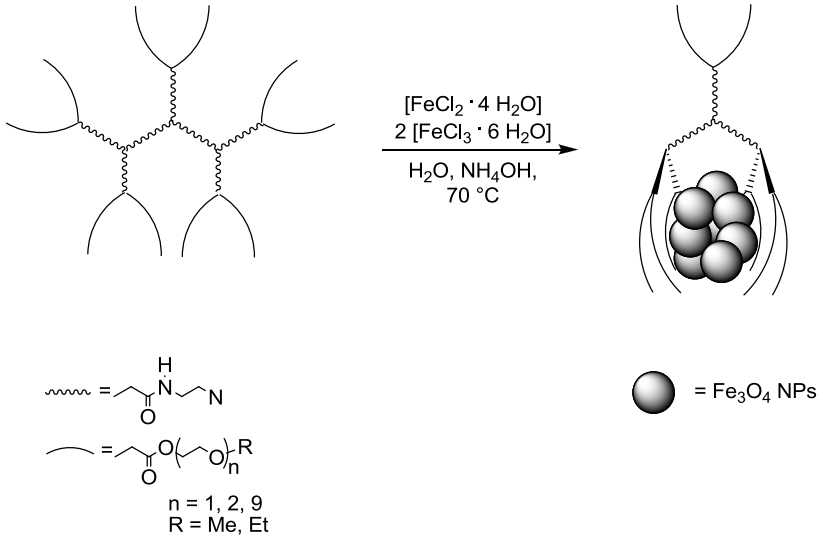

Scheme F2. Schematic illustration of *in-situ* dendrimer-stabilized Fe_3O_4 NP formation by the co-precipitation method.

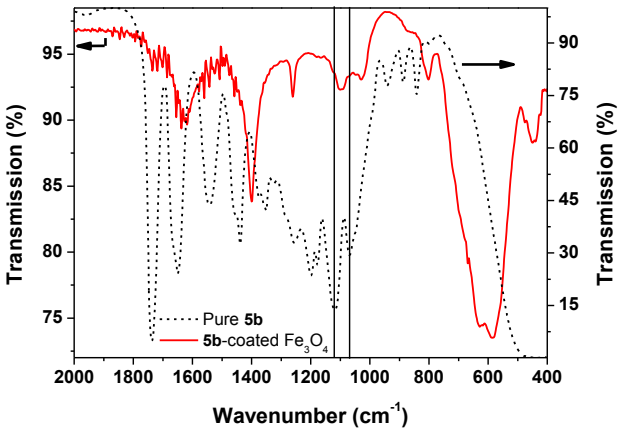

Figure F1. FT-IR spectra of pure **5b** and **5b**-coated Fe_3O_4 MNPs.

As an evidence for surfacing the colloids by the applied dendritic stabilizers the strong band at around 1095 cm^{-1} can be cited attributing to the C−O−C vibrations of the terminal (poly)ethylene glycol ether units. This absorption is bathochromic shifted by approximately 30 cm^{-1}, when compared to the parent dendrimers **5a** – **5c** [F20]. Furthermore, the broad bands

between 1620 and 1700 cm^{-1} can be assigned to both the amide and the ester functionalities of the dendritic scaffold.

The phase and crystalline nature of dendrimer stabilized Fe_3O_4 MNPs were confirmed by XPRD analysis of **5b**-coated Fe_3O_4 colloids (**5b**:Fe_3O_4 = 1:100) as shown exemplarily in Figure F2. The revealed powder diffraction pattern is consistent with standard Fe_3O_4 reflections reported in literature and in Joint Committee on Powder Diffraction Standards (JCPDS Card No. 19-629) [F23], confirming the formation of magnetite NPs with the space group *Fd-3m*. The characteristic diffraction peaks could be well indexed to the inverse cubic spinel structure of Fe_3O_4. The crystallite size of magnetite as calculated by the Scherrer formula was found to be ≈ 8.2 nm [F23]. From the color of the precipitate as well as from the XRPD and FT-IR results, it is justified to conclude that the formed nanoparticles are that of Fe_3O_4. However, further experiments are necessary to exclude the presence of traces of Fe_2O_3, if any.

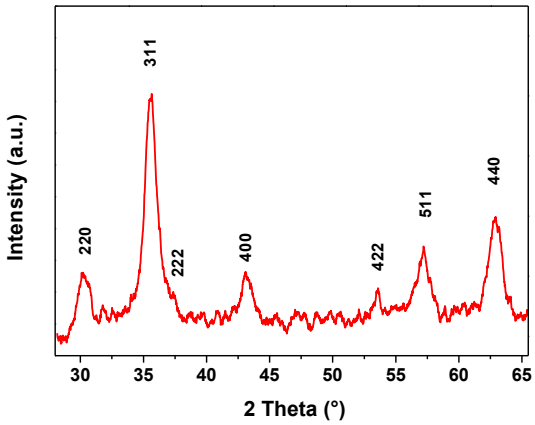

Figure F2. X-ray powder diffraction patterns derived from **5b**-stabilized Fe_3O_4 NPs (**5b**:Fe_3O_4 = 1:100).

The magneto-dendrimer NPs were imaged by TEM. Figure F3 depicts representative TEM images of Fe_3O_4 NPs stabilized by **1** (surfactant:Fe_3O_4 = 1:100; Ø = 10.1 (± 1.9) nm), **5b** (surfactant:Fe_3O_4 = 1:10; Ø = 5.6 (± 1.4) nm) and **5b** (surfactant:Fe_3O_4 = 1:100; Ø = 7.3 (± 1.3) nm). The mean particle diameters and standard deviations were determined from TEM micrographs from the statistics of at least 300 particles. The corresponding particle sizes of **1** – **4** and **5a** – **5c**-surfaced Fe_3O_4 NPs are presented in Table F1. Although negligible cluster aggregation occurs in all specimens as a result of drying effects in the sample preparation, the herein implemented co-precipitation method gives reproducible, well-defined spherical magnetite NPs embedded in biocompatible organic coatings of slightly decreased sizes compared to

other approaches in literature [F24]. To some extent the resulting particle sizes can be affected by variation of the donation capabilities of the applied dendritic protective coatings and the adjusted molar surfactant-to-Fe_3O_4 ratio [F20].

a)

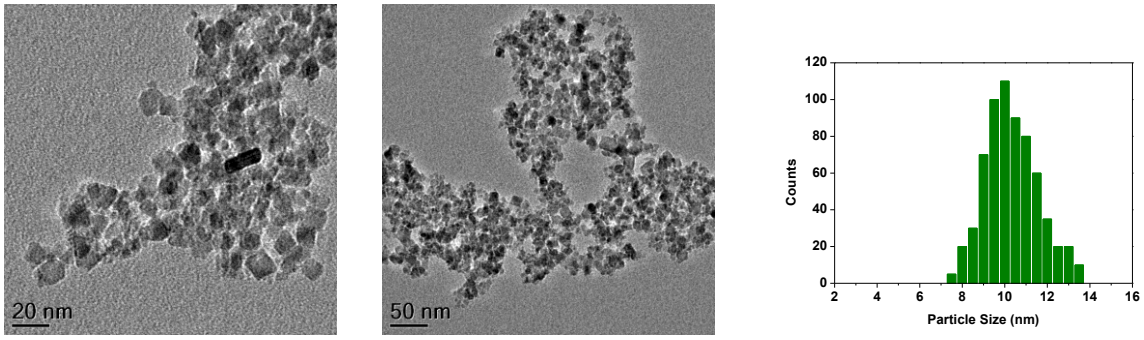

b)

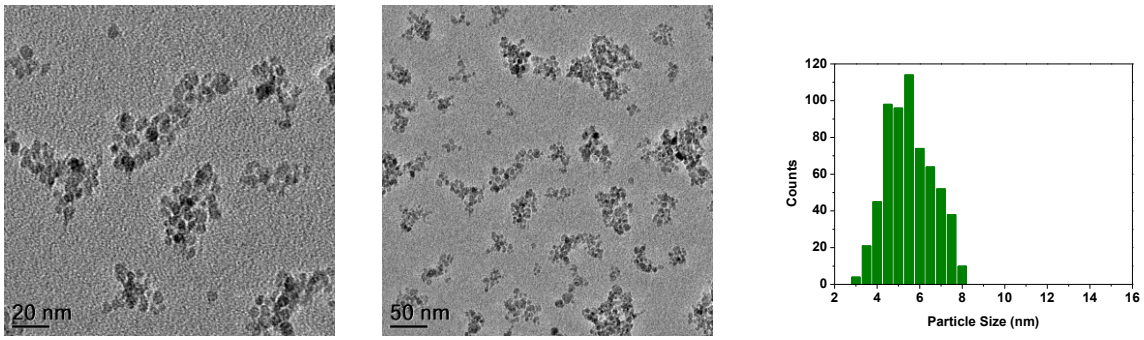

c)

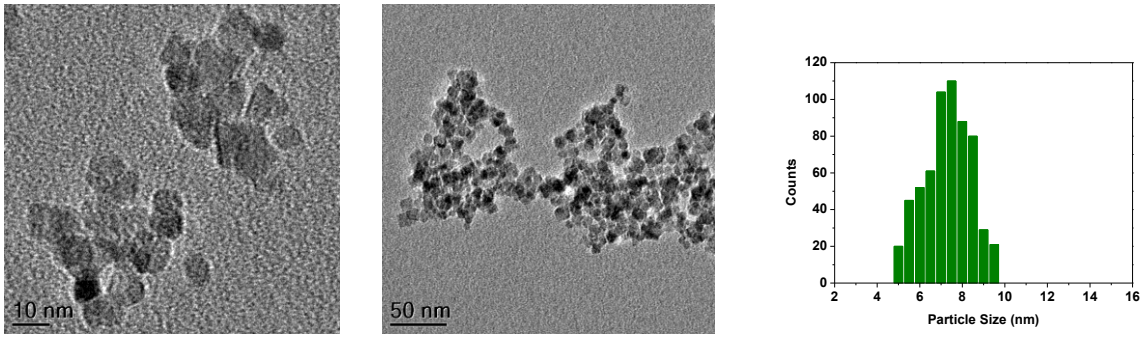

Figure F3. TEM images and particle size distributions of a) **1-** (surfactant:Fe_3O_4 = 1:100; ø = 10.1 (± 1.9) nm), b) **5b-** (surfactant:Fe_3O_4 = 1:10; ø = 5.6 (± 1.4) nm) and c) **5b-** (surfactant:Fe_3O_4 = 1:100; ø = 7.3 (± 1.3) nm) coated Fe_3O_4 NPs. Note the difference in scale bar in 3 c) compared to panels in a) and b)).

From Table F1 it can be seen that increasing the number of peripheral attached ether tentacles, using longer ethylene glycol ether termini at the amidoamine-based stabilizer´s scaffold as well as higher molar surfactant-to-Fe_3O_4 ratios led to the formation of smaller colloidal iron oxide composites as the dendritic-constrained nanoreactors provide a confinement that restricts particle nucleation and growth. However, the control of the particle size distribution is limited, because the crystal growth in co-precipitation method is mainly influenced by kinetic factors [F25].

The TEM determined particle size for, *e.g.* **5b**-surfaced Fe_3O_4 colloids (molar ratio surfactant:Fe_3O_4 = 1:100) is in good accordance with the crystallite size obtained by line profile fitting of the XRPD using Scherrer equation (Figure F2).

Table F1. Particle sizes generated by surfactants **1** – **4** and **5a** – **5c** for varied molar stabilizer:Fe_3O_4 ratios.

Surfactant	Ratio	Particle Size
1	1:100	10.1(± 1.9) nm
2	1:100	9.8 (± 2.1) nm
3	1:100	9.1 (± 2.6) nm
4	1:100	8.2 (± 1.4) nm
5a	1:1000	9.0 (± 1.7) nm
5b	1:10	5.6 (± 1.4) nm
5b	1:100	7.3 (± 1.3) nm
5b	1:1000	8.8 (± 2.0) nm
5c	1:1000	7.3 (± 1.9) nm

The thermal decomposition of the hybrid-material **5b**:Fe_3O_4 (1:100) was studied by thermogravimetric experiments in a dinitrogen atmosphere and a temperature range of 40 °C – 700 °C using a heating rate of 10 K min^{-1} (Figure F4). Decomposition and transformation processes of both the organics and the iron oxide material within the applied composite occur in various steps between 70 °C and 550 °C resulting in an overall mass diminution of 12.3

wt%. Furthermore, in mass spectrometry-coupled thermogravimetric studies only m/z = 44 amu was detected during the decomposition process. This mass fragment can be assigned to $[CO_2]^+$, $[CONH_2]^+$ as well as $[C_2H_4O]^+$ representing sample specific components of **5b**:Fe_3O_4 (1:100).

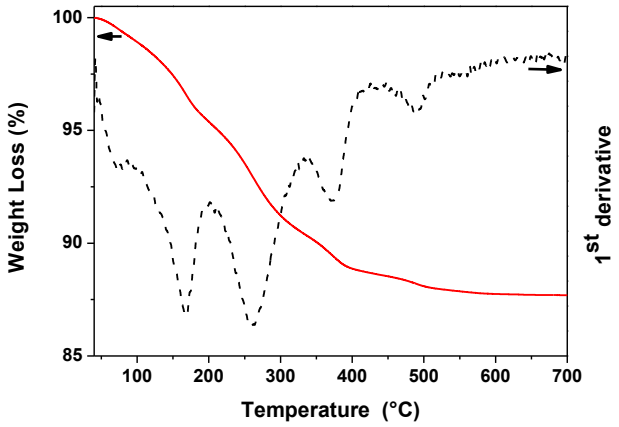

Figure F4. Thermogravimetric analysis of hybrid-material **5b**:Fe_3O_4 (1:100) in a dinitrogen atmosphere (20 mL min^{-1}) using a heating rate of 10 K min^{-1}.

3.2. Magnetic Characterization of Dendrimer-Coated Fe_3O_4 Nanoparticles

Magnetic measurements were carried out on all samples in powder form using a SQUID-VSM. FC and ZFC magnetization recorded at two different fields for colloids **5b**:Fe_3O_4 = 1:100 is, for example, shown in Figure F5.

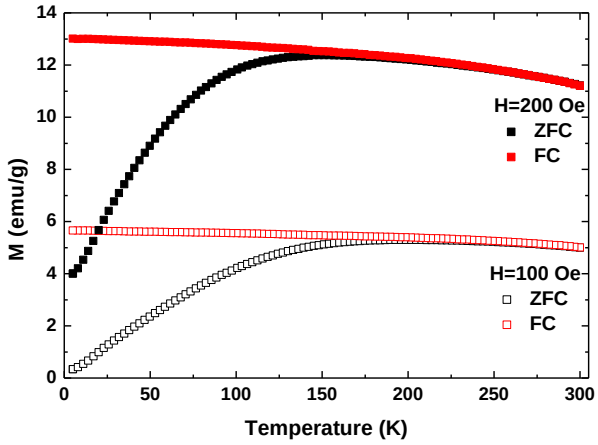

Figure F5. FC and ZFC magnetizations of colloids **5b**:Fe_3O_4 = 1:100 as a function of temperature recorded at magnetic fields H = 100 Oe and H = 200 Oe, respectively.

In the FC mode, the magnetization increases slightly as the temperature is swept from 300 K to 5 K, whereas the ZFC magnetization exhibits a maximum followed by a steady decrease of magnetization in the low-temperature regime. This type of magnetization behavior is expected for superparamagnetic particles which show ferrimagnetic characteristics at temperatures below the blocking temperature T_B. Here, T_B is defined as $T_B = KV/k_B\ln(\tau_m/\tau_0)$ where K is the crystalline anisotropy constant, k_B is the Boltzmann constant, V is the volume of the particle, τ_m is the measurement time (typically 100 s) and τ_0 is the inverse of the attempt frequency associated with magnetic moments overcoming field-dependent energy barriers [F26].

In the ZFC mode during cooling, for temperatures lower than T_B, the magnetization of each particle aligns with the direction of the easy axes and because of the random orientation of easy axes of the nanoparticles, the total magnetization approaches zero at low temperatures. However, when the sample is warmed up to 300 K, an increasing number of particles will acquire thermal energy to switch their magnetization from the easy axes to the direction of the applied magnetic field. This leads to an increase in magnetization of the sample. At temperatures higher than T_B, the nanoparticles undergo superparamagnetic relaxation, where the magnetization of each particle fluctuates in between the easy axis. TEM investigations showed that there is a distribution in MNPs sizes. Hence, a distribution in blocking temperature is expected. In a system consisting of non-interacting magnetic nanoparticles, the derivative of $(M_{ZFC}-M_{FC})$ with respect to temperature T is a representative of the blocking temperature distribution [F27]. Here, M_{ZFC} is the ZFC magnetization and M_{FC} is the FC magnetization. In order to investigate this, $-d(M_{FC}-M_{ZFC})/dT$ as a function of temperature T, is plotted in Figure F6.

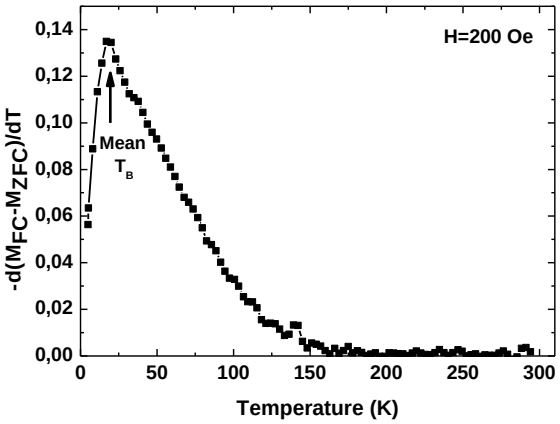

Figure F6. Derivative of difference in FC and ZFC magnetization of **5b**:Fe_3O_4 = 1:100 with respect to temperature plotted as a function of temperature.

It was found that for sample **5b**:Fe_3O_4 = 1:100 there is a distribution in T_B and mean T_B was around 20 K. From this value, a rough estimate of the mean particle size can be obtained using the equation $T_B = KV/25k_B$ [F28]. Here, we assumed the anisotropy constant K as $1.35 \cdot 10^4$ J m^{-3} that of bulk Fe_3O_4 [F29]. NPs diameters thus obtained are around 10 nm which is in the range of particle sizes found from the TEM images and the calculation by the Scherrer formula. Slight discrepancies in the sizes can be due to the assumption of bulk anisotropy constant for Fe_3O_4 nanoparticles as well as due to the dipole-dipole interactions between the nanoparticles.

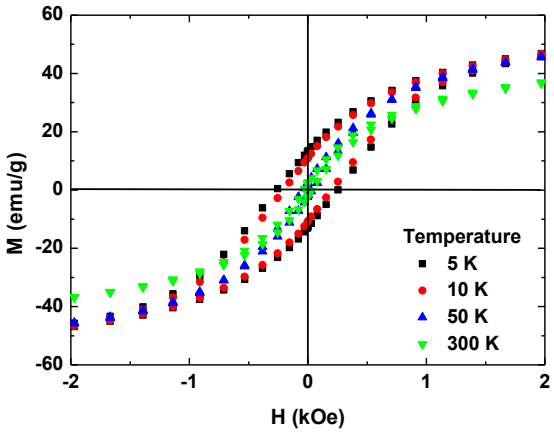

Figure F7. M-H loops for sample **5b**:Fe_3O_4 = 1:100 recorded at temperatures 5 K, 10 K, 50 K and 300 K.

Figure F7 shows M-H loops recorded for **5b**:Fe_3O_4 = 1:100 at 5 K, 10 K, 50 K and 300 K. M-H loops at 5 K and 10 K show hysteretic behavior as expected for superparamagnetic nanoparticles in a blocked state. The coercive field, H_c determined from the loop is 258 Oe and 202 Oe for 5 K and 10 K, respectively. M-H loops recorded at 300 K shows negligible remanence and coercivity, which is characteristic of magnetic nanoparticles where thermal fluctuations are sufficient to overcome the anisotropy energy barrier, allowing the magnetization to spontaneously reverse direction. It has to be noted that the MNPs obtained in the present experiment are in a size range well below 20 nm, a value often proposed as the superparamagnetic limit for Fe_3O_4 particles. For a comparison, magnetic properties of dendrimer-coated Fe_3O_4 NPs obtained from different synthesis conditions are summarized in Table F2. Not much difference was observed in the coercivity and mean blocking temperature for the four samples except for the magnetization values. Magnetization of a composite consisting of dendrimer-coated Fe_3O_4 nanoparticles is mainly influenced by the volume fraction of Fe_3O_4 NPs in the composite matrix and the differences in magnetization observed in the sample series are

in accordance with the composition analyzed using inductively coupled plasma mass spectrometry (ICP-MS).

Table F2. Magnetic properties of dendrimer-stabilized magnetite NPs.

Sample	5 K		300 K		Mean T_B (K)
	H_c (Oe)	M @ 70 kOe (emu/g)	H_c (Oe)	M @ 70 kOe (emu/g)	
5a:Fe_3O_4 (1:100)	214±3	74.5	32±3	61.5	20±2
5b:Fe_3O_4 (1:10)	232±3	88.9	33±3	75.4	20±2
5b:Fe_3O_4 (1:100)	258±3	66.9	32±3	56.5	20±2
5b:Fe_3O_4 (1:1000)	228±3	54.2	33±3	45.7	20±2

4. Conclusion

Fe_3O_4 nanoparticles stabilized by biocompatible low-generation (poly)amidoamine-based dendrimers modified with end-grafted ethylene glycol ether moieties of type $(N(CH_2CH_2C(O)NHCH_2CH_2NR_2)_3$ (R = $CH_2CH_2C(O)O(CH_2CH_2O)_2C_2H_5$), $[CH_2N(CH_2CH_2C(O)NHCH_2CH_2NR_2)_2]_2$ (R = $CH_2CH_2C(O)O(CH_2CH_2O)_2C_2H_5$) and $(R_2NCH_2CH_2NHC(O)CH_2CH_2)N[CH_2CH_2N(CH_2CH_2C(O)NHCH_2CH_2NR_2)_2]_2$ (R = $CH_2CH_2C(O)OCH_2CH_2OCH_3$; R = $CH_2CH_2C(O)O(CH_2CH_2O)_2C_2H_5$; R = $CH_2CH_2C(O)$-$O(CH_2CH_2O)_9CH_3$) were synthesized using Fe^{2+} and Fe^{3+} mixed aqueous salt solutions in the chemical co-precipitation method. The implemented synthesis protocol yielded Fe_3O_4 MNPs of sizes in the range of 5 nm to 10 nm depending on the applied molar stabilizer-to-Fe_3O_4 ratio = 1:10, 1:100, 1:1000 as well as the number of ethylene glycol tentacles and the intrinsic donation capabilities of the utilized stabilizer. TEM studies revealed that increasing the number of tentacles and donation capabilities as well as higher molar ratios of the applied dendritic surfactants results in the formation of ultrafine magnetite colloids. The obtained NPs are superparamagnetic at ambient temperatures and thus the present synthesis method is capable

of obtaining biocompatible well-defined dendrimer-embedded Fe_3O_4 colloids for potential medical applications.

5. Acknowledgement

This study was generously supported by the Deutsche Forschungsgemeinschaft, the Fonds der Chemischen Industrie, the German Academic Exchange Service (DAAD) and the State of Saxony (Landesgraduierten Stipendium S.D.).

6. References

[F1] S. Sun, C.B. Murray, D. Weller, L. Folks, A. Moser, *Science* **2000**, *287*, 1989.

[F2] W. Voit, W. Zapka, L. Belova and K.V. Rao, *IEE Proc.-Sci. Meas. Technol.* **2003**, *150*, 252.

[F3] (a) M.M. Miller, G.A. Prinz, S.F. Cheng, S. Bounnak, *Appl. Phys. Lett.* **2002**, *81*, 2211;

(b) X. Chen, X. Sun, Y. Liu, B. Luo, C. Wang, Y. Bao, H. Xu, H. Peng, *Angew. Chem.* **2011**, *123*, 5600.

[F4] (a) T.K. Jain, M.A. Morales, S.K. Sahoo, D.L. Leslie-Pelecky, V. Labhasetwar, *Mol. Pharm.* **2005**, *2*, 194;

(b) I. Chourpa, L. Douziech-Eyrolles, L. Ngaboni-Okassa, J.F. Fouquenet, S. Cohen-Jonathan, M. Souce, H. Marchais, P. Dubois, *Analyst* **2005**, *130*, 1395.

[F5] (a) S. Boutry, S. Laurent, L. van der Elst, R.N. Muller, *Contrast Med. Mol. Imaging* **2006**, *1*, 15;

(b) C. Corot, P. Robert, J.M. Idee, M. Port, *Adv. Drug Deliv. Rev.* **2006**, *58*, 1471.

[F6] H.Maeda, J.Wu, T. Sawa, Y. Matsumura, K. Hori, *J. Control. Release* **2000**, *65*, 271.

[F7] (a) M.R. Saboktakin, A. Maharramov, M.A. Ramazanov, *New York Science Journal* **2008**, *1*, 14;

(b) K. Krogars, J. Heinamaki, J. Vesalahti, M. Marvola, O. Antikainen, J. Yliruusi, *Int. J. Pharma.* **2000**, *199*, 187.

[F8] J. Qin, S. Laurent, Y.S. Jo, A. Roch, M. Mikhaylova, Z.M. Bhujwalla, R.N. Muller, M. Muhammed, *Adv. Mater.* **2007**, *19*, 1874.

[F9] (a) Y. Sahoo, H. Pizem, T. Fried, D. Golodnitsky, L. Burstein, C.N. Sukenik, G. Markovich, *Langmuir* **2001**, *17*, 7907;

(b) Y. Sahoo, A. Goodarzi, M.T. Swihart, T.Y. Ohulchanskyy, N. Kaur, E.P. Furlani, P.N. Prasad, *J. Phys. Chem. B* **2005**, *109*, 3879.

[F10] (a) Y. Zhang, N. Kohler, M. Zhang, *Biomaterials* **2002**, *23*, 1553;

(b) L.M. Lacava, Z.G.M. Lacava, M.F. da Silva, O. Silva, S.B. Chaves, R.B. Azevedo, F. Pelegrini, C. Gansau, N. Buske, D. Sabolovic, P.C. Morais, *Biophys. J.* **2001**, *80*, 2483.

[F11] C. Zhang, B. Wangler, B. Morgenstern, H. Zentgraf, M. Eisenhut, H. Untenecker, R. Kruger, R. Huss, C. Seliger, W. Semmler, F. Kiessling, *Langmuir* **2007**, *23*, 1427.

[F12] J.W. Bulte, M. de Cuyper, *Methods Enzymol.* **2003**, *373*, 175.

[F13] (a) S.H. Wang, X. Shi, M. van Antwerp, Z. Cao, S.D. Swanson, X. Bi, J.R. Baker Jr., *Adv. Funct. Mater.* **2007**, *17*, 3043;

(b) E. Strable, J.W.M. Bulte, B. Moskowitz, K. Vivekanandan, M. Allen, T. Douglas, *Chem. Mater.* **2001**, *13*, 2201.

[F14] S. Xiangyang, T.P. Thomas, L.A. Myc, A. Kotlyar, J.R. Baker, *Phys. Chem. Chem. Phys.* **2007**, *9*, 5712.

[F15] M.R. Saboktakin, A. Maharramov, M.A. Ramazanov, *Polymer-Plastics Technol. Engn.* **2010**, *49*, 104.

[F16] A.L. Martin, L.M. Bernas, B.K. Rutt, P.J. Foster, E.R. Gillies, *Bioconj. Chem.* **2008**, *19*, 2375.

[F17] D. Chandrasekar, R. Sistla, F.J. Ahmad, R.K. Khar, P.V. Diwan, *J. Biomed. Mater. Res. A* **2007**, *82*, 92.

[F18] **Z**. Sideratou, D. Tsiourvas, C.M. Paleos, *J. Colloid Interface Sci.* **2001**, *242*, 272.

[F19] A.-H. Lu, E.L. Salabas, F. Schüth, *Angew. Chem. Int. Ed.* **2007**, *46*, 1222.

[F20] (a) S. Chandra, S. Dietrich, H. Lang, D. Bahadur, *J. Mater. Chem.* **2011**, *21*, 5729;

(b) S. Dietrich, S. Schulze, M. Hietschold, H. Lang, *J. Colloid Interface Sci.* **2011**, *359*, 454;

(c) S. Dietrich, A. Nicolai, H. Lang, *J. Organomet. Chem.* **2011**, *696*, 739.

[F21] (a) K. Hervé, L. Douziech-Eyrolles, E. Munnier, S. Cohen-Jonathan, M. Soucé, H. Marchais, P. Limelette, F. Warmont, M.L. Saboungi, P. Dubois, I. Chourpa, *Nanotechnology* **2008**, *7*, 465608;

(b) S. Mornet, J. Portier, E. Duguet, *J. Magn. Magn. Mater.* **2005**, *293*, 127;

(c) M. Mikhaylova, D.K. Kim, C.C. Berry, A. Zagorodni, M. Toprak, A.S.G. Curtis, M. Muhammed, *Chem. Mater.* **2004**, *16*, 2344;

(d) Y.S. Kang, S. Risbud, J.F. Rabolt, P. Stroeve, *Chem. Mater.* **1996**, *8*, 2209.

[F22] H. Xia, P. Foo, J. Yi, *Chem. Mater.* **2009**, *21*, 2442.

[F23] (a) H. Xia, J. Yi, P. Foo, B. Lui, *Chem. Mater.* **2007**, *19*, 4087;

(b) A. Guinier, *X-Ray Diffraction in Crystals, Imperfect Crystals and Amorphous Bodies* **1994**, Dover Publications, New York.

[F24] (a) A.-H. Lu, E.L. Salabas, F. Schüth, *Angew. Chem.* **2007**, *119*, 1242;

(b) S. Wan, J. Huang, H. Yan, K. Liu, *J. Mater. Chem.* **2006**, *16*, 298;

(c) M. Aydın, Z. Durmus, H. Kavas, B. Esat, H. Sözeri, A. Baykal, F. Yilmaz, M.S. Toprak, *Polyhedron* **2011**, *30*, 1120;

(d) Z. Li, M. Kawashita, N. Araki, M. Mitsumori, M. Hiraoka, M. Doi, *Mater. Sci. Eng. C-Mater. Biol. Appl.* **2010**, *30*, 990;

(e) L.A. Thomas, L. Dekker, M. Kallumadil, P. Southern, M. Wilson, S.P. Nair, Q.A. Pankhurst, I.P. Parkin, *J. Mater. Chem.* **2009**, *19*, 6529;

(f) A.P. Herrera, C. Barrera, C. Rinaldi, *J. Mater. Chem.* **2008**, *18*, 3650;

(g) G. Marinescu, L. Patron, D.C. Culita, C. Neagoe, C.I. Lepadatu, I. Balint, L. Bessais, C.B. Cizmas, *J. Nanopart. Res.* **2006**, *8*, 1045;

(h) B. Unal, Z. Durmus, H. Kavas, A. Baykal, M.S. Toprak, *Mater. Chem. Phys.* **2010**, *123*, 184.

[F25] S. Laurent, D. Forge, M. Port, A. Roch, C. Robic, L. van der Elst, R.N. Muller, *Chem. Rev.* **2008**, *108*, 2064.

[F26] (a) T.N. Narayanan, A.P. Reena Mary, P.K. Anas Swalih, D. Sakthu Kumar, D. Makarov, M. Albrecht, J. Puthumana, A. Anas, M.R. Anantharaman, *J. Nanosci. Nanotechnol.* **2011**, *11*, 1958;

(b) B.D. Cullity, C.D. Graham, *Fine Particles and Thin Films*, in *Introduction to Magnetic Materials*, Second Edition **2008**, John Wiley & Sons, Inc., Hoboken, NJ, USA.

[F27] H. Mamiya, M. Ohnuma, I. Nakatani, T. Furubayashim, *IEEE Trans. Magn.* **2005**, *41*, 3394.

[F28] C.P. Bean, J.P. Livingston, *J. Appl. Phys.* **1959**, *30* 120.

[F29] D.J. Dunlop, Ö. Özdemir, *Rock Magnetism Fundamentals and Frontiers*, Cambridge University Press **1997**, Cambridge.

G Dendrimer - Doxorubicin Conjugate for Enhanced Therapeutic Effects for Cancer

Sudeshna Chandra, Sascha Dietrich, Heinrich Lang and Dhirendra Bahadur

Published in *J. Mater. Chem.* **2011**, *21*, 5729 − 5737.

The results in the succeeding Chapter were accomplished in a fertile inter-institutional collaboration with Dr. Sudeshna Chandra in the research group of Prof. Dr. Dhirendra Bahadur at the Indian Institute of Technology Bombay (India).

Whereas the synthesis and characterization of amidoamine **1** and OEGylated **2** was performed by the author of the present doctoral thesis in Chemnitz, drug loading of dendrimer **2** with doxorubicin to give a dendrimer-drug conjugate and subsequent *in vitro* cell studies were realized by Dr. Sudeshna Chandra and Prof. Dr. Dhirendra Bahadur in Bombay.

1. Introduction

Exceptional structural properties such as monodispersity, high density peripheral functional groups, globular structure and multivalency of dendrimers [G1] make them an efficient nanodevice for controlled and targeted delivery of therapeutic compounds. Low-generation dendrimers possess open conformations and empty internal cavities which make them possible to encapsulate drug molecules. [G2] They also have more functional groups at the periphery in comparison to conventional macromolecules which enhance the applications of the dendrimers in various ways. The surface functional groups on the dendrimers are responsible for high reactivity and thus a dendrimer can be suitably modified for conjugation and encapsulation of drugs. [G3] However, out of many considerations like hemocompatibility, cytotoxicity, immunogenicity and biodistribution for *in vivo* use of any dendritic system, cytotoxicity remains the most critical factor. The dendritic cytotoxicity is related not only to generations, but also to the charges of the surface groups and it has been well reported that the cytotoxicity of the dendrimers increases with the increase in generation and concentration. [G4] Among dendrimers, the cationic dendrimers were found to be more toxic than the anionic ones due to the fact that the cationic dendrimers interact with the lipid bilayers thereby causing a disturbance in the electrolyte flux resulting in the cell death. [G5, G6] The toxicity from the dendrimers can

be used to enhance the therapeutic efficacy of a drug which when programmed carefully can be used to reduce the dosage of a toxic drug, increase the bioavailability and also provide stability to the drug. [G7] In this way, the dendrimer can act as a shell encapsulating the drug (dendrimer-drug conjugate), which can enhance the delivery of the cytotoxic drug by releasing it in the target site as and when required while minimizing the collateral damage to the normal cells. The loading ability of the drug onto the dendrimers can be tuned by using different linkers between the dendrimer and the drug and thus dendrimer based therapeutics can be formulated. Drugs can be appropriately attached to the dendritic nanodevices by various linkages like ester or amide connectivity which can later be hydrolyzed inside the cell. However, when drugs are loaded non-covalently into the dendrimers, they are rapidly released which make them inefficient for targeted delivery. [G8] Thus, improvement in loading efficiency and release properties remain as major challenges in the dendrimer based drug delivery systems. Since a dendrimer can provide a single molecule character along with their low cost synthesis, toxicology profile and permeability, they can be used not only as a drug carrier but can also be used to facilitate improved internalization over free drug.

Another important factor is the biodistribution of the dendrimers which has been widely studied. Usually, smaller generation dendrimers show rapid renal elimination while higher generation dendrimers show accumulation in the liver. [G9, G10] Binding of the PEG units into a dendrimer scaffold not only helps in reducing toxicity but also increases circulation time in the blood thereby reducing its accumulation in the liver or kidney. This is due to the shielding of the positive charge on the dendrimer by the PEG chains. [G11] Further, enhanced permeation and retention (EPR) can be achieved if the drugs are encapsulated within the PEG moiety of the dendrimer. [G12] In addition to this, there are many reports which demonstrated that PEG chains, when grafted to the polymer micelles and liposomes, suppress their interaction with the plasma proteins cells thereby prolonging the circulation time in blood. [G13, G14] Thus, it is expected that the dendrimers covered with PEG entity make them attractive drug carriers *in vivo*.

To this end, we wish to report an amidoamine dendrimer with an oligo(ethylene glycol) graft (OEG) in the periphery which serves not only as an efficient drug delivery vehicle by loading the drug, but also enhances the sensitivity of the cells towards the drug. Doxorubicin (DOX) was employed as drug molecule and its interaction with the dendrimer was characterized by NMR and HPLC. The release properties of the doxorubicin from the dendrimer-DOX conjugate were studied under hyperthermic condition. As a proof of concept, we also report hyper-

thermia studies through a biphasic suspension [G15] of this dendrimer-drug conjugate. Further, their *in vitro* cell viability and cellular uptake of the dendrimer-DOX conjugate were studied for their potential in therapeutic applications.

2. Experimental Section

2.1. Materials and Methods

Syntheses of dendrimers were performed under dry and deoxygenated N_2 atmosphere using standard Schlenk techniques unless otherwise stated. All solvents were dried by standard procedures over the appropriate drying agents and distilled immediately before use. The reagents purchased commercially (Sigma Aldrich) were used without further purification. Di(ethylene glycol)ethyl ether acrylate was distilled prior to use. Dendrimer **1** was synthesized according to the published procedure. [G16] Doxorubicin hydrochloride was obtained from Sigma Aldrich.

^{1}H and $^{13}C\{^{1}H\}$ NMR spectra were recorded with a Bruker Avance III 500 MHz spectrometer. Chemical shifts δ are given in ppm (parts per million) using $CDCl_3$ solvent as the reference signal. Coupling constants *J* are given in Hertz (Hz). FT-IR spectra were recorded with a FT Nicolet IR 200 instrument in the range of 500 to 4000 cm^{-1}. UV/Vis spectra were obtained with a CECIL CE 3021 spectrophotometer in the wave length range of 200 to 600 nm. High resolution mass spectra were recorded using a micrOTOF QII Bruker Daltonite workstation. The surface charges on samples (pH = 6.6 ± 0.4) were measured using a zeta plus zeta potential analyzer (Brookhaven Instruments) at 25 °C. DLS measurements to determine the size of the OEGylated dendrimer and drug-loaded dendrimer were performed using a Malvern 4800 Autosizer employing a 7132 digital correlator. The light source was an argon ion laser operated at 514.5 nm with a maximum output of 2 W. The concentrations of dendrimer and drug loaded dendrimer were 1 mg · mL^{-1} in the 0.1 M PBS (pH 7.4).

Evidence of the chemical stability of the drug and the interaction of the drug and dendrimer was followed using HPLC using a reversed phase Thermohypersil 28905-020 column (250 × 4.6 mm 5 μ pore size BDS phenyl) operated at room temperature with a Perkin Elmer Series 200 Pump equipped with an UV detector (Varian Prostar). A linear gradient mixture of water/acetonitrile/methanol/H_3PO_4 (540:290:170:2, v/v/v/v) + 1 g SLS was used as a mobile phase at a flow rate of 1.5 mL · min^{-1}. Detection of DOX was done by measuring its UV absorbance at 485 nm. Samples of free DOX and DOX loaded dendrimer were analyzed and a

calibration curve was constructed using the area under the curve (AUC) method and the total amount of DOX was calculated by summing up all AUC, attributed to DOX and its degradation products.

2.2. Synthesis of OEGylated Poly(amidoamine) Dendrimer 2

Molecule **1** (0.9 g, 1.35 mmol) dissolved in 20 mL of methanol was mixed with 5 mL (5.0 g, 27 mmol) of di(ethylene glycol)ethyl ether acrylate. The resulting reaction mixture was stirred for 15 days at 25 °C. After evaporation of all volatiles in oil-pump vacuum, dendrimer **2** (Scheme G1) was obtained as pale yellow oil (3.4 g, 98 %, based on **1**). ^{1}H NMR (δ, $CDCl_3$): 1.20 (t, 30 H, $^{3}J_{HH}$ = 7.0 Hz, CH_3), 2.35 (t, 10 H, $^{3}J_{HH}$ = 6.8 Hz, $CH_2CH_2C(O)NH$), 2.42 (t, 20 H, $^{3}J_{HH}$ = 6.8 Hz, $NCH_2CH_2C(O)$), 2.54 (t, 10 H, $^{3}J_{HH}$ = 6.1 Hz, $HNCH_2CH_2N$), 2.56 (m, 8 H, NCH_2CH_2N), 2.74 – 2.78 (m, 30 H, $NCH_2CH_2C(O)$ / $CH_2CH_2C(O)NH$), 3.25 (dd, 10 H, $^{3}J_{HH}$ = 5.9 Hz, $^{3}J_{HH}$ = 11.6 Hz, $HNCH_2CH_2N$), 3.53 (q, 20 H, $^{3}J_{HH}$ = 7.0 Hz, CH_2CH_3), 3.59 (m, 20 H, $CH_2OCH_2CH_3$), 3.67 (m, 20 H, $CH_2CH_2OCH_2CH_3$), 3.73 (m, 20 H, $C(O)OCH_2CH_2$), 4.24 (m, 20 H, $C(O)OCH_2CH_2$), 7.15 (m, 5 H, C(O)N*H*). $^{13}C\{^{1}H\}$ NMR (δ, $CDCl_3$): 15.1 (CH_3), 32.7 ($NCH_2CH_2C(O)$), 33.8 ($CH_2CH_2C(O)NH$), 37.2 ($HNCH_2CH_2N$), 49.3 ($NCH_2CH_2C(O)$), 50.2 ($CH_2CH_2C(O)NH$), 51.6 ($HNCH_2CH_2N$), 53.0 (NCH_2CH_2N), 63.1 ($C(O)OCH_2CH_2$), 66.7 (CH_2CH_3), 68.6 ($C(O)OCH_2CH_2$), 69.9 ($CH_2OCH_2CH_3$), 72.5 ($CH_2CH_2OCH_2CH_3$), 172.3 (*C*(O)NH), 173.0 (*C*(O)). FT-IR (NaCl, cm^{-1}): 3330 (m, ν_{NH}), 1735 (vs, $\nu_{C(O)}$), 1650 (s, $\nu_{C(O)}$, amide I), 1540 (m, $\nu_{C(O)}$, amide II), 1120 (s, ν_{COC}). HR MS: *m*/*z* calcd. for $C_{99}H_{183}N_{13}O_{37}$: 2148.2942, found 2148.3087 $[M - C_{20}H_{40}O_8 + H]^+$. UV/Vis ($C_2H_5OH$) [$\lambda_{max}$ (ε)]: 231 (3500).

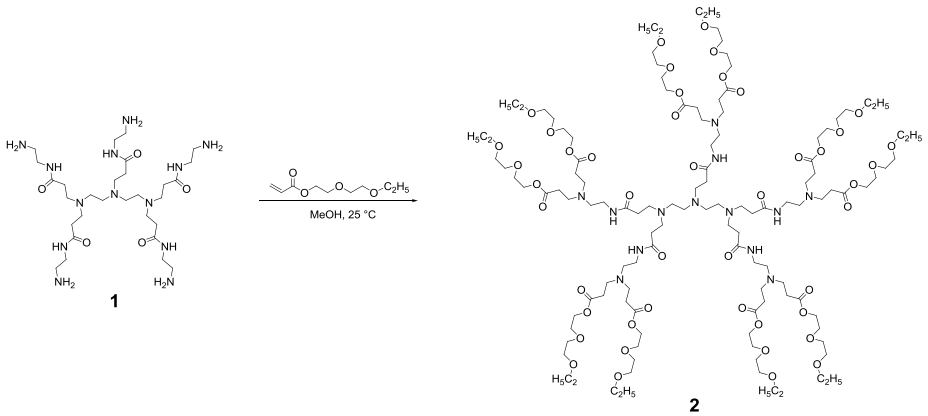

Scheme G1. Synthesis of OEGylated poly(amidoamine) dendrimer **2**.

2.3. Cell Viability Studies

Cytotoxicity of dendrimer **2** and the dendrimer-drug conjugate were determined by 3-(4,5-dimethylthiazol-2-yl)-5-(3-carboxymethoxyphenyl)-2-(4-sulfophenyl)-2H-tetrazolium (MTS) assay. HeLa (cervical cancer cell line) and MCF-7 (breast cancer cell line) cells were cultured in MEM and DMEM respectively, supplemented with 10 % fetal bovine serum and penicillin/streptomycin at 37 °C in a 5 % carbon dioxide atmosphere. For subculture, cells were washed once with phosphate buffer saline (PBS) and incubated with trypsin-EDTA solution (0.25 % trypsin, 1 mM EDTA) for 10 min at 37 °C to detach the cells. The complete medium was then added to the flask at ambient temperature to inhibit the effect of trypsin. The cells were re-suspended in the complete medium for reseeding and growth in the new culture medium. Cell viability was determined through staining with Trypan blue and cells were counted using a hemocytometer. Cell density was estimated using a 0.9 mm^3 counting chamber.

For viability measurements, cells were plated at the density of 10^4 cells per well in a flat bottomed 96 well plates. Later they were incubated with different concentrations of dendrimers (in PBS) for 24 h. After this incubation, the cell viability was determined by MTS assay. In short, after the period of incubation, the medium was removed from each well and 90 µL of the fresh medium and 10 µL of the MTS assay (CellTiter 96® Aq_{ueous} One solution Reagent; Promega, Madison, WI) were added to each well according the manufacturer´s instructions. After 4 hrs in culture, the cell viability was determined by measuring absorbance at 490 nm using 1420 Multilabel counter, Victor V^3 (Perkin Elmer). Results were plotted in reference to 100 % control cells using the following Equation G1:

$$Cell\ viability\ (\%) = \frac{absorbance\ of\ treated\ cells}{absorbance\ of\ control\ cells} \times 100 \qquad \text{(Eq. G1)}$$

where, control was the absorbance of 10 µL CellTiter 96® Aq_{ueous} One solution Reagent in 100 µL culture medium. The same set of experiments was carried out with DOX loaded dendrimer **2** and the half maximal inhibitory concentration (IC_{50}) was determined by using Bio-Data Fit website (www.changbioscience.com/stat/ec50.html).

2.4. Doxorubicin Loading and Release

Fluorescence spectroscopy was followed to evaluate the drug loading onto dendrimer **2** and was recorded by exciting the DOX solution at 490 nm and recording the emission at 500 –

800 nm (excitation slit: 5 nm; emission slit: 2.5 nm) on a Hitachi F-2500 Fluorescence Spectrophotometer. The calibration curve of DOX was obtained at 535 nm (Figure S1, ESI†) and a linear relationship was observed between enhanced fluorescence intensities and the concentrations of doxorubicin in the range of 0.2 to 20 mM with a correlation coefficient of 0.9979. 4 mg · mL^{-1} stock solution of dendrimer **2** was prepared in PBS (pH 7.4). From this solution, 250 mL of dendrimer **2** was taken out in the sample tube and the volume was made up to 1 mL by adding 750 μL of PBS. 100 μL of the diluted solution of the dendrimer was added after every 15 min to the DOX solution (concentration: 10 mg mL^{-1}). After each addition, the solution was mixed well and incubated at ambient temperature for 15 min. The addition of the dendrimer was continued till no further decrease in emission was observed. Once a constant emission was achieved, the sample from the vial was taken out and put under dialysis in PBS in reservoir-sink condition for 24 hrs to remove the unloaded drug. After 24 h, the sink was analyzed by measuring the fluorescence and the loading efficiency was calculated as follows (Equation G2):

$$\%\ Efficiency = \frac{initial\ flourescence\ intensity - final\ flourescence\ intensity}{initial\ flourescence\ intensity} \times 100 \qquad \text{(Eq. G2)}$$

To assess the drug release profile of the DOX loaded dendrimer, we monitored the release of DOX in phosphate buffer (0.1 M, pH 7.4) and simulated body fluid (SBF, pH 7.4) using a dialysis membrane of 2.5 nm pore size under reservoir-sink condition. [G17] Specifically, a solution of DOX loaded dendrimer **2** was prepared using the encapsulation procedure described before and the drug concentration in the solution was determined. The drug loaded dendrimer was then transferred to the dialysis membranes which were placed in 250 mL beakers containing 200 mL of release medium (PBS and SBF) to maintain the sink conditions. The beakers containing the dialysis bag were placed over a magnetic stirrer and continuously stirred over the entire period of the drug release experiment. The dialysis was carried out at 37 °C and 43 ± 1 °C and samples (1 mL) from each sink were collected at predetermined time intervals of 1 h to 24 hrs with replacement of equal amount of the solutions. The amount of DOX released was quantified by the 1420 Multilabel Counter, Victor V^3 (Perkin Elmer) UV spectrophotometer at 490 nm using a validated analytical method. Hyperthermia experiments were done as described earlier. [G18]

2.5. *In Vitro* Cellular Uptake of Dendrimer-DOX Conjugate

HeLA cells were seeded in 24-well plates at 10^5 cells per well having a cover slip and grown overnight. The media were discarded after 24 hrs and the cells were incubated for 3 hrs with DOX, dendrimer **2** and dendrimer-DOX conjugate. After incubation, the media were again discarded and the cells were washed with PBS three times. 1 mL of 10 % formalin was added to each well and kept for 10 min. The cover slip was mounted on glass slides with DPX mount and the photographs of the cells after incubation were taken in phase contrast and fluorescence mode with fixed exposure time using Olympus Inverted Confocal Microscope Model IX 81.

3. Results and Discussion

3.1. Drug Loading and Release

Fluorescence spectroscopy has been successfully used to study the interaction between DOX and its surrounding molecules. Figure G1a shows the fluorescence spectra of DOX and DOX loaded dendrimer **2** assemblies and significant differences are seen in these spectra. The concentration of DOX was kept constant and the concentration of the dendrimer was varied as mentioned in the Experimental section. The loading of DOX within dendrimer **2** is indicated by predominant quenching of the DOX fluorescence.

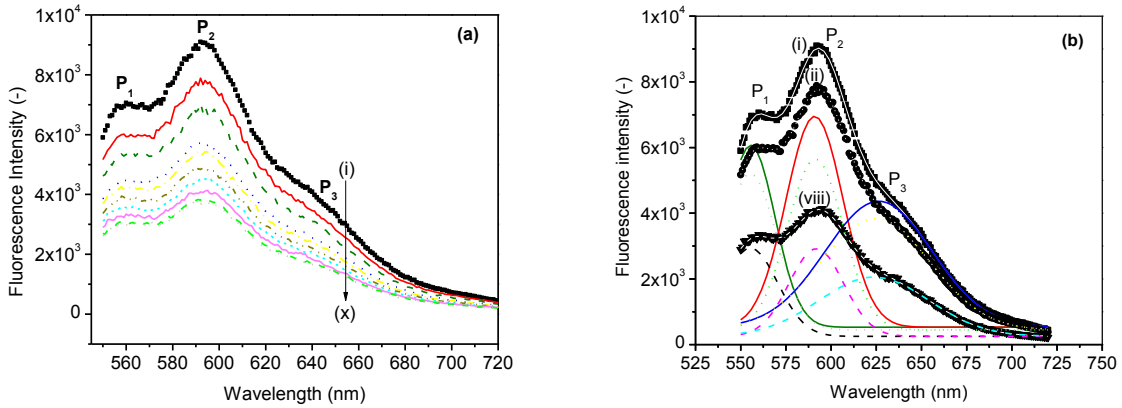

Figure G1. (a) Fluorescence spectra of (a) pure DOX (i) and DOX-dendrimer conjugate (10 μg · L^{-1} of DOX) recorded at initial (ii) and after 15 (iii), 30 (iv), 45 (v), 60 (vi), 75 (vii), 90 (viii), 105 (ix) and 120 min. (x); (b) Gaussian profiles for the fluorescence spectra (i), (ii) and (viii).

It has been observed that the fluorescence intensity of DOX decreases monotonically on increasing the interaction/loading time of DOX with the dendrimer till a saturation loading of DOX is achieved. The drug loading efficiency was calculated out to be 52 % where 10 μg · mL^{-1} of DOX was reacted with 450 μg · mL^{-1} of the dendrimer for 90 min, after which the intensity begins to remain constant. The loading was continued further for another 30 min till saturation is achieved.

The fluorescence spectrum of DOX showed three emission bands at ca. 555 nm (P_1 band), 590 nm (P_2 band) and 626 nm (P_3 band). To understand the interaction between the DOX and the dendrimer, select fluorescence spectra were further analyzed by multiple peak Gaussian curve fitting analysis using Origin 7.2 data processing software. The area under each emission bands and correlation factor R^2 values are shown in Figure G1b and Table S1 (see ESI†). Any change in the position of the peak maximum, spectral shape and ratios of area under the peak 1 (A_1) to peak 2 (A_2) and peak 3 (A_3) to peak 2 (A_2) tells us about the nature of interaction between drug and dendrimer. When compared to pure DOX, A_1/A_2, A_3/A_2 values for DOX loaded dendrimer at t = 0 and t = 90 min show progressive increase which indicates that there is a significant interaction between the DOX and dendrimer **2**. The ethylene glycol moiety of the dendrimer exhibits π – π stacking interaction with the quinine portion of DOX developing hydrophobicity in the conjugate. In addition to this, the NH_2 and the OH groups of DOX also participate in hydrogen bonding with the dendrimer.

3.2. Surface Potential of the Dendrimer-Drug Assembly

Zeta potential (ζ-potential) is the difference in the electrical charge developed between the dense layers of ions surrounding the molecule and gives information about the overall surface charge of the particles thereby indicating their stability. The interactions between the molecules play an important role in determining the colloidal stability and the ζ-potential measurements may be used to quantify such interactions.

The values of ζ-potential for unloaded and drug loaded dendrimer **2** are summarized in Table G1 which clearly indicate that loading of doxorubicin onto dendritic arena increases positive potential of the entire molecule. The observed increase may be explained by the fact that drug molecules bear a positive charge and due to their loading onto the dendrimers, the positive charge increases which also supports the dendrimer-drug interaction. Further characterization of the structure of the drug-loaded dendrimer was carried out to investigate their size change before and after loading of DOX using dynamic light scattering measurements. Figure

S2 (ESI†) shows the size distributions of dendrimer and DOX loaded dendrimer. The effective diameter of the dendrimer increased from 215 to 432 nm after loading DOX.

Table G1. Surface potential of the dendrimer-drug assembly, EMF data have been expressed as mean ± S.D. of at least three determinations.

pH	EMF / mV Buffer solution	EMF / mV Unloaded	EMF / mV Loaded
1.4	275.2	258.4	283.3
7.5	-34.2	-36.7	-20.7
9.2	-80.4	-84.1	-43.2

3.3. Structural Analysis of Dendrimer-DOX Conjugate

FT-IR spectroscopy was used to confirm the successful loading of DOX into OEGylated dendrimer **2** (Figure G2). Doxorubicin exhibits characteristic FT-IR modes at 1742 cm^{-1} (C═O stretching vibration at position C13), 1630 and 1552 cm^{-1} (stretching vibration of the C═O groups of the anthracene ring (C6, C12)), 1412 cm^{-1} (C–H bending), ≈ 1250cm^{-1} (skeleton vibration of the DOX molecule) and a band at 992 cm^{-1} (νC–O bonds). [G19] The broad band appears in the range of 2800 – 3000 cm^{-1} which is attributed to the stretching vibrations of the C–H and OH groups of DOX along with a contribution of NH_2 within this band.

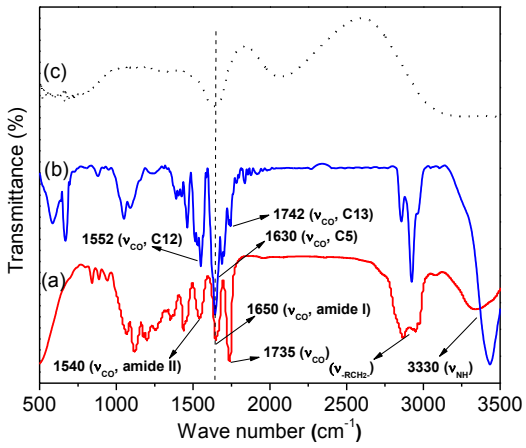

Figure G2. FT-IR spectra of (a) dendrimer **2**, (b) DOX and (c) dendrimer-drug conjugate.

In the FT-IR spectra of dendrimer-DOX conjugate, the shift of the 1735 cm^{-1} and 1742 cm^{-1} bands of the dendrimer and the DOX molecule respectively to 1630 cm^{-1} gives an evidence of formation of mutual hydrogen bonds between the carbonyl group of DOX (which acts as an hydrogen acceptor) and NH groups (hydrogen donors) of the dendrimer and *vice versa*. In this way, there exists a mutual interaction between the host dendrimer and the guest doxorubicin. Further, the broad peak at ≈ 3400 cm^{-1} and the shift in the absorption peaks are attributed to the intermolecular interaction of the DOX molecule with the dendrimer. The proposed interaction of the dendrimer with DOX is shown in Scheme G2.

The interaction of DOX with the dendrimer was also investigated by comparing the UV/Vis spectra of dendrimer-DOX conjugate with those of the pure dendrimer and DOX (see ESI†, Figure S3). UV/Vis absorption spectra of the DOX showed absorption bands at 485, 275 and 257 nm. Bands corresponding to n → π* absorption of the carbonyl groups of DOX (275 and 257 nm) exhibit blue shift in the UV/Vis spectra of the dendrimer-DOX conjugate. The observed blue shift may be due to the formation of hydrogen bond between the dendrimer and the DOX molecule.

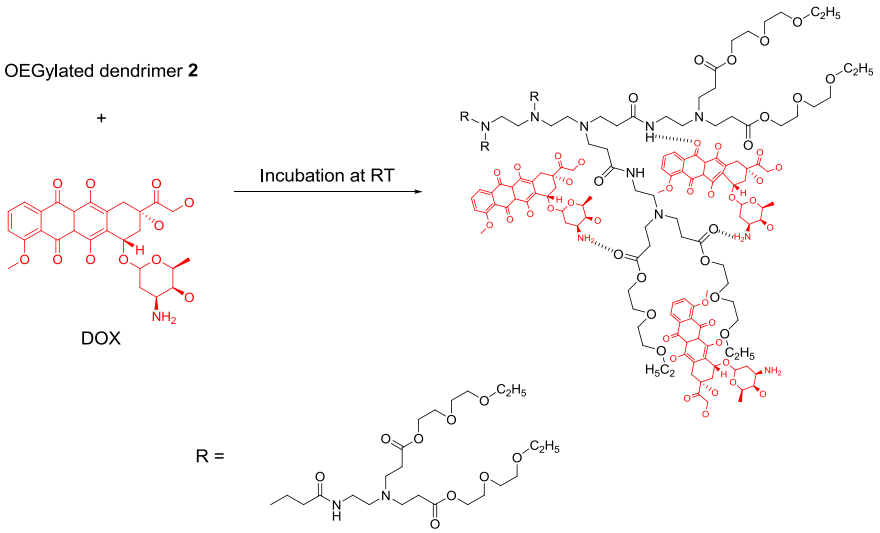

Scheme G2. Proposed interactions of the dendrimer with doxorubicin.

DOX in dendrimer **2** was analyzed by reverse phase HPLC which gave evidence that most of the DOX was loaded without degradation (Figure G3). Free DOX eluted as a single sharp peak at 7.0 min. After encapsulation within the dendrimer, one new peak appeared at 7.4 along with a slight shift in the peak of the free DOX. It may be due to the fact that the doxorubicin is encapsulated within the dendritic arms with reduced polarity thereby increasing the elution time and appearing as the second peak. The intensity of the first peak reduced

which may be due to the unencapsulated DOX in solution. Thus, reverse phase HPLC demonstrated the interaction between DOX and dendrimer **2**.

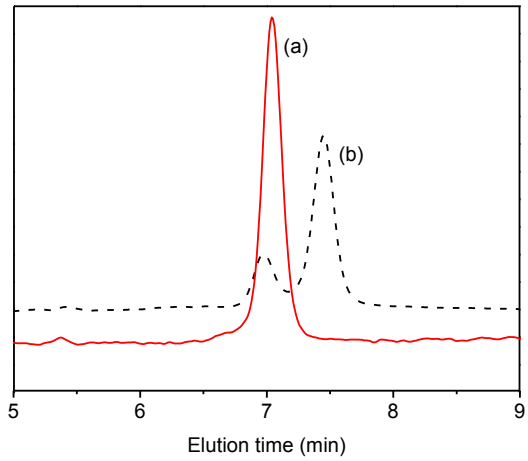

Figure G3. Reverse phase HPLC chromatogram of pure DOX (a) and dendrimer-drug conjugate (b).

NMR is a real time, *in-situ* and one of the powerful tools to give information regarding loading in a host-guest system in a surrounding electronic environment and helps in predicting the interactions in it. [G20] Any change in the electronic environment around the target nucleus caused by the inclusion of any guest will induce a shield/deshield effect for the nucleus. Therefore, it can directly predict the intramolecular/intermolecular interactions in the system. [G21, G22] NMR characterization of the drug loaded dendrimer **2** was carried out to establish the loading of the drug within the dendrimer. The ^{1}H NMR spectra of the dendrimer-drug conjugate in $CDCl_3$ showed prominent resonance peaks at 7.2 – 7.6 and 1.6 – 2.5 ppm corresponding to aromatic protons of the anthraquinone ring and the proton signals from the sugar moiety of doxorubicin. In addition to this, the signals of the ethylene glycol group (OCH_2CH_2O) at ≈ 3.1 to 3.5 ppm of the OEG moiety of dendrimer **2** were also seen (see ESI†, Figure S4). DOX is inherently less hydrophobic due to its polar hydroxyl and amino groups and thus is likely to be entrapped within dendrimer **2** by hydrogen bond interactions.

Evidence for the chemical stability of doxorubicin contained in dendrimer **2** was further revealed by visible spectroscopy (Figure G4). The absorbance of the free doxorubicin at 485 nm showed a decrease in absorbance from 0.25 to 0.045 over a period of 240 hrs (10 days), probably due to chemical degradation of pure DOX. [G23] However, the absorbance of DOX loaded onto dendrimer **2** was essentially constant over the same period of time. It showed negligible decrease in the absorbance from 0.20 to 0.17. This may be due to the fact that the cavities of

the dendrimer encapsulate the DOX molecules thereby preventing the hydrolytic reaction of DOX. This, in turn, gives an evidence of the dendrimer-drug interaction. Besides, giving the evidence of chemical stability of DOX and the interaction of the dendrimer with drug, the visible spectroscopy also suggests that the DOX is not released under the same experimental conditions. This suggests that some external stimuli are required for the release of the drug from the dendritic carrier.

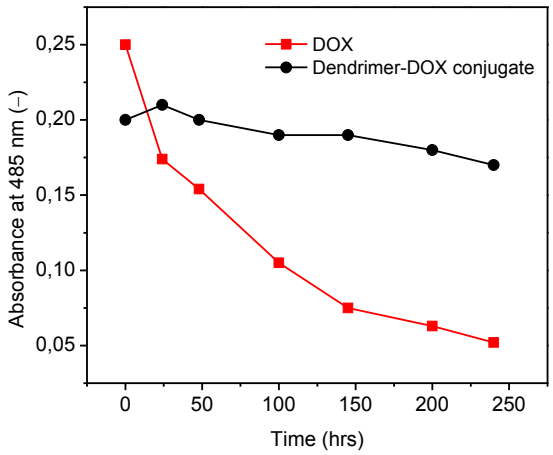

Figure G4. Chemical stability of pure DOX and dendrimer–DOX conjugate over a period of time.

3.4. *In Vitro* DOX Release Profile from Dendrimer-Drug Conjugate

In vitro release profiles of DOX from DOX loaded dendrimer **2** in PBS (pH 7.4) and SBF (pH 7.4) as a function of time were studied at temperatures of 37 and 43 °C (Figure G5a and b). It is encouraging to note that while at the physiological temperature at 37 °C, the release is limited to about 10 % over a period up to 1400 min, this goes up to about 90 % at 43 °C, a possible hyperthermic temperature. An initial fast and burst release of DOX was observed at 43 °C probably due to the breaking of the hydrogen bridge formed between DOX and the dendrimer. The burst release was observed within 1 h in both the release media (PBS and SBF), thereafter a slow release was observed for another 2.5 h. About 85 % of the DOX was released in 5 hrs in PBS after which a plateau was attained; the release in SBF was slightly higher (90 %) than in PBS medium. The release was monitored for 24 hrs and no change was observed in the release percentage and hence, complete release was not achieved. The release observation may prove to be very beneficial as a certain initial burst drug release is preferable to achieve sufficient initial dosage of the anticancer drug to inhibit the tumor cell growth for

further treatment. For the cancer cells that are not inhibited by the initial stage of the DOX release, the slow DOX release is necessary to prevent their further proliferation. Therefore, based on the release profile of the conjugate, it is inferred that the dendrimer **2** makes it a promising candidate for tumor treatment. The next step of our studies will be devoted to the *in vitro* assessment of the cytotoxic activity of the dendrimer.

The release fraction of DOX was plotted against the square root of time to assess the release mechanism of DOX from DOX loaded dendrimer **2**. As it can be seen from the inset of Figure G5a and b, a linear relationship between the drug release and $t^{1/2}$ is obtained in the first stage which shows that the DOX release process is diffusion-controlled. In the second stage also, a linear relationship between the drug release and the square root of time is observed, however, the slope of the second line is much less than the first stage. This indicates that the release rate was slower in the second stage probably due to the fact that the DOX loaded within the dendritic cavity took a longer time to get released. The results of DOX release indicate that the drug is not only encapsulated within the ethylene glycol moiety of the dendrimer **2**, but also may be entrapped within matrix of the dendrimer. In this case, the triggering of the drug release is initiated by change in temperature, which acts as an external stimulus. The hydrogen bonds formed between the dendrimer and the DOX molecule break at higher temperature, which instantly release the DOX. Due to the presence of amide backbones in the OEGylated PAMAM dendrimers, degradation takes place only at harsh conditions and not in the physiological conditions. OEGylated dendrimers are possibly degraded into smaller units and are easily eliminated from the body. [G24] The linking chemistry in the dendrimer-drug conjugate governs the drug release thereby enhancing the therapeutic index.

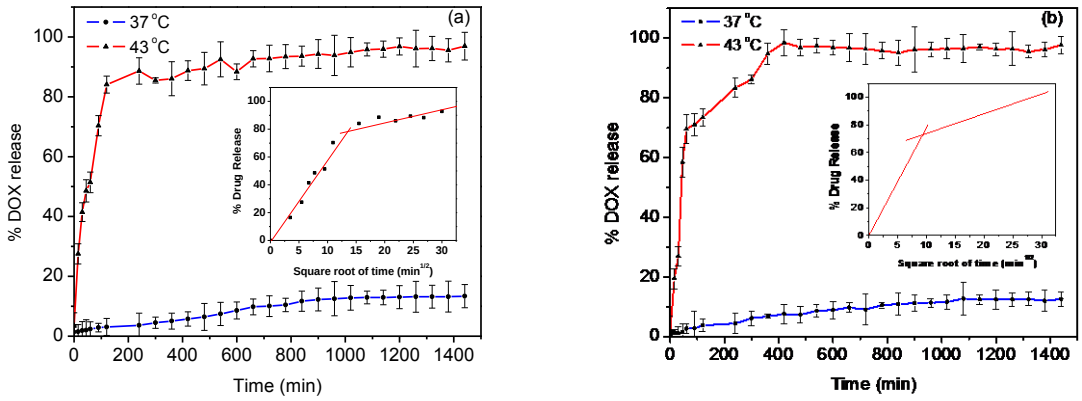

Figure G5. Drug release profile of DOX from dendrimer-drug conjugate in PBS (a) and SBF (b) at 37 °C and 43 °C. Inset shows curves of (a) and (b) replotted against the square root of time at 43 °C.

In view of the interesting observation of a large difference in the drug release between physiological conditions (37 °C) and hyperthermic condition (43 °C), we were motivated to carry out some preliminary *in vitro* hyperthermic experiments through a biphasic suspension of the dendrimer-drug conjugate and a ferrofluid, which is an aqueous suspension of iron oxide magnetic nanoparticles. [G18] Magnetic fluids generate heat when exposed to the AC magnetic field and thus the induction heat is not only useful for hyperthermia treatment but also acts as driving force for drug release. Keeping this in mind, the release of the drug from the dendrimer-drug conjugate assisted by the magnetic fluid (iron concentration 10 mg · mL^{-1} with a SAR value of 19 W · g^{-1} Fe) was studied under AC magnetic field through a biphasic suspension consisting of dendrimer-drug conjugate and the magnetic fluid. This was taken in a falcon tube which was put inside a circular coil attached to a RF generator at 423 kHz fixed frequency and 10 kA · m^{-1} field and was exposed to AC magnetic field. It took only 4 minutes to raise the temperature of the suspension to 43 °C, which could be a possible temperature for magnetic hyperthermia. Figure G6 shows the release of DOX from the solution triggered by on–off switching of the AC magnetic field. In this experiment, the percentage of cumulative release DOX was calculated using the formula (Equation G3):

$$C = \frac{C_f}{C_i} \times 100 \qquad \text{(Eq. G3)}$$

where C_i is the initial amount of the DOX and C_f is the cumulative amount of released DOX.

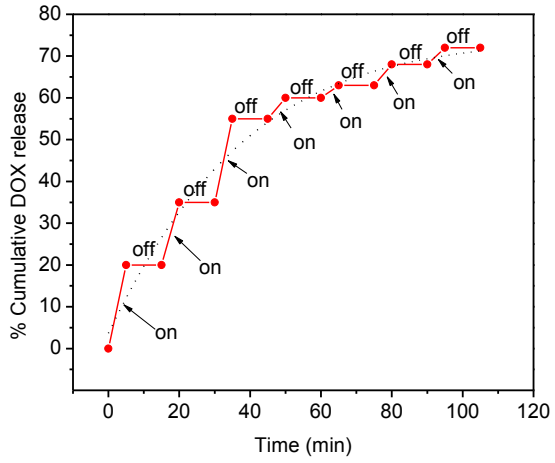

Figure G6. Controlled release of DOX from the conjugate by switching the AC magnetic field on-off.

It is interesting that DOX gets released during application of the field (switch on mode) and it stops on removal of the field (switch off mode). It has been found that ≈ 70 % DOX is re-

leased on application of AC magnetic field for 35 minutes. The sigmoidal profile of the graph shows that there is a fast release during the first 15 minutes under "switch on" mode of AC magnetic field and later on, the release is slow. This allows the controlled release of the DOX from the conjugate to its delivery to remote tumor locations. Moreover, the heat generated can be used for magnetic hyperthermia treatment and also for enhancing the drug effect (chemo-therapy). [G25]

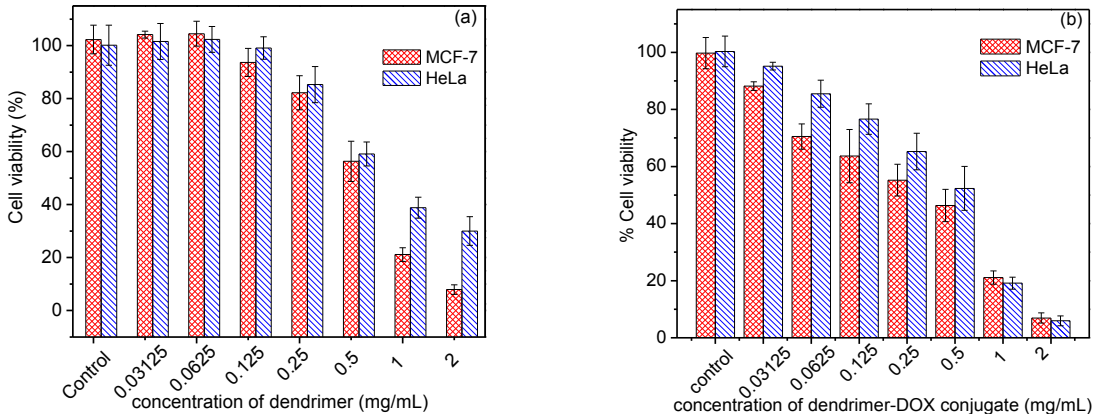

Figure G7. Viabilities of MCF-7 and HeLa cells incubated with MEM media containing (a) dendrimers and (b) dendrimer-drug conjugate.

3.5. Cell Viability Studies of the Dendrimer-DOX Conjugate

The cell viability of the dendrimer **2** and the dendrimer-DOX conjugate is shown in Figure G7. The MTS assay showed that about 90 % of the HeLa and the MCF-7 cells were viable after 24 hrs of incubation with dendrimer concentration of 0.25 mg · mL^{-1}, however, they are affected by the presence of the dendrimers above this limit. The IC_{50}, defined as the concentration of the material which results in a 50 % inhibition of cellular process, was found to be 0.87 μM and 0.76 μM for HeLa and MCF-7 cells, respectively. The *in vitro* cytotoxicity of DOX-dendrimer conjugate was found to decrease the IC_{50} of DOX for HeLa cells to 0.711 μM (the reversal fold was 1.2) and for MCF-7 to 0.37 μM (reversal fold was 2.0) indicating that dendrimer **2** can enhance the sensitivity of the cancer cells (HeLa and MCF-7) to DOX. Cytotoxicity experiments performed led to the conclusion that the toxicity from the dendrimer can also be used for formulation of a therapeutic drug specific to the cancer cells. [G26] However, as with the formulation of any drug, biological activity is not the sole determinant, hence, based on the *in vitro* results, detailed *in vivo* experiments will be designed to evaluate the therapeutic potential of the proposed dendrimer-drug conjugate in due course of time.

3.6. Cellular Uptake by the Dendrimer-DOX Conjugate

Confocal microscopy was performed on the HeLa cells following 3 hrs incubation with free DOX, dendrimer **2** and the dendrimer-DOX conjugate at 37 °C. The control cells did not show any fluorescence under same microscopic settings (Figure G8a and b), while the cells exposed to free DOX showed nuclear internalization as the DOX has an inherent property to fluoresce (Figure G8c).

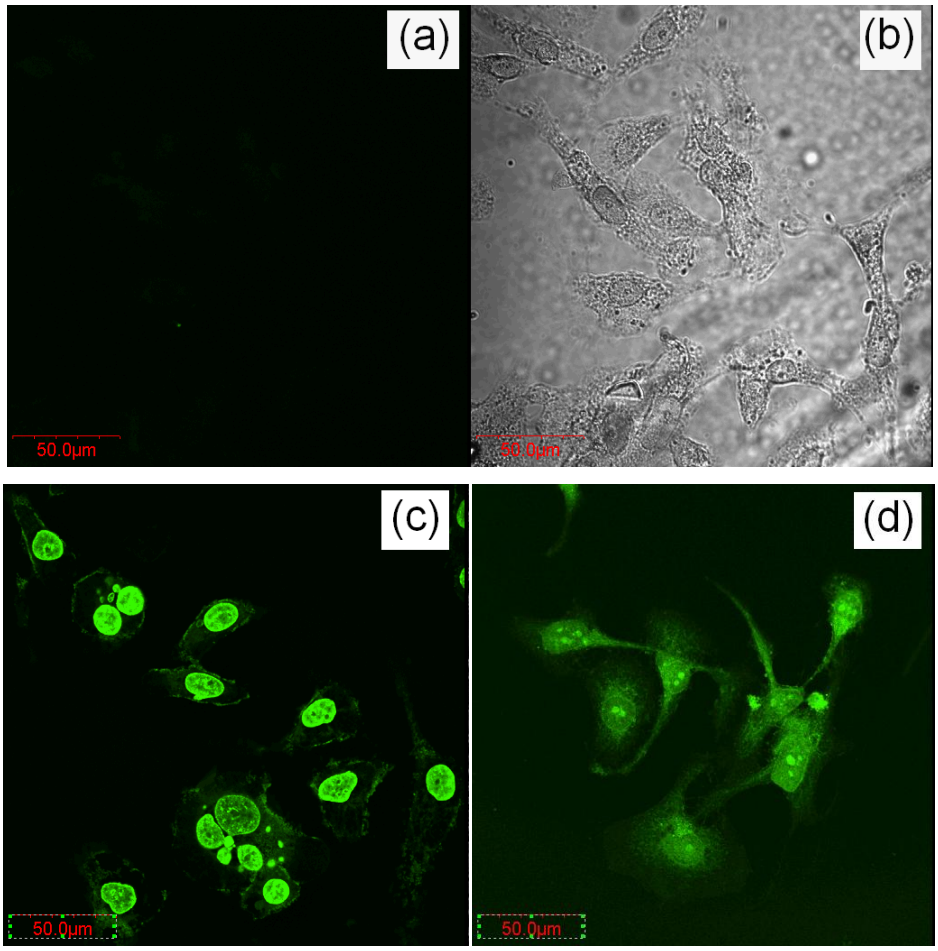

Figure G8. Cellular uptake as evidenced by confocal microscopy images: (a) control cells showing no fluorescence, (b) phase contrast image of the control cells, (c) HeLa cells incubated with free DOX and (d) cells incubated with dendrimer-DOX conjugate. All the cells were grown on sterilized cover slips and incubated for 24 h. Magnification is 60×.

The conjugation of the DOX with the dendrimer also enables confocal microscopic imaging of the cellular uptake. The cells treated with the dendrimer-DOX conjugate displayed fluorescence signals, which are associated with the uptake of the dendrimer-DOX conjugate in to the cytoplasm as well as on the membrane of the cells within 3 hrs (see Figure G8d). The intensity of the fluorescence is, however, less in the cell nuclei when they were incubated with the dendrimer-DOX conjugate which suggests that the drug is still intact and does need some

trigger for the release. During this period of study, no toxicity was observed from the dendrimer-drug conjugate. Based on the confocal images, it was possible to determine the intracellular location of the dendrimer-DOX conjugate, however, further detailed microscopy will be carried out to ascertain the effects of cell type, incubation period and fixation.

3.7. Protein Adsorption Studies

Oligomers of ethylene glycol moieties are known to provide protein resistance in aqueous medium where the oxygen of the ethylene glycol forms hydrogen bonds with water thereby preventing hydrophobically driven protein adsorption. The chain mobility of the ethylene glycol segments results in steric hindrances which are also responsible for resistance to protein adsorption. To study the nonspecific protein adsorption onto the oligo(ethylene glycol)-grafted amidoamine dendrimer, bovine serum albumin (BSA) and immunoglobulin (IgG) was used as test proteins and ζ potentials were recorded. The dendrimer (0.125 mg · mL^{-1}) was incubated with the test proteins, BSA (0.5 mg · mL^{-1}) and IgG (0.25 mg · mL^{-1}) in PBS at room temperature for 2 h. The ζ potential of pure dendrimer, pure BSA and pure IgG was -9.8 ± 3.0 mV, -11 ± 1.8 mV, -16.0 ± 3.8 mV respectively, in PBS (pH 7.4). The ζ potential of the incubated dendrimer-BSA and dendrimer-IgG sample was found to be -7.5 ± 4.7 and -13.5 ± 3.2 mV, respectively; the change in ζ potentials are significantly small (≈ 4 mV) depicting resistance of the dendrimer to BSA and IgG adsorption.

4. Conclusions

The present study reports synthesis of a novel OEGylated dendrimer and its conjugate with doxorubicin. An important observation of the present work is that dendrimer **2** is not only an efficient carrier for the cancer drug, doxorubicin, as could be seen from the results of fluorescence spectroscopy in terms of the quenching of fluorescence intensity as well as the change in band positions and spectral shapes, but also an effective therapeutic. The IC_{50} of the dendrimer-DOX conjugate towards the HeLa and MCF-7 cell lines were lowered suggesting that the loading of DOX in dendrimer increased its potency. Further, the dendrimer encapsulate the doxorubicin molecule without altering its chemical integrity as evidenced by HPLC, which is also an important aspect for drug delivery. The uptake by HeLa cells of the dendrimer-DOX conjugate is also promising for use as scaffolds in the development of drug carriers. The combined effect of loading and release pattern of DOX from the dendritic carrier and the

enhanced potency of the dendrimer-drug conjugate will certainly make them an efficient system for cancer treatment. It is also interesting to observe the release of the DOX from the conjugate using a biphasic suspension with magnetic fluid under AC magnetic field. This study exhibits a strong potential for a combination therapy involving chemotherapy and hyperthermia. However, additional studies are required to establish the precise *in vivo* action of the dendrimer-drug conjugate and also to ascertain whether the dendrimer-DOX conjugate behaves as potent antitumor agent when acting on larger tumors.

5. Acknowledgements

The author SC acknowledges Department of Science and Technology (DST), for awarding DST Young Scientist fellowship. Financial support from Alexander-von-Humboldt Foundation (AvH), Germany, Department of Information Technology (DIT) and Nanomission of DST, Govt. of India is also gratefully acknowledged. Author SD thanks the Landesgraduiertenförderung des Freistaates Sachsen and Fonds der Chemischen Industrie, Germany for financially supporting his PhD studies. Authors are also thankful to Mr Imtyaz Mohammed and Mr Lathiesh Srinivasan for carrying out HPLC experiments.

6. Supplementary Material

Electronic supplementary information (ESI) available.

See DOI:10.1039/c0jm04198j

7. References

[G1] T. Sakthivel, A.T. Florence, *Drug Deliv. Technol.* **2003**, *3*, 73.

[G2] J.F.G.A. Jansen, E.M.M. Debrabandervandenberg, E.W. Meijer, *Science* **1994**, *266*, 1226.

[G3] H. Yang, J.J. Morris, S.T. Lopina, *J. Colloid Interface Sci.* **2004**, *273*, 148.

[G4] R. Jevprasesphant, J. Penny, D. Attwood, N.B. Mckeown, A. D´Emanuele, *Pharm. Res.* **2003**, *20*, 1543.

[G5] N. Malik, R. Wiwattanapatapee, R. Klopsch, K. Lorenz, H. Frey, J.W. Weener, E.W. Meijer, W. Paulus, R. Duncan, *J. Control. Release* **2000**, *65*, 133.

[G6] H.-T. Chen, M.F. Neerman, A.R. Parrish, E.E. Simanek, *J. Am. Chem. Soc.* **2004**, *126*, 10044.

[G7] R.X. Zhuo, B. Du, Z.R. Lu, *J. Control. Release* **1999**, *57*, 249.

[G8] A.K. Patri, J.F. Kukowska-Latallo, J.R.J. Baker, *Adv. Drug Deliv. Rev.* **2005**, *57*, 2203.

[G9] S.-E. Stiriba, H. Frey, R. Haag, *Angew. Chem. Int. Ed.* **2002**, *41*, 1329.

[G10] R. Duncan, L. Izzo, *Adv. Drug Deliv. Rev.* **2005**, *57*, 2215.

[G11] D. Bhadra, S. Bhadra, S. Jain, N.K. Jain, *Int. J. Pharm.* **2003**, *257*, 111.

[G12] K. Kono, M. Liu, J.M.J. Frechet, *Bioconjugate Chem.* **1999**, *10*, 1115.

[G13] H. Namazi, M. Adeli, *Biomaterials* **2005**, *26*, 1175.

[G14] S. Chen, X.-Z. Zhang, S.-X. Cheng, R.-X. Zhuo, Z.-W. Gu, *Biomacromolecules* **2008**, *9*, 2578.

[G15] N.K. Prasad, L. Hardel, E. Duguet, D. Bahadur, *J. Magn. Magn. Mater.* **2009**, *321*, 1490.

[G16] (a) S. Dietrich, A. Nicolai, H. Lang, *J. Organomet. Chem.* **2011**, *696*, 739;
(b) D.A. Tomalia, *US Patent* **1985**, *4507466*.

[G17] S. Chandra, S. Mehta, S. Nigam, D. Bahadur, *New J. Chem.* **2010**, *34*, 648.

[G18] N.K. Prasad, K. Rathinasamy, D. Panda, D. Bahadur, *J. Mater. Chem.* **2007**, *17*, 5042.

[G19] S. Li, Y. Ma, X. Yue, Z. Cao, Z. Dai, *New J. Chem.* **2009**, *33*, 2414.

[G20] T. Brand, E.J. Cabrita, S. Berger, *Prog. Nucl. Magn. Reson. Spectrosc.* **2005**, *46*, 159.

[G21] M.A.C. Broeren, B.F.M. de Waal, M.H.P. van Genderen, H.M.H.F. Sanders, G. Fytas, E.W. Meijer, *J. Am. Chem. Soc.* **2005**, *127*, 10334.

[G22] J.J. Hu, Y.Y. Cheng, Y.R. Ma, Q.L. Wu, T.W. Xu, *J. Phys. Chem. B* **2009**, *113*, 64.

[G23] M. Yokoyama, M. Miyauchi, N. Yamada, T. Okano, Y. Sakurai, K. Kataoka, S. Inoue, *Cancer Research* **1990**, *50*, 1693.

[G24] C.C. Lee, J.A. Mackay, J.M.J. Frechet, F.C. Szoka, *Nat. Biotechnol.* **2005**, *23*, 1517.

[G25] P. Pradhan, J. Giri, F. Rieken, C. Koch, O. Mykhaylyk, M. Döblinger, R. Banerjee, D. Bahadur, C. Plank, *J. Control. Release* **2010**, *142*, 108.

[G26] M.J. Vicent, L. Dieudonné, R.J. Carbajo, A.P. Lucena, *Expert Opin. Drug Delivery* **2008**, *5*, 593.

H Summary

1. Summary

The present work describes the synthesis, characterization and application of (poly)amidoamine-based low-generation dendrimers. The main emphasis is focused on specific peripheral organometallic, metal-organic as well as biochemical modifications. The versatility of thus dendritic architectures formed is reflected in various applications, as *e.g.* catalysts in homogeneous cross-coupling reactions, templates for metal/metal oxide nanoparticles formation and drug delivery vehicles for therapeutic anticancer drugs.

The results gained in this work can be subdivided into five topics according to the following Chapters:

Chapter C:	Amidoamine-based Dendrimers with End-grafted Pd-Fe Units: Synthesis, Characterization and Their Use in the Heck Reaction
Chapter D:	A Preparation of Planar-Chiral Multidonor Phosphanylferrocene Carboxamides and Their Application as Ligands for Palladium-Catalyzed Asymmetric Allylic Alkylation
Chapter E:	Au Nanoparticles Stabilized by PEGylated Low-Generation PAMAM Dendrimers: Design, Characterization and Properties
Chapter F:	Design, Characterization and Magnetic Properties of Fe_3O_4-Nanoparticle Arrays Coated with PEGylated-Dendrimers
Chapter G:	Dendrimer-Doxorubicin Conjugate for Enhanced Therapeutic Effects for Cancer

The most relevant results are discussed below.

Chapter C

The synthesis and characterization of amidoamine-based metallodendrimers with heterobimetallic end-grafted amidoferrocenyl-palladium-allyl chloride units is described. The dendritic starting materials as well as the corresponding metallodendrimers were prepared by a consecutive divergent synthesis methodology including addition-amidation cycles, standard pep-

tide coupling and coordination procedures (Scheme H1). Using $[Pd(\eta^3\text{-}C_3H_5)Cl]_2$ as palladium source the heterobimetallic metallodendrimers **7-Fe-Pd** − **9-Fe-Pd** as well as (amido)amine-functionalized model compounds **5-Fe-Pd** and **6-Fe-Pd** were synthesized (Figure H1).

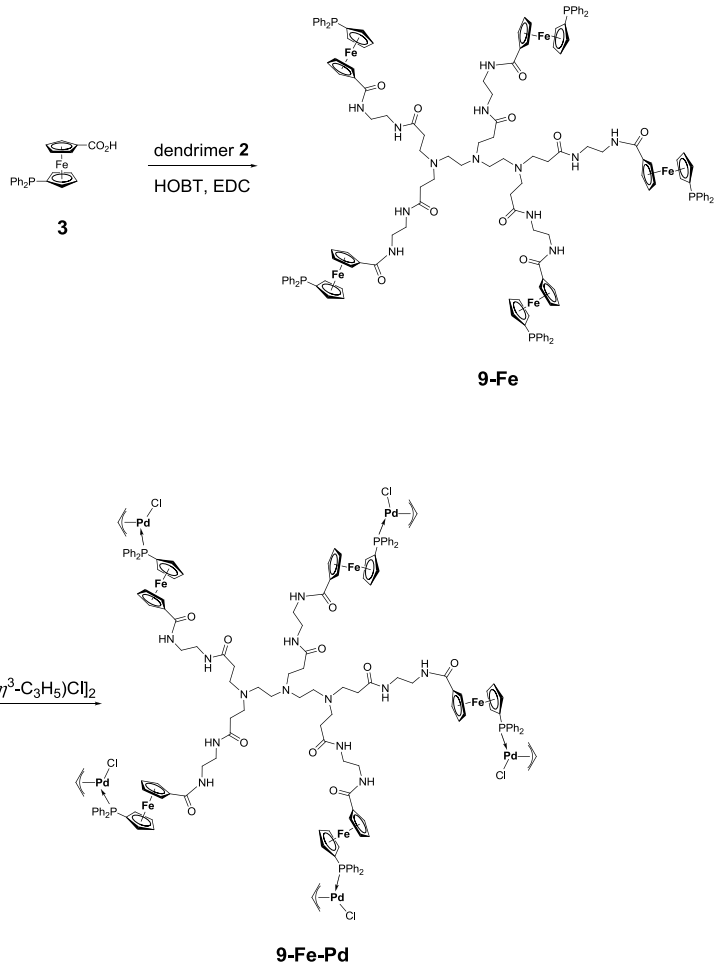

Scheme H1. Synthesis of heterobimetallic **9-Fe-Pd**.

The individual heterobimetallic Fe-Pd phosphines **5-Fe-Pd** – **9-Fe-Pd** were applied as homogeneous Heck-catalysts in carbon-carbon cross coupling reactions of iodobenzene with *tert*-butyl acrylate. The highest productivity was achieved with catalyst **9-Fe-Pd** possessing five terminal heterobimetallic Fe-Pd-units. Furthermore, synergistic and cooperative effects resulting in higher yields and productivities can be recognized most pronounced between metallodendrimers **5-Fe-Pd** / **6-Fe-Pd**, **7-Fe-Pd** / **8-Fe-Pd** and **9-Fe-Pd**.

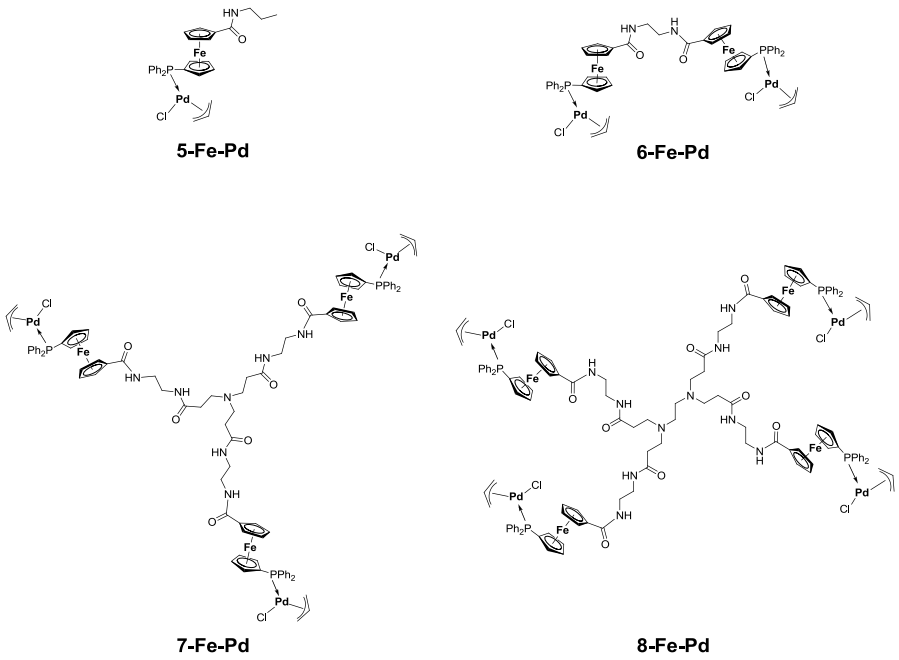

Figure H1. Heterobimetallic amidoamines **5-Fe-Pd** – **8-Fe-Pd**.

Chapter D

A series of oligoamides bearing one to three (S_p)-2-(diphenylphosphanyl)ferrocen-1-yl pendant groups at the periphery were designed by the amide coupling reactions of (S_p)-2-(diphenylphosphanyl)ferrocene-1-carboxylic acid [(S_p)–**1**] with appropriate terminal amines in the presence of peptide coupling agents (Scheme H2).

The obtained chiral dendrimer-supported phosphines **2** – **5** were combined with [Pd(η^3-C_3H_5)Cl]$_2$ as a metal source and applied for asymmetric palladium-catalyzed allylic alkylation reactions. Therein, the alkylation of the symmetrical 1,3-diphenylprop-2-en-1-yl acetate with *in situ* generated malonate anion was employed. The results indicate only relatively minor variation in the *ee* upon increasing the number of the chiral 2-phosphanylferrocenyl units per ligand molecule. Furthermore, the conversions achieved after 24 hrs for the applied ligands **2** – **5** varied greatly, being lower for donor molecules exhibiting a larger dendritic scaffold.

Chapter E

In a two-step synthesis methodology a series of well-defined low-generation (poly)amidoamine-based dendrimers and related (amido)amine model compounds functionalized with terminal ethylene glycol ethers of various chain lengths were prepared (Chart H1).

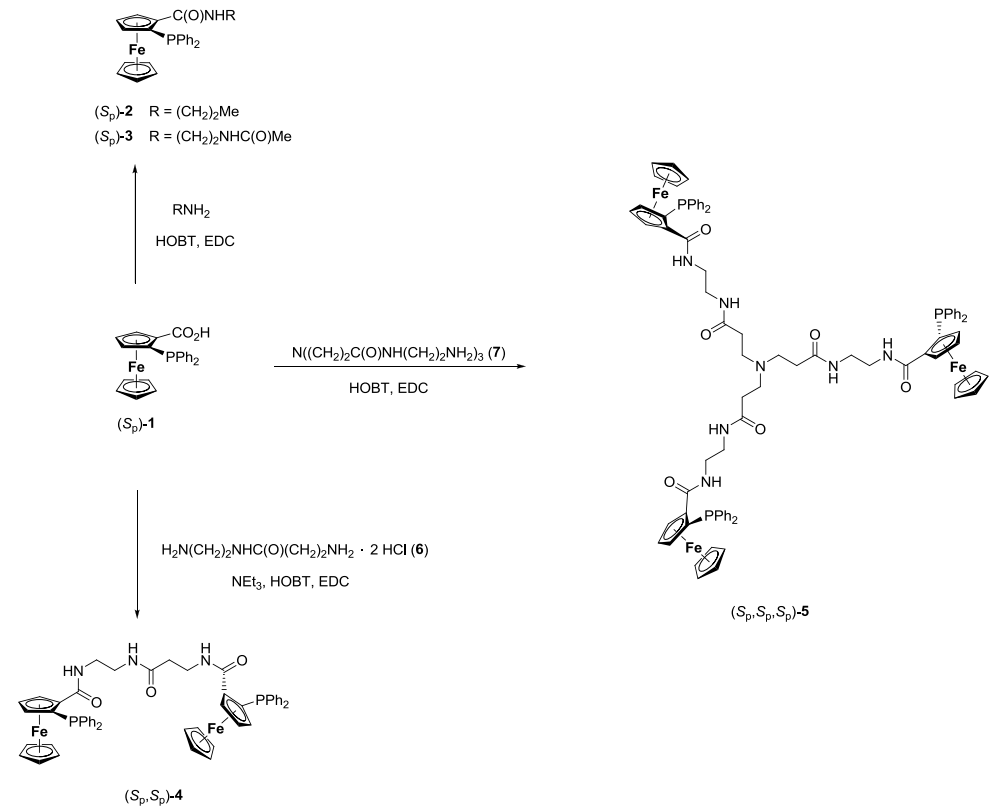

Scheme H2. Preparation of phosphane-amides **2** – **5** (EDC = 1-ethyl-3-[3-(dimethylamino)propyl]carbodiimide, HOBT = 1-hydroxybenzotriazole).

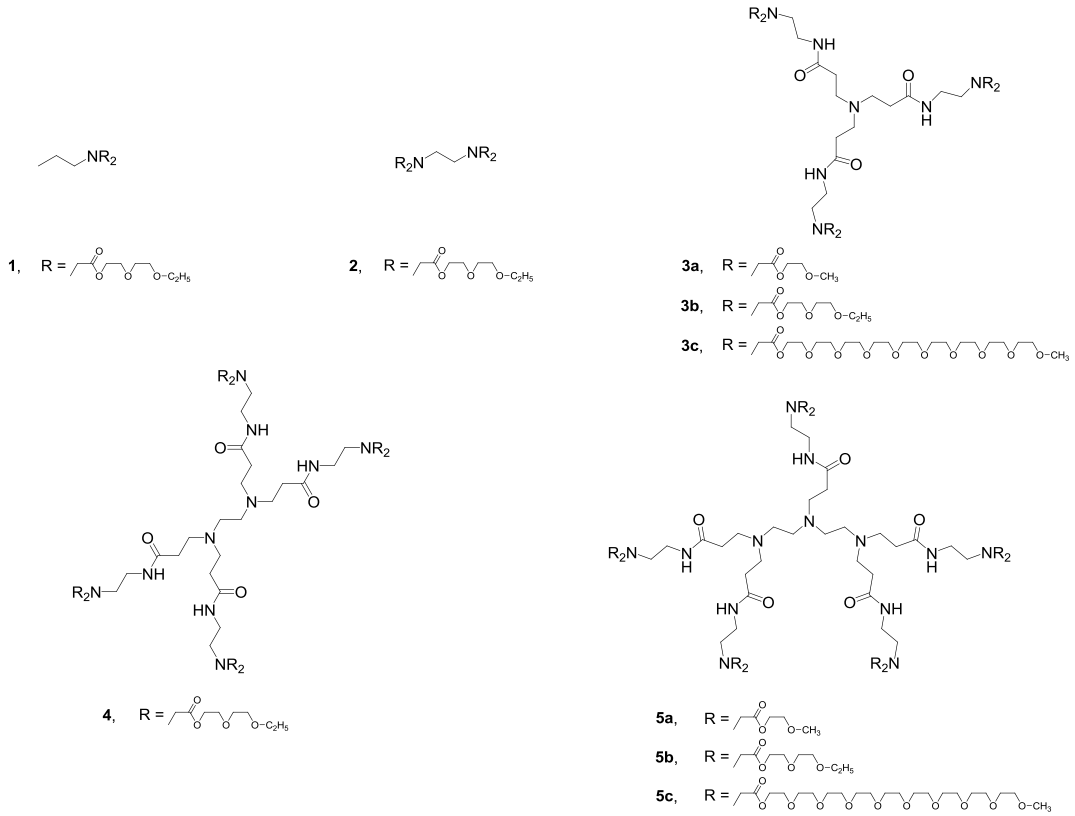

Chart H1. Synthesized (poly)ethylene glycol-functionalized PAMAM dendrimers **3a** – **3c**, **4**, **5a** – **5c** and for comparison, amines **1** and **2**.

The obtained biocompatible dendritic architectures **3a** – **3c**, **4**, **5a** – **5c** featuring 6, 8, or 10 ethylene glycol ether-termini of various sizes provide multiple donating capabilities. The intrinsic nanotemplating properties were examined for the stabilization of Au NPs. Therefore, the appropriate templates **1**, **2**, **3a** – **3c**, **4** and **5a** – **5c** were loaded with $H[AuCl_4]$. Subsequent reduction of the respective metallodendrimers with $Na[BH_4]$ produced dendrimer encapsulated gold colloids. The dendritic scaffold, the length of the ethylene glycols, the adjusted stabilizer to gold ratio and the duration of reaction time affected the morphology and the average Au NPs diameter in a range of 4.0 (± 0.9) to 58.5 (± 14.5) nm. Characterization by transmission electron microscopy (TEM), dynamic light scattering (DLS), UV/Vis and FT-IR spectroscopy revealed that Au NPs are formed and protected inside the dendrimer scaffold.

Chapter F

Stable magnetic magnetite nanoparticles (Fe_3O_4 NPs) were synthesized using the chemical co-precipitation method of ferrous (Fe^{2+})/ferric (Fe^{3+}) mixed aqueous salt solutions in presence of well-defined biocompatible low generation (poly)amidoamine (PAMAM)-based dendrimers with end-grafted *n* (oligo)ethylene glycol ether (*n* = 1, 2, 9) moieties, accessible by means of straightforward consecutive divergent synthesis methodologies including addition and amidation cycles (Scheme H3).

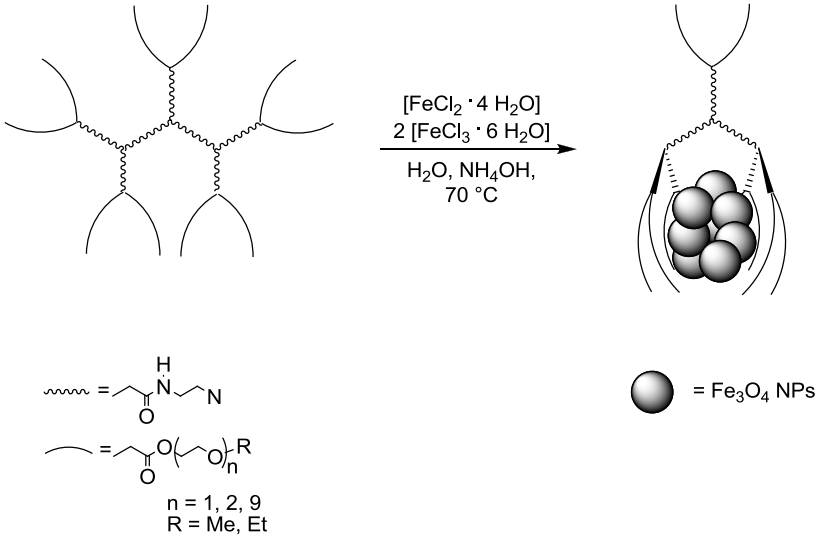

Scheme H3. Schematic illustration of *in-situ* dendrimer-stabilized Fe_3O_4 NP formation by the co-precipitation method.

The structural properties of Fe_3O_4 NPs were analyzed by FT-IR spectroscopy, thermogravimetry (TGA), X-ray powder diffraction (XRPD) and transmission electron microscopy (TEM) experiments.

Magnetic measurements, performed in the temperature range of 5 K to 300 K and at magnetic fields of -70 kOe to +70 kOe, were carried out on Fe_3O_4-magnetodendrimers using a SQUID-VSM to record field cooled (FC) and zero field cooled (ZFC) magnetizations. The determination revealed superparamagnetic metal oxide colloids, possessing ferrimagnetic characteristics at temperatures below the blocking temperature T_B (≈ 20 K).

Chapter G

The (oligo)ethylene glycol grafted amidoamine dendrimer **2** was synthesized, characterized and evaluated as drug delivery vehicle for therapeutic doxorubicin (DOX). While fluorescence spectroscopy was performed to monitor the drug loading process onto dendrimer **2**, the successful loading was confirmed by FT-IR spectroscopy, displaying characteristic vibration modes of the resulting dendrimer-DOX conjugate (Scheme H4).

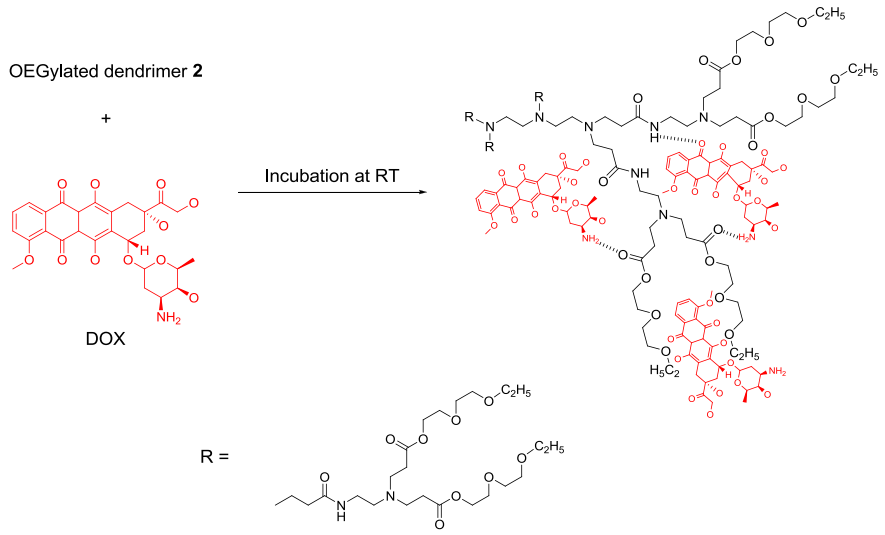

Scheme H4. Proposed interactions of the dendrimer with doxorubicin.

Temperature stimulated *in vitro* release studies of DOX from DOX-loaded dendrimers were carried out. An initial fast and burst release of DOX was observed in hyperthermic conditions at 43 °C, achieved by breaking off the intermolecular hydrogen bonds formed. The dendrimer-DOX conjugate´s efficacy was evaluated *in vitro* against HeLa and MCF-7 cancer cell lines and the IC_{50} was estimated, indicating an enhancement in cytotoxicity DOX loaded on dendrimer **2**.

2. Zusammenfassung

Die vorliegende Arbeit befasst sich mit der Darstellung, Charakterisierung und Anwendung (Poly)amidoamin-basierender Dendrimere kleiner Generationen. Den Mittelpunkt des Interesses stellt dabei die gezielte Modifikation der dendritischen Peripherie durch das Einführen von metallorganischen, komplexchemischen und biochemischen Funktionalitäten dar. Die Vielseitigkeit der auf diesem Wege erhaltenen dendritischen Strukturen spiegelt sich in einer Vielzahl von Einsatzmöglichkeiten wie bspw. als Katalysatoren in homogen-katalytisch geführten *C,C*-Kreuzkupplungsreaktionen, als Template für die Metall- bzw. Metalloxid-Nanopartikelgenerierung sowie als spezifische Wirtsmoleküle für Zytostatika wieder.

Die Ergebnisse, welche im Rahmen dieser Promotionsarbeit erzielt wurden, sind in fünf einzelne Themengebiete unterteilt und in den entsprechenden Kapiteln ausgewiesen:

Kapitel C: Amidoamine-based Dendrimers with End-grafted Pd-Fe Units: Synthesis, Characterization and Their Use in the Heck Reaction

Kapitel D: A Preparation of Planar-Chiral Multidonor Phosphanylferrocene Carboxamides and Their Application as Ligands for Palladium-Catalyzed Asymmetric Allylic Alkylation

Kapitel E: Au Nanoparticles Stabilized by PEGylated Low-Generation PAMAM Dendrimers: Design, Characterization and Properties

Kapitel F: Design, Characterization and Magnetic Properties of Fe_3O_4-Nanoparticle Arrays Coated with PEGylated-Dendrimers

Kapitel G: Dendrimer-Doxorubicin Conjugate for Enhanced Therapeutic Effects for Cancer

Kapitel C

In diesem Kapitel wird die Darstellung und Charakterisierung Amidoamin-basierender Metallodendrimere mit heterobimetallischen, endständigen Amidoferrocenyl-Palladium-allylchlorid-Funktionalitäten vorgestellt. Mittels konsekutiver, divergenter Synthesestrategien konnten sowohl die dendritischen Ausgangsverbindungen als auch die entsprechenden Metallodendrimere zugänglich gemacht werden. Durch Zugabe von $[Pd(\eta^3\text{-}C_3H_5)Cl]_2$ wurden die heterobimetallischen Metallodendrimere **7-Fe-Pd** − **9-Fe-Pd** als auch die (Amido)amin-funktionalisierten Modellsysteme **5-Fe-Pd** und **6-Fe-Pd** erhalten (Schema H1, Figur H1).

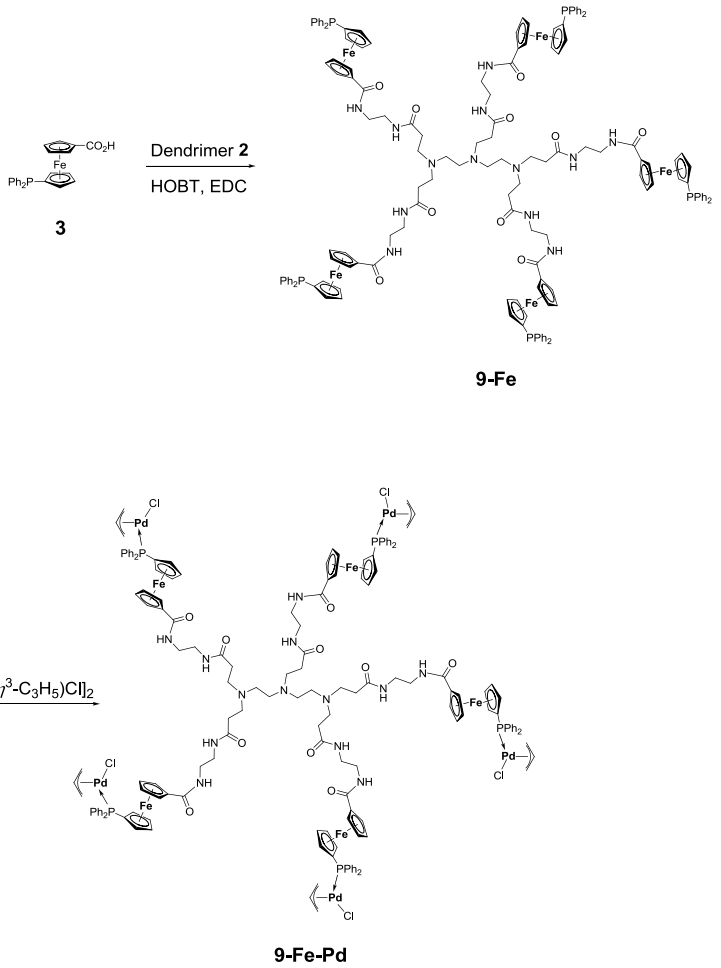

Schema H1. Darstellung des heterobimetallischen Dendrimers **9-Fe-Pd**.

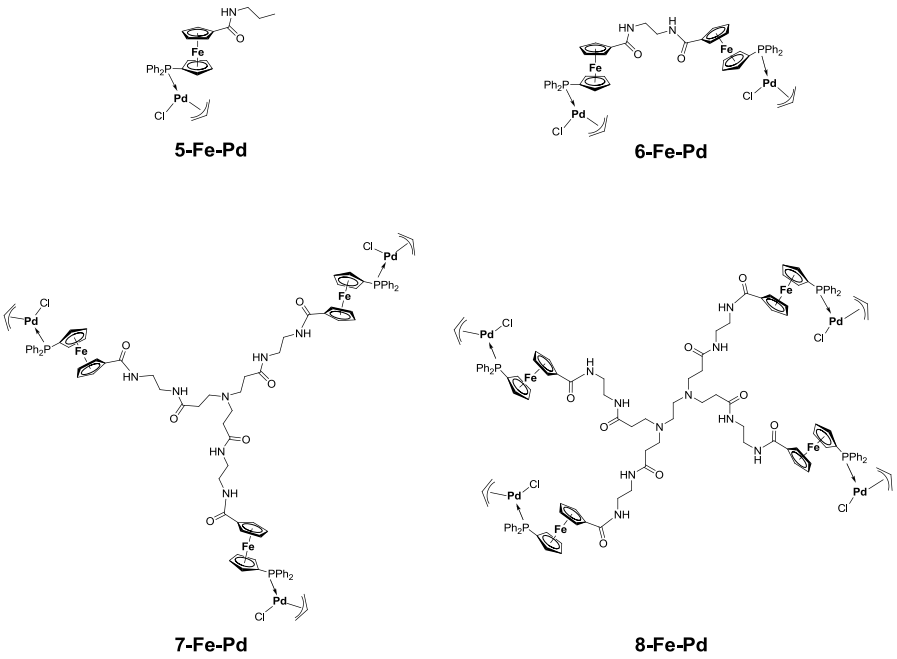

Figur H1. Heterobimetallische Amidoamine **5-Fe-Pd** – **8-Fe-Pd**.

Nachfolgend fanden die entsprechenden heterobimetallischen Systeme **5-Fe-Pd** – **9-Fe-Pd** Einsatz als Präkatalysatoren in einer *C,C*-Kreuzkupplungsreaktion nach Heck. Bei der homogen-katalytisch geführten Umsetzung von Iodbenzol mit *tert*-Butylacrylat zeigte Verbindung **9-Fe-Pd** mit fünf terminalen heterobimetallischen Fe-Pd-Einheiten die höchste Produktivität. Darüber hinaus konnte das Auftreten gesteigerter Umsätze als Resultat synergistischer, kooperativer Effekte für die Metallodendrimere **5-Fe-Pd** / **6-Fe-Pd**, **7-Fe-Pd** / **8-Fe-Pd**, und **9-Fe-Pd** beobachtet werden.

Kapitel D

Eine Oligoaminserie mit peripherer Mono-, Di- und Tri-Funktionalisierung durch (S_p)-2-(Diphenylphosphan)ferrocen-1-yl-Substituenten konnte mittels Peptidknüpfungsreaktionen ausgehend von (S_p)-2-(Diphenylphosphan)ferrocen-1-carbonsäure [(S_p)–**1**] und den entsprechenden terminalen Aminen in Gegenwart geeigneter Peptidkupplungsreagenzien dargestellt werden (Schema H2).

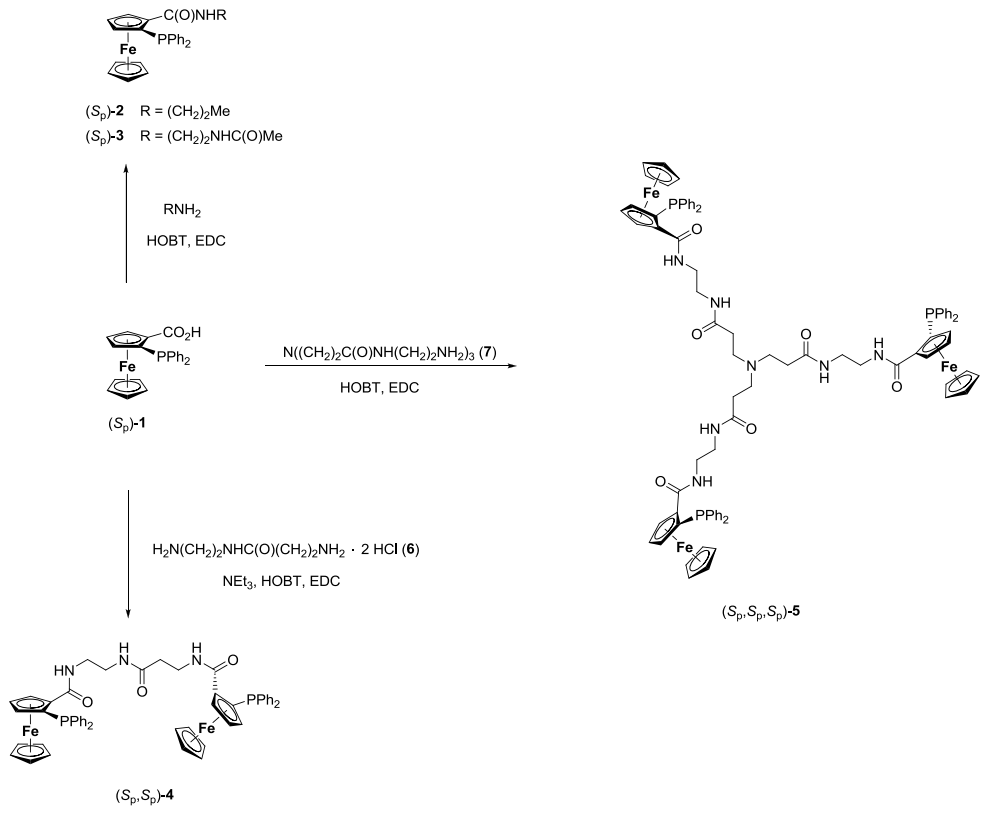

Schema H2. Darstellung der Phosphanamid-Moleküle **2** – **5** (EDC = 1-Ethyl-3-[3-(dimethylamino)propyl]carbodiimid, HOBT = 1-Hydroxybenzotriazol).

Die erhaltenen chiralen, Dendrimer-geträgerten Phosphane **2** – **5** wurden mit $[Pd(\eta^3\text{-}C_3H_5)Cl]_2$ zur Reaktion gebracht und im Anschluss als Präkatalysatoren in einer asymmetrischen Palladium-katalysierten allylischen Substitutionsreaktion eingesetzt. Die Ergebnisse der Umsetzung von 1,3-Diphenylprop-2-en-1-yl-acetat mit Malonat zeigen eine relativ geringe Veränderung des *ee* in Bezug auf die Anzahl chiraler 2-Phosphanylferrocenyl-Einheiten. Weiterhin sind die erhaltenen Umsätze nach 24 Stunden stark verschieden, wobei größere Dendrimerstrukturen geringere Umsätze zur Folge haben.

Kapitel E

Über eine zweistufige Synthesestrategie wurde die Darstellung einer Serie von (Poly)amidoamin-basierenden Dendrimeren sowie entsprechender (Amido)amin-Modellverbindungen mit terminal funktionalisierten Ethylenglykolethern unterschiedlicher Kettenlänge ermöglicht (Abbildung H1).

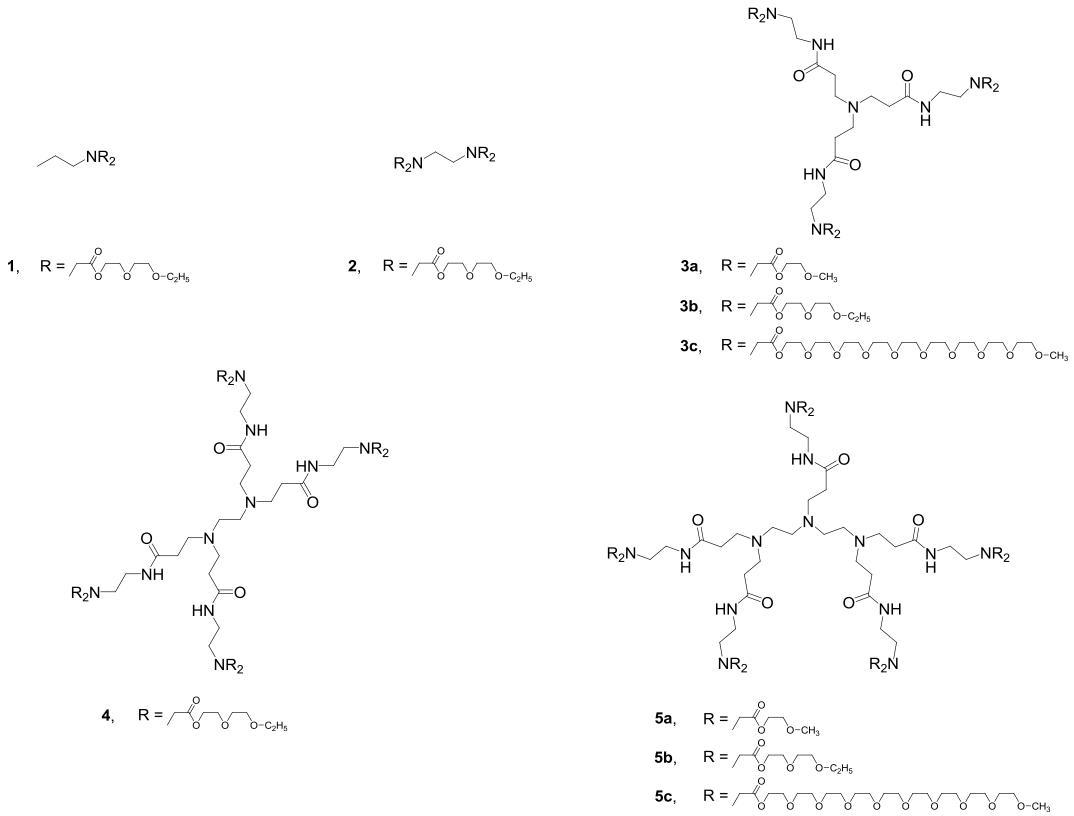

Abbildung H1. Dargestellte (Poly)ethylenglykol-funktionalisierte PAMAM Dendrimere **3a** – **3c**, **4**, **5a** – **5c** und Modellverbindungen **1** und **2**.

Die erhaltenen, biokompatiblen dendritischen Strukturen **3a** – **3c**, **4** und **5a** – **5c** mit sechs, acht und zehn Ethylenglykolether-Endgruppen verschiedener Kettenlänge weisen eine große Anzahl von Donoratomen auf. Folglich wurden die intrinsischen koordinativen Eigenschaften

bei der Stabilisierung von Gold-Nanopartikeln eingehend untersucht. Die jeweiligen Template **1**, **2**, **3a** – **3c**, **4** und **5a** – **5c** wurden mit $H[AuCl_4]$ zur Reaktion gebracht, und durch anschließende Reduktion mit $Na[BH_4]$ konnte die Generierung der entsprechenden Dendrimer-stabilisierten Goldkolloide realisiert werden. Es zeigte sich, dass neben der dendritischen Struktur selbst, auch die Größe der Ethylenglykolether-Funktionalitäten, das eingestellte Stabilisator-Gold-Verhältnis sowie die Reaktionszeit einen erheblichen Einfluss auf die Morphologie und den durchschnittlichen Goldpartikeldurchmesser haben. Die Charakterisierung der Dendrimer-Gold-Hybridmaterialien mittels Transmissionselektronenmikroskopie (TEM), dynamischer Lichtstreuung (DLS), UV/Vis- und FT-IR-Spektroskopie belegen die Bildung 4.0 (± 0.9) nm bis 58.5 (± 14.5) nm großer Goldkolloide innerhalb der dendritischen Strukturen.

Kapitel F

Stabile, magnetische Magnetitnanopartikel (Fe_3O_4) konnten durch Anwendung der Mitfällungsmethode ausgehend von wässrigen Fe^{2+}/Fe^{3+}-Lösungen in Gegenwart entsprechender biokompatibler (Poly)amidoamin-basierender Dendrimere mit endständigen Ethylenglykolether-Einheiten erhalten werden (Schema H3).

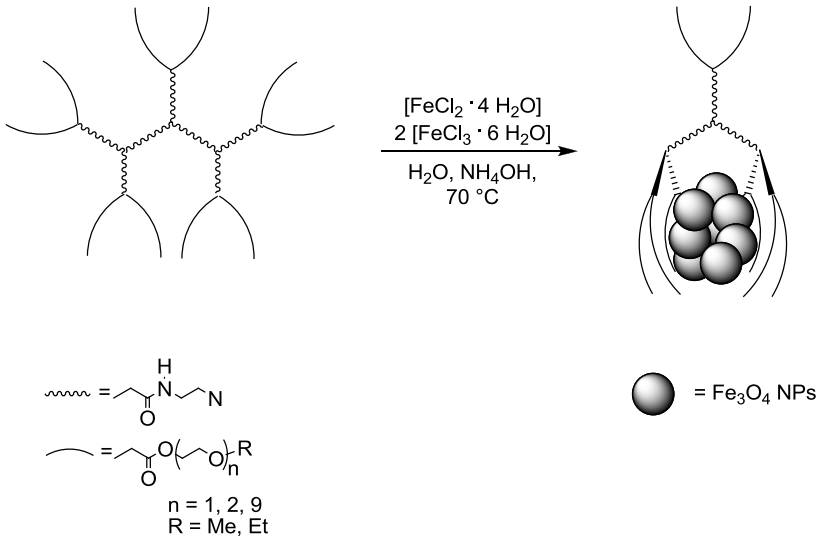

Schema H3. Schematische Darstellung der *in-situ* Generierung Dendrimer-stabilisierter Fe_3O_4-Nanopartikel durch die Mitfällungsmethode.

Die strukturellen Besonderheiten der Dendrimer-stabilisierten Fe_3O_4-Kolloide wurden mittels FT-IR-Spektroskopie, Thermogravimetrie (TGA), Röntgenpulverdiffraktometrie (XRPD)

und Transmissionselektronenmikroskopie (TEM) bestimmt. Magnetische Messungen wurden bei verschiedenen Temperaturen (5 K bis 300 K) und variierten magnetischen Feldern (-70 kOe bis +70 kOe) an ausgewählten Fe_3O_4-Magnetodendrimeren durchgeführt. An einem SQUID-VSM-Gerät konnten die FC- (field cooled) und ZFC- (zero field cooled) Magnetisierungen der Metalloxid-Proben ermittelt werden. Aus den erhaltenen Ergebnissen wird ein superparamagnetisches Verhalten der Kolloide oberhalb einer Blocking-Temperatur von $T_B \approx$ 20 K deutlich.

Kapitel G

Das (Oligo)ethylenglykol-funktionalisierte Amidoamin-Dendrimer **2** konnte erfolgreich dargestellt und charakterisiert werden. Bei einer anschließenden biochemischen Evaluierung erwies es sich als geeignete Wirtsverbindung für das Zytostatikum Doxorubicin (DOX). Mittels Fluoreszenzspektroskopie wurde die Beladung des Dendrimers **2** mit DOX verfolgt. Charakteristische Schwingungsbanden im anschließend aufgenommenen FT-IR-Spektrum bestätigten die Bildung eines Dendrimer-DOX-Konjugates (Schema H4).

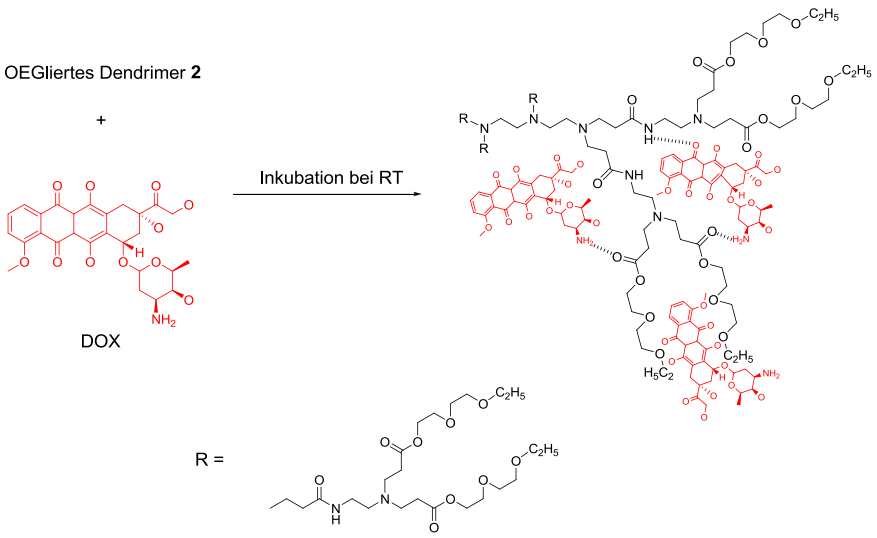

Schema H4. Postulierte intermolekulare Wechselwirkungen im Dendrimer-DOX-Konjugat.

In vitro Untersuchungen zur temperaturgesteuerten Wirkstoffabgabe des Doxorubicins aus dem Konjugat zeigen eine schnelle Freisetzung des Therapeutikums unter hyperthermischen Bedingungen von 43 °C in Folge des Aufbrechens intermolekularer Wasserstoff-Brücken-Bindungen. Die Wirksamkeit des Dendrimer-DOX-Konjugates bei der Behandlung von HeLa- und MCF-7-Krebszellen konnte durch die Bestimmung der jeweiligen IC_{50}-Werte nach-

gewiesen werden. Es zeigte sich eine erhöhte Zytotoxizität des Doxorubicin-beladenen Dendrimers **2** gegenüber des ungeträgerten Wirkstoffes.

Danksagung

Ich möchte diese Gelegenheit nutzen und mich bei einer Vielzahl von Menschen bedanken, die zum Gelingen dieser Arbeit maßgeblich beigetragen haben.

Mein besonderer Dank gilt Herrn Prof. Dr. Heinrich Lang für die Möglichkeit, diese interessante und vielseitige Aufgabenstellung bearbeiten zu können, für das in mich gesetzte Vertrauen, die stets gewährte Unterstützung sowie die zahlreichen anregenden Diskussionen.

Bei Prof. Dr. Michael Mehring bedanke ich mich für die Anfertigung des Zweitgutachtens.

Prof. Dr. Dhirendra Bahadur und Dr. Sudeshna Chandra danke ich für die Möglichkeit einen DAAD-geförderten Auslandsaufenthalt am IIT Bombay (Indien) durchführen zu können und die stets gute Zusammenarbeit.

(Dr.) Alexander Hildebrandt, André Tuchscherer und Dieter Schaarschmidt gilt mein ganz besonderer Dank für die zahllosen befruchtenden Diskussionen auf vielen chemischen und nicht-chemischen Gebieten sowie der stets freundschaftliche Umgang miteinander.

Allen Mitgliedern der Arbeitsgruppe Anorganische Chemie danke ich für das stets freundliche und hilfsbereite Arbeitsklima. Ich danke Dr. Roy Buschbeck für das Korrekturlesen der vorliegenden Arbeit.

Frau Ruder und Frau Stöß möchte ich für ihre stets aufopferungsvolle und fürsorgliche Unterstützung in allen organisatorischen Angelegenheiten während der letzten Jahre meinen Dank aussprechen.

Zum Schluss gehört ein ganz großes Dankeschön meiner Familie für die Geduld, das Verständnis, die Führung und die mir stets gewährte Unterstützung während meines bisherigen persönlichen und beruflichen Werdegangs. Meinen Eltern, meinem Bruder und meiner lieben Sophia soll diese Arbeit als Dank gewidmet sein.

Meinen "außerchemischen" Freunden sowie vielen, hier nicht genannten Personen danke ich für die schönen Erlebnisse und die Motivationen in den vergangenen Jahren.

I Appendix

1. Appendix Chapter C

Amidoamine-based Dendrimers with End-grafted Pd-Fe Units: Synthesis, Characterization and Their Use in the Heck Reaction

Sascha Dietrich, Anja Nicolai and Heinrich Lang

(Published in *J. Organomet. Chem.* **2011**, *696*, 739 – 747.)

Technische Universität Chemnitz, Fakultät für Naturwissenschaften, Institut für Chemie, Lehrstuhl für Anorganische Chemie, Straße der Nationen 62, 09111 Chemnitz (Germany)

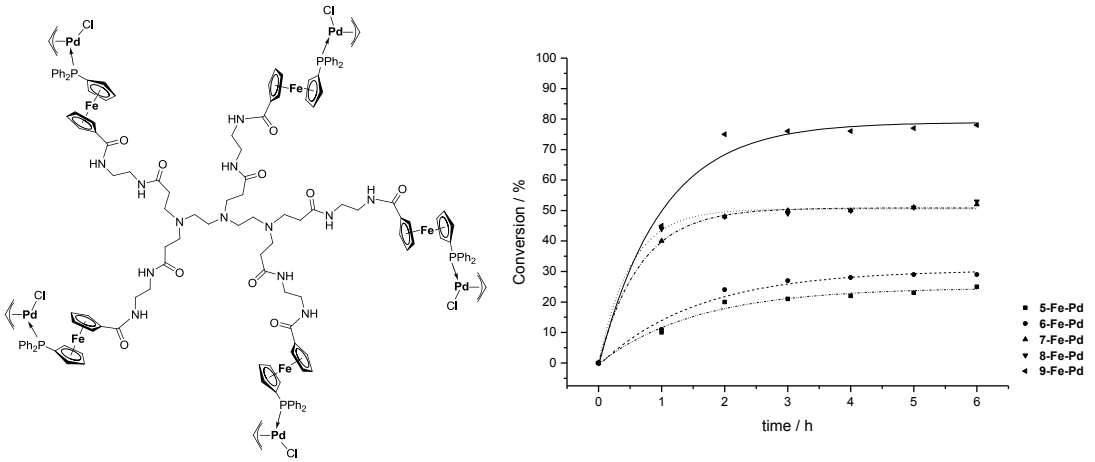

Abstract

The synthesis and characterization of novel amidoamine-based metallodendrimers with heterobimetallic end-grafted amidoferrocenyl-palladium-allyl chloride units is described. Dendrimer (Fe((η^5-$C_5H_4PPh_2$)(η^5-C_5H_4))C(O)HNCH$_2$CH$_2$NHC(O)CH$_2$CH$_2$)N[CH$_2$CH$_2$N(CH$_2$CH$_2$-C(O)NHCH$_2$CH$_2$NHC(O)(Fe(η^5-C_5H_4)(η^5-$C_5H_4PPh_2$)))$_2$]$_2$ (**9-Fe**) and the corresponding metallodendrimer (Fe((η^5-$C_5H_4PPh_2$(Pd(η^3-C_3H_5)Cl))(η^5-C_5H_4))C(O)HNCH$_2$CH$_2$NHC(O)-

$CH_2CH_2)N[CH_2CH_2N(CH_2CH_2C(O)NHCH_2CH_2NHC(O)(Fe(\eta^5\text{-}C_5H_4)(\eta^5\text{-}C_5H_4PPh_2(Pd(\eta^3\text{-}C_3H_5)Cl))))_2]_2$ (**9-Fe-Pd**) were prepared by a consecutive divergent synthesis methodology including addition-amidation cycles, standard peptide coupling and coordination procedures. For comparative reasons also the monomeric and dimeric molecules ($Fe(\eta^5\text{-}C_5H_4(PPh_2)(\eta^5\text{-}C_5H_4C(O)NH^nC_3H_7))$) (**5-Fe**) and $[Fe(\eta^5\text{-}C_5H_4(PPh_2))(\eta^5\text{-}C_5H_4C(O)NHCH_2)]_2$ (**6-Fe**) as well as $N(CH_2CH_2C(O)NHCH_2CH_2NHC(O)(Fe(\eta^5\text{-}C_5H_4)(\eta^5\text{-}C_5H_4PPh_2)))_3$ (**7-Fe**) and $[CH_2N\text{-}(CH_2CH_2C(O)NHCH_2CH_2NHC(O)(Fe(\eta^5\text{-}C_5H_4)(\eta^5\text{-}C_5H_4PPh_2)))_2]_2$ (**8-Fe**) were prepared from $Fe(\eta^5\text{-}C_5H_4(PPh_2))(\eta^5\text{-}C_5H_4CO_2H)$ (**3**). Using $[Pd(\eta^3\text{-}C_3H_5)Cl]_2$ (**4**) as palladium source heterobimetallic metallodendrimers $(Fe(\eta^5\text{-}C_5H_4PPh_2(Pd(\eta^3\text{-}C_3H_5)Cl))(\eta^5\text{-}C_5H_4C(O)\text{-}NH^nC_3H_7))$ (**5-Fe-Pd**), $[Fe(\eta^5\text{-}C_5H_4(PPh_2(Pd(\eta^3\text{-}C_3H_5)Cl))(\eta^5\text{-}C_5H_4C(O)NHCH_2))]_2$ (**6-Fe-Pd**), $N(CH_2CH_2C(O)NHCH_2CH_2NHC(O)(Fe(\eta^5\text{-}C_5H_4)(\eta^5\text{-}C_5H_4PPh_2(Pd(\eta^3\text{-}C_3H_5)Cl))))_3$ (**7-Fe-Pd**) and $[CH_2N(CH_2CH_2C(O)NHCH_2CH_2NHC(O)(Fe(\eta^5\text{-}C_5H_4)(\eta^5\text{-}C_5H_4PPh_2(Pd(\eta^3\text{-}C_3H_5)Cl))))_2]_2$ (**8-Fe-Pd**) were synthesized. Additionally, seleno-phosphines of **5-Fe-Se** and **9-Fe-Se**, respectively, were prepared by addition of elemental selenium to **5-Fe** or **9-Fe** to estimate their σ- donor properties.

The palladium-containing amidoamine supports are catalytically active in the Heck-Mizoroki cross-coupling of iodobenzene with *tert*-butyl acrylate. The catalytic data are compared to those obtained for the appropriate mononuclear and dinuclear compounds **5-Fe-Pd** and **6-Fe-Pd**. This comparison confirms a positive cooperative effect. The mercury drop test showed that (nano)particles were formed during catalysis, following on heterogeneous carbon-carbon cross-coupling.

2. Appendix Chapter D

A Preparation of Planar-Chiral Multidonor Phosphanyl-Ferrocene Carboxamides and Their Application as Ligands for Palladium-Catalyzed Asymmetric Allylic Alkylation

Martin Lamač, Jiří Tauchman, Sascha Dietrich, Ivana Císařová, Heinrich Lang and Petr Štěpnička

(Published in *Appl. Organometal. Chem.* **2010**, *24*, 326 – 331.)

Technische Universität Chemnitz, Fakultät für Naturwissenschaften, Institut für Chemie, Lehrstuhl für Anorganische Chemie, Straße der Nationen 62, 09111 Chemnitz (Germany)

Charles University in Prague, Faculty of Science, Department of Inorganic Chemistry, Hlavova 2030, 128 40 Prague (Czech Republic)

Abstract

Amide coupling of (S_p)-2-(diphenylphosphanyl)ferrocene-1-carboxylic acid with appropriate terminal amines mediated by 1-hydroxybenzotriazole and a carbodiimide affords multi-donor amides terminally functionalized with planar-chiral (S_p)-2-(diphenyl-phosphanyl)ferrocen-1-yl moieties in good to excellent yields. Palladium catalysts based on these ligands efficiently promote asymmetric allylic alkylation of 1,3-diphenylallyl acetate with *in-situ* generated dimethyl malonate anion to give the C-alkylated product with *ee*s up to 93 % at room temperature.

3. Appendix Chapter E

Au Nanoparticles Stabilized by PEGylatedLow-Generation PAMAM Dendrimers: Design, Characterization and Properties

Sascha Dietrich, Steffen Schulze, Michael Hietschold and Heinrich Lang

(Published in *J. Colloid Interface Sci.* **2011**, *359*, 454 – 460.)

Technische Universität Chemnitz, Fakultät für Naturwissenschaften, Institut für Chemie, Lehrstuhl für Anorganische Chemie, Straße der Nationen 62, 09111 Chemnitz (Germany)

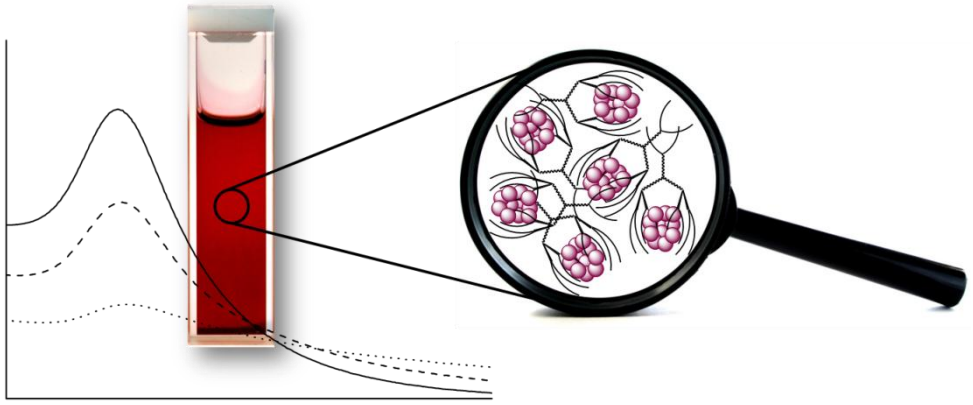

Abstract

The preparation and characterization of a series of well-defined low-generation (poly)amidoamine (PAMAM)-based dendrimers with end-grafted ethylene glycol ether moieties of type $N(CH_2CH_2C(O)NHCH_2CH_2NR_2)_3$ (**3a**, R = $CH_2CH_2C(O)OCH_2CH_2OCH_3$; **3b**, R = $CH_2CH_2C(O)O(CH_2CH_2O)_2C_2H_5$; **3c**, R = $CH_2CH_2C(O)O(CH_2CH_2O)_9CH_3$), $[CH_2N(CH_2CH_2C(O)NHCH_2CH_2NR_2)_2]_2$ (**4**, R = $CH_2CH_2C(O)O(CH_2CH_2O)_2C_2H_5$) and $(R_2NCH_2CH_2NHC(O)CH_2CH_2)N[CH_2CH_2N(CH_2CH_2C(O)NHCH_2CH_2NR_2)_2]_2$ (**5a**, R = $CH_2CH_2C(O)OCH_2CH_2OCH_3$; **5b**, R = $CH_2CH_2C(O)O(CH_2CH_2O)_2C_2H_5$; **5c**, R = $CH_2CH_2C(O)O(CH_2CH_2O)_9CH_3$) and their application for the stabilization of gold nanopar-

ticles (Au NPs) is described. These dendrimers were prepared by a consecutive divergent synthesis methodology including Michael addition and amidation cycles. For comparison, amidoamine related model compounds $N(C_3H_7)R_2$ (**1**, R = $CH_2CH_2C(O)O(CH_2CH_2O)_2C_2H_5$) and $[CH_2NR_2]_2$ (**2**, R = $CH_2CH_2C(O)O(CH_2CH_2O)_2C_2H_5$) were also synthesized to estimate the minimum required donating capabilities of the stabilizer. Loading the appropriate dendritic templates with $H[AuCl_4]$ (**12**) and subsequent reduction of the respective metallodendrimers with $Na[BH_4]$ produced dendrimer encapsulated gold colloids. The dendrimeric scaffold, the length of the ethylene glycols, the adjusted stabilizer:gold ratio and the duration of reaction time affects the average Au particle diameter in a range of 4.0 (± 0.9) to 58.5 (± 14.5) nm. Furthermore, depending on the nature of the stabilizer, nanoparticles were formed having spherical or multiple morphologies. Characterization by transmission electron microscopy (TEM), dynamic light scattering (DLS), UV/Vis and FT-IR spectroscopy revealed that Au NPs are formed and protected inside the dendrimer scaffold.

4. Appendix Chapter F

Design, Characterization and Magnetic Properties of Fe_3O_4-Nanoparticle Arrays Coated with PEGylated-Dendrimers

Sascha Dietrich, Sudeshna Chandra, Colin Georgi, Senoy Thomas, Denys Makarov, Steffen Schulze, Michael Hietschold, Manfred Albrecht, Dhirendra Bahadur and Heinrich Lang

(Submitted to *Mat. Chem. Phys.* **2011**.)

Technische Universität Chemnitz, Fakultät für Naturwissenschaften, Institut für Chemie, Lehrstuhl für Anorganische Chemie, Straße der Nationen 62, 09111 Chemnitz (Germany)

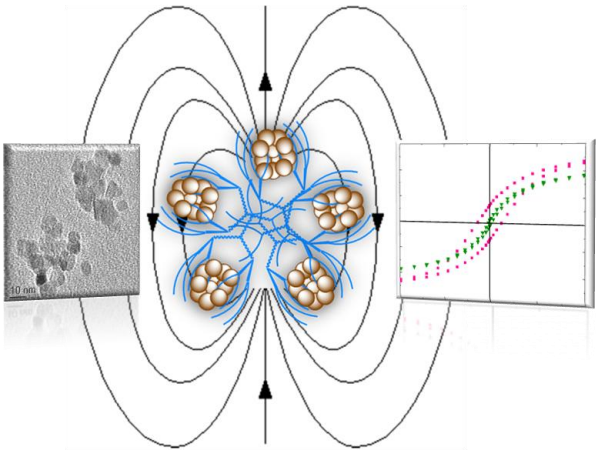

Abstract

Stable magnetic magnetite nanoparticles (Fe_3O_4 NPs) were synthesized using the chemical co-precipitation method of ferrous (Fe^{2+})/ferric (Fe^{3+}) mixed aqueous salt solutions in presence of well-defined biocompatible low-generation (poly)amidoamine (PAMAM)-based dendrimers with end-grafted n ethylene glycol ether (n = 1, 2, 9) moieties, accessible by means of straightforward consecutive divergent synthesis methodologies including addition and amidation cycles. Addition of NH_4OH to the respective dendritic nanoreactor containing iron salt solution produced dendritic stabilized uniform shaped magnetite nanoparticles. The structural and magnetic properties of Fe_3O_4 NPs were analyzed by FT-IR spectroscopy, ther-

mogravimetry (TGA), X-ray powder diffraction (XRPD), transmission electron microscopy (TEM) and superconducting quantum interference device (SQUID) vibrating sample magnetometry (VSM). The coherence of affecting the average magnetite particle diameter in range of 5.6 (± 1.4) nm to 10.1 (± 1.9) nm by the dendritic scaffold, the number and length of the attached ethylene glycol ether termini as well as the adjusted stabilizer-to-Fe_3O_4 ratio is discussed along with their magnetic peculiarities.

5. Appendix Chapter G

Dendrimer – Doxorubicin Conjugate for Enhanced Therapeutic Effects for Cancer

Sudeshna Chandra, Sascha Dietrich, Heinrich Lang and Dhirendra Bahadur

(Published in *J. Mater. Chem.* **2011**, *21*, 5729 – 5737.)

Abstract

An oligo(ethylene glycol)-grafted amidoamine dendrimer was synthesized and characterized by FT-IR, MS, ^{1}H and ^{13}C NMR. The dendritic scaffold was evaluated for its potential to load doxorubicin and its release, thereafter. The interaction between drug and the dendrimer was reviewed by ζ potential, HPLC, NMR and FT-IR spectroscopy. The drug encapsulation efficiency was as high as 52 %. The temperature stimulated release characteristics of the DOX loaded dendrimers were studied in PBS and SBF at 37 °C (physiological temperature) and 43 °C (hyperthermic temperature). A biphasic suspension of the dendrimer-drug conjugate and a magnetic fluid entitles release of the drug under AC magnetic field which can simultaneously be used for hyperthermia treatment of cancer. The efficacy of dendrimer-DOX conjugate was evaluated *in vitro* against cancer cell lines and the IC_{50} was estimated.

Lebenslauf

Persönliche Daten

Name:	Sascha Dietrich
Geburtsdatum:	15.10.1982
Geburtsort:	Stollberg/Erzgebirge
Anschrift:	Mosenstrasse 6 09130 Chemnitz
Familienstand:	ledig
Staatsangehörigkeit:	deutsch

Berufserfahrung

seit 11/2007	Wissenschaftlicher Mitarbeiter am Lehrstuhl für Anorganische Chemie, TU Chemnitz (Prof. Dr. Heinrich Lang)

Ausbildung

09/2007	Diplomverteidigung (Gesamtprädikat: sehr gut)
11/2006 – 09/2007	Diplomarbeit: "Metallodendrimere: Synthese und Charakterisierung", Lehrstuhl für Anorganische Chemie, TU Chemnitz (Prof. Dr. Heinrich Lang)
10/2006	Diplomhauptprüfung
10/2004 – 09/2006	Diplomstudiengang Chemie, Hauptstudium, TU Chemnitz, Schwerpunkt: Anorganische Chemie
09/2004	Vordiplomprüfung
10/2002 – 09/2004	Diplomstudiengang Chemie, Grundstudium, TU Chemnitz
08/2001 – 07/2002	Zivildienst bei AWO Seniorenpflegeheim "Willy-Brandt-Haus", Chemnitz
08/1993 – 07/2001	Gymnasium Einsiedel, Chemnitz Abschluss: Allgemeine Hochschulreife
09/1989 – 07/1993	Grundschule Neukirchen

Auszeichnungen

04/2008 – 03/2011	Landesgraduiertenstipendium, Freistaat Sachsen
02/2010 – 04/2010	DAAD-Kurzzeitstipendium, Auslandsaufenthalt am Indian Institute of Technology (IIT) Bombay (Prof. Bahadur)

Praktika

02/2005 – 03/2005	"Synthesis of New Macrocyclic Ligands", Universitat Autònoma de Barcelona (Prof. Llobet/Prof. Casabo)
02/2006 – 03/2006	"C-H Activation in New Macrocyclic Copper(I) Complexes", Universitat Autònoma de Barcelona (Prof. Llobet/Prof. Casabo)

Liste der Publikationen, Vorträge und Posterpräsentationen

Publikationen

1. A Preparation of Planar-Chiral Multidonor Phosphanyl-Ferrocene Carboxamides and Their Application as Ligands for Palladium-Catalyzed Asymmetric Allylic Alkylation.
   M. Lamač, J. Tauchman, S. Dietrich, I. Císařová, H. Lang, P. Štěpnička,
   Appl. Organomet. Chem. **2010**, *24*, 326 – 331.

2. Amidoamine-based Dendrimers with End-grafted Pd-Fe Units: Synthesis, Characterization and Their Use in the Heck Reaction.
   S. Dietrich, A. Nicolai, H. Lang,
   J. Organomet. Chem. **2011**, *696*, 739 – 747.

3. Dendrimer-Doxorubicin Conjugate for Enhanced Therapeutic Effects for Cancer.
   S. Chandra, S. Dietrich, H. Lang, D. Bahadur,
   J. Mater. Chem. **2011**, *21*, 5729 – 5737.

4. Alkynyl Ti–M Complexes with M = Cd and Hg: Synthesis, Characterization and Reaction Chemistry.
   S. Dietrich, N. Mansilla, A. Hildebrandt, N. Wetzold, G. Rheinwald, T. Rüffer, H. Lang,
   J. Organomet. Chem. **2011**, *696*, 2491 – 2498.

5. Au Nanoparticles Stabilised by PEGylated Low Generation PAMAM Dendrimers: Design, Characterization and Properties.
   S. Dietrich, S. Schulze, M. Hietschold, H. Lang,
   J. Colloid Interface Sci. **2011**, *359*, 454 – 460.

6. Design, Characterization and Magnetic Properties of Fe_3O_4 Nanoparticle Arrays Coated with PEGylated-Dendrimers.
   S. Dietrich, S. Chandra, C. Georgi, S. Thomas, D. Makarov, S. Schulze, M. Hietschold, M. Albrecht, D. Bahadur, H. Lang
   Mat. Chem. Phys. **2011**, submitted.

Poster

1. Immobilisierte Ferrocenylphosphan-Palladium-Komplexe für die Heck-Mizoroki-Reaktion.
   S. Dietrich, C. Schreiner, H. Lang,
   42. Jahrestreffen Deutscher Katalytiker 2009, 11. – 13.03.2009, Weimar.

2. New Materials and Chemistry: Small Molecules – Great Progress.
   R. Mothes, A. Jakob, A. Tuchscherer, S. Dietrich, Y. Shen, T. Waechtler, S.E. Schulz, T. Gessner, S. Jahn, R.R. Baumann, H. Lang,
   Global Challenges for Sustainable Development 2010, 25. – 26.02.2010,
   Rennes/Frankreich.

3. Metal- and Metal Oxide Nanoparticles.
   A. Jakob, A. Tuchscherer, S. Dietrich, R. Mothes, H. Lang,
   6. Thüringer Grenz- und Oberflächentage (ThGOT) 2010, 07. – 09.09.2010, Gera.

4. Synthese und Charakterisierung von Precursoren zur Erzeugung magnetischer Schichten und Nanopartikel.
   C. Georgi, M. Reichel, S. Dietrich, A. Jakob, H. Lang,
   NANETT-Projekttreffen, Öffentliches Statusseminar 2010, 09.11.2010, Chemnitz.

5. Immobilized Ferrocenyl Phosphine Palladium Complexes for the Heck-Mizoroki Reaction.
   S. Dietrich, C. Schreiner, H. Lang,
   9^{th} Ferrocene Colloquium 2011, 14. – 16.02.2011, Chemnitz.

Vorträge

1. Immobilisierung und Heterogenisierung homogen-katalytisch aktiver Katalysatoren.
   S. Dietrich, H. Lang,
   1st International Main-Group-Element and Organometallic Meeting, 25. – 28.09.2008, Graz/Österreich.

2. NANOPARTIKEL – Klein an Größe, Groß an Potential.
   S. Dietrich, H. Lang,
   2nd International Main-Group-Element and Organometallic Meeting, 24. – 27.09.2009, Bad Schandau.

3. Dendrimer-stabilized Metal Nanoparticles and their Applications.
   S. Dietrich, H. Lang,
   International Conference on Nano Science and Technology (ICONSAT) 2010,
   17. – 20.02.2010, Mumbai/Indien.

4. Towards Smart Materials – Design and Application.
   S. Dietrich, H. Lang,
   Doktorandenseminar IfC, TU Chemnitz 2011, 08.06.2011, Chemnitz.

5. Nanoparticles: Synthesis, Properties and Application.
   S. Dietrich, H. Lang,
   IRTG Block Courses, Summer Semester 2011, 18.07.2011, Chemnitz.

6. Nanoparticle Arrays Coated with OEGylated-Dendrimers.
   S. Dietrich, H. Lang,
   9. Mitteldeutsches Anorganiker-Nachwuchssymposium (MANS),
   22.09.2011, Leipzig.